THESIS CONFIDENTIAL STATUS

UNIVERSITI MALAYSIA PAHANG

DECLARATION OF THE THESIS AND COPYRIGHT

Author's full name : Masood Kamal

Date of birth : 21/02/1981

Title : A new hybrid multiaxial fatigue life model based on critical plane

continuum damage mechanics and genetic algorithm

Academic Session :

I declared that this thesis is classified as:

☐ **CONFIDENTIAL** (Contains confidential information under the official Secret Act 1972)

☐ **RESTRICTED** (Contains restricted information as specified by the organization where research is done)

■ **OPEN ACCESS** I agree that my thesis to be published as online open access (Full text)

I acknowledge that Universiti Malaysia Pahang reserves the right as follows:

1. The thesis is the property of Universiti Malaysia Pahang.
2. The library of Universiti Malaysia Pahang has the right to make copies for the purpose of the research only.
3. The library has the right to make copies of the thesis for academic exchange.

Certified by:

|	
(Student's Signature)	(Signature of Supervisor)
AE4202263	Prof. Dr. Md. Mustafizur Rahman
New IC / Passport Number	Name of Supervisor
Date:	Date:

STATEMENT OF AWARD FOR DEGREE

Thesis submitted in fulfillment of the requirements for the award of the degree of Doctor of Philosophy (Mechanical Engineering).
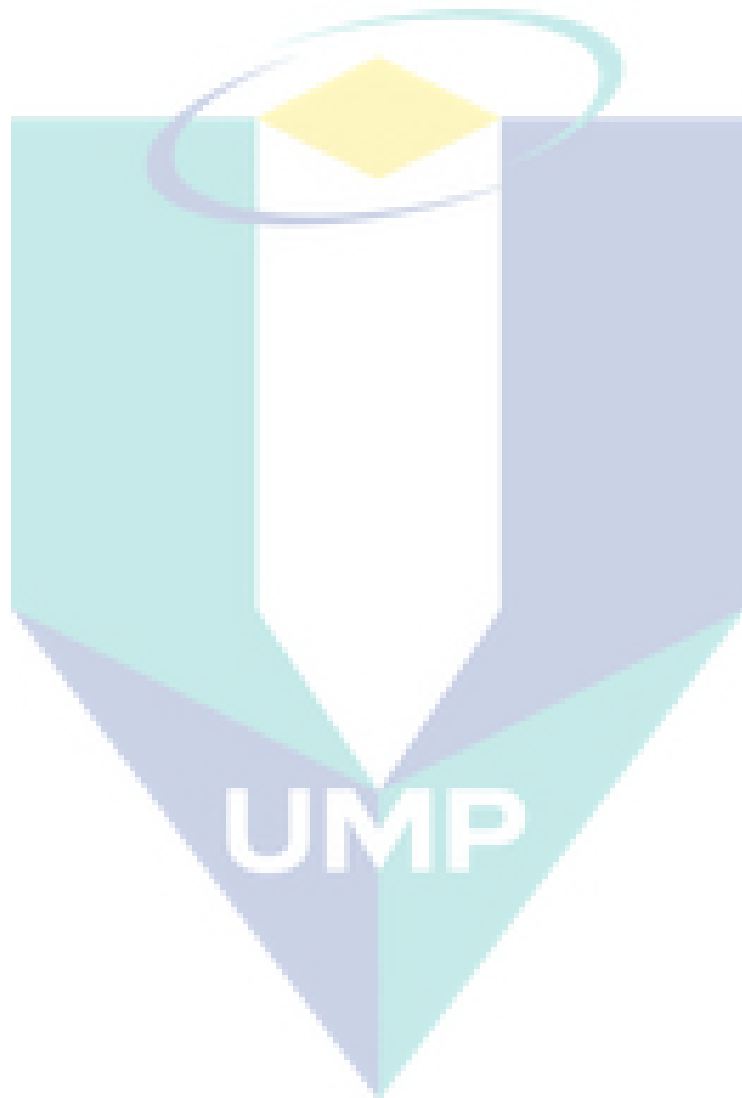
A NEW HYBRID MULTIAXIAL FATIGUE LIFE MODEL BASED ON CRITICAL PLANE, CONTINUUM DAMAGE MECHANICS AND GENETIC ALGORITHM

MASOOD KAMAL

Thesis submitted in fulfilment of the requirements
for the award of the degree of
Doctor of Philosophy in Mechanical Engineering

Faculty of Mechanical Engineering
UNIVERSITI MALAYSIA PAHANG
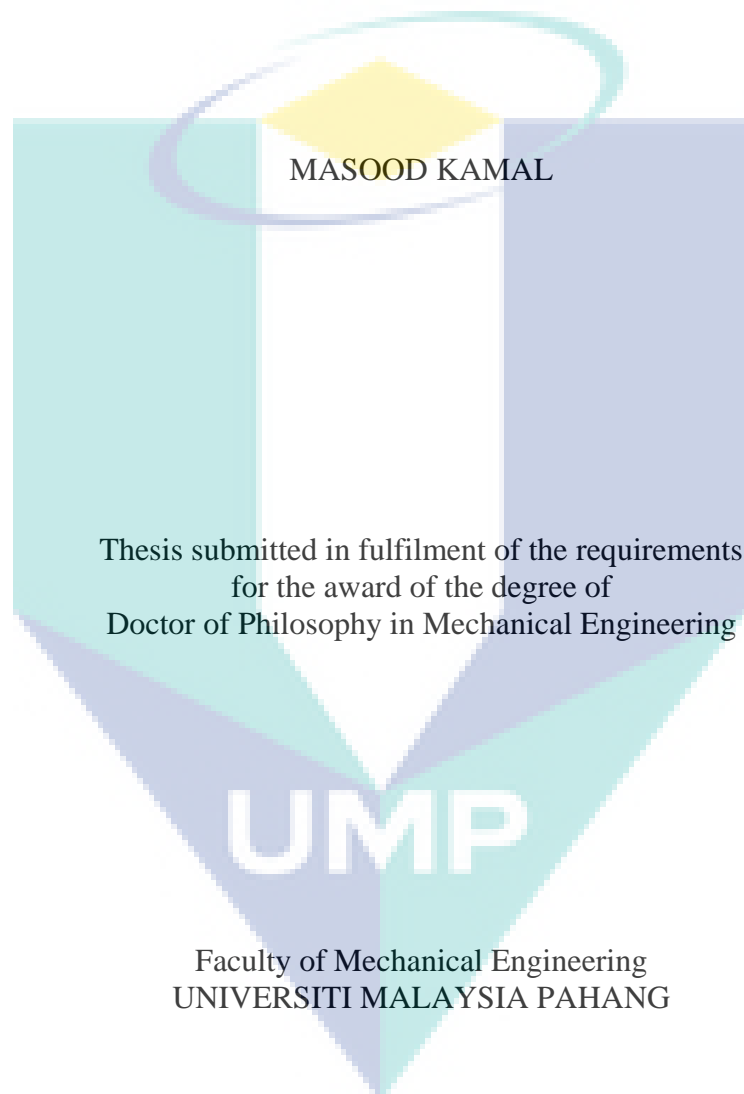
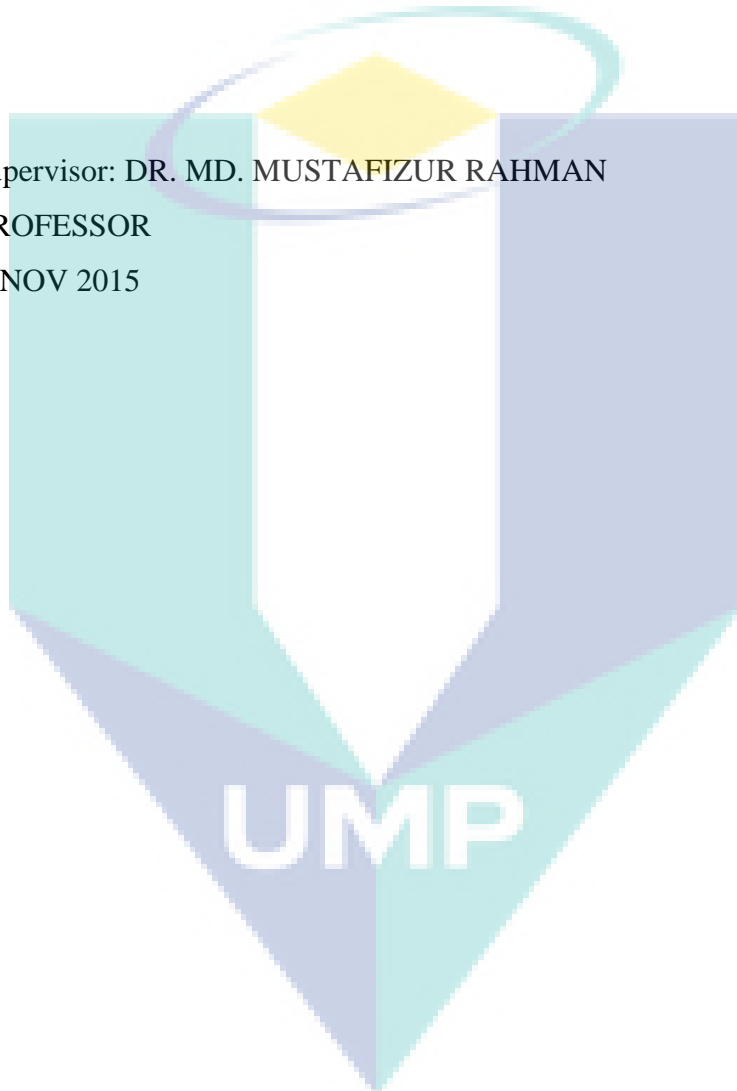NOVEMBER 2015

SUPERVISORS' DECLARATION

I hereby declare that I have checked this thesis and in my opinion, this thesis is adequate in terms of scope and quality for the award of the degree of Doctor of Philosophy in Mechanical Engineering.

Signature

Name of Supervisor: DR. MD. MUSTAFIZUR RAHMAN

Position: PROFESSOR

Date: 03 NOV 2015

STUDENT'S DECLARATION

I hereby declare that the work in this thesis is my own except for quotations and summaries which have been duly acknowledged. The thesis has not been accepted for any degree and is not concurrently submitted for award of other degree.

Signature   :
Name   : MASOOD KAMAL
ID Number : PMA11001
Date: 03 NOV 2015

Dedicated To

My Parents; Beloved Wife; Lovely son; Brother, sister and Extended family
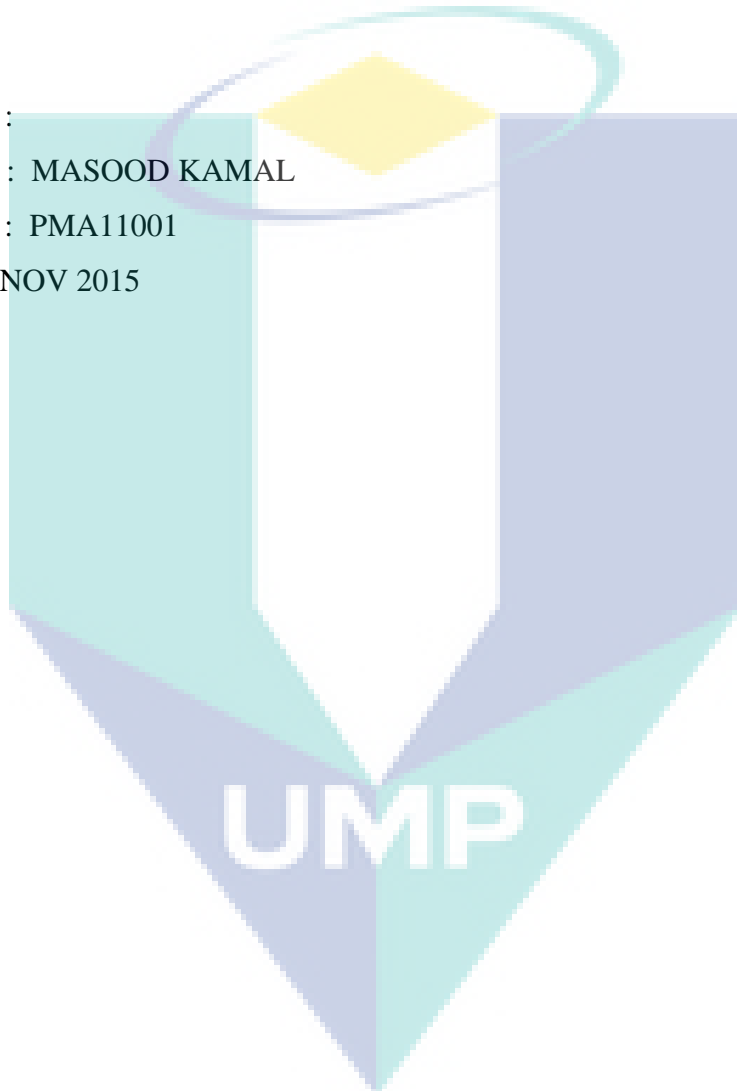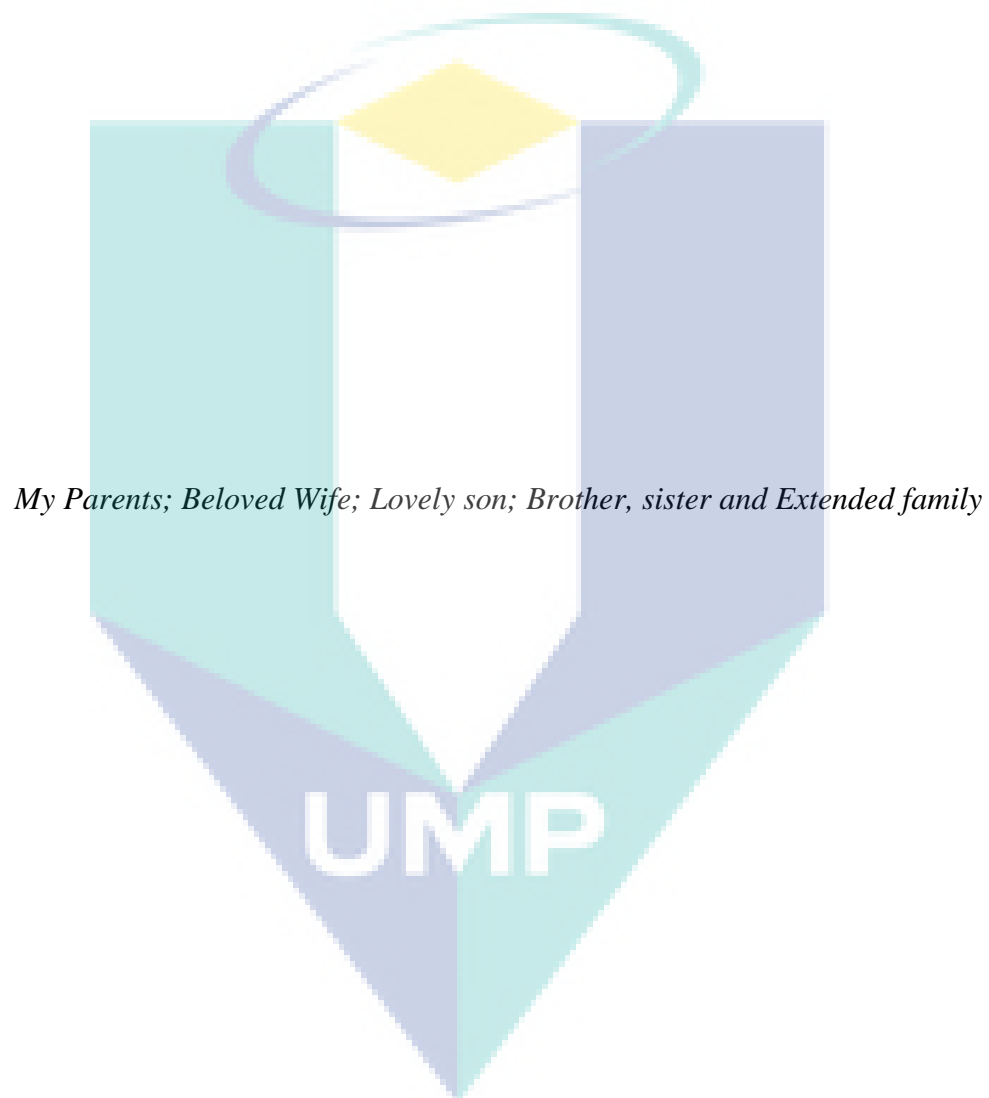
ACKNOWLEDGEMENTS

In the name of Allah, the Most Gracious, the Most Merciful. Praise be to Allah, the Lord of the Worlds; peace and blessings of Allah be upon the noblest of the Prophets and Messengers, our Prophet Mohammed and upon his family, companions and who follows him until the last day. It is only through Allah's mercy and help that this work could be completed, and it is ardently desired that this little effort be accepted by Him to be of some service to the cause of humanity. I am truly and deeply indebted to so many people that there is no way to acknowledge them all or even any of them properly. Thus, I offer my sincerest apologies to anyone I ungratefully omitted from explicit mention.

First of all, I wish to express my deep sense of gratitude and indebtedness to my supervisor Professor Dr. Md. Mustafizur Rahman. I am grateful and would like to express my sincere obligations to my supervisor Professor Rahman for his novel ideas, invaluable guidance, continuous encouragement and constant support in making this research possible. I really appreciate his consistent support since the beginning of this research till these concluding moments. I am truly indebted for his tolerance to many of my naive mistakes and his progressive vision and commitment to research. His perpetual energy and enthusiasm in research had motivated me to complete my Ph.D. I also sincerely thanks for the time spent proofreading and correcting my many mistakes. I wish to thank him for his valuable time and resources, to make this thesis a success.

I would like to acknowledge the support of Universiti Malaysia Pahang (UMP) for funding under University grant no. (RDU 110332) and Graduate Research Scheme (GRS140309). I want to thank all the people at UMP. Furthermore, special thanks to the academic, management and technical staff in Faculty of Mechanical Engineering in UMP. I wish to thank everyone who has helped me throughout my attachment period at Universiti Malaysia Pahang. I thank all my friends and colleagues for every bit of support; I thank to all Malaysian people whom I met, for their openness, friendship and hospitality.

I acknowledge my sincere indebtedness and gratitude to my parents for their love and prayers for me. I acknowledge the consistent encouragement of my mother-in-law. I am also grateful to my beloved wife, Syeda Najiha Masood and son, Faaiz, for their sacrifice, patience, and understanding that were inevitable to make this work possible. I cannot find the appropriate words that could properly describe my appreciation for their devotion, support and faith in my ability to attain my goals. Special thanks should be given to my committee members. I would like to acknowledge their comments and suggestions, which were crucial for the successful completion of this study.

ABSTRACT

Multiaxial fatigue is one of the most common failure mechanisms encountered by the mechanical components during service life. For reliability assessment of the components under real-life service conditions, and maintenance, the understanding of multiaxial fatigue phenomenon is essential. Despite extensive research in this area, the fatigue life prediction is still a challenging task. The application of analytical and numerical methods in fatigue life analysis under real-life service conditions is becoming more significant, given the time and costs considerations in experimental testing. This study aims to develop a hybrid multiaxial fatigue model capable of estimating fatigue life independent of applied loading-path-shape with the application of the most commonly available material property. A new fatigue parameter is formulated based on stress-strain variables identified from various fatigue life models in order to deal with mean stress effects and non-proportional hardening. Continuum damage mechanics approach is applied to develop damage expression as a continuously damage-accumulative function in terms of fatigue parameter. Genetic algorithm is also applied for the calibration of proposed model in terms of calibrated coefficients. The developed hybrid model is calibrated using complex profiles for proportional and non-proportional loading under in-phase and out-of-phase loading conditions. The model is validated against the published experimental results under various loading and material conditions including SS304, carbon steel C40, EN3B, Steel20 and Titanium alloy BT9. Interpolation scheme for calibrated model coefficients is applied for loading cases with same profiles and different magnitude. For in-phase and out-of-phase loading with zero and positive mean stress the proposed model provides good correlation with experimental data (min. 4% diff.) for C40, EN3B and Steel 20. For SS304 predicted fatigue life from proposed model for complex profiles, calibrated with characteristic profiles, correlates well with the experimental data with an agreeable difference (min.6%). The results of the proposed model for Titanium alloy BT9 and steel 20 with block loading correlates reasonably well with experimental data (min. 4-10% diff.). The proposed model serves as path-independent fatigue life estimating tool hence can be used with any type of loading conditions. The notion of characteristic profiles for the calibration of the model is also coherent with the application of equivalent fatigue loading in generating experimental data for calibration. The model is simple in application with the use of genetic algorithm for model calibration making use of only the material fatigue limit. Thus the proposed model is more accurate for variety of loading and material conditions. The hybrid approach of critical plane, continuum damage mechanics and calibration through genetic algorithm provided a strong basis for a universally accepted multiaxial fatigue life model. Interpolation scheme based on the multiaixality of stresses is suggested for the determination of coefficients of the model for different loading paths. Material parameter including stress sensitivity factor for normal or shear stress can be incorporated to improve the calibration process. The proposed model can serve as an efficient tool for multiaxial fatigue life analysis in academics as well as commercial applications, especially automotive and aircraft industry, due to inherent flexibility of the model for accommodating different loading conditions.

ABSTRAK

Kelesuan berbilang paksi adalah salah satu mekanisma kegagalan biasa yang terjadi ke atas komponen mekanikal semasa digunakan. Kefahaman yang mendalam untuk fenomena kelesuan berbilang paksi adalah amat penting apabila pengukuran kebolehpercayaan komponen di buat dalam keadaan pengunaan sebenar dan proses membaikpulih. Walaupun banyak kajian telah di lakukan untuk bidang ini, kajian jangkaan hayat kelesuan masih merupakan satu tugas yang mencabar. Penggunaan kaedah analisis dan berangka dalam analisis ketahanan keleusuan di dalam keadaan pengunaan sebenar menjadi lebih penting dan diberi pertimbangan masa dan kos dalam kajian. Kajian ini bertujuan untuk membangunkan model kelesuan berbilang paksi hibrid yang mampu menganggarkan kelesuan yang bebas daripada beban gunaan laluan-bentuk dengan sifat bahan yang sedia ada. Parameter keletihan baru digubal berdasarkan pembolehubah tegasan-terikan yang dikenal pasti dari pelbagai model keleusuan yang sedia ada untuk menangani kesan-kesan tekanan yang minima dan pengerasan bukan berkadar. Pendekatan kontinum mekanik digunakan untuk membangunkan kerosakan terkumpul secara berterusan sahaja kerosakan dari segi parameter kelesuan. Algoritma genetik juga digunakan untuk penentukuran model yang dicadangkan dari segi pekali-terukur. Model hibrid yang telah di bina ditentukur menggunakan profil kompleks untuk bebanan berkadar dan bukan berkadar di dalam dan di luar fasa benanan tersebut. Model yang telah disahkan dengan keputusan ujikaji yang diterbitkan di bawah pelbagai keadaan bebanan dan bahan termasuk SS304, keluli karbon C40, EN3B, Steel20 dan Titanium aloi BT9. Sisipan skim bagi model pekali yang telah disahkan telah digunakan untuk bebanan kes profil yang sama dan berlainan magnitud. Bagi di dalam dan di luar fasa bebanan sifar dan positif bermaksud tekanan model cadangan memberi hubungan yang baik dengan data ujikaji (minima kelainan 4%) untuk bahan C40, EN3B dan Steel20. Untuk SS304 tahap kelesuan diramalkan dari model yang dicadangkan untuk profil kompleks, ditentukan dengan ciri-ciri profil, di sahkan dengan data ujikaji dengan perbezaan yang di persetujui (minima 6%). Keputusan untuk model yang dicadangkan untuk bahan BT9 aloi dan Steel20 adalah di sahlkan dengan baik dengan data ujikaji (minima kelainan 4%). Model yang dicadangkan telah digunakan sebagai kaedah kelesuan bebas untuk membuat pengganggaran dengan mana-mana jenis bebanan. Konsep ciri-ciri profil untuk penentukuran model ini juga koheren dengan kelesuan bebanan setara untuk menjana data-data ujikaji penentukuran. Model yang mudah dalam aplikasi menggunakan algoritma genetik untuk penentukuran model menggunakan hanya had lesu bahan. Oleh itu model yang dicadangkan adalah lebih tepat bagi pelbagai jenis pembebanan dan keadaan bahan. Pendekatan hibrid satah kritikal, mekanik kontinum dan penentukuran melalui algoritma genetik memberikan asas yang kukuh untuk penerimaan universal untuk kelesuan berbilang paksi. Skim sisipan yang berdasarkan tegasan berbilang paksi dicadangkan untuk penentuan pekali untuk model bagi bebanan yang berbeza. Parameter bahan termasuk faktor sensitiviti tekanan biasa atau tegasan ricih boleh digunakan bersama untuk meningkatkan kuality proses penentukuran. Model yang dicadangkan boleh dijadikan cara yang cekap untuk menanalisa kelesuan berbilang paksi di dalam kajian akademik serta penggunaan komersil, terutama di dalam bidang automotif dan industri pesawat, kerana model ini memberikan keadaan fleksibiliti bagi menampung bebanan yang pelbagai.

TABLE OF CONTENTS

CHAPTER 4   RESULTS AND DISCUSSION

CHAPTER 5   CONCLUSIONS AND RECOMMENDATIONS

APPENDICES

LIST OF TABLES

LIST OF FIGURES

LIST OF SYMBOLS

Symbols	Description
$\Delta\varepsilon_{eq}$	Equivalent strain range
$\Delta\varepsilon_1$	Principal strain range
$\Delta\varepsilon_n,\ \Delta\varepsilon$	Normal strain range
ε_n^*	Normal strain excursion between turning points on critical plane
$\varepsilon(t)$	Strain at time (t)
$\Delta\varepsilon_{gen}^*$	Maximum generalized strain amplitude
$\Delta\varepsilon_n^e$	Elastic normal strain range
$\Delta\varepsilon_n^p$	Plastic normal strain range
$\varepsilon_n,\ \varepsilon_c$	Nucleation and coalescence strains
$\sigma_f^{'}$	Fatigue strength coefficient
$\tau_f^{'}$	Shear fatigue strength coefficient
$\tau(t),\ \tau_q(t)$	Instantaneous shear stress
$\varepsilon_f^{'}$	Fatigue ductility coefficient
γ_f	Shear fatigue ductility coefficient
b	Fatigue strength exponent
$b\gamma$	Shear fatigue strength exponent
c	Fatigue ductility exponent
$c\gamma$	Shear fatigue ductility exponent
$N_f,\ N$	Fatigue life
σ_o	Endurance limit
$\Delta\sigma_0$	Range of uniaxial plain fatigue limit
σ_y	Yield stress

Symbols	Description
σ_h	Hydrostatic stress
$\sigma_h(t)$	Instantaneous hydrostatic stress
σ_{hmax}	Maximum hydrostatic stress
σ_{uts}	Ultimate tensile strength
$\sigma_{n,max}$, N_a	Maximum normal stress
σ_n	Normal stress
$\Delta\sigma_n$	Normal stress range
$\sigma_{n,mean}$ N_m	Mean normal stress
σ_p	Principal stress (p = 1,2,3)
$\sigma_{1,a}$	Amplitude of maximum principal stress
σ_{pmax}	Maximum principal stresses
$\sigma_{equ,a}$, σ_E, σ_{eq}, f	Equivalent stress amplitude
σ_{mr}	memory stress
$\sigma_{eff,a}$	Amplitude of effective stress
σ_E	Non linear equivalent stress
σ_c	Material parameter for cyclic stress
σ_{ac}	Normal stress amplitude on critical plane
σ_{mc}	Mean normal stress on critical plane
$\tau_{\gamma\phi m}$, $\sigma_{\gamma\phi m}$	Static shear and normal stress on plane $\gamma\phi$
τ_{ac}	Shear stress amplitude on critical plane
$\tau_{n,max}$, C_a	Shear stress on considered plane
$\Delta\tau_{oct}$	Octahedral stress (von mises)
$\Delta\tau_{max}$	Maximum shear stress range
$\Delta\tau$	Shear stress range

Symbols	Description
$\Delta\gamma_{max}$	Maximum shear strain range
$\Delta\gamma$	Shear strain range
$\Delta\gamma^e$	Elastic shear strain range
$\Delta\gamma^p$	Plastic shear strain range
$\tau_{A,Ref}(\rho_{eff})$	Reference shear stress amplitude at considered limit to cycles to failure
T_a	Resolved shear stress amplitude
T_1, T_2	Threshold functions
T	Stress triaxiality
s_e	Effective deviatoric stress tensor
$d\varepsilon^p$	Plastic strain increment due to normal stress
$d\gamma^p$	Plastic strain increment due to shear stress
$t_{A,B}$	Shear fatigue strength
f_{-1}, S_e	Fatigue limit in fully reversed axial and torsion
f_0	Fatigue limit in repeated axial loading
t_{-1}, T_e	Fatigue limit in fully reversed torsion
k	Fatigue limit ratio ($k = f_{-1} / k_{-1}$)
$k^{'}$	Normal stress sensitivity factor
$k_\tau(\rho_{eff})$	Negative inverse slope of Wholer Curve
ρ_{eff}	Critical plane stress ratio
D	Damage
$D_{cr}(\rho_{eff})$	Critical damage sum dependent on degree of multiaixiality
L	Material characteristic length
L_M	Critical distance in medium cycle fatigue regime

Symbols	Description
$\Delta K_{I,th}$	Range of threshold value if stress intensity factor under Mode I loading
$\Delta K_{mixed,eq}$	Equivalent stress intensity factor
ΔK_{th}	Fatigue threshold stress intensity factor
$\omega_a{}^D(C_i, \text{load})$	Volumetric mean value of strain energy volumetric density around critical point
W_a	Strain energy volumetric density
$W_a{}^*$	Strain energy volumetric density at critical point C_i
I_1, I_2, I_3	Stress Invariants
J_1, J_2, J_3	Deviatoric stress invariants
$\sqrt{J_{2a}}$	Amplitude of second invariant of stress deviator (or equivalent shear stress amplitude)
$J_2{}'$	Second invariant of deviator of the amplitude of stress tensor
E	Elastic modulus
ν_{eff}	Effective poisson's ratio
W_{geqdam}	Damaging part of strain work density
W_{geq}	Equivalent strain work density
$W_g{}^*$	Minimum strain work volumetric density (per load cycle) necessary to create irreversible damage in a representative elementary volume
W^*_{gen}	Maximum generalized strain energy
P_l	Proportionality factor
α_m	represents evolution of stress / strain tensors and sequence duration (equal to 1 for constant amplitude loading)
G, μ	Shear modulus
ΔW	Virtual strain energy (VSE) parameter
ψ_e	Free energy

Symbols	Description
λ_a^e (a=1,2,3)	Eigen values of elastic finger tensor
k_B	Bulk modulus
$\eta(t)$	void nucleation at time 't'
K_{IC}	Critical stress intensity factor
f_{Nf}	Normal stress at N_f cycles
t_{Nf}	Shear stress at N_f cycles
a_i, 1-5	Amplitude of deviatoric stresses
a_1, a_2	Half-length of sides of rectangular hull loading path
l, m, n	Directional cosines of vector normal to plane
ϕ, θ, ψ	Angle locating material plane
χ	Angle between major axis and resolved shear stress
$V^*(C_i)$	Volume at critical point
d	Length scale parameter
α^d, α^p	Damage and plastic internal variables
$\alpha^{'}$	Slip system index
$dD^{(\alpha)}$	Damage parameter increment on slip system (α)
$dY^{(\alpha)}$	Plastic strains energy increment on slip system (α)
$G^{'}$	Notch gradient correction factor
k_1, k_2, k^H	Loading related parameter
t	time
$a, b, m, n, A, B,$ $S, C_{coeff}, \sigma_c, m^{'}$ $\delta^{'}, d_1, d_2, a_0 - a_3$ $\sigma_0, \gamma_1, \gamma_2, \gamma_3^{'}, \eta_{Nf},$ $a_c, b_c, \alpha, \beta, \gamma, \delta, k,$ $f, a^{'}, b^{'}, c, m, n, \lambda$	Material parameters / model constants

LIST OF ABBREVIATIONS

ANN   Artificial Neural Network

APDL   Ansys Parametric Design Language

CARLOS   Car Loading Standard

CPU   Central Processing Unit

DASA   Differential Ant Stigmergy Algorithm

EFL   Equivalent Fatigue Loads

FE   Finite Element

FEA   Finite Element Analysis

FEM   Finite Element Method

GA   Genetic Algorithm

MOGA-II   Multi Objective Genetic Algorithm II

SAE   Society of Automotive Engineers

VB   Visual Basic
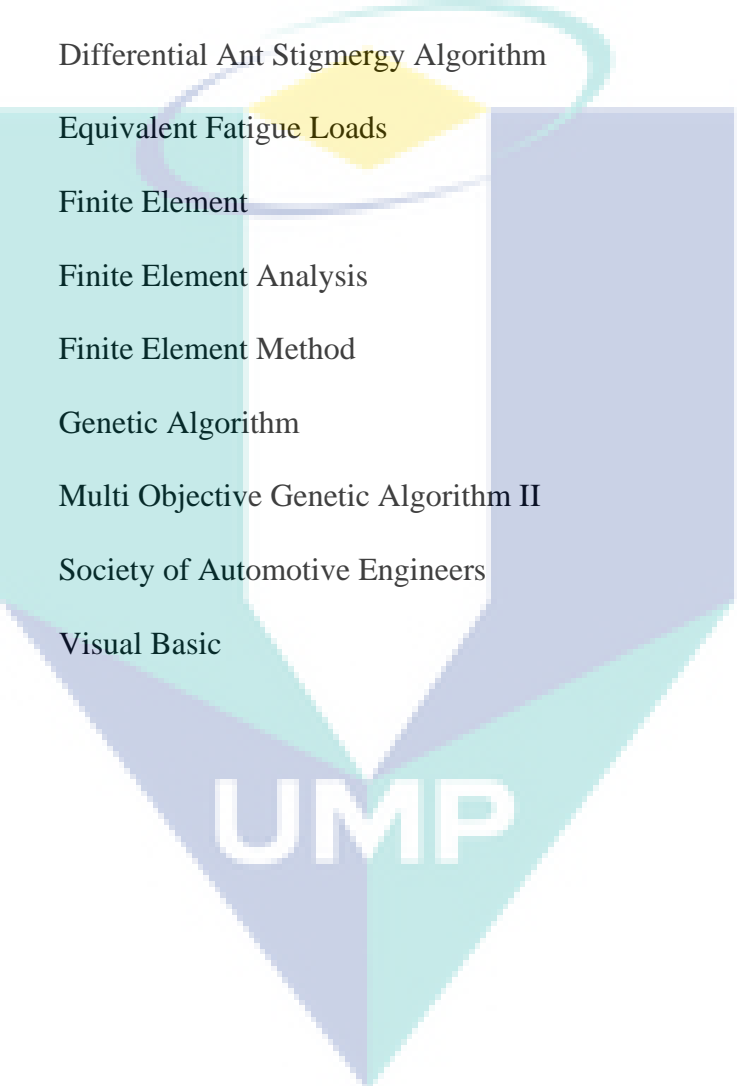
CHAPTER 1

INTRODUCTION

1.1   INTRODUCTION

Fatigue is a common phenomenon during the service life of machines, equipment, vehicles, buildings, aircraft and several other structures subjected to time variable combined tension, bending and torsion load. These complex cyclic loadings are defined as multiaxial loadings, where the principal stresses rotate and change their magnitude non-proportionally during loading (Suman, 2013). The fatigue is classified on the basis of the state of stress and the load level. On the basis of the stress state, fatigue is divided into the two categories of uniaxial and multiaxial fatigue (Milella, 2013). For uniaxial fatigue, the cyclic stresses do not change direction, such as in the case of axial and bending loadings. In the case of multiaxial fatigue, the time-varying loads in the cyclic stress change direction and act as combined axial and torsion out-of-phase loading. Moreover, based on the level of loading, fatigue is classified as either low-cycle fatigue (LCF) or high-cycle fatigue (HCF). For LCF, the amplitude of loading is high enough that the component fails in less than approximately 10^3–10^4 cycles. However, fatigue life greater than 10^4-10^6 cycles is referred to as HCF due to the low magnitude of the applied loading (Manson and Halford, 2006). During HCF, deformations in components are mainly elastic, but for LCF deformations can be both elastic and plastic. As multiaxial fatigue is a time-dependent phenomenon, the modelling of physical conditions with mathematical models to predict the damage is certainly a challenging task (Sun et al., 2013). Unfortunately, the combination of multiaxial loading paths and complex geometries of components cannot be avoided in real-world scenarios and durability test experiments in most situations are not feasible due to time and cost considerations (Ince, 2013). Therefore, analytical and numerical

methods are an essential approach to perform fatigue and durability analysis in designing mechanical components.

A number of studies for the estimation of multiaxial fatigue life have been performed by researchers over the past 60 years. Various innovative techniques and approaches have been proposed during this period to address the complex phenomenon of multiaxial fatigue (Kenmeugne et al., 2012; Macha and Niesłony, 2012). These approaches include continuum damage mechanics (CDM) (Khandelwal and El-Tawil, 2014), modified rainflow cycle counting (Meggiolaro and de Castro, 2012), optimization algorithms (Klemenc and Fajdiga, 2013) and critical-plane based fatigue life estimation models (Ince and Glinka, 2014). CDM is based on the framework of the thermodynamics of an irreversible process with damage as an irreversible and continuously increasing function (Chaboche, 1998a, b; Ottosen et al., 2008; Khandelwal and El-Tawil, 2014). Cycle counting methods are used to identify individual cycles from a variable loading history. Fatigue life is then estimated for the cycles identified from the fatigue data and curves obtained with simple constant amplitude load cycles (Manson and Halford, 2006; Meggiolaro and de Castro, 2012), however with the loss of the sequence of loading information (Anes et al., 2014).

Optimization is the act of obtaining the best solution under given circumstances (Pinto, 2007), and in the last decade evolutionary optimization algorithms have gained popularity in formulating fatigue life estimation methodologies (Krishnapillai and Jones, 2009; Brighenti and Carpinteri, 2012; Klemenc and Fajdiga, 2013). Critical plane models are based on experimental observations that cracks nucleate and grow on specific planes known as critical planes, and these models relate fatigue damage to stresses and strains on these planes. These models can predict fatigue life as well as the orientation of the cracks (Stephens et al., 2000). With all these efforts, the need to fully understand the multiaxial behaviour of different materials under various loading conditions is a special focus of this research. In spite of the importance of understanding multiaxial fatigue behaviour, limited literature exists on the subject due to the inherent complexities in studying this topic (Shamsaei, 2010; Gates and Fatemi, 2014).

Considering the effectiveness of the CDM and critical plane methods, a hybrid approach with the flexibility of evolutionary optimization algorithms has been proposed to estimate the multiaxial fatigue life. The proposed methodology does not require cycle counting and thus avoids the loss of loading sequence data by treating the damage as a continuously increasing function as the load time history advances. The proposed method incorporates the benefits of the critical plane estimation to predict the fatigue life as well as the direction of crack growth. Multi-objective optimization based on genetic algorithm (GA) has been used to calibrate the model coefficients as well as to predict the critical plane using more than one critical plane determination criterion.

1.2   RESEARCH MOTIVATIONS

Most components in real-life scenarios have a multiaxial state of stress and are subjected to random loading conditions. Therefore, the study of multiaxial fatigue under complex loading conditions is of great practical significance (Reis et al., 2003; Rahman et al., 2009; Marquis, 2010; Gates et al., 2014). Models for fatigue life prediction in the case of uniaxial loadings are well established; however, for multiaxial as well as random amplitude loading conditions, research is still in progress. Very few methods are proposed in the literature addressing fatigue life estimation for non-proportional multiaxial loading (Shamsaei, 2010; Gates and Fatemi, 2014). However, while many fatigue parameters to address multiaxial fatigue have been proposed during recent decades, due to the challenging nature of the problem, a universally accepted model which can be used in various loading and material conditions is still needed for reliable multiaxial fatigue life estimation (Ganjidoust and Shariyat, 2009; Fatemi and Shamsaei, 2011; Gómez et al., 2011; Ince, 2013; Ince and Glinka, 2014). The requirement to produce highly reliable products, with a cost-effective design process in terms of prototyping and testing is always the prime concern of design engineers (Ince, 2012). Testing and analysis are two essentials tools for design against fatigue failure. In order to reduce the design cost, it is essential to reduce the experimental testing and prototyping cost (Shamsaei, 2010). This goal can be achieved by replacing experimental testing with accurate analysis, especially in the early design stages. In order to evaluate fatigue life accurately, a technique is required which is capable of handling various

loading and material conditions and is adaptable for both academic and industrial applications.

1.3   PROBLEM STATEMENT

Most machine components are subjected to combined cyclic tension, bending and torsional loads during their service life. In addition, many machine components have complex geometries as per design requirements, which can cause stress concentration areas (Acevedoa and Nussbaumer, 2009). With multiaxial loads, complex stress–strain states occur around stress concentration points and can cause fatigue failure without any apparent large-scale plastic deformations (Schijve, 2009; Schmid et al., 2013). To address this issue, various models have been proposed for multiaxial fatigue life estimation. However, most of these work accurately only for certain material and loading conditions (Marquis, 2010; Gómez et al., 2011; Ince and Glinka, 2014). In addition, as experimental testing for fatigue life becomes unfeasible in most situations, especially in the early design stages, the requirement for a fatigue life model that can serve as a general purpose model as well as for various materials and loading conditions is therefore indispensable to bring down the cost of product design (Ince, 2012; Suman, 2013).

While the development of uniaxial fatigue models is at a quite mature stage, the modelling of multiaxial fatigue damage is still an active area of research (Liu, 2006; Habtour et al., 2014). Multiaxial fatigue modelling can generally be classified in three major categories: equivalent stress/strain-based, energy-based and critical plane-based. Equivalent stress/strain theories use the von Mises or Tresca failure criterion for an equivalent representation of stress and strain. These criteria cannot distinguish between proportional and non-proportional loading. Energy-based theories determine the strain energy within a material during the loading cycle and compare it with a critical value. Since energy is a scalar quantity, these criteria do not provide physical interpretations of the process by which fatigue cracks initiate and propagate along certain directions or planes in the material (Suman, 2013). The third theory was initially proposed by Findley (1959), based on orientation planes having cracks in the material, and is thus named critical plane methodology. This technique has gained widespread acceptance and many

improvements have been proposed by researchers, including Brown and Miller (1973), Fatemi and Socie (1988), Dang Van (1993), Lazzarin and Susmel (2003) and Susmel (2010), to name a few. Thus the critical plane concept is a better option to use as the basis of new fatigue life models.

Real-life loading conditions are variable in amplitude, while most multiaxial fatigue life models are formulated on the basis of constant amplitude loading (Suman, 2013). In order to estimate the fatigue life for variable amplitude loading, cycle counting methods are applied to compare the effect of variable amplitude loading histories to fatigue data obtained with simple constant amplitude load cycles (Stephens et al., 2000). Fatigue life is estimated for each of the counted constant amplitude cycle set and cumulative damage is determined with respect to the number of cycles counted for each magnitude determined from the variable loading history. The main drawback of the cycle counting method is the loss of the sequence of loading data, which can lead to ignoring any effect it might have on fatigue life (Gao et al., 2014). The concept of continuum damage mechanics deals with fatigue damage as a constantly increasing function, where the damage is accumulated as the loading history progresses with time (Bobyr et al., 2014). The essential feature of CDM theory is that it is formulated by means of incremental relations and not changes per cycle, so it contains in itself the damage accumulation; thus the cycle counting method is no longer required and the loss of data can be avoided (Ottosen et al., 2008).

The application of evolutionary optimization algorithms in fatigue life estimation is a relatively new research domain (Zhou et al., 2012). Approaches like genetic algorithms (GA) and artificial neural networking (ANN) are employed to estimate the model parameters. Complex interrelationships can be established between physical and theoretical correlations with experimental observations (Bukkapatnam and Sadananda, 2005; Roux et al., 2013). These approaches can be termed as material-independent data-driven methods correlating input and output parameters and establishing the relationship between them. Thus, with an adequate amount of data, these models can be used with any material and loading configurations (Vassilopoulos et al., 2008; Brighenti and Carpinteri, 2012; Klemenc and Fajdiga, 2013).

This research aims at finding a hybrid approach incorporating the multi-objective optimization algorithm with a critical plane-based fatigue estimation model. The model should be independent of the loading path shape and work with various material conditions. Implementation of the model should be easy enough to make it easily adaptable by industry. To achieve this, a methodology is proposed to integrate the benefits of the concepts which have been successfully applied before for various specific loading and material conditions but were not suitable as a general purpose or universal approach. The first step is the proposal of a new fatigue parameter expression based on the stress–strain parameters identified from the earlier published fatigue models, which are used to handle the effects of mean stress, high-cycle and low-cycle fatigue and non-proportional hardening. The proposed model is developed on the basis of the critical plane method, where the fatigue parameter is maximized as a whole to locate the critical plane. Secondly the calibration methodology is proposed to estimate the coefficients of the fatigue model expressions with the application of optimization algorithms by using the known experimental data about fatigue life and fatigue limit. This formulation is proposed on the assumption that, as per the continuum damage mechanics approach, damage is a continuously increasing function until unity or failure. This approach will allow the damage estimation to be independent of the loading path, as damage will follow the loading path as it progresses and not depend on the cycle counting methods. In the case of loading blocks or constant amplitude cycles, the Palmgren–Miner linear damage rule will be applied to determine the number of cycles or blocks of loading to failure.

1.4   OBJECTIVES OF THE STUDY

The objectives of the study are summarized as follows:

i.   To develop a multiaxial fatigue life estimation model based on the continuum damage mechanics approach and critical plane method.

ii. To determine calibrated coefficients for the proposed model utilizing optimization algorithms.

iii. To validate and analyse the performance of the proposed multiaxial fatigue model against various multiaxial loadings and material conditions from published results.

iv. To develop a critical plane estimation method for complex random loading conditions in order to identify an increased number of planes for maximum damage compared to established models.

1.5 SCOPE OF THE STUDY

The scope of the study are as follows:

i. A multiaxial fatigue life estimation model is developed based on a hybrid approach using continuum damage mechanics and critical plane theory with crack initiation considered as failure.

ii. Maximum normal and shear strain ranges, normal and shear stress and mean normal and shear stress on the critical plane are used in establishing the fatigue model equations.

iii. Non-linear finite element analysis was performed based on various specimen geometries to generate the stress response time histories against the applied loading.

iv. Calibrated coefficients for the proposed model are determined by employing a genetic algorithm.

v. The proposed model is validated by testing the fatigue life prediction performance for various multiaxial loadings and materials, i.e., EN3B steel alloy, carbon steel C40, SS304, titanium alloy BT9 and low carbon steel (steel 20) with experimental fatigue lives. Experimental fatigue related data of various materials and loading conditions were taken from the published literature, as it is sufficient to validate the model and demonstrate the capability of the proposed model.

vi. Model performance is analyzed in handling complex profiles and block loading for factors including two-principal strain directions, fully reversed loading, rotational principal strain direction, load step length and direction of loading path.

vii.   A multi-parameter method is devised to locate the critical plane using the multi-objective optimization feature of GA.

1.6   OVERVIEW OF THE THESIS

Chapter 1 includes a brief description of continuum damage mechanics, the critical plane method, evolutionary optimization algorithms, research motivations, the problem statement, research objectives and the scope of study. **Chapter 2** presents a literature review of fatigue life estimation models with the emphasis on highlighting the latest advances in recent years. A brief review of the application of optimization algorithms in fatigue life estimation models is also given. **Chapter 3** describes the developed fatigue life model, with detailed discussion of the calibration process using the optimization algorithm and working of the proposed model. Details are given of the validation exercise performed for the proposed model, with material and loading conditions taken from published literature, and the FEA models, developed for acquiring the stress–strain response, are shown. **Chapter 4** presents the results of the proposed model validation exercise and discusses the performance of the proposed model in various material and loading conditions. Calibration of model coefficients is performed using characteristic profiles and the effects of these calibrated coefficients on fatigue life estimation for complex loadings are analysed. The efficiency of the interpolation of the estimated coefficients method is discussed, and performance analysis of the multi-parameter critical plane estimation method is presented. **Chapter 5** presents the conclusions of the study, its contribution, and recommendations for future studies.

CHAPTER 2

LITERATURE REVIEW

2.1   INTRODUCTION

The purpose of this chapter is to provide a survey of past research efforts linked with the development of fatigue life estimation models. In the survey, the main objective is to identify new ideas fo2011r fatigue life estimation other than the classical models and their hybrids. Various techniques to estimate fatigue life have been identified, including critical plane deviation, 5D deviatoric space enclosed surface, and modified Wholer curve. But the most distinguished one found is the application of evolutionary optimization algorithms for, e.g., genetic algorithms, artificial neural networking and differential ant-stigmergy algorithms. In this chapter first a brief history of fatigue life estimation and modelling is presented. In subsequent sections some well-known classical models are discussed and then various innovative approaches to fatigue life prediction are reviewed. The survey is fairly detailed and best efforts have been made to net in as many new methodologies as possible. The review is organized to offer insight on how past research efforts have provided the groundwork for subsequent studies, including the present research effort. The present research effort can be properly tailored to add to the present body of literature as well as to justify its own scope and trends.

2.2   FATIGUE LIFE ESTIMATION

The importance of fatigue is evident from the estimate that almost half of all mechanical failures are due to fatigue, which constitutes approximately 4% of the gross national product of USA (Stephens et al., 2000). It is essential to understand the physics

of fatigue and develop a fatigue life estimation methodology which can help reduce the probability of such failures (Sangid, 2013). Since the investigations by Wohler in 1860, fatigue experiments and predictions have played a major role in mechanical design (Lee et al., 2005; Manson and Halford, 2006). Addressing the fatigue problem, huge efforts have been made to devise sound methodologies suitable for safely assessing mechanical components subjected to time-variable loadings (Schijve, 2003; Rahman et al., 2007; Abdullah et al., 2008; Li et al., 2011; Mamiya et al., 2011; Papuga, 2011; Kenmeugne et al., 2012; Meggiolaro and de Castro, 2012a; Susmel and Taylor, 2012; Saintier et al., 2013). It is an acknowledged fact that to estimate fatigue life accurately in real-world scenarios is a complex task in which numerous variables have to be taken into account in order to avoid unwanted and dangerous failures (Brighenti and Carpinteri, 2012). The reliability of a fatigue estimation technique depends on its ability to model damage due to non-zero superimposed static stresses, the degree of multiaxiality in the stress field and the effects of stress concentration phenomena (Susmel and Taylor, 2008). For the cases of cyclic and random multiaxial loading conditions, it is difficult to estimate fatigue life as damage is dependent on all the stress components and their variations during the whole duration of load application (Susmel and Taylor, 2008; Macha and Niesłony, 2012). A brief classification of fatigue analysis types is summarized in Table 2.1 (Liu, 2006). To predict fatigue estimation results accurately, the fatigue assessment method should be calibrated with reference to some experimental information that can be easily obtained through tests run in accordance with the pertinent standard codes (Atzori et al., 2006; Susmel and Taylor, 2008; Susmel and Tovo, 2011; Brighenti and Carpinteri, 2012; Susmel and Taylor, 2012). Stress analysis is conducted to correctly estimate fatigue damage by directly post-processing a simple linear elastic finite element model (Bishop and Sherratt, 2000; Rahman et al., 2009; Pinto et al., 2010).

2.3   MULTIAXIAL MATERIAL FATIGUE MODELLING

Fatigue is defined as the process of progressive localized permanent structural change occurring in a material subjected to conditions that produce fluctuating stresses and strains at some point or points, and which may culminate in cracks or complete fracture after a sufficient number of fluctuations (ASM, 1996). In common engineering

terminology, it refers to the damage and failure of materials under cyclic loads, including mechanical loads, thermal loads, etc. (Liu, 2006). Fatigue damage is characterized by nucleation, coalescence and stable growth of cracks, leading ultimately to net section yielding or brittle fracture (Varvani-Farahani, 2005). An evaluation of fatigue of structures and materials in the 20th century raises the question what happened in the 19th century? The answer is that fatigue of structures became evident as a by-product of the industrial revolution in the 19th century (Schijve, 2009). A fundamental step in fatigue analysis was made at the beginning of the 20th century by Ewing and Humfrey (1903). The authors carried out a microscopic investigation which showed that fatigue crack nuclei start as micro-cracks in slip bands (Schijve, 2003). When components are stressed in the high-cycle fatigue or very high-cycle fatigue regime, most load cycles in realistic in-service loading sequences are at stress amplitudes that are too low to cause failure under constant amplitude loading conditions (Mayer, 2009). Constant amplitude cycling below the endurance limit does not lead to fracture, but it can cause fatigue damage. Several investigations show that short fatigue cracks may be initiated by cycling carbon steels below the endurance limit (Chapetti et al., 2001; Mayer, 2009).

Table 2.1: Classification of various types of fatigue analysis.

Classification basis	Fatigue analysis type	Description
Loading	Uniaxial	One cyclic stress or strain component dominates during the life
	Multiaxial	Multiaxial cyclic stress or strain components dominate during the life
Fatigue life	High-cycle	Fatigue life $>10^{4-6}$ cycles
	Low-cycle	Fatigue life $<10^{3-4}$ cycles
Damage stage	Crack initiation	From no crack to macro crack
	Crack propagation	From macro crack to final failure
Analysis approach	Stress-life approach (S-N)	Stress is used to predict fatigue life
	Strain-life approach (e-N)	Strain is used to predict fatigue life
	Energy approach	Energy is used to predict fatigue life
	Fracture mechanics approach	Fracture parameters are used to predict fatigue life

In real-world scenarios loading conditions are variable and complex and the resulting stress states are also multiaxial. Multiaxial loads, which can be in-phase (proportional) or out-of-phase (non-proportional), are common for many components and structures (Suman, 2013). Even under uniaxial loads. multiaxial stresses often exist, although typically in-phase, for example due to geometric constraints at notches. Such multiaxial loads and stress states are frequently encountered in many industries, including automotive, aerospace, and power generation, among others (Fatemi and Shamsaei, 2011). Non-proportional multiaxial fatigue damage occurs when the principal stress directions vary during the loading induced by several independent sources, such as out-of-phase bending and torsion moments (Meggiolaro and de Castro, 2012a). The methodologies for the more complex case of multiaxial variable amplitude loading are not yet well established, particularly when the loads are non-proportional (Ghalami and Fatemi, 2013). In the following section, fatigue life models are presented which were proposed in the last century and are well discussed and known in published literature, mentioned here as classical models.

2.4   CLASSICAL MULTIAXIAL FATIGUE LIFE ESTIMATION MODELS

This section presents a brief review of the fatigue life models which are most popular in the published literature, and many of the models proposed more recently lately are their hybrids.

2.4.1   Stress-Based Models

Sines (1955, 1959) proposed that octahedral (von Mises) shear stress is used as a fatigue damage criterion as expressed in Eq. (2.1), but this model is incapable of handling non-proportional loading.

$$\frac{\Delta \tau_{oct}}{2} + \alpha\left(3\sigma_h\right) = \beta \tag{2.1}$$

where $\Delta\tau_{oct}$ = octahedral stress (von Mises) range, σ_h = hydrostatic stress, α and β are material parameters.

Crossland (1956) proposed a similar parameter to that of Sines but used maximum hydrostatic stress (σ_{hmax}) instead of mean, as expressed in Eq. (2.2). This also faces problems in dealing with out-of-phase multiaxial loading (Papuga, 2011).

$$\frac{\Delta \tau_{oct}}{2} + \alpha\left(3\sigma_{h\max}\right) = \beta \tag{2.2}$$

Findley (1959) proposed a fatigue life parameter, as expressed in Eq. (2.3), based on a combination of shear stress range and normal stress on the plane having the maximum value of the parameter.

$$\left(\frac{\Delta \tau}{2} + k\sigma_n\right)_{\max} = f \tag{2.3}$$

where $\Delta\tau$ = shear stress range, σ_n = normal stress, k = material constant.

McDiarmid (1991, 1994) proposed a model similar to Findley's, as expressed in Eq. (2.4), in which the critical plane is identified as the plane with the maximum shear stress range, but has a large scatter in results.

$$\frac{\Delta \tau_{\max}}{2t_{A,B}} + \frac{\sigma_{n,\max}}{2\sigma_{uts}} = 1 \tag{2.4}$$

where $\Delta\tau_{max}$ = maximum shear stress range, $t_{A,B}$ = shear fatigue strength, σ_{uts} = ultimate tensile strength.

Dang Van (1993) proposed an endurance limit criterion, also known as the Dang Van model, based on the concept of micro-stresses within a critical volume of material, expressed in Eq. (2.5). Recently, Hofmann et al. (2009) and Charkaluk et al. (2009) revisited the Dang Van model and suggested a finer qualitative analysis to better understand the ability of the model.

$$\tau(t) + a\sigma_h(t) = b \tag{2.5}$$

where $\tau(t)$ = instantaneous shear stress, $\sigma_h(t)$ = instantaneous hydrostatic stress, a and b = material constants

2.4.2 Strain-Based Models

Brown and Miller (1973); Brown and Miller (1982) and Kandil et al. (1982) proposed a parameter based on the maximum shear strain range and normal strain range on the plane experiencing the maximum shear strain range, as expressed in Eq. (2.6).

$$\frac{\Delta\gamma_{max}}{2} + S\Delta\varepsilon_n = A\frac{\sigma_f' - 2\sigma_{n,mean}}{E}\left(2N_f\right)^b + B\varepsilon_f'\left(2N_f\right)^c \qquad (2.6)$$

where $\Delta\gamma_{max}$ = maximum shear strain range, $\Delta\varepsilon_n$ = normal strain range, $\sigma_{n,mean}$ = mean normal stress, S, A and B = material constants.

Wang and Brown (1993) proposed a modification of the model proposed by (Brown and Miller, 1982), adding the capability to handle the strain path effect. The model is expressed in Eq. (2.7).

$$\frac{\Delta\hat{\gamma}}{2} = \frac{\Delta\gamma_{max}}{2} + S\varepsilon_n^* = \left(1 + \nu_e + (1-\nu_e)S\right)\sigma_f'\left(2N_f\right)^b + \left(1 + \nu_p + (1-\nu_p)S\right)\varepsilon_f'\left(2N_f\right)^c \quad (2.7)$$

where $\Delta\hat{\gamma}$ = equivalent shear strain connection, $\Delta\gamma_{max}$ = maximum shear strain range, ε_n^* = normal strain excursion between two turning points of γ_{max}, ν_e and ν_p = elastic and plastic Poisson ratio, S = a material parameter representing the influence of normal strain on fatigue crack growth.

2.4.3 Strain Energy-Based Models

Smith et al. (1970) proposed a damage model also known as the Smith Watson Topper (SWT) model, including the cyclic normal strain range and maximum normal stress, as expressed in Eq. (2.8); the critical plane is identified as the plane of maximum

normal stress. This model was originally developed and is still used for mean stress correction.

$$\sigma_{n,\max} \frac{\Delta\varepsilon_1}{2} = \frac{\sigma_f^{'2}}{E}\left(2N_f\right)^{2b} + \sigma_f^{'}\varepsilon_f^{'}\left(2N_f\right)^{b+c} \quad (2.8)$$

where $\sigma_{n,max}$ = maximum normal stress, $\Delta\varepsilon_1$ = principal strain range, $\sigma_f^{'}$ = fatigue strength coefficient, $\varepsilon_f^{'}$ = fatigue ductility coefficient, E = elastic modulus, N_f = fatigue life, b = fatigue strength coefficient, c = fatigue ductility exponent.

Fatemi and Socie (1988) suggested a modification to the Brown and Miller model by replacing the normal strain term with normal stress. Eq. (2.9) represents the Fatemi–Socie model when shear fatigue properties are used (Stephens et al., 2000) and also in the form of uniaxial fatigue properties (Fatemi and Socie, 1988; Fatemi and Gladskyi, 2013). Additional cyclic hardening developed during out-of-phase loading is included in the normal stress term. Mean stress can also be accounted for by adding the normal mean stress across the maximum shear plane to the alternating normal stress across the same plane.

$$\frac{\Delta\gamma}{2}\left(1+k\frac{\sigma_{n,\max}}{\sigma_y}\right) = \frac{\tau_f^{'}}{G}\left(2N_f\right)^{b\gamma} + \gamma_f^{'}\left(2N_f\right)^{c\gamma} = \left[(1+v_e)\frac{\sigma_f^{'}}{E}\left(2N_f\right)^b + (1+v_p)\varepsilon_f^{'}\left(2N_f\right)^c\right]\left[1+k\left(\frac{\sigma_f^{'}}{2\sigma_y}\left(2N_f\right)^b\right)\right] \quad (2.9)$$

where $\Delta\gamma$ = shear strain range, σ_y = yield stress, $\tau_f^{'}$ = shear fatigue strength coefficient, $\gamma_f^{'}$ = shear fatigue ductility coefficient, G = shear modulus, b_γ = shear fatigue strength exponent, c_γ = shear fatigue ductility exponent, v_e and v_p = elastic and plastic Poisson ratio.

Liu (1993) proposed a model based on virtual strain energy (VSE), i.e., the product of the stress and strain ranges, expressed in Eqs. (2.10)–(2.11). The critical plane is defined by the value of maximum normal work and the VSE quantity is the sum of normal work and shear work on the critical plane for tensile failure dominant materials, and vice versa for shear failure dominant materials.

For tensile failure:

$$\Delta W = \left(\Delta\sigma_n \Delta\varepsilon_n\right)_{\max} + \left(\Delta\tau\Delta\gamma\right) \tag{2.10}$$

For shear failure:

$$\Delta W = \left(\Delta\sigma_n \Delta\varepsilon_n\right) + \left(\Delta\tau\Delta\gamma\right)_{\max} \tag{2.11}$$

where ΔW = virtual strain energy parameter, $\Delta\sigma_n$ = normal stress range, $\Delta\varepsilon_n$ = normal strain range, $\Delta\tau$ = shear stress range, $\Delta\gamma$ = shear strain range.

Liu and Wang (2001) revisited the VSE model and evaluated its effectiveness, stating the strengths of the method as its ability to predict the physical characteristics of fatigue cracks, such as initiation sites, fracture modes and crack orientations. The method under-predicted in the case of superimposed compressive mean stress for torsional fatigue life. Núñez et al. (2011) introduced a probabilistic formulation in Liu's model based on a perturbation method to obtain two statistical moments (mean and variance) of the random variable fatigue lifetime. They compared their results with analysis done with a Monte Carlo simulation approach, and good agreement was found. But no experimental results are used in the study for comparison of model performance.

Chu (1995) proposed a similar parameter to Liu's model to combine shear and normal work, but replaced stress ranges with maximum stresses to include the mean stress effect, as expressed in Eq. (2.12). The critical plane is defined by the plane having the maximum fatigue parameter value.

$$\Delta W = \left(\tau_{n,\max}\,\frac{\Delta\gamma}{2} + \sigma_{n,\max}\,\frac{\Delta\varepsilon}{2}\right)_{\max} \tag{2.12}$$

where $\tau_{n,\max}$ = maximum shear stress on plane.

Glinka et al. (1995) proposed a shear strain energy model that includes the effects from both tensile and shear mean stresses, as expressed in Eq. (2.13). The critical plane is identified as the plane experiencing the largest shear work.

$$\Delta W = \frac{\Delta \tau}{2} \frac{\Delta \gamma}{2} \left(\frac{\sigma_f^{'}}{\sigma_f^{'} - \sigma_{n,max}} + \frac{\tau_f^{'}}{\tau_f^{'} - \tau_{n,max}} \right) \qquad (2.13)$$

Summary of the prediction capability of the models is presented in Table 2.2. The next section outlines the models proposed in the last 30 years which presented new proposals and expressions to estimate multiaxial fatigue damage.

Table 2.2: Prediction capability of fatigue life models

Fatigue model	Load type handling capability	Capable to handle mean stress effect
Sines (1955, 1959)	Proportional	No
Crossland (1956)	Proportional	No
Findley (1959)	Proportional	No
McDiarmid (1991, 1994)	Proportional / non-proportional	Yes
Dang Van (1993)	Proportional and random loading	Yes
Brown and Miller (1973); Brown and Miller (1982) and Kandil et al. (1982)	Proportional / non-proportional	No
Wang and Brown (1993)	Proportional / non-proportional	Yes
Smith et al. (1970)	Proportional / non-proportional	Yes
Fatemi and Socie (1988)	Proportional / non-proportional	Yes
Liu (1993)	Proportional / non-proportional	No
Chu (1995)	Proportional / non-proportional	Yes
Glinka et al. (1995)	Proportional / non-proportional	Yes

2.5   ADVANCES IN MULTIAXIAL FATIGUE LIFE ESTIMATION MODELS

The above discussion gives a brief introduction to the fatigue models that have gained widespread acceptance. The following section discusses some less known models, which may not be widely used but present new concepts and fatigue parameter expressions to estimate multiaxial fatigue life. This review is not exhaustive but best efforts have been made to gather as much data as possible about the development of fatigue life models from the previously published literature. The reviewed models are categorized with respect to basic concepts for example the critical plane, enclosed surface methods, integral type models, material structure-based models, stress invariants-based models, statistical assessment models, plasticity framework models. To highlight the stress–strain parameters involved for defining the model expressions quantifying fatigue damage and fatigue life.

2.5.1   Critical Plane Models

Susmel and Lazzarin (2002) and Lazzarin and Susmel (2003) proposed a critical plane model, i.e., the plane of maximum shear stress amplitude, then calculated both the maximum shear stress amplitude and the maximum normal and mean stress relative to that plane. Their modified Wholer curve method (MWCM) is expressed in Eqs. (2.14)–(2.15).

$$k_\tau\left(\rho_{eff}\right) = a\,\rho_{eff} + b \tag{2.14}$$

$$\tau_{A,\mathrm{Re}f}\left(\rho_{eff}\right) = \alpha\,\rho_{eff} + \beta \tag{2.15}$$

where $k_\tau(\rho_{eff})$ = negative inverse slope of Wholer curve, ρ_{eff} = critical plane stress ratio, $\tau_{A,Ref}(\rho_{eff})$ = reference shear stress amplitude at considered limit to cycles to failure, a, b, α, β = material constants.

Susmel and Taylor (2006) proposed a simplified approach to apply the theory of critical distances (TCD) (Taylor, 1999), as defined in Eq. (2.16), to predict the fatigue behaviour of notched components subjected to torsional fatigue loading. TCD was

found to be a useful tool for assessing fatigue life, as the experimental results generated using uniaxial testing equipment and linear elastic FE models are the only two pieces of information needed for its application.

$$L = \frac{1}{\pi}\left(\frac{\Delta K_{I,th}}{\Delta\sigma_0}\right)^2 \tag{2.16}$$

where L = material characteristic length, $\Delta K_{I,th}$ = fatigue threshold stress intensity factor, $\Delta\sigma_0$ = range of uniaxial plane fatigue limit.

Susmel and Taylor (2008) later proposed a method which combines the MWCM and TCD methods to estimate fatigue life under multiaxial loadings. They concluded that the proposed method is efficient, provided that it is calibrated by using appropriate pieces of experimental information. Susmel (2010) formulated a critical plane determination method based on the concept that the material plane where the crack initiation phenomenon takes place is the one containing the direction along which variance of the resolved shear stress reaches its maximum. Expressions defining the variance are shown in Eqs. (2.17)–(2.19). The main feature of the method is the speed of critical plane determination, as the time needed to find the global maximum is not dependent on the length of load history under study.

$$Var\left[\tau_q(t)\right] = d^T[C]d \tag{2.17}$$

where d = direction cosines, $[C]$ = matrix consisting of variance V_i, covariance $C_{i,j}$ terms defined as:

$$V_i = Var\left[\sigma_i(t)\right] \quad for\ i = x, y, z, xy, xz, yz \tag{2.18}$$

$$C_{i,j} = CoVar\left[\sigma_i(t), \sigma_j(t)\right] \quad for\ i = x, y, z, xy, xz, yz \tag{2.19}$$

Susmel and Taylor (2011) proposed a reformulation of the TCD method so that it can be used to estimate the fatigue life of notched components facing variable amplitude uniaxial fatigue loading. They also highlighted three forms of application of

TCD: the point method, line method and area method, of which the point method is said to be the easiest to apply in terms of the calculation load. Susmel and Tovo (2011) presented the methodology of estimating fatigue life under variable amplitude loading conditions, using MWCM along with MVM for critical plane determination. They also introduced a material parameter critical damage sum, expressed in Eqs. (2.20)–(2.21), determined experimentally, where this parameter can vary with the degree of multiaxiality and non-proportionality.

$$D_{CR}(\rho_{eff}) = d_1 \cdot \rho_{eff} + d_2 \qquad (2.20)$$

where d_1 and d_2 = material fatigue properties to be determined experimentally, ρ_{eff} = critical plane stress ratio, defined by

$$\rho_{eff} = \frac{m \cdot \sigma_{n,m} + \sigma_{n,a}}{\tau_a} \qquad (2.21)$$

where m = mean stress sensitivity index, $\sigma_{n,m}$ and $\sigma_{n,a}$ = mean and amplitude of stress perpendicular to critical plane, τ_a = shear stress amplitude.

Susmel and Taylor (2012) devised a technique for fatigue assessment of notched components subjected to variable amplitude fatigue loading. They used MWCM along with TCD in the form of the point method, where the critical plane is determined using MVM. They concluded that their method provided a high level of accuracy and that real components can be designed against variable amplitude uniaxial/multiaxial loading by direct post-processing of the relevant stress fields determined through conventional linear-elastic FE models. Susmel et al. (2014b) investigated the MVM method to determine whether, independently from the degree of multiaxiality and non-proportionality of the applied loading history, the direction of maximum variance of the resolved shear stress is also capable of accurately estimating the orientation of Stage I crack paths. The study showed that MVM is seen to be capable of estimating the orientation of the Stage I crack paths under non-proportional loading with an adequate level of accuracy. Susmel et al. (2014a) performed a validation exercise to judge the effectiveness of TCD in the form of the point method along with MCWM in estimating

fatigue life for uniaxial/multiaxial loading cases by directly post-processing linear elastic stress fields calculated from commercial finite element software. A high level of accuracy was observed in the calculated fatigue life results.

Mahadevan and Liu (2005) proposed a fatigue model based on the concept of critical plane deviation, as expressed in Eq. (2.22), where first a search for the fracture plane is conducted and then the critical plane is found at a certain deviation from the fracture plane. The concept is based on the idea that a crack initiates on one plane and then propagates along a distinct plane orientation. The model is tested for constant amplitude loading and is found to give results in good agreement with experimental data. Later, Mahadevan and Liu (2007) extended the application domain of their model from isotropic materials to anisotropic materials and composite materials. But, due to the non-availability of experimental fatigue data on anisotropic materials in the literature, they suggested testing the proposed model with more experimental data available in future studies.

$$\frac{1}{\beta}\sqrt{\left[\sigma_{a,c}\left(1+\eta_{N_f}\frac{\sigma_{m,c}}{f_{N_f}}\right)\right]^2 + \left(\frac{f_{N_f}}{t_{N_f}}\right)^2(\tau_{a,c})^2 + k(\sigma_{a,c}^H)^2} = f_{N_f} \qquad (2.22)$$

where $\sigma_{a,c}$ = normal stress amplitude on critical plane, $\sigma_{m,c}$ = mean normal stress on critical plane, f_{Nf} = normal stress at N_f cycles, t_{Nf} = shear stress at N_f cycles, $\tau_{a,c}$ = shear stress amplitude on critical plane, $\sigma_{a,c}^H$ = hydrostatic stress amplitude on critical plane.

Ninic and Stark (2007) proposed a non-linear fatigue damage function based on the critical plane concept expressed in Eq. (2.23), rightly named as the quadratic critical plane formula by Papuga (2011). The critical plane is identified as the plane experiencing the maximum value of damage function. Their study concluded that the proposed fatigue damage function is dependent on the normal stress sensitivity factor for accurate predictions, and also identified that the endurance strength ratio is important for multiaxial fatigue analysis.

$$D(l,m,n) = \left[\left(\frac{\tau_a(l,m,n)}{T_e} \right)^2 + k \cdot \left(\frac{\sigma_{eq}(l,m,n)}{S_e} \right)^2 \right]^{\frac{1}{2}}$$

(2.23)

where D = damage on critical plane, τ_a = shear stress amplitude, T_e = fatigue limit in fully reversed torsion, σ_{eq} = equivalent stress amplitude, S_e = fatigue limit in fully reversed axial and torsion, (l,m,n) = direction cosines of vector normal to plane, k = normal stress sensitivity factor.

Papuga and Ruzicka (2008) proposed two criteria with a similar damage parameter with the emphasis on the effects of shear stress in comparison to normal stress. The criteria for the search for the critical plane are expressed in Eqs. (2.24)–(2.26). The two methods derived here are to study whether it is more effective to integrate the load effect or to maximize it. Both methods provide very similar results as regards the presented data set of 119 experimental results.

$$\sqrt{a_c \cdot C_a^2 + b_c \cdot \left(N_a + \frac{t_{-1}}{f_0} \cdot N_m \right)} \leq f_{-1}$$

(2.24)

where

$$k < \sqrt{\frac{4}{3}} \cong 1.155: \quad a_c = \frac{k^2}{2} + \frac{\sqrt{k^4 - k^2}}{2}, \quad b_c = f_{-1}$$

(2.25)

$$k \geq \sqrt{\frac{4}{3}} \cong 1.155: \quad a_c = \left(\frac{4k^2}{4+k^2} \right)^2, \quad b_c = \frac{8f_{-1}k^2(4-k^2)}{(4+k^2)^2}$$

(2.26)

where k, a_c, b_c = material parameter, C_a = shear stress on considered plane, N_a = maximum normal stress, N_m = mean normal stress, t_{-1} = fatigue limit in fully reversed torsion, f_0 = fatigue limit in repeated axial loading, f_{-1} = fatigue limit in fully reversed axial loading.

Lu and Liu (2009) proposed a critical plane model with the equivalent initial flaw size expressed in Eqs. (2.27)–(2.28). The critical plane is determined by the maximum normal stress plane and the ratio of mode II and mode I stress intensity factor

coefficients corresponding to a specific crack growth rate. This means that critical plane determination is dependent on stress states as well as material properties.

$$N = \int_{a_i}^{a_c} \frac{1}{C\left[\Delta K_{eq} - \Delta K_{th}\right]^m} \, da \tag{2.27}$$

$$K_{mixed,eq} = \frac{1}{B} \sqrt{(k_1)^2 + \left(\frac{k_2}{s}\right)^2 + A\left(k^H\right)^2} \tag{2.28}$$

where N = fatigue life, ΔK_{eq} = equivalent stress intensity factor, ΔK_{th} = threshold stress intensity factor, a = crack length, A, B, C, m = material parameters, $K_{mixed,\,eq}$ = equivalent stress intensity factor under general mixed mode loading, k_1, k_2 and k^H = loading related parameters, s = ratio of stress intensity factors for mode II and mode I.

Shang et al. (2010) proposed a damage parameter based on a critical plane having maximum shear strain and a higher value of normal strain excursion, as expressed in Eq. (2.29). The proposed parameter shows good correlation with the multiaxial fatigue lives of different materials in low cycle loading cases.

$$\left(\varepsilon_n^{*2} + \frac{\upsilon_{eff}\left(2 - \upsilon_{eff}\right)}{\left(1 + \upsilon_{eff}\right)^2}\left(\frac{\Delta\gamma_{max}}{2}\right)^2\right)^{1/2} = \frac{\sigma_f'}{E}\left(2N_f\right)^b + \varepsilon_f'\left(2N_f\right)^c \tag{2.29}$$

where ε_n^* = normal strain excursion between turning points on the critical plane, υ_{eff} = effective Poisson ratio, $\Delta\gamma_{max}$ = maximum shear strain range.

Li et al. (2010) and Li et al. (2011) presented a simple critical plane type method to assess the fatigue life of metallic materials subjected to proportional and non-proportional loading, and their model is expressed in Eq. (2.30). The model has maximum shear strain range ($\Delta\gamma_{max}$), normal strain range ($\Delta\varepsilon_n$) and the maximum normal stress ($\sigma_{n,max}$) on the maximum shear strain range plane.

$$\frac{\Delta\varepsilon_{eq}^*}{2} = \frac{\Delta\gamma_{max}}{2} + \left(1 + \frac{\sigma_{n,max}}{\sigma_y}\right)\frac{\Delta\varepsilon_n}{2} = \left[\frac{\sigma_f'}{E}(2N_f)^b + \varepsilon_f'(2N_f)^c\right]\left(1 + \frac{\sigma_f'}{\sigma_y}(2N_f)^b\right) \quad (2.30)$$

Ince and Glinka (2014) proposed two different forms of fatigue damage parameter related to the maximum fatigue damage plane. The two forms are the generalized strain energy damage parameter expressed in Eq. (2.31) and the generalized strain amplitude damage parameter expressed in Eq. (2.32).

$$W_{gen}^* = \left(\tau_{max}\frac{\Delta\gamma^e}{2} + \frac{\Delta\tau}{2}\frac{\Delta\gamma^p}{2} + \sigma_{n,max}\frac{\Delta\varepsilon_n^e}{2} + \frac{\Delta\sigma_n}{2}\frac{\Delta\varepsilon_n^p}{2}\right)_{max} = f(N_f) \quad (2.31)$$

$$\frac{\Delta\varepsilon_{gen}^*}{2} = \left(\frac{\tau_{max}}{\Delta\tau/2}\frac{\Delta\gamma^e}{2} + \frac{\Delta\gamma^p}{2} + \frac{\sigma_{n,max}}{\Delta\sigma_n/2}\frac{\Delta\varepsilon_n^e}{2} + \frac{\Delta\varepsilon_n^p}{2}\right)_{max} = f(N_f) \quad (2.32)$$

where W_{gen}^* = maximum generalized strain energy, τ_{max} = maximum shear stress, $\Delta\gamma^e$ and $\Delta\gamma^p$ = elastic and plastic strain range, $\Delta\tau$ = shear stress range, $\sigma_{n,max}$ = maximum normal stress, $\Delta\varepsilon_n^e$ and $\Delta\varepsilon_n^p$ = elastic and plastic normal strain range, $\Delta\sigma_n$ = normal stress range, $\Delta\varepsilon_{gen}^*$ = maximum generalized strain amplitude.

2.5.2 Enclosed Surface Models

Mamiya et al. (2005) proposed a multiaxial high-cycle fatigue endurance criterion for sinusoidal iso-frequency in-phase and out-of-phase loading conditions based on the idea of the minimum circumscribed ellipse in Illyushin's deviatoric space, as expressed in Eq. (2.33). The mean stress effect is conservative on fatigue life results compared to other models used in the study. One limitation is that the model application is restricted to iso-frequency loading cases.

$$\sqrt{\sum_{i=1}^{5}a_i^2} + k\sigma_{p\,max} \leq \lambda \quad (2.33)$$

where $a_{i(1-5)}$ = amplitude of deviatoric stress, k = fatigue limit ratio, $\sigma_{p,max}$ = maximum principal stress, λ = material parameter.

Leila et al. (2010) proposed the enclosing path method with prismatic hulls on principal axes directions, as expressed in Eq. (2.34). This technique is effective in the sense that it is easy to capture the equivalent stress parameter with different loads causing the same value of stress parameter.

$$\sqrt{J_{2,a}} = \sqrt{R_1^2 + R_2^2 + R_3^2 + R_4^2 + R_5^2} \tag{2.34}$$

where $R_1 - R_5$ = amplitudes of stresses in principal directions in 5D Euclidean space,

$\sqrt{J_{2,a}}$ = amplitude of second invariant of stress deviator.

Araujo et al. (2011) proposed the maximum rectangular hull method to define the equivalent shear stress amplitude, as expressed in Eqs. (2.35)–(2.36), where a rectangle is fitted on a complex loading path by maximizing its size. The method is capable of distinguishing between proportional and non-proportional loading. The method predicted better results than the minimum rectangular hull method when compared with experimental data.

$$\tau_a^{max} = \max\left\{\tau_a(\phi,\theta)\right\} \tag{2.35}$$

where

$$\tau_a = \max\sqrt{a_1^2(\varphi) + a_2^2(\varphi)} \tag{2.36}$$

where τ_a^{max} = maximum equivalent shear stress amplitude, $\tau_a(\phi, \theta)$ = equivalent shear stress on plane located by ϕ and θ, φ = angle locating rectangular hull on plane.

Mamiya et al. (2011) proposed a fatigue life estimation model in terms of a piecewise ruled S-N surface. The first surface is defined as the sum of deviatoric stress amplitude (τ_a) and maximum hydrostatic stress (σ_{Hmax}) as the exponential function of fatigue life, as expressed in Eq. (2.37); for the second surface only the deviatoric stress amplitude is used, as expressed by Eq. (2.38), for cases where hydrostatic stresses have a small magnitude. The maximum prismatic hull method is used to calculate the deviatoric stress amplitude. The proposed model performed in the same way as the other

earlier proposed model included in the study, but better in the situation of mean normal stress.

$$\tau_a + \sigma_{H\max} = \alpha N_f^{\beta} \quad if \ \sigma_{H\max} \geq \alpha\left(\frac{\tau_a}{\gamma}\right)^{\beta/\delta} - \tau_a \tag{2.37}$$

$$\tau_a = \gamma N_f^{\delta} \tag{2.38}$$

where N_f = fatigue life, α, β, γ, δ = material parameters.

Meggiolaro and de Castro (2012a, 2012b) proposed an enclosing surface model with a modified Wang–Brown rainflow counting method. They identified discrepancies in the previously defined enclosing surface methods: only the minimum ball method has a physical foundation, the considered portion of the path should have more than one cycle or else, if it is considered as a single cycle, the actual damage might be underestimated, with a loss of information as the enclosing surface algorithms do not take into account the actual loading path, but only the convex hulls associated with them. For loading histories with more than one cycle counted by the rainflow method before applying the moment of inertia method, in the second part they have shown the shortcoming of the original Wang–Brown model, which can lead to non-conservative predictions by incorrectly filtering out significant events within a multiaxial loading cycle. The two improvements they proposed are, first, related to choosing the starting point of the cycle, so that the cycle counting is modified, and secondly that the algorithm implementation is simplified by formulating it in a reduced five-dimensional Euclidean space.

2.5.3 Integral Type Models

Papadopoulos (1994) proposed an integral type fatigue life criterion where all components are integrated over all planes at the point of consideration, with an extra integration of resolved shear stress over shear plane as expressed in Eqs. (2.39)–(2.40). This places a high demand on computation time, thus preventing its use in commercial fatigue solvers (Papuga, 2011). This model is best suited for hard metals (Papadopoulos et al., 1997).

$$\sqrt{\left\langle T_a^2 \right\rangle} + \alpha \sigma_{h,\max} \leq \beta \tag{2.39}$$

$$\sqrt{\left\langle T_a^2 \right\rangle} = \sqrt{5}\sqrt{\frac{1}{8\pi^2} \int_{\varphi=0}^{2\pi} \int_{\theta=0}^{\pi} \int_{\chi=0}^{2\pi} \left(T_a(\varphi,\theta,\chi)\right)^2 d\chi \sin\theta d\theta d\varphi} \tag{2.40}$$

where T_a = resolved shear stress amplitude, φ and θ = angle locating the plane, χ = angle between major axis and resolved shear stress, α and β = material constant.

Lasserre and Palin-Luc (1998) proposed an energy density model expressed in Eq. (2.41), based on the idea of volumetric distribution of strain energy density around the critical point considered for fatigue failure. The model predicted results with good agreement with uniaxial and multiaxial experimental data of smooth cylindrical specimens.

$$\omega_a^D(C_i, load) = \frac{1}{V^*(C_i)} \iiint_{V^*(C_i)} \left[W_a(x,y,z,load) - W_a^*(C_i,load) \right] d\upsilon \tag{2.41}$$

where ω_a^D = volumetric mean value of strain energy volumetric density, $V^*(C_i)$ = volume at critical point, W_a = strain energy volumetric density, W_a^* = strain energy volumetric density at critical point C_i.

Later, Palin-Luc et al. (2003) improved the volumetric density model by modifying the damage part of the model so as to overcome the limitation of fully reversed sinusoidal loading in the (Lasserre and Palin-Luc, 1998) model. Saintier et al. (2013) reformulated the model, as expressed in Eq. (2.42), and suggested improvements in the criterion for multiaxial variable amplitude loading, where originally only constant amplitude loadings are considered. The model also improved the incremental fatigue life assessment method for proportional and non-proportional multiaxial variable amplitude loadings. The proposed model estimated fatigue life results with good accuracy within the considered experimental cases, and it was also suggested that a more thorough study with variety of materials is required.

$$W_{geqdam}(M) = \left\langle W_{geq}(M) - \sum_{l=1}^{6} P_l(M)\alpha_{M,l} W_g^* \right\rangle \qquad (2.42)$$

where W_{geqdam} = damaging part of strain work density, W_{geq} = equivalent strain work density, P_l = proportionality factor, α_M = represents evolution of stress / strain tensors and sequence duration, W^*_g = minimum strain work volumetric density to create irreversible damage.

Zenner et al. (2000) proposed a fatigue life estimation criterion based on an integral type approach and shear stress intensity expressed in Eq. (2.43), which can result in good estimation in the case of complex periodical loadings. But due to stress quantities, this is not valid for a low-cycle fatigue regime, as strain-based parameters are required to deal with plastic deformations (Zenner et al., 2000).

$$\sigma_{equ,a} = \left\{ \frac{15}{8\pi} \int_{\gamma=0}^{\pi} \int_{\varphi=0}^{2\pi} \left[a\tau_{\gamma\varphi a}^2 \left(1 + m\tau_{\gamma\varphi m}^2\right) + b\sigma_{\gamma\varphi a}^2 \left(1 + n\sigma_{\gamma\varphi m}\right) \right] \sin\gamma\, d\gamma\, d\varphi \right\}^{1/2} \qquad (2.43)$$

where $\sigma_{equ,a}$ = equivalent stress amplitude, $\tau_{\gamma\varphi m}$, $\sigma_{\gamma\varphi m}$ = static shear and normal stress on plane $\gamma\varphi$, $\tau_{\gamma\varphi a}$, $\sigma_{\gamma\varphi a}$ = alternating shear and normal stress on plane $\gamma\varphi$, a, m, b, n = obtained from the tensile-compressive fatigue strength, torsional fatigue strength, pulsating tensile strength and pulsating torsional strength.

Papuga and Ruzicka (2008) proposed two criteria with a similar damage parameter with the emphasis on the effects of shear stress in comparison to normal stress. The criteria integrate a fatigue parameter over all planes, expressed in Eqs. (2.44)–(2.45). The two methods derived here are to study whether to integrate the load effect or to maximize it is the more effective approach. Both methods provide very similar results as regards the presented data set of 119 experimental results.

$$\sqrt{\frac{1}{4\pi} \int_\varphi \int_\psi \left[a_1 \cdot C_a^2 + b_I \cdot \left(N_a + \frac{f_{-1}}{t_{-1}} N_m \right) \right] \sin\psi\, d\psi\, d\varphi_{-1}} \leq f \qquad (2.44)$$

where

$$a_I = \frac{5}{2}k^2, \quad b_I = f_{-1}\left(3 - k^2\right) \tag{2.45}$$

where k, a_I, b_I = material parameter, C_a = shear stress on considered plane, N_a = maximum normal stress, N_m = mean normal stress, t_{-1} = fatigue limit in fully reversed torsion, f_0 = fatigue limit in repeated axial loading, f_{-1} = fatigue limit in fully reversed axial loading, ψ and φ = Euler angles of planes examined in local coordinate system.

2.5.4 Material Structure-Based Models

Luo and Chattopadhyay (2011) proposed a multi-scale damage criterion for initial stage crack prediction expressed in Eqs. (2.46)–(2.47). The local damage state is derived using optimization theory, and then passed on to grain level. The damage for a meso representative volume element (RVE), which contains several grains, is determined. The estimation results of RVE failure at a structural hotspot match the experimental results. Also, the damage criterion is working on microscale (grain level) thus it has the capability to provide the potential directions for crack growth. This model can be good for application in case studies, but due to its complex application method and dependence on grain structure, it may be not applicable in early stages of design process. Due to rapid changes in design prototypes with respect to shapes and materials, a quick analysis of various designs are required. Hence, the macroscale performance and behavior is preferable to perform a rapid and inexpensive analysis to select the best designs for detailed analysis.

$$dD^{(\alpha)} = \left\langle \frac{\sigma_{mr}}{\sigma_o} - 1 \right\rangle^{m'} \left(1 + \frac{\sigma_n^{(\alpha)}}{\sigma_f}\right) dY^{(\alpha')} \tag{2.46}$$

$$dY^{(\alpha')} = \delta' \sigma_n^{(\alpha')}\left(d\varepsilon^p\right)^{(\alpha')} + \frac{1-\delta'}{2} \sigma_s^{(\alpha')}\left(d\gamma^p\right)^{(\alpha')} \tag{2.47}$$

where $dD^{(\alpha)}$ = damage parameter increment on slip system (α), $dY^{(\alpha)}$ = plastic strains energy increment on slip system (α), σ_{mr} = memory stress, σ_o = endurance limit, $\sigma_n^{(\alpha)}$ = normal stress on slip system (α), σ_f = true fracture stress, m, δ = material constants, $d\varepsilon^p$

= plastic strain increment corresponding to $\sigma_n^{(\alpha)}$, $\sigma_s^{(\alpha)}$ = shear stress on slip system (α), $d\gamma^p$ = plastic strain increment corresponding to $\sigma_s(\alpha)$.

2.5.5   Stress Invariants-Based Models

Horstemeyer and Gokhale (1999) proposed a void crack nucleation model for ductile metals with second phases, as expressed in Eq. (2.48). The model is a function of the fracture toughness of the aggregate material, length scale parameter, the volume fraction of the second phase, strain level and stress state. Later, Lugo et al. (2011), using an acoustic emission method, showed the effectiveness of the proposed model.

$$\eta(t) = C_{coeff} \exp\left(\frac{\varepsilon(t)d^{1/2}}{K_{IC}f^{1/3}} \left\{ a' \left[\frac{4}{27} - \frac{J_3^2}{J_2^3} \right] + b' \cdot \frac{J_3}{J_2^{3/2}} + c' \cdot \left\| \frac{I_1}{\sqrt{J_2}} \right\| \right\} \right) \tag{2.48}$$

where $\eta(t)$ = void nucleation at time t, C_{coeff} = material constant, $\varepsilon(t)$ = strain at time t, d = length scale parameter, K_{IC} = critical stress intensity factor, f = equivalent stress amplitude, a', b' and c' = material constants determined from different stress states, I_1 = stress invariant, J_2, J_3 = deviatoric stress invariants.

Vu et al. (2010) proposed a fatigue life criterion based on stress invariants and they introduced a quantity $J_{2,mean}$, shown in Eqs. (2.49)–(2.51), which captures the shear stress effect and phase shift effect. The model performed well within the considered set of experimental data. It was also suggested that a more detailed study is required to validate the model's reliability.

$$f = \sqrt{\gamma_1 J_2'(t)^2 + \gamma_2 J_{2,mean}^2 + \gamma_3 I_f\left(I_{1,a}, I_{1,m}\right)} \leq \beta \tag{2.49}$$

where

For low-strength metals

$$I_f\left(I_{1,a}, I_{1,m}\right) = I_{1,a} + I_{1,m} \tag{2.50}$$

For high-strength metals

$$I_f\left(I_{1,a}, I_{1,m}\right) = I_{1,a} + \frac{f_{-1}}{t_{-1}} I_{1,m} \tag{2.51}$$

where γ_1, γ_2, γ_3, β = material parameters, J_2' = second invariant of deviator of the amplitude of stress tensor, $J_{2,mean}$ = mean value of $J_2'(t)$ over a period, I_f = function of $I_{1,a}$ and $I_{1,m}$, I_1 = first stress invariant (a − amplitude and m − mean), f_{-1} = fatigue limit in fully reversed axial and bending, t_{-1} = fatigue limit in fully reversed torsion.

2.5.6   Statistical Assessment Models

Pinto et al. (2010) proposed a Weibull regression model based on the Weibull model for statistical assessment of stress–life data for probabilistic definition of the strain–life field. This provides an analytical probabilistic definition of the whole strain–life field as quantile curves, both in the low-cycle and high-cycle fatigue regions. The proposed model deals directly with the total strain, without the need to separate its elastic and plastic strain components, which represents a significant advantage over the classical approaches, permitting it to deal with run-outs, and it can be applied for probabilistic lifetime prediction using damage accumulation.

2.5.7   Plasticity Framework Models

Emuakpor et al. (2012) developed a fatigue life assessment expression for multiaxial loading, shown in Eq. (2.52), incorporating non-linear plastic stress−strain relations in distortion theory for a case of cyclic loading. The idea behind the criterion is that the physical damage quantity for failure is equal to the accumulated strain energy in a monotonic fracture, which is also equal to the strain energy during fatigue failure.

$$\sigma_E = \frac{\sigma_C}{2} \ln\left(\sum_{p=1}^{3} e^{2\sigma_P/\sigma_C}\right) \tag{2.52}$$

where σ_E = non-linear equivalent stress, σ_C = material parameter for cyclic stress, σ_P = principal stress ($p = 1,2,3$).

Chaussumier et al. (2013) proposed a fatigue life prediction model based on experimental results, including multi-site crack consideration, coalescence between neighbouring cracks, a short crack growth stage and a long crack propagation stage. This model is built from experimental topography measurements of pickled surfaces which make it possible to detect pits and to characterize their sizes. The model was developed specifically for 7050 aluminium alloy, but its application and effectiveness should be tested for a greater variety of materials before considering it for widespread use.

Khandelwal and El-Tawil (2014) proposed a damage mechanics-based model to simulate ductile fracture in structural steels. The model, expressed in Eqs. (2.53)–(2.55), is based on the concept of the principle of effective stress and strain equivalence in a plasticity framework. The proposed model is implemented in finite element code, the model parameters are mesh-dependent and the model has to be recalibrated if a different material or mesh size is employed.

$$\dot{\alpha}^d = a_0 \, T_1\left(\alpha^p\right)\dot{\alpha}^P + a_1 \, \mathrm{T}T_1\left(\alpha^P\right)\dot{\alpha}^P + a_2 \exp\left(a_3 \, \alpha^P\right)T_2\left(\alpha^P\right)\dot{\alpha}^P \tag{2.53}$$

$$\begin{cases} T_1\left(\alpha^P,\varepsilon_n,\Delta\varepsilon\right)=0 & \textit{if } \alpha^P < \varepsilon_n \\[2mm] T_1\left(\alpha^P,\varepsilon_n,\Delta\varepsilon\right)=\dfrac{\left(\alpha^P-\varepsilon_n\right)^2}{\Delta\varepsilon^2}\left[3-\dfrac{2\left(\alpha^P-\varepsilon_n\right)}{\Delta\varepsilon}\right] & \textit{if } \varepsilon_n < \alpha^p < \varepsilon_n+\Delta\varepsilon \\[2mm] \textit{and } T_1\left(\alpha^P,\varepsilon_n,\Delta\varepsilon\right)=1 & \textit{if } \alpha^P \geq \varepsilon_n+\Delta\varepsilon \end{cases} \tag{2.54}$$

$$\begin{cases} T_2\left(\alpha^P,\varepsilon_c,\Delta\varepsilon\right)=0 & \textit{if } \alpha^P < \varepsilon_c \\[2mm] T_2\left(\alpha^P,\varepsilon_c,\Delta\varepsilon\right)=\dfrac{\left(\alpha^P-\varepsilon_c\right)^2}{\Delta\varepsilon^2}\left[3-\dfrac{2\left(\alpha^P-\varepsilon_c\right)}{\Delta\varepsilon}\right] & \textit{if } \varepsilon_c < \alpha^p < \varepsilon_c+\Delta\varepsilon \\[2mm] \textit{and } T_2\left(\alpha^P,\varepsilon_c,\Delta\varepsilon\right)=1 & \textit{if } \alpha^P \geq \varepsilon_c+\Delta\varepsilon \end{cases} \tag{2.55}$$

where α^d and α^p = damage and plastic internal variables, T_1 and T_2 = threshold function, T = stress tri-axiality, a_0, a_1, a_2, a_3 = material parameters, ε_n = nucleation strain, $\Delta\varepsilon$ = smoothing factor, ε_c = coalescence strain

2.6   OPTIMIZATION ALGORITHM IN FATIGUE ANALYSIS

Bukkapatnam and Sadananda (2005) proposed a framework to model crack growth dynamics in materials under alternative service environments without resorting to extensive experimentation. The model structures are derived based on the unified approach (including all the observed effects of load ratio, short cracks, shielding of dislocations, overload and underload, surface crack, etc.), and a genetic algorithm is used to parameterize the models. The GAs allow reconciliation of the known, complicated physical relationships with empirical observations. The presence of physically motivated mathematical structures renders these phenomena predictive and easier to analyse than the use of purely empirical approaches such as neural networks. A fatigue crack growth model derived from the application of the proposed framework was found to predict crack growth rates to within 12% error. Thus they offer the potential to reduce the extent of the experimentation needed for fatigue crack growth analysis.

Liu (2006) proposed a simulation based calculation procedure for multiaxial fatigue life prediction, which combines a Monte Carlo simulation technique with stochastic process theory and a response surface method. The proposed method can include randomness in material properties, applied loading and geometry. Time-dependent failure probability is evaluated, where the failure is defined as occurring when the accumulated damage exceeds an acceptable value or the crack exceeds a critical value. A Monte Carlo simulation method is used to calculate the probabilistic life distribution. A response surface method combined with design of experiments is used to obtain a simplified empirical formula for the damage accumulation process, considering several sources of variation. Field failure data was in very good agreement with numerically predicted results.

Vassilopoulos et al. (2007) proposed a procedure using an artificial neural network to model the fatigue life of multidirectional composite laminates made of

GFRP composite materials and tested these under constant amplitude loading patterns. The prediction accuracy of the artificial neural network (ANN) was validated using experimental data available from the literature. Only 50% of the experimental data is required by the ANN to model the fatigue life of the material in comparison to the data required by conventional methods.

Vassilopoulos et al. (2008) presented a comparative study of fatigue life estimation of composite materials using the GA tool, with conventional methods. They concluded that the fatigue life results are more accurate than the results produced by conventional methods. The advantages of GA highlighted in this paper are that the modelling is not based on any assumption, such as that the data follow a specific statistical distribution, or that the SN curve follows a power curve equation. It is a material-independent data-driven method which correlates input with output in order to establish a model describing the relationship between them. Thus the model can be applied to any material provided that an adequate amount of data is available. For future research related to GA-based fatigue modelling, they proposed to use more complex genetic programming configurations by introducing models with multiple inputs, e.g. stress amplitude, maximum stress, stress ratio and off-axis angle, and to try to assign a corresponding number of cycles to failure to every set of input.

Franulovic et al. (2009) proposed a material model describing the elasto-plastic behaviour of materials under cyclic loading. The material constitutive model for description of low-cycle fatigue behaviour is highly non-linear and therefore its parameter identification requires a complex numerical procedure, such as a genetic algorithm. A GA is a stochastic search method for obtaining good approximate solutions in complex problems. The calculation resulted in the identification of material parameters that are validated by comparing the material response of the numerical solution with experimental data. The GA for the parameter identification in a particular problem, using a finite element method to simulate the materials' response, proved to be a very good choice. The use of suitable genetic operators in the GA calculation procedure made it possible to achieve very fast and reliable convergence to accurate results.

Krishnapillai and Jones (2009) proposed a structural optimization procedure that integrates geometrical modelling, structural analysis and optimization into one complete and automated computer-aided design process. They illustrated a procedure for the design of lightweight structures using fatigue-based optimization in conjunction with a genetic algorithm. It provides a robust methodology and also has the potential to be applied to structures with complex structural configurations with multiple optimum peaks.

Brighenti and Carpinteri (2012) proposed a continuum mechanics-based endurance function which quantifies the damage accumulation in the material up to final failure, under an arbitrary multiaxial loading history. The proposed model is characterized by several parameters, so a genetic algorithm is employed to numerically evaluate their values once the effects of some experimental complex stress history on the fatigue life are known. The GAs have some advantages with respect to classical techniques, since they allow us to solve problems characterized by both multiple minima and non-convexity properties, avoiding numerical instabilities and the risk of missing the global optimum. Furthermore, the GAs can handle any kind of objective function, and simply operate by using basic concepts such as generation of random numbers, choice, switching and combination of such generated numbers. No critical plane or loading cycle counting algorithm is needed, as the proposed model simply analyses damage accumulation during the loading process. The fatigue life was assumed to be dominated by crack-nucleation, i.e., the fatigue life for crack propagation is negligible with respect to the total life. They concluded that the fatigue life results using the proposed endurance function show satisfactory agreement with the experimental data. Kamal et al. (2013) studied the endurance function model and suggested a simplification by reducing the number of parameters needed to calibrate the model and also developed a methodology to use FE analysis stress results to estimate fatigue life using the model.

Roux et al. (2013) proposed a method to define Equivalent Fatigue Loads (EFL) from in-service load measurement in the case of a structure subjected to multiple variable fatigue loadings. EFL can be used in order to define tests on full-scale structures for an experimental validation approach. A mathematical method is proposed

to find EFL, which uses a genetic algorithm in order to compute an accurate EFL for the whole structure. This method to find the best EFL for a structure can be used to perform a validation test on a bench and can also be used during the design phase to optimize the structure geometry for a specific use.

Lotfi and Beiss (2013) showed the application of an ANN as an effort to predict the effect of various powder metallurgy processing parameters on the endurance limit of powder metallurgy steel specimens. The study applies the existing data which was collected from published experimental investigations. Fabrication and testing parameters together with corresponding fatigue limit records were used as sets of data for network training. A genetic algorithm was also included to optimize the experimental conditions, subject to practical limitations, in order to achieve the desired fatigue strength values. The GA with a trained neural network is found to be a powerful optimization and cost reduction tool, as it makes it possible to select optimum material compositions and processing conditions for a specific fatigue strength.

Niesłony and Böhm (2013) presented a stress-based approach to take into account the influence of the mean stress value on the fatigue strength of constructional materials. The proposed fatigue life estimation model implemented a locally developed optimization algorithm to ensure maximum precision in the fatigue life calculations. The key assumption in the proposed solution is the use of fatigue strength amplitudes for calibration, gained for two boundary states: tension and compression with the stress ratio R = 1 and another one with a significant mean stress value, e.g. the popular unilateral tension R = 0, which is also mentioned by the authors as the main limitation.

Klemenc and Fajdiga (2012); Klemenc and Fajdiga (2013) proposed a technique for estimating ε-N curves and their scatter. They introduced five parameters: four parameters of the Coffin–Manson equation for the scale parameter of the Weibull distribution and the shape parameter of the Weibull distribution. Then they used GA and the differential ant-stigmergy algorithm (DASA) to estimate the five parameters on the basis of the known fatigue life data (mainly median EN curves) to obtain not only the trend of the ε-N curve, but also its scatter. Both algorithms were found to be capable of

estimating the five parameters correctly with as small a set as 25 data points of experimental data as input. GA was found to be faster than DASA.

2.7   FINITE ELEMENT ANALYSIS IN FATIGUE LIFE ESTIMATION

Maksimovic (2005) defined a computation procedure in conjunction with Neuber rule and strain-life criterions in order to predict fatigue life using analytical and finite element analysis (FEA) methods. The analytical method is easier while FEM is adequate for application with complex structures. FEM is favorable for detection of critical locations. Additionally, FEM is reliable method for the stress analysis for linear as well as elastic-plastic domain. Liu (2006) applied the FEA to determine the stress–strain response of rolling contact of rail head and railroad wheel and then used the S-N curves to predict the fatigue life. The parametric study was performed to study the effect of geometrical parameters and material parameters on fatigue damage. Ninic (2006) was used FEA to determine the stress–strain response around the critical areas of lubrication holes and shaft minor diameter transition of transmission shaft. These stress–strain results were used for fatigue life estimation by fatigue life criterion i.e. McDiarmid's criterion, Carpinteri and Spangoli's criterion and fatigue damage function. Ås (2006) was used FEA simulation to determine the topography of rough surface from white light interferometry. The geometry of grooves were modelled and fine meshed for stress determination around the groove area. Finite element analysis of the rough surfaces showed a clear trend that crack initiation occurred in grooves where stresses are higher than for other grooves. The fatigue life was estimated with the stress fields from the surface geometry topography measurements. This detailed stress fields in turn improved the characterization of fatigue initiation life.

Krishnapillai and Jones (2009) applied FEA in fatigue based optimization study. A parametric study was performed on the geometric parameters and the effects were studied on the performance against fatigue life. Tarar (2008) proposed a new finite element procedure from an energy-based fatigue life prediction framework developed for prediction of axial, bending and multi-axial fatigue life. The prediction of fatigue life through energy analysis consists of constitutive laws, which correlate the cyclic energy to the amount of energy required to fracture. The energy expressions that

construct the new constitutive laws were integrated into finite elements for fatigue life prediction of structural components subjected to axial, bending and multi-axial cyclic loads. Miao et al. (2009) implemented FEA in a multi-disciplinary method to estimate fatigue for the railway car body. FEA along with multibody simulation was performed to simulate the rigid and flexible dynamic property of the full vehicle complex system. Then, optimization of the vehicle body was performed based on results of multi-body simulation. This method proved to be an alternative to expensive field dynamic tests.

Zhang et al. (2012) developed an FEA based method coupled with a non-linear continuum damage model and validated for uniaxial and multiaxial plain fatigue, un-notched and notched conditions. The method was applied to a fretting fatigue of round on flat surface for the effect of slip on life. Susmel et al. (2014a) applied the FEA with sub-modelling technique to generate the stress fields around the notch areas. Then, the fatigue life is estimated by post processing the stress results. Khandelwal and El-Tawil (2014) implemented coupling the plasticity damage model and explicit finite element analysis program. A set of model parameters are proposed for ASTM A36 steel and the simulation results. The finite element analysis was shown that the proposed constitutive model able to successfully predict the failure due to ductile fracture under varied stress-states by comparing the with experimental results.

Ince and Glinka (2014) implemented a finite element-integrated simplified analytical modeling approach to determine the stress–strain response at notch area of notched shaft. It is used to assess the prediction capability of the proposed fatigue damage models by comparing with experimental results. Gates and Fatemi (2014) implemented the finite element analysis with linear elastic analysis with Neuber correction and elastic–plastic analysis for determining the notch root stress–strain quantities. It was used them to estimate fatigue life using the Fatemi Socie fatigue parameter and successfully correlate the predicted fatigue life results with experimental results.

2.8   SUMMARY

A review is presented about the periodic development of fatigue life estimation modelling. The reviewed models incorporate various methods to estimate fatigue damage, including different combinations of stress and strain quantities, mean stress effects, critical planes, micro-stresses, virtual strain energy, enclosing surface methods, 5D Euclidean space, optimization algorithms, etc. New concepts developed in order to model the fatigue behaviour of materials are reviewed and it is observed that the proposed models are still limited to certain conditions, i.e., high-cycle or low-cycle fatigue, uniaxial and multiaxial loading, constant and variable amplitude loading and material type such as brittle, hard and ductile materials. However, no model can yet be declared as a universal or generalized model for various loading and material conditions, so additional research and development work is still needed for accurate and reliable multiaxial fatigue life estimation. The main objective of this review is to explore the new concepts and methods to estimate fatigue life, unlike the classical ones which do not lead to any universal or generalized fatigue models. The most promising methods for fatigue life estimation from the recently proposed models involve the application of evolutionary optimization algorithms like GA, ANN, DASA etc. The most attractive feature of these types of models is the inherent flexibility in model training/calibration due to the application of evolutionary algorithms. This can lead to more flexible formulation of model expressions with a higher number of parameters. The concept of using optimization algorithms should be explored in detail to utilize the full potential of this simple, versatile and easy to implement technique for fatigue life estimation modelling. In the next chapter a new method is proposed to incorporate the genetic algorithm in a fatigue life estimation method which is capable of handling a variety of loading and material conditions.

CHAPTER 3

METHODOLOGY

3.1   INTRODUCTION

This chapter describes the identification of the stress and strain parameters to be used in modelling the proposed fatigue model expressions. The two developed expressions and the process flow of the proposed model are explained. Details of the application of a genetic algorithm in the calibration of the proposed model equations and critical plane identification are presented. The validation procedure of the proposed model is described with the loading conditions, materials and details of FEA models being used and mesh convergence study is also presented.

3.2   FLOW CHART OF THE STUDY

The flow chart of the study is presented in Figure 3.1. This flow chart shows the flow of steps in the development and evaluation of the proposed model. Stress and strain parameters are identified to include in the proposed model from stress–strain history results. These parameters are able to capture the effects of proportionality of stress, mean stress effects and strain hardening. The selected stress–strain parameters are assembled in fatigue parameter expressions in the form of strain energy named as Model-1 and summation of terms named as Model-2, an expression to account the evolution of stresses and an expression to quantify the damage. A genetic algorithm based calibration method is developed to determine the value of coefficients and material constants based on previously published experimental fatigue life results. A comparison of prediction accuracy and ease of calibration between the proposed model Model-1 and Model-2 are performed. Performance study of the proposed fatigue model

with the selected fatigue parameter expression is done against various material and loading conditions. Results are analyzed and findings of the study are concluded on the basis of the obtained results.
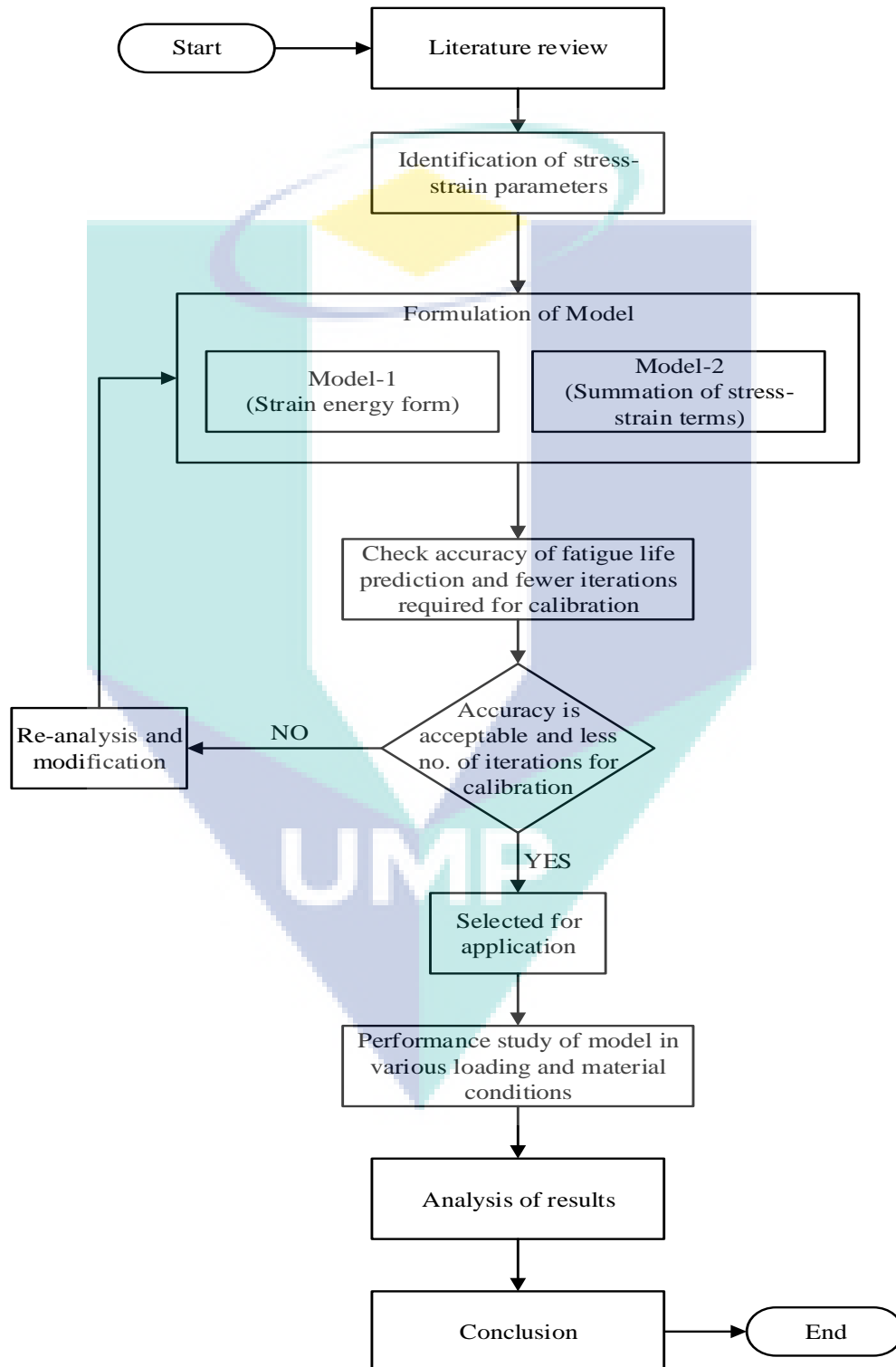
Figure 3.1: Flow chart of the study.

3.3   STRESS AND STRAIN PARAMETERS

From more than 50 years, researchers have put a great amount of effort into proposing new models to estimate fatigue life that can deal with various complex real-world scenarios, as reviewed in Chapter 2. But in the end it all comes down to the fact that the proposed expressions to determine equivalent stress / strain or fatigue parameters are combinations of certain stress and strain quantities, a fact also identified by (Socie and Marquis, 2000). A list of highlighted parameters is given in Table 3.1. The variables mentioned in Table 3.1 are those that have been most commonly used to establish the fatigue models studied in chapter 2. As mentioned by (Socie and Marquis, 2000; Ince, 2012), successful models have included features like being simple, efficient and applicable to various types of loading conditions, applicable in low and high cycle regimes, being able to include mean stress effect and able to handle non-proportional hardening effects, being physically correct from the continuum mechanics viewpoint, without any additional material coefficients, being load path dependent and able to determine failure planes and include tensile and shear failure modes. In their respective models, the stress / strain quantities identified in Table 3.1 define the mentioned features that are required for a model to able to be acknowledged as ready for real-world applications.

3.3.1 Selection of Stress and Strain Parameters

The first and most important requirement put forward for the proposed model is to keep the implementation procedure simple and easy to use. Thus the stress and strain quantities which are to be used in defining the proposed model should be easily determined. Keeping this in focus, stress–strain parameters are selected such that they can be directly calculated from the stress–strain tensor defining the state of stress and strain at a predetermined location. This avoids the extra calculation effort needed for secondary stress–strain quantities like 5D Euclidean stress, stress invariants, stress amplitudes derived from enclosing surface methods etc.

Table 3.1: List of stress / strain components used in fatigue models.

Stress / Strain parameter		References
τ_{oct}	Octahedral stress (von Mises)	Sines (1955, 1959), Crossland (1956)
$\Delta\tau/2, \tau_a$	Shear stress amplitude	Findley (1959), McDiarmid (1991, 1994), Liu (1993), Glinka et al. (1995), Mahadevan and Liu (2005), Ninic and Stark (2007)
$\Delta\tau_{max}$	Maximum shear stress range	McDiarmid (1991, 1994)
$\Delta\gamma, \Delta\gamma_{max}$	Maximum shear strain range	Brown and Miller (1973); Kandil et al. (1982), Fatemi and Socie (1988), Liu (1993), Chu (1995), Glinka et al. (1995), Li et al. (2011), Ince (2012)
$\tau_{n,max}$	Shear stress on considered plane	Chu (1995), Glinka et al. (1995), Papuga and Ruzicka (2008), Ince (2012)
$\Delta\varepsilon_n$	Normal strain range	Smith et al. (1970), Brown and Miller (1973), Liu (1993), Chu (1995), Li et al. (2011), Ince (2012)
σ_h	Hydrostatic stress	Sines (1955), Sines (1959), Crossland (1956), Dang Van (1993), Mahadevan and Liu (2005)
$\sigma_{n,max}$	Maximum normal stress	Findley (1959), McDiarmid (1991), Smith et al. (1970), Fatemi and Socie (1988), Chu (1995), Glinka et al. (1995), Papuga and Ruzicka (2008), Li et al. (2011), Ince (2012)
σ_m	Mean normal stress	Morrow and Socie (1980); Papuga and Ruzicka (2008)
I_1, I_2, I_3 (a – amplitude, m – mean)	Stress invariants	Horstemeyer and Gokhale (1999), Vu et al. (2010), Brighenti and Carpinteri (2012)
J_1, J_2, J_3	Deviatoric stress invariants	Horstemeyer and Gokhale (1999), Vu et al. (2010), Brighenti and Carpinteri (2012)

According to the above-mentioned criteria, the stress–strain parameters selected for the proposed model are shear strain range ($\Delta\gamma$), maximum shear stress (τ_{max}), normal strain range ($\Delta\varepsilon$), maximum normal stress ($\sigma_{n,max}$) and mean stress (σ_{mean}). These parameters are used in various already recognized models to define plasticity, non-proportionality of load, mean stress effects, strain hardening etc. The shear strain range ($\Delta\gamma$) is the maximum shear strain range on a plane having the maximum fatigue parameter value, i.e. the critical plane. Brown and Miller (1973), Fatemi and Socie

(1988), and Liu (1993) used the cyclic shear strain in their models as it helps cracks to nucleate and also cyclic plasticity can be included through it. Maximum shear stress (τ_{max}) is used by Chu (1995), Glinka et al. (1995) and Ince (2012), to capture mean stress effects and for handling torsion test data. In the proposed model it is the maximum resultant shear stress of the two components acting on the critical plane. The normal strain range ($\Delta\varepsilon$) is the maximum normal strain range on the critical plane. It is used by Smith et al. (1970), Liu (1993), Ince (2012) and Ince and Glinka (2014) to include fatigue failure of the material failing on planes having the maximum tensile strain or stress. Maximum normal stress ($\sigma_{n,max}$), i.e. on the critical plane, is included to reflect mean stress effects and non-proportional hardening. As it was found by Fatemi and Socie (1988) that strain terms alone cannot reflect the mean stress effect, Smith et al. (1970) define load path dependent hardening, the difference between tension and torsion loading. Mean stress (σ_{mean}) on many occasions is included as Morrow correction (Morrow and Socie, 1980), but sometimes directly as a term of fatigue parameter, as by Papuga and Ruzicka (2008). In the proposed model, mean stress is included as shear (τ_{mean}) and normal (σ_{mean}) mean stresses on the critical plane.

3.3.2 Stress and Strain on a Plane

To evaluate the fatigue damage caused by applied loads on an arbitrary plane, the local stress and strain components acting on that plane must be known. The fatigue damage parameter on a plane can be expressed in terms of stress and strain quantities as a function of the plane orientation. Stress and strain at a point are defined by an array of nine components each shown in Eqs. (3.1)–(3.2), where only six of each are needed because $\tau_{xy} = \tau_{yx}$, $\tau_{yz} = \tau_{zy}$, $\tau_{xz} = \tau_{zx}$ for isotropic materials and similarly for strain.

$$\sigma = \begin{bmatrix} \sigma_x & \tau_{xy} & \tau_{xz} \\ \tau_{yx} & \sigma_y & \tau_{yz} \\ \tau_{zx} & \tau_{zy} & \sigma_z \end{bmatrix} \tag{3.1}$$

$$\varepsilon = \begin{bmatrix} \varepsilon_x & \gamma_{xy}/2 & \gamma_{xz}/2 \\ \gamma_{yx}/2 & \varepsilon_y & \gamma_{yz}/2 \\ \gamma_{zx}/2 & \gamma_{zy}/2 & \varepsilon_z \end{bmatrix} \tag{3.2}$$

Now to define the stresses and strains on an arbitrary plane in three dimensions located by angle θ and ϕ, as shown in Figure 3.2. Two coordinate transformations are needed to transform stresses from the XYZ coordinate system to the X'Y'Z' coordinate system. The direction cosines for these transformations are given in Table 3.2.

3.3.3 Stress Strain Plasticity Modelling

Generally, components are designed such that the stresses should never exceed the yield stress. However, local plastic deformations are common in stress concentration areas under cyclic loadings. Even though the material behaviour in the net section area is in the elastic range, the stress–strain response at the concentration areas may often show elastic-plastic behaviour. The stress (σ) strain (ε) elastic-plastic relationship of materials for FEA is defined by the Romberg–Osgood relationship expressed in Eq. (3.5) or data acquired from stress–strain curves available in already published literature.

$$\varepsilon = \frac{\sigma}{E} + \left(\frac{\sigma}{K}\right)^{1/n} \tag{3.5}$$

where K = strength coefficient, n = strength exponent and E = elastic modulus.

Table 3.2: Direction cosines for coordinate transformation.

	X	Y	Z
X'	$a_{11} = \cos\theta \sin\phi$	$a_{12} = \sin\theta \sin\phi$	$a_{13} = \cos\phi$
Y'	$a_{21} = -\sin\theta$	$a_{22} = \cos\theta$	$a_{23} = 0$
Z'	$a_{31} = -\cos\theta \cos\phi$	$a_{32} = -\sin\theta \cos\phi$	$a_{33} = \sin\phi$
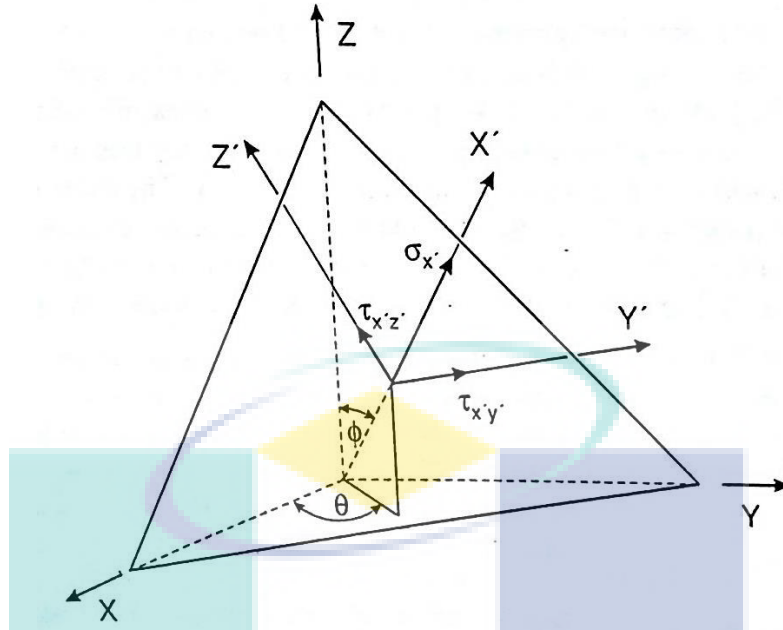
Figure 3.2: Plane location defined by angle θ and ϕ.

The following are the transformation equations in the form of matrices for stress Eq. (3.3) and strains Eq. (3.4):

$$\begin{bmatrix} \sigma_{x'} \\ \sigma_{y'} \\ \sigma_{z'} \\ \tau_{x'y'} \\ \tau_{x'z'} \\ \tau_{y'z'} \end{bmatrix} = \begin{bmatrix} a_{11}^2 & a_{12}^2 & a_{13}^2 & 2a_{11}a_{12} & 2a_{11}a_{13} & 2a_{13}a_{12} \\ a_{21}^2 & a_{22}^2 & a_{23}^2 & 2a_{21}a_{22} & 2a_{21}a_{23} & 2a_{23}a_{22} \\ a_{31}^2 & a_{32}^2 & a_{33}^2 & 2a_{31}a_{32} & 2a_{31}a_{33} & 2a_{33}a_{32} \\ a_{11}a_{21} & a_{12}a_{22} & a_{13}a_{23} & (a_{11}a_{22}+a_{12}a_{21}) & (a_{13}a_{21}+a_{11}a_{23}) & (a_{12}a_{23}+a_{13}a_{22}) \\ a_{11}a_{31} & a_{12}a_{32} & a_{13}a_{33} & (a_{11}a_{32}+a_{12}a_{31}) & (a_{13}a_{31}+a_{11}a_{33}) & (a_{13}a_{32}+a_{12}a_{33}) \\ a_{21}a_{31} & a_{22}a_{32} & a_{23}a_{33} & (a_{21}a_{32}+a_{22}a_{31}) & (a_{23}a_{31}+a_{21}a_{33}) & (a_{22}a_{33}+a_{23}a_{32}) \end{bmatrix} \begin{bmatrix} \sigma_x \\ \sigma_y \\ \sigma_z \\ \tau_{xy} \\ \tau_{xz} \\ \tau_{yz} \end{bmatrix} \quad (3.3)$$

$$\begin{bmatrix} \varepsilon_{x'} \\ \varepsilon_{y'} \\ \varepsilon_{z'} \\ \frac{\gamma_{x'y'}}{2} \\ \frac{\gamma_{x'z'}}{2} \\ \frac{\gamma_{y'z'}}{2} \end{bmatrix} = \begin{bmatrix} a_{11}^2 & a_{12}^2 & a_{13}^2 & 2a_{11}a_{12} & 2a_{11}a_{13} & 2a_{13}a_{12} \\ a_{21}^2 & a_{22}^2 & a_{23}^2 & 2a_{21}a_{22} & 2a_{21}a_{23} & 2a_{23}a_{22} \\ a_{31}^2 & a_{32}^2 & a_{33}^2 & 2a_{31}a_{32} & 2a_{31}a_{33} & 2a_{33}a_{32} \\ a_{11}a_{21} & a_{12}a_{22} & a_{13}a_{23} & (a_{11}a_{22}+a_{12}a_{21}) & (a_{13}a_{21}+a_{11}a_{23}) & (a_{12}a_{23}+a_{13}a_{22}) \\ a_{11}a_{31} & a_{12}a_{32} & a_{13}a_{33} & (a_{11}a_{32}+a_{12}a_{31}) & (a_{13}a_{31}+a_{11}a_{33}) & (a_{13}a_{32}+a_{12}a_{33}) \\ a_{21}a_{31} & a_{22}a_{32} & a_{23}a_{33} & (a_{21}a_{32}+a_{22}a_{31}) & (a_{23}a_{31}+a_{21}a_{33}) & (a_{22}a_{33}+a_{23}a_{32}) \end{bmatrix} \begin{bmatrix} \varepsilon_x \\ \varepsilon_y \\ \varepsilon_z \\ \frac{\gamma_{xy}}{2} \\ \frac{\gamma_{xz}}{2} \\ \frac{\gamma_{yz}}{2} \end{bmatrix} \quad (3.4)$$

Unlike the uniaxial cycle stress–strain curve, the multiaxial stress–strain state during cyclic plastic deformation requires a cyclic plasticity model to model the multiaxial stress–strain behaviour of a material. An appropriate cyclic plasticity model includes three major components: a yield function, flow rule and hardening rule. A yield function describes the combinations of stress that are needed to initiate plastic

deformation, a flow rule defines the relationship between stresses and plastic strains during plastic deformation, and a hardening rule describes how the yield surfaces are altered due to plastic strain.

Yield Function

The yield criterion determines the stress level at which yielding is initiated. For multi-component stresses, this is represented as a function of the individual components, $f(\sigma_{ij})$, and yield strength σ_y. The yield function $F(\sigma_{ij})$ is defined as Eq. (3.6).

$$F(\sigma_{ij}) = f(\sigma_{ij}) - \sigma_y = 0 \tag{3.6}$$

Flow Rule

The flow rule determines the direction of plastic straining and is defined as Eq. (3.7), as proposed by (Drucker, 1952), where $d\varepsilon_{ij}$ is plastic strain increment, F is a yield function and $d\lambda$ is a scalar valued function (which determines the amount of plastic straining). This postulate implies that the increment of plastic strain is in the normal direction to the yield surface during plastic deformation.

$$d\varepsilon_{ij}^p = d\lambda \frac{\partial F}{\partial \sigma_{ij}} \tag{3.7}$$

Hardening Rule

The hardening rule describes the changing of the yield surface with progressive yielding, so that the conditions (i.e. stress states) for subsequent yielding can be established. Generally, there are two alternatives to explain the evolution of the yield surface: isotropic hardening where the yield surface expands with plastic loading, and kinematic hardening where the yield surface translates without any expansion with plastic loading. In a general form, the hardening rule can be written as Eq. (3.8), where α_{ij} defines the movement of the centre of the yield surface, $g(\varepsilon^p)$ is a function relating

plastic strain to yield strength, and f() is commonly the von Mises yield function. When $g(\varepsilon^p)$ is a constant equal to σ_{ys}^2, the hardening is kinematic. When $\alpha_{ij} = 0$, it is isotropic.

$$F = f(\sigma_{ij} - \alpha_{ij}) + g(\varepsilon^p) = 0 \qquad (3.8)$$

Isotropic hardening describes the expansion of the yield surface during plastic deformation. In other words, the yield surface grows. However, the centre of the yield surface remains fixed. Such behaviour for the stress–strain curve is plotted in Figure 3.3. In kinematic hardening, the yield surface is allowed to translate in stress space with no change in size or shape. Kinematic hardening on the stress–strain curve is shown in Figure 3.4. Real materials exhibit some aspects of both kinematic and isotropic hardening until they become cyclically stable. After stabilization, they exhibit only kinematic hardening. If transient behaviour is not of interest, as in most cases of fatigue analysis, a cyclically stable material is assumed and only kinematic hardening models are used (Socie and Marquis, 2000).
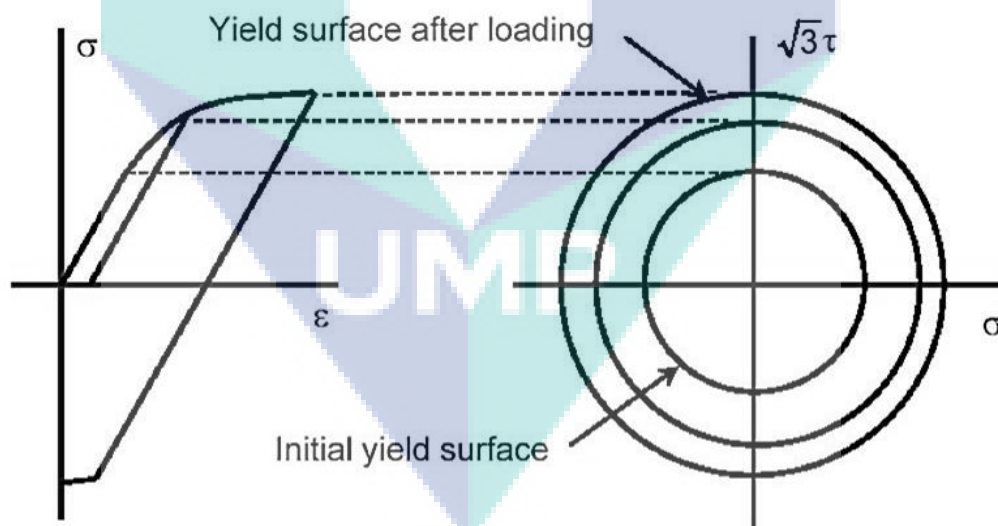
Figure 3.3: Yield surface after isotropic hardening.
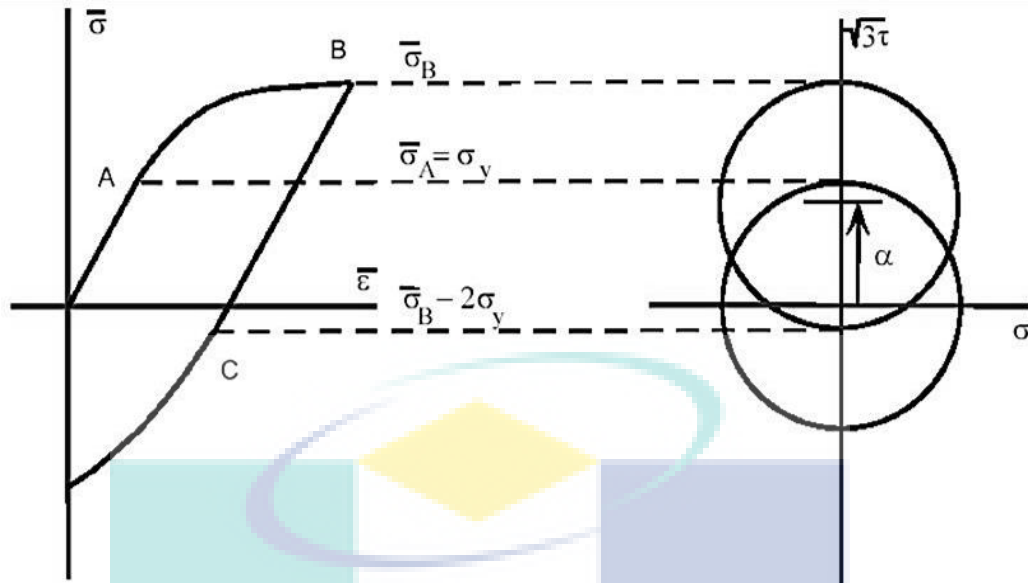
Figure 3.4: Yield surface after kinematic hardening.

3.4   PROPOSED MULTIAXIAL FATIGUE MODELS

A significant work has been done in the last century to develop models to estimate multiaxial fatigue damage as discussed in Chapter 2. However, critical plane-based damage parameters have gained wide acceptance due to their reasonably accurate life prediction capabilities. But, a universally acceptable model that can perform in various type of loading and stress-strain state conditions is not proposed till now (Mahadevan and Liu, 2005; Papuga, 2011). To fulfill the requirement of general acceptance with ease of application, a critical plane-based fatigue model is proposed that considers specific planes experiencing maximum fatigue damage. The proposed model use continuum damage mechanics approach and use incremental damage sum to quantify the fatigue damage.

The proposed fatigue model is described in two forms; energy type combination and summation of stress-strain terms. The energy type combination termed as Model-1 is defined as a function of strain energy by Liu (1993); Chu (1995); Ince (2012). The function can be expressed mathematically as Eq.(3.9);

$$W = f\left(\sum\left(shear\,strain\,energy, normal\,strain\,energy\right)\right) = f\left(\Delta\gamma\cdot\tau + \Delta\varepsilon\cdot\sigma\right) \qquad (3.9)$$

Similarly, the proposed fatigue parameter 'P' is defined as a function of normal and shear strain energy;

$$P = f(\Delta\gamma \cdot \tau + \Delta\varepsilon \cdot \sigma) \tag{3.10}$$

Expression for fatigue parameter 'P' can be written as **Model-1** in Eq.(3.11);

$$P = a_1\left(\frac{\Delta\gamma \cdot \tau}{\sigma_y}\right) + a_2\left(\frac{\Delta\varepsilon \cdot \sigma}{\sigma_y}\right) - fatigue\ material\ property\ term \\ - stress\ evolution\ term \tag{3.11}$$

The form with summation of stress-strain terms is termed as Model-2. It is defined as a function of normal and shear strain range and shear and normal stress similar to the concept defined by Li et al. (2010); Li et al. (2011); Ince (2012). On the basis of this theory, the function can be expressed mathematically as Eq.(3.12);

$$W = f\left(\sum(shear\ strain\ range, shear\ stress, normal\ strain\ range, normal\ stress)\right) \\ = f(\Delta\gamma + \tau + \Delta\varepsilon + \sigma) \tag{3.12}$$

Similarly, the proposed fatigue parameter 'P' (Model-2) is defined as in Eq. (3.10);

$$P = f(\Delta\gamma + \tau + \Delta\varepsilon + \sigma) \tag{3.13}$$

Expression for fatigue parameter 'P' can be written as **Model-2** in Eq.(3.14);

$$P = a_1(\Delta\gamma) + a_2\left(\frac{\tau}{\sigma_y}\right) + a_3(\Delta\varepsilon) + a_4\left(\frac{\sigma}{\sigma_y}\right) - fatigue\ material\ property\ term \\ - stress\ evolution\ term \tag{3.14}$$

where fatigue material property 'σ_L' is defined as a representation of material fatigue limit (Brighenti and Carpinteri, 2012) and its range of values is defined from available fatigue limit data. The fatigue parameter can now be written as in Eq. (3.11);

$$P = a_1\left(\frac{\Delta\gamma \cdot \tau}{\sigma_y}\right) + a_2\left(\frac{\Delta\varepsilon \cdot \sigma}{\sigma_y}\right) - \frac{\sigma_L}{E} - stress \; evolution \; term \qquad (3.15)$$

And Eq.(3.14) can be written as;

$$P = a_1(\Delta\gamma) + a_2\left(\frac{\tau}{\sigma_y}\right) + a_3(\Delta\varepsilon) + a_4\left(\frac{\sigma}{\sigma_y}\right) - \frac{\sigma_L}{E} - stress \; evolution \; term \quad (3.16)$$

Stress evolution term 'ev' is added to account for hardening produced due to strain or non-proportionality during the applied loading (Ottosen et al., 2008; Noradila et al., 2013). 'ev' is expressed through Eq.(3.17), including maximum and mean stresses, where stress evolution is proportional (through material parameter 'V') to the power 'm' of damage parameter increment (dP) during a load step. Normally it is safe to assume as ($m=1$) or linear relationship between ev and dP, if no specific information is available for rate dependence on induced hardness in material.

$$ev = V.dP^m\left(\frac{\tau_{max} - \tau_m}{E}\right)\left(\frac{\sigma_{max} - \sigma_m}{E}\right) \qquad (3.17)$$

Critical plane is defined for both cases with maximizing the value of "P" on a plane, with coefficients of stress-strain quantities ($a_1 - a_4$) taken as one and neglecting σ_L and ev terms. Based on the assumptions, all stress-strain components contribute in fatigue damage and plane with the maximum combined effect of these components are the plane with maximum fatigue damage. Elastic modulus 'E' and yield strength 'σ_Y' is for normalizing. Finally, the proposed parameter expression for Model-1 and Model-2 can be written as;

Model-1:
$$P = a_1 \left(\frac{\Delta\gamma.\tau_{\max}}{\sigma_y} \right) + a_2 \left(\frac{\Delta\varepsilon.\sigma_{n,\max}}{\sigma_y} \right) - \frac{\sigma_L}{E} - ev \qquad (3.18)$$

Model-2:
$$P = a_1 \cdot \Delta\gamma. + a_2 \cdot \left(\frac{\tau_{\max}}{\sigma_Y} \right) + a_3 \, \Delta\varepsilon + a_4 \cdot \left(\frac{\sigma_{n,\max}}{\sigma_Y} \right) - \frac{\sigma_L}{E} - ev \qquad (3.19)$$

The incremental damage 'D_n' in each load step is defined as a function of damage parameter 'P' and its increment 'dP' (Ottosen et al., 2008). It can be mathematically expressed as;

$$D_n = dP \, f(P) \qquad (3.20)$$

where $f(P)$ is assumed to increase nonlinearly with damage parameter 'P' (Ottosen et al., 2008). Hence, $f(P)$ is expressed as in Eq. (3.21);

$$f(P) = K \cdot P^R \qquad (3.21)$$

where 'K' and 'R' are material parameters. Hence D_n is proportional (through 'K') to the fatigue parameter 'P' (to the power 'R') multiplied by increment in fatigue parameter 'dP' (Ottosen et al., 2008). Hence, substituting Eq.(3.21) in Eq.(3.20) we have the expression for damage D_n as Eq.(3.22).

$$D_n = K \cdot P^R \cdot dP \qquad (3.22)$$

The process of fatigue estimation using the proposed model is highlighted in the subsequent section. The calibration and critical plane determination using the proposed methodology is explained in detail as follows.

3.5 WORKING OF PROPOSED FATIGUE MODEL

In order to implement the equations defined in the previous section for any component subjected to a multiaxial loading, an algorithm has been developed. The fatigue life estimation process is presented in Figure 3.5. The process starts with stress

analysis using FEA for each of the load cases under study. A macro in APDL was written to extract the required stress–strain values on the predetermined location susceptible to fatigue failure. As a first step, calibration of the model is conducted using the GA against the selected / experimental load cases. GA is used for calibration through an integrated software environment between the spreadsheet application and modeFrontier. The advantage of using GA is that it can handle situations with multiple minima and non-convexity properties, thus avoiding numerical instability or missing the global optimum (Davis, 1991). It uses basic concepts like random number generation, choice, switching and combination of such generated numbers to get a new population which performs better than the previous generation (Franulovic et al., 2009). This process is repeated iteratively until the required tolerance is achieved or the set number of iterations are completed and thus the optimal condition can be achieved (Gantovnik et al., 2003). In the present research GA is implemented by using a Multi-objective Genetic Algorithm with II designating the proprietary version (MOGA-II). A macro written in Visual Basic programing language is added in MS-Excel to implement the proposed fatigue model equations.

Two methods for determining the critical plane are implemented. One is the conventional incremental angle with a certain step size to locate the maximum fatigue parameter plane, and the second is the newly developed method based on GA optimization. The calibrated model is then implemented in ANSYS using a macro developed in APDL to predict the fatigue life. ANSYS Parametric Design Language is a scripting language that can be used to build any FEA model in terms of parameters (variables). APDL encompasses all ANSYS commands as part of the scripting language, as well as a wide range of other features such as repeating a command, macros, if-then-else branching, do-loops, and scalar, vector and matrix operations. APDL combines ANSYS commands with FORTRAN-like functions and can be used to do many of the operations done by user-subroutines in other FE codes.
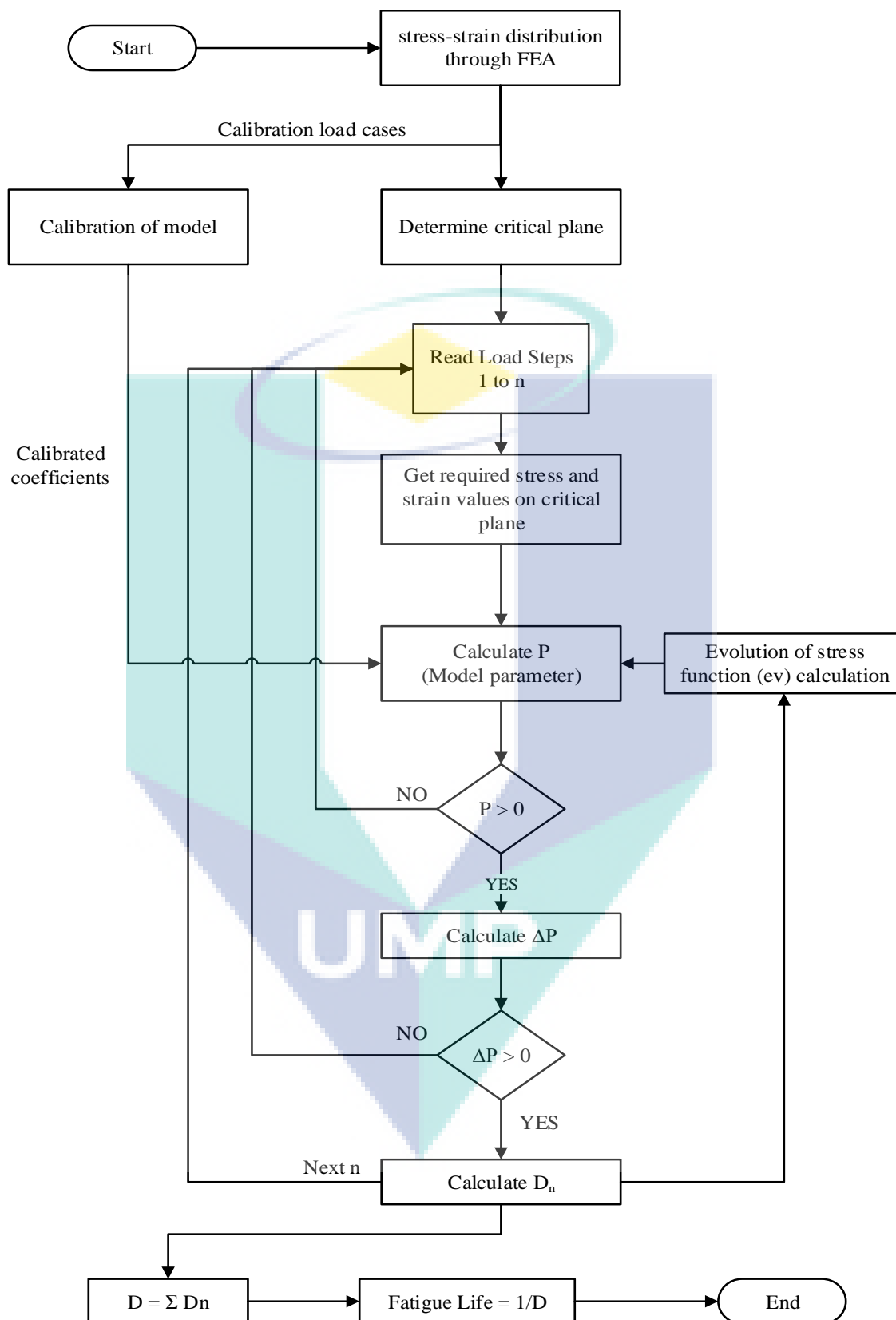
Figure 3.5: Fatigue life estimation process for the proposed model.

The fatigue life estimation process is summarized as follows:

Determine the state of stress–strain time history at the location susceptible to fatigue failure through structural analysis using FEA.

1. ***If*** *applied load is to be used for calibration then determine coefficients as per procedure defined in Section 3.7.*

2. ***For*** *fatigue life estimation, determine critical plane as per Section 3.7.1.*

3. ***For*** *load step 1 to n;*

    a. *Get stress–strain values on critical plane from FEA results (Appendix A4).*

    b. ***Calculate P using Model-1 or Model-2 :*** *P defines the state of material at certain load step.*

    c. ***If P > 0 then :*** *The stress-strain state has overcome the material threshold defined by the fatigue material property term and evolution of stress term, and cause damage to the material.*

       calculate ΔP : *Change in P from last load step*

       else;

       Next load step (n+1) : *For P < 0 there will be no damage.*

    d. ***If ΔP > 0 then :*** *As P is defined as an incremental function and if* $\Delta P \leq 0$ *it shows that no damage occur in this step as there is no positive increment in P.*

       calculate 'ev' as per Eq.(3.17) : *With a damage occurred in material there is effects on the stress response in material*

       calculate damage for each load step 'Dₙ' as per Eq.(3.22)

       else;

       Next *load step (n+1).*

    Next *load step (n+1)*

4. *Calculate total damage from the applied load profile (D=Σ Dₙ.)*

5. *Calculate fatigue life as 1/D (no. of repetitions of applied load profile)*

3.6   MULTI-OBJECTIVE GENETIC ALGORITHM

A multi-objective genetic algorithm (MOGA-II) is used for optimization. A randomly generated set between defined ranges serves as the "*initial population*". This initial population consists of sets of chromosomes. The chromosomes evolve during several iterations called generations (Routara et al., 2012). The best individuals are evaluated, recombined and mutated to constitute a new population. MOGA was the first generation genetic algorithm (Fonseca and Fleming, 1993), while MOGA-II is a second generation evolutionary algorithm with elitism. The work flow chart for the MOGA-II is given in Figure 3.6. The basic concept of using a genetic algorithm for optimization is that the genetic collection of a given population contains better solutions to a given problem. The general operators applied in evolutionary algorithms are selection, mutation and crossover. The MOGA-II algorithm implements a fourth operator, i.e. multi-search elitism. The selection operator shifts designs to the next generation, selection being based on the best fitness of the function. Designs with a higher fitness value are more likely to be replicated into the next generation, ensuring a higher survival probability for the more fit solutions. The new generations are generated utilizing the crossover and mutation technique. Crossover splits chromosomes in two and then combines one half of each chromosome with the other pair. Mutation involves flipping a single bit of a chromosome (Routara et al., 2012). The chromosomes are then evaluated against certain fitness criteria and the best ones are retained while the others are rejected. The elitism operator is able to preserve all non-dominated solutions from the initial population, thus enhancing the convergence speed. Pseudo codes for the GA-based optimization algorithms are given as follows:

***Algorithm 1*:   Pseudo code for MOGA-II (overall algorithm main loop)**

Input: *Np (Population size)*

                G (Maximum number of generations)

Output: *Non-dominated set A*

1.   *Objective functions $f_1(x) \ldots \ldots .. f_k(x), x = (x_1 \ldots \ldots .. x_n)$*

2.   *Initialize the population $P_o = (x_1 \ldots \ldots .. x_n)$ (Initial population = DOE)*

3.   *Elite set $E = \Theta$ (Null set). Set g = 0.*

> **for** $j = 1$ to N (points on Pareto frontier)
>
> > **while** $(g < G)$

4. *Evaluate fitness (objective values)*

5. *Assign rank on the basis of Pareto dominance-'Sort'*

6. *Generate next generation population*

   a. *Combine both population P_o and elite set E into $P' = P_o U E$*

   b. *If the cardinality of P' is greater than cardinality of P_o reduce P' by removing exceeding individuals.*

   c. *Perform the evolution of P' to P'' by applying MOGA reproduction operators randomly (selection, single-point crossover, directional crossover, bit flip mutation) (with regard to the pre-defined operator probabilities).*

7. *If $g > G$ or another stopping criterion is satisfied then set A equal to the set of decision vectors represented by the non-dominated individuals in P''. Stop.*

8. *Evaluate objective values of population P''.*

9. *Assign ranks to P'' individuals based on Pareto dominance. 'Sort'.*

10. *Copy all non-dominated designs from P'' to E. 'Sort'.*

11. *Remove the duplicated and dominated designs from E.*

12. *Resize the elite set E if it is bigger than generation size N by randomly removing the exceeding individuals.*

13. *Repeat evaluation of the objective values (step 4) for the sets of P'' with P'' as the new population.*

14. *Continue till termination.*

Algorithm 2: Pseudocode for reproduction used in MOGA-II

with *(individual $Ind_i \in$ generation G)* **do**

    choose reproduction operator

    if *(operator is one-point crossover)* **then**

        $j \leftarrow$ TournamentSelection, where $j \neq i$

        $NewInd_i \leftarrow$ OnePointCrossover (Ind_i, Ind_j)

    else if *(operator is directional crossover)* **then**

        $j \leftarrow$ RandomWalk(i)

        $k \leftarrow$ RandomWalk(i), where $k \neq j \neq i$

NewInd$_i$ ← DirectionalCrossover(Ind$_i$, Ind$_j$, Ind$_k$)

else if *(operator is mutation)* **then**

NewInd$_i$ ← Mutation (Ind$_i$)

else if *(operator is selection)* **then**

NewInd$_i$ ← Ind$_i$

end if

end with
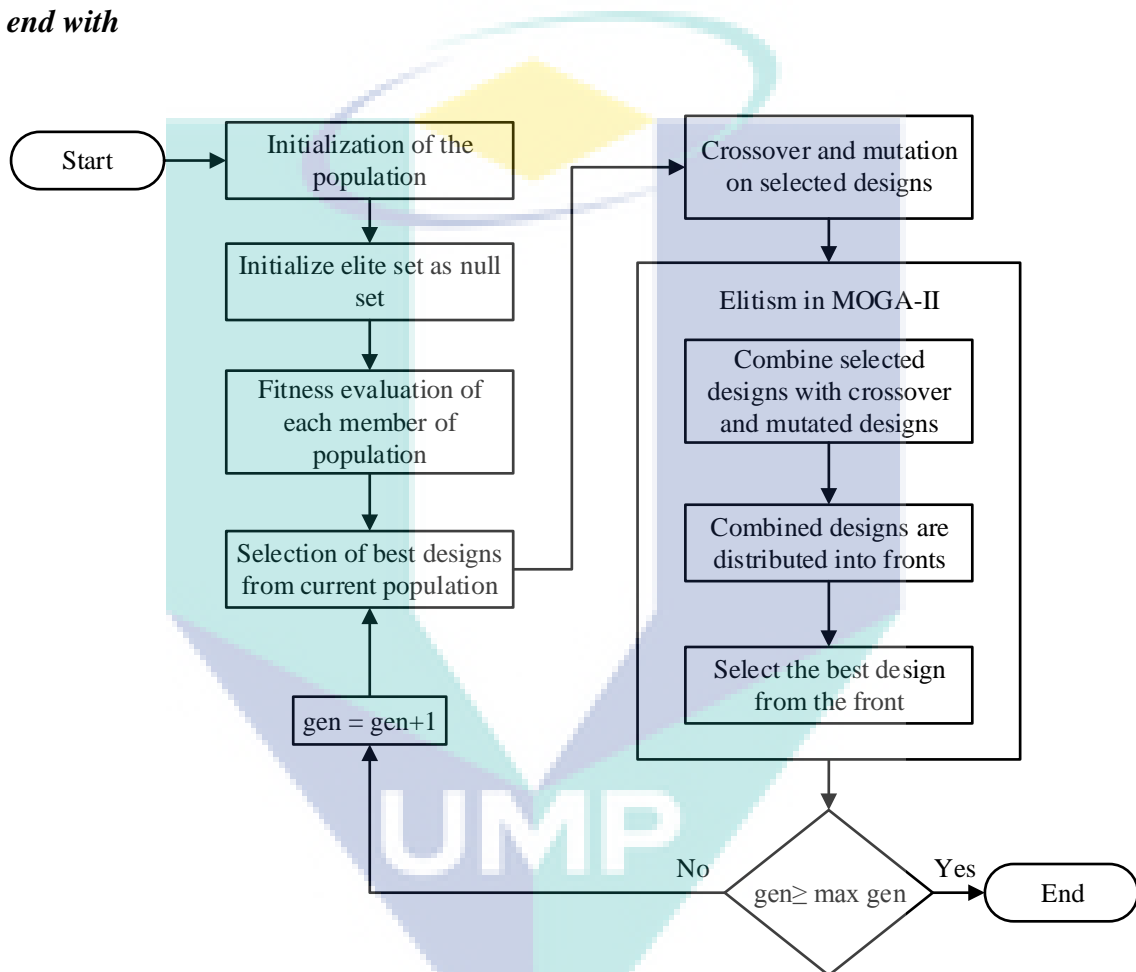
Figure 3.6: MOGA-II algorithm flow chart.

3.7   MODEL CALIBRATION METHOD

In order to calibrate the formulated model equations, the coefficients in Eq. (3.9) or Eqs. (3.10)–(3.12), i.e. a_1-a_4, σ_L, V, m, K and R, have to be calculated by using experimental life data for known loading conditions. The steps involved in the calibration process are as follows, and shown in Figure 3.7:

1. *Determine the state of stress–strain time history at the location susceptible to fatigue failure through structural analysis using FEA.*

2. *The location of the critical plane is determined by maximizing the fatigue parameter 'P', as per Section 3.7.1.*

3. *Time histories of stress–strain quantities required for the fatigue model are projected on the critical plane and extracted through APDL code (Appendix A4).*

4. *The extracted stress–strain time history data is imported into an MS Excel spreadsheet, as an integrated environment between MS Excel and modeFrontier is used to apply the GA for calibration of fatigue model coefficients.*

5. *modeFrontier supplies the values of coefficients generated by the GA algorithm to MS Excel, where the damage per cycle is calculated from the stress–strain data and the coefficients supplied by the GA and sent back to modeFrontier for evaluating the objective function defined to be minimized by the GA.*

6. *After the complete run of the GA, where the number of iterations to be performed is decided by the size of the initial population and number of generations to be generated by the GA, the sets of coefficients, i.e. generated by the GA, are selected with respect to the minimum value of the objective function, as per Section 3.8.2.*

7. *The calibrated coefficients are determined by taking the weighted average of selected sets of coefficients, on the basis of the objective function, as per Section 3.9.3.*
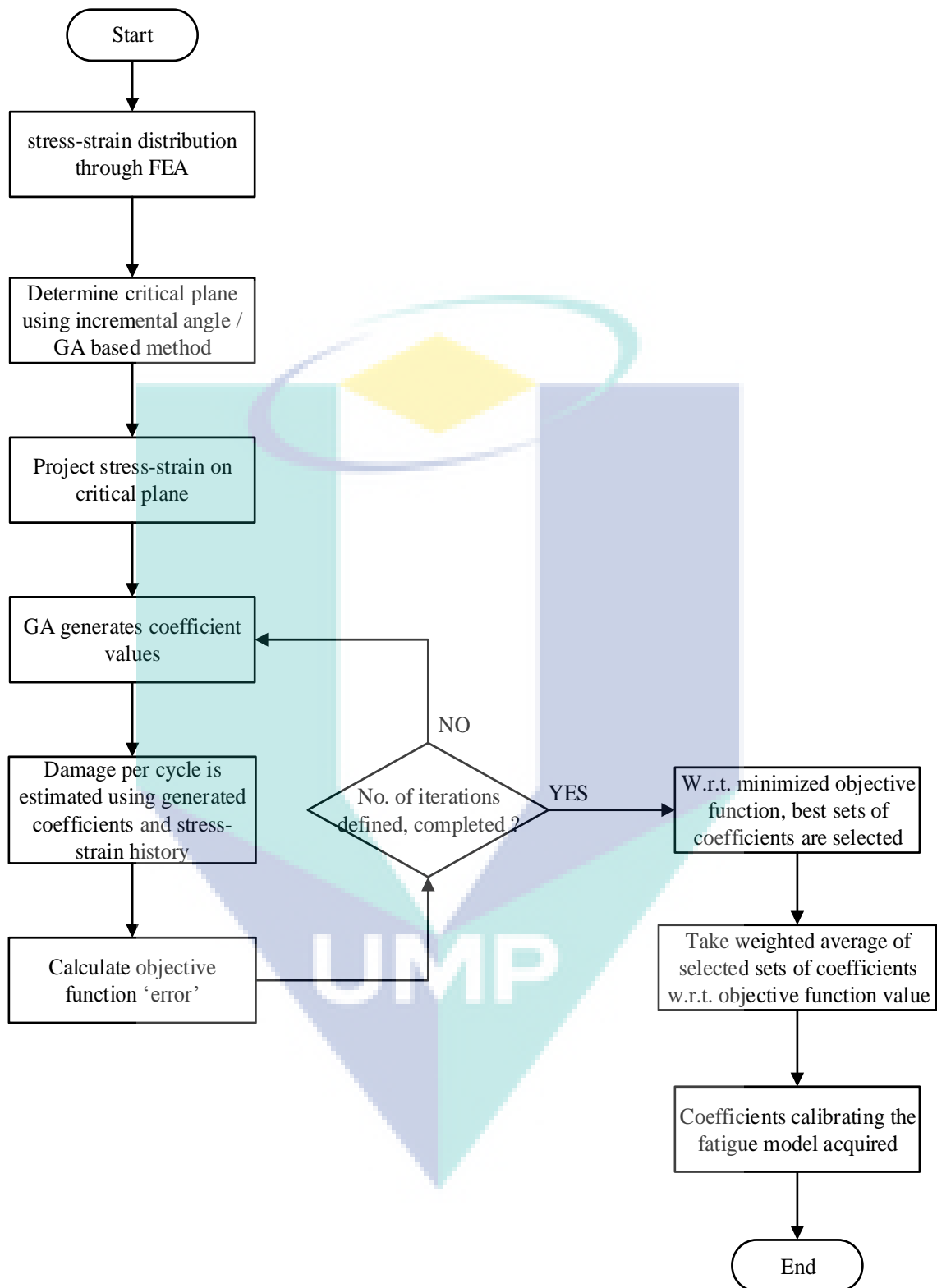
Figure 3.7: Calibration process flow chart for proposed model.

3.7.1   Incremental Angle Method

The conventional method of locating the critical plane is to calculate the fatigue parameter on each plane, i.e. located by θ and ϕ as shown in Figure 3.2, where θ and ϕ vary from 0 to 180° with a set step size. Then the plane with the maximum fatigue parameter, i.e. plane having the maximum effect of stress and strain, is declared as the plane having maximum damage. For this study, the step size for θ and ϕ is set as 5° as this gives reasonable accuracy in critical plane determination (Ince, 2012). The APDL code developed to implement the method in ANSYS is shown in Appendix A1 and the flow chart for the algorithm is shown in Figure 3.8.
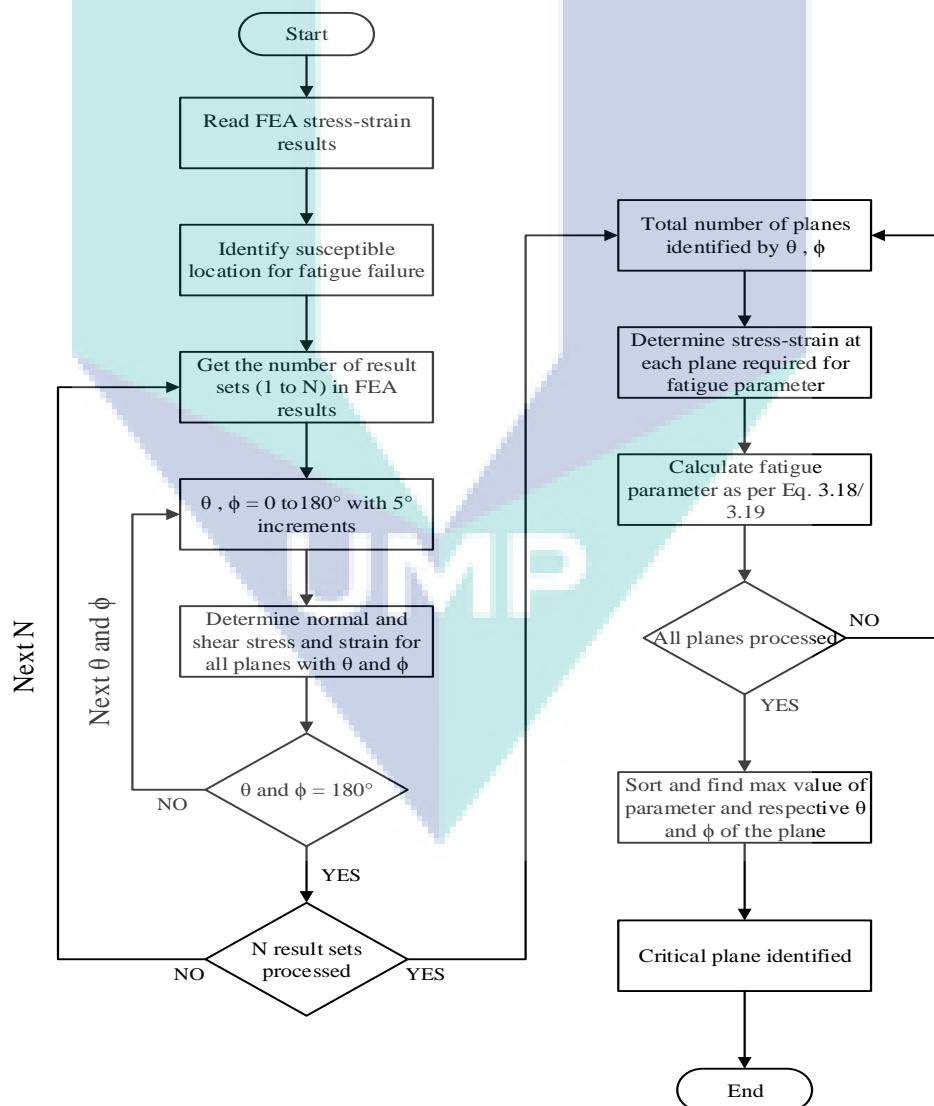
Figure 3.8: Incremental angle method flow chart.

3.7.2   Critical Plane Method

One of the major drawbacks of the conventional method of locating the critical plane, i.e. the angle increment, is that the number of iterations rises rapidly if greater accuracy is required in determining the critical plane orientation. A solution to this problem is proposed by formulating a GA-based critical plane method, which can yield very accurate results for critical plane orientation with very few iterations. Another major benefit is that more than one criterion or fatigue parameter can be simultaneously used to locate the critical plane, using the multi-objective optimization capability of the GA. To demonstrate this feature, a two-parameter method is developed where the two parameters applied are the fatigue parameter from the current study and the maximum variance of shear stress, where variance is defined by Eq. (3.23) (Susmel, 2010).

$$Var[\sigma_i(t)] = \frac{1}{T} \int_0^T [\sigma_i(t) - \sigma_{i,m}]^2 \, dt \qquad (3.23)$$

The GA set-up generates the θ and ϕ values (Figure 3.2), a VB code is developed to handle the incoming θ and ϕ values, and projects the stress–strain response time history at the susceptible location for fatigue failure, acquired from the FEA simulation, on the plane defined by θ and ϕ using direction cosines, as shown in Eq. (3.8) (Socie and Marquis, 2000), and then calculates the fatigue parameter. The calculated fatigue parameter is sent back to the GA. The GA set-up is shown in Figure 3.9, the VB coding is shown in Appendix A2 and the flow chart of the process is shown in Figure 3.10. For the two-parameter method a modified GA set-up is shown in Figure 3.11 and additional VB code to implement the maximum variance parameter is shown in Appendix A3. Note that the inherent optimization module of the maximum variance method (Susmel, 2010) is excluded here as the GA is being used for optimization. A combined flow chart highlighting the difference between the conventional incremental angle method, GA-based method and multi-parameter model is shown in Figure 3.12.
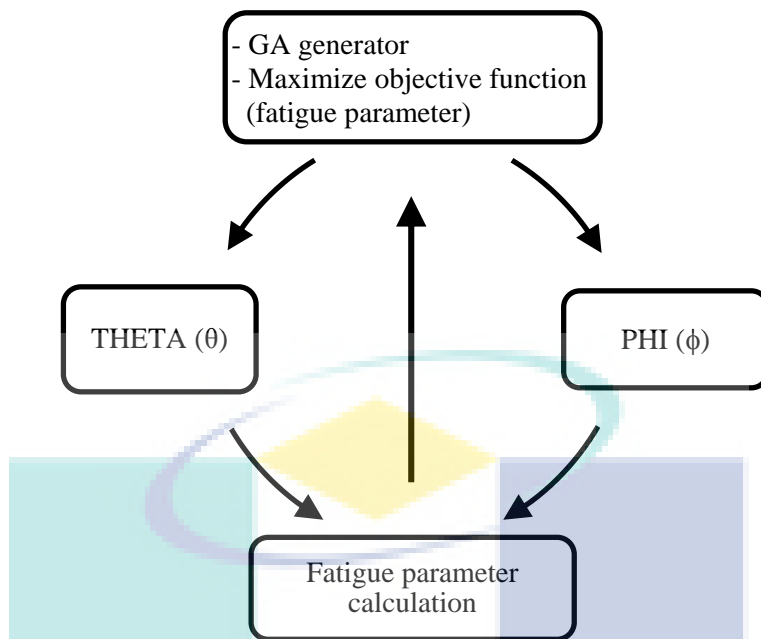
Figure 3.9: GA based critical plane set-up diagram.
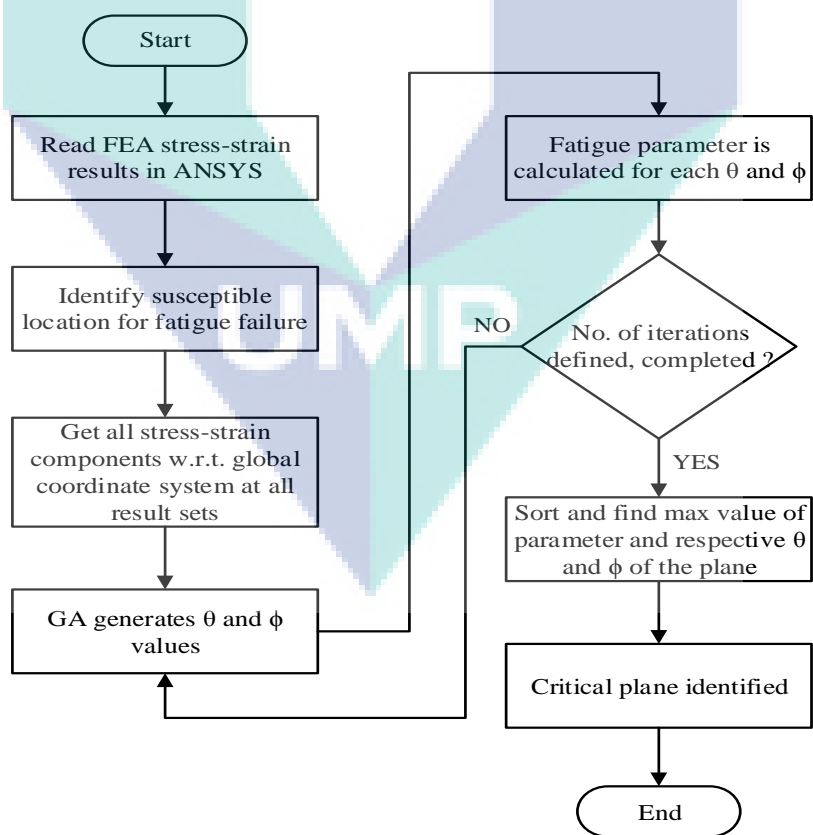
Figure 3.10: GA-based critical plane method flow chart.
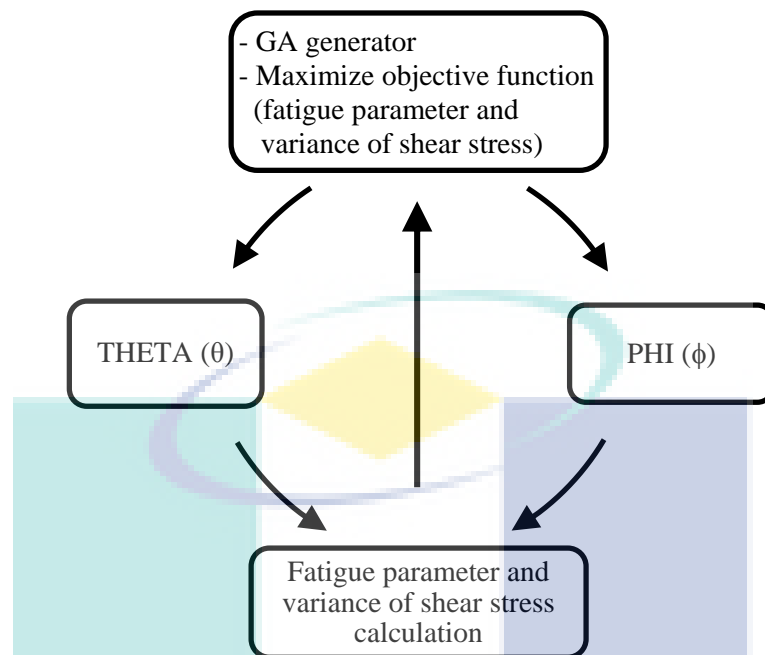
Figure 3.11: Two-parameter GA-based critical plane set-up diagram.

3.8   DEVELOPMENT OF DAMAGE ESTIMATION CODE

As the critical plane has been located at the susceptible location for fatigue failure, with the help of the APDL code stated in Appendix A4, the angles θ and ϕ locating the critical plane are now used to extract the response time history of stress–strain quantities projected on the critical plane, required in Eq.(3.17-3.19) and Eq.(3.22) for fatigue model calibration. The extracted response time histories with the VB code stated in Appendix A5, developed to implement the fatigue model, receives the values of coefficients generated by the GA and returns the fatigue damage per cycle. The process flow chart is shown in Figure 3.13. As the whole time history has been used for calibration, the predicted values of coefficients are the best possible representation of the fatigue behaviour under the considered calibration loading profile.
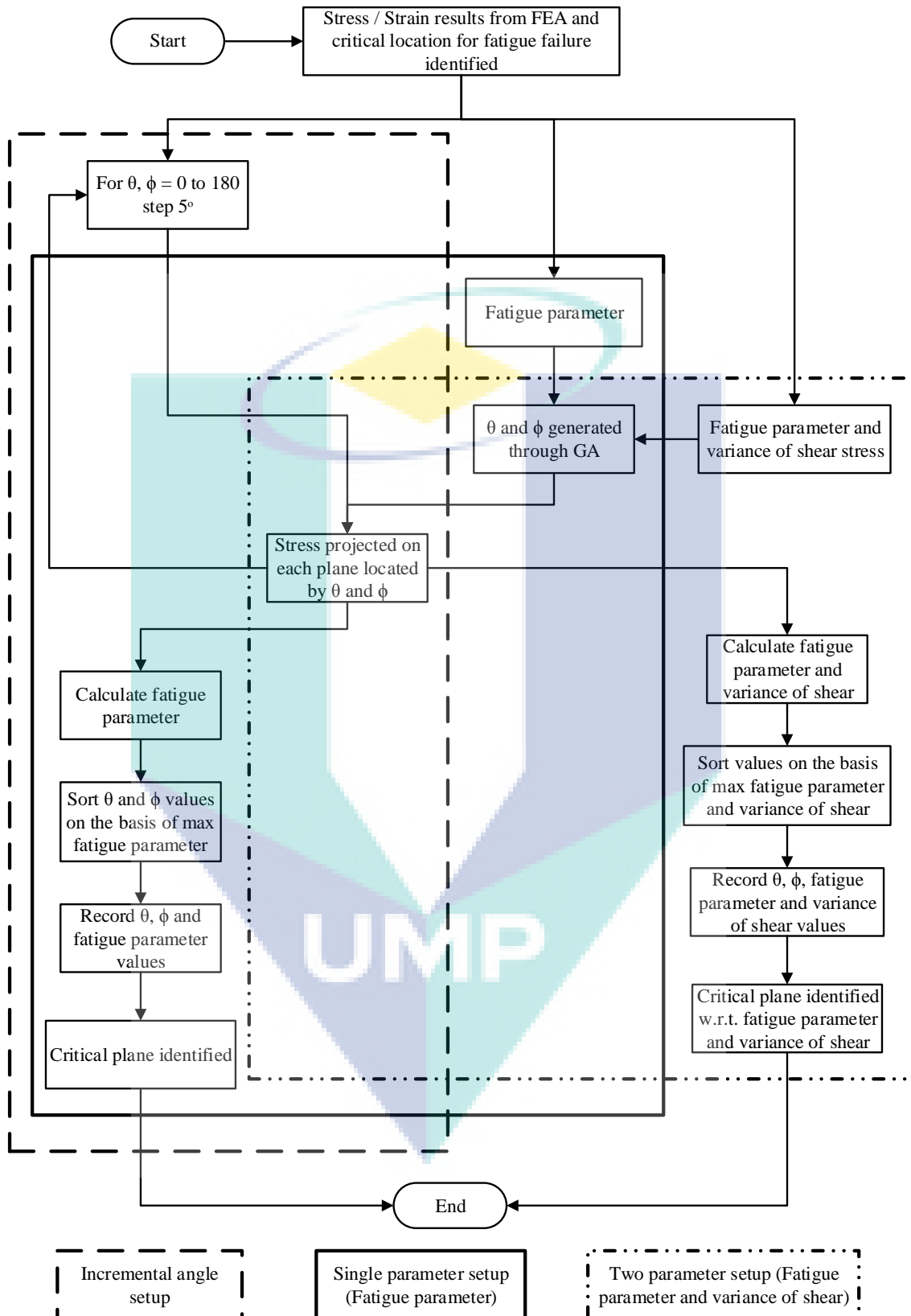
Figure 3.12: Combined flow chart for incremental angle and GA-based critical plane methods.
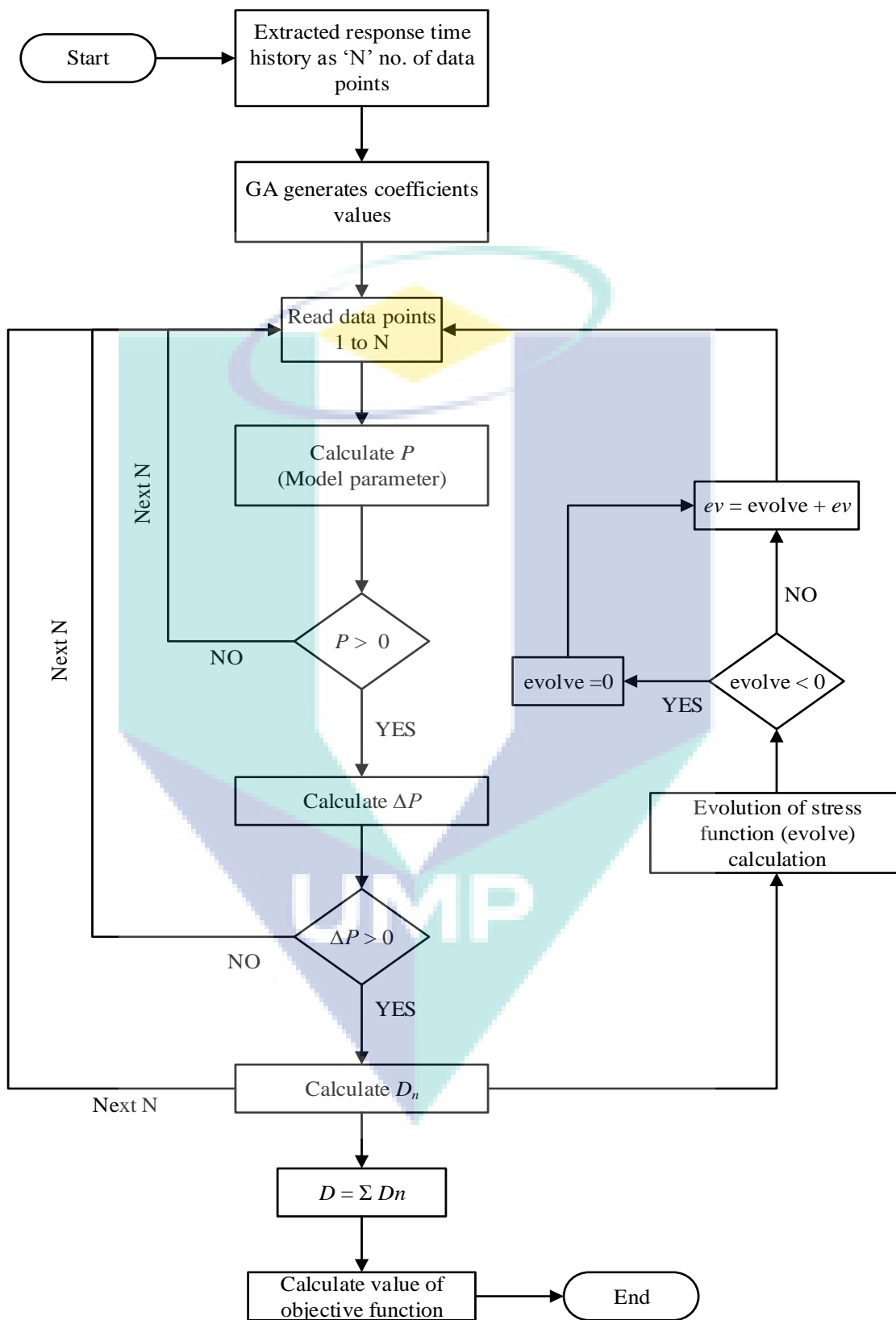
Figure 3.13: Process flow chart for calibration of fatigue model.

3.9   DEVELOPMENT OF GENETIC ALGORITHM MODEL

The GA set-up generates coefficient values and sends them for damage per cycle calculation. The amount of damage calculated is returned to the GA where the objective function is minimized, i.e. the difference of damage per cycle calculated and the experimental damage per cycle. The workflow diagram of the GA set-up is shown in Figure 3.14.
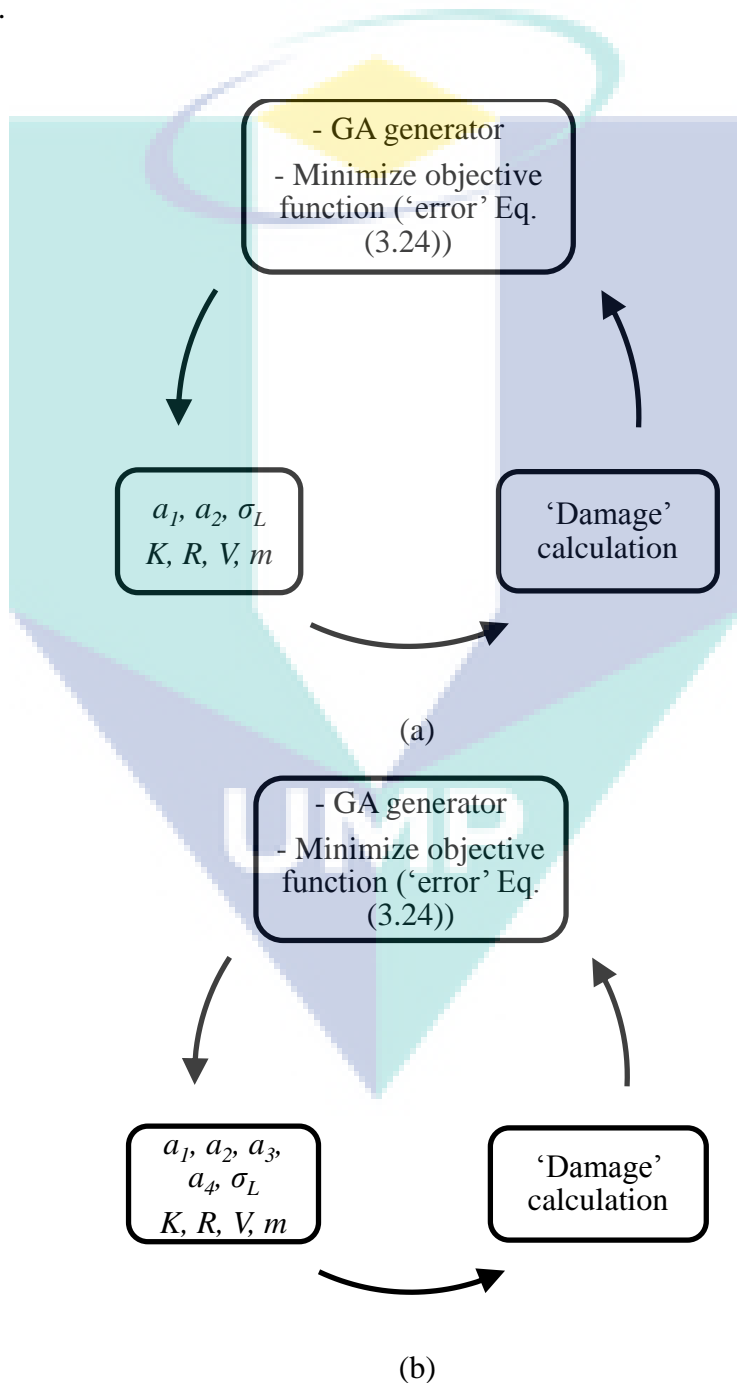
Figure 3.14: GA workflow diagrams for calibration of fatigue model: (a) Model-1, (b) Model-2.

3.9.1 Initialization

To start the GA simulation, the limits of the input variables have to be defined, between which the GA will work and attempt to achieve the condition defined in the objective function. For the current research, the coefficients are initialized by assuming values within a range of one to two decimal places of values which can balance the model equations. This will narrow down the limits of the coefficients which can later be modified to represent the calibrated model coefficients. σ_L is a material constant equivalent to the fatigue limit and its limits for GA can be assumed from the fatigue limit values determined for the loading profile, as similar as possible to the profile that for which the calibration is going to be done. If the fatigue limit is not available for the specific loading conditions, uniaxial fatigue limits can also be used by assuming the limits of σ_L below the uniaxial fatigue limit, which can be modified later as needed.

3.9.2 Convergence Criteria

Due to the random nature of the GA, a well-defined termination criterion to stop GA simulation cannot be pre-determined and no conditional stop can be set. This is because if, for the current research, the minimum value of the objective function 'error' is set to be a convergence criterion, expressed in Eq. (3.24), there is a chance that it can result in declaring the wrong coefficient set as calibrated if the set has resulted in the minimum value of 'error', when actually the coefficient set is a random combination generated by the GA which, by chance, resulted in the minimum error while in reality it is not the correct representation of the fatigue behaviour.

$$error = damage\ per\ cycle\ calculated - damage\ per\ cycle\ experimental \qquad (3.24)$$

To solve this problem, the method adopted in the current situation is that, after every predetermined number of GA iterations (Eq. (3.15)) the value of minimum error is checked. For the current study, a rule is adopted that the error should be two orders less than the corresponding damage value to be considered as a selected solution. Now, from this short-listed group we select the top coefficient sets (approximately ten in number) with respect to the minimum value of 'error'. Coefficient values near the

global minimum of 'error' must be close with respect to the corresponding value in the selected sets. A deviating value for any model coefficients suggests that the set does not belong to the global minimum sets and the minimum error resulting from that coefficient set arises because it is a random combination and should thus be discarded from further processing. If the total number of selected sets is small, for example less than ten, then the GA simulation should continue to the next predetermined number of iterations until the required number of resulting selected sets is acquired. If, after the GA iterations, none of the coefficient sets results in an 'error' value of less than two orders of damage per cycle, this means that the limits set for coefficients in the initialization phase have to be modified. The limits are modified for those coefficients that have reached the earlier defined limiting values at minimum 'error'. The number of GA iterations, as expressed in Eq. (3.25), is decided by the size of the initial population and the number of generations set for the GA to generate during the process run. The number of generations is set to 50 (ESTECO, 2003) and the initial population size is to be generated randomly from the ranges defined for coefficients; thus the number is set to 150, decided by hit and trial which can make the number of GA iterations sufficient to get the required convergence of coefficients.

$$\text{number of GA iterations} = \text{size of initial population} \times \text{number of generations} \qquad (3.25)$$

3.9.3   Determination of Calibrated Coefficients

Now the limits are modified accordingly to determine the fatigue model coefficients values at the global minimum. We select the top ten or more (as required) coefficient sets with respect to the minimum value of 'error', and take the weighted average of the coefficients among the selected sets with respect to the reciprocal of 'error', as this will give the highest weight for the coefficients set with the lowest 'error' value. This weighted average is to compensate for the randomness in determination of coefficient sets by the GA.

3.10   FATIGUE LIFE ESTIMATION PROCEDURE

After the calibration process coefficients defining the proposed model equations have been determined, as stated in the previous section, the next step is to estimate the fatigue life using the calibrated model. The process flowchart of the fatigue life estimation process was shown in Figure 3.5. The loading conditions against which the fatigue life is to be determined are simulated in an FEA environment to get the stress–strain response time history. The critical plane is determined through the process explained in the previous section during calibration of the fatigue model. These calibrated coefficients are now used with the APDL code developed to predict fatigue life using the proposed model. The process flow chart and APDL code are shown in Figure 3.15 and Appendix A6. Generally, two types of case are encountered during fatigue life estimation. The first is where the model is calibrated with a load profile at a certain magnitude, and the loading for which the fatigue life is to be determined is only different in magnitude. In this type of situation, an interpolation scheme is proposed, where more than one calibration load is used with respect to magnitude, the coefficients set for each load is determined, and then each coefficient's value is interpolated with respect to the load value at which the fatigue life has to be determined. Here it is recommended that the calibration loads are selected such that they can cover as much of the working range for the fatigue life estimation model as possible, so that any error due to extrapolation can be avoided. To accommodate any change in slope of S-N curve when moving from low to high cycle fatigue regime, more calibration load points are required. Such that at-least two load points can cover each region of curve divided with respect to slope of the curve.

The second type is where the fatigue estimation model is calibrated with a load profile of a certain shape, assumed to be a characteristic profile which can represent a range of different shapes of load profiles. Here care should be taken when selecting calibration profiles that those selected should have similar shape and load variations to the load profiles for which the fatigue life has to be determined. As can be seen in Figure 3.16, the profile shown in Figure 3.16(a) can be used as the calibrating profile for the fatigue life predicted for the profile in Figure 3.16(b) as it is nearly proportional

(Itoh et al., 1995; Kida et al., 1997). Interpolation of coefficients is not applicable in this case, as there is no reference quantity against which coefficients can be interpolated.

Figure 3.15: Flow chart of fatigue life estimation process.
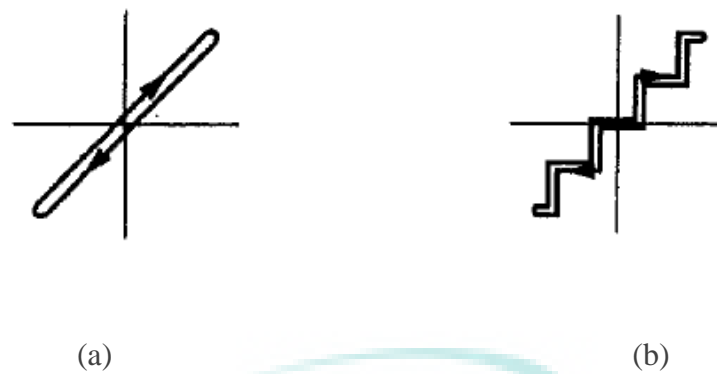
Figure 3.16: Normal strain (x-axis) and shear strain (y-axis) loading profile: (a) fully proportional, (b) nearly proportional with small steps.

For block loads, after the calibration of the model, the general step is to get the stress–strain response history for the block loading and then estimate the fatigue life. Simplification can be made for handling of the block loading so to reduce the processing time and storage requirement, where allowed by the material and loading conditions. For example, the block loading can be dealt with in segments of constant amplitude loads of different magnitude and phase difference (Fatemi et al., 2010). And if the material does not experience any effect of the sequence of loading segments, then these segments can be analysed separately and the cumulative fatigue damage can then be calculated. In the current study, the linear damage rule is applied and for each segment of load, the damage is estimated for one cycle of load then multiplied by the number of cycles in that load segment to estimate the total damage done by that load segment. Then the cumulative damage is determined by summing the damage of all segments included in the block load, as expressed in Eq. (3.26).

$$\text{Tot.cuml. damage} = \sum_{1}^{n} \text{damage by 1 cycle of segment } (n) \times \text{no. of cycles in segment} \quad (3.26)$$

3.11   VALIDATION OF MODEL

To validate and assess the performance of the proposed model, the fatigue life obtained from the model is compared with various sets of published experimental data to analyse the prediction capabilities. The model is checked for in-phase, out-of-phase and complex multiaxial loading cases, including different materials to check the ability

to handle various load cases and material behaviour. Two types of cases defined in previous section including first case, the data sets from published literature with continuous data are used. Each set is divided into two subsets, one is used for calibration and the other is used for validation of the proposed model's fatigue life prediction capability with effectiveness of interpolation of coefficients. For second case, the data from published literature consists of various profile shapes and block loads. The proposed model fatigue life estimation was validated with the concept of load profiles representing the characteristics of the applied load are used for calibration and fatigue life estimated for other complex load profiles and blocks.

3.11.1 Load Cases

For the above-mentioned activity, Table 3.3 is the tabulated list of published experimental data used for assessing the correlation between predicted and experimental fatigue life. The applied loads are in the form of applied normal and shear stress or strain load histories with the profile shape as sinusoidal or complex with normal and shear stress / strain with $\varphi = 0°$ to $90°$ phase difference. The sinusoidal profile for applied stress or strain is defined by Eq. (3.27-3.28), where ε_a, σ_a are normal strain / stress amplitude and γ_a, τ_a are shear strain / stress amplitude. Table 3.4 state the various profile paths of different shapes used in study.

$$\varepsilon_{app} \, or \, \sigma_{app} = \varepsilon_a \, or \, \sigma_a \sin(\omega t) \tag{3.27}$$

$$\gamma_{app} \, or \, \tau_{app} = \gamma_a \, or \, \tau_a \sin(\omega t - \varphi) \tag{3.28}$$

3.11.2 Materials Properties

Table 3.5 and Table 3.6 list the mechanical and material properties including the fatigue limits considered for the materials involved in the validation exercise. In the case of any missing data, other published literature sources or general properties for the group of materials are used.

Table 3.3: Loading and material detail used in the study.

Type of Loading Profile	Materials involved	Reference
Fully reversed in-phase and out-of-phase, with zero and positive mean	EN3B	Susmel and Taylor (2008)
Fully reversed in-phase and out-of-phase, with zero and positive mean	C40	Atzori et al. (2006)
Various loading paths of different shapes (Table 3.4)	SS304	Itoh et al. (1995); Meggiolaro and de Castro (2012)
Constant amplitude axial and torsion, and block loading	Low carbon steel (steel 20) (0.24% C, 0.25% Si, 0.45% Mn, 0.2% Cr)	Fatemi and Gladskyi (2013)
Block loading of axial, torsion and 90° out-of-phase axial and torsion	Titanium alloy (BT9) (0.081% Fe, 0.06% C, 0.3% Si, 3.4% Mo, 0.018% N, 6.5% Al, 1.58% Zr, 0.006% H)	Fatemi et al. (2010)

Table 3.4: Profile paths for SS 304 (ε – x axis and γ – y axis).

Path no.	Path shape	Path no.	Path shape	Path no.	Path shape
1		6		11	
2		7		12	
3		8		13	
4		9			
5		10			

Table 3.5: Properties of materials used in the study.

Material	Elastic modulus, E (MPa)	Poisson ratio (ν)	Tensile strength (MPa)	Ultimate tensile strength (MPa)	Strain hardening Exponent (n)	Strength coefficient (K) (MPa)
EN3B	208500 Susmel and Taylor (2010)	0.3 ---	571 Susmel and Taylor (2010)	622 Susmel and Taylor (2010)	0.1635 Susmel and Taylor (2010)	890.7 Susmel and Taylor (2010)
C40	206000 Atzori et al. (2006)	0.3 ---	537 Atzori et al. (2006)	715 Atzori et al. (2006)	0.131 SAE-J1009 (2002)	915 SAE-J1009 (2002)
SS304	197000 Meggiolaro and de Castro (2012)	0.29 ---	240 Narayanasamy and Loganathan (2007)	898 Narayanasamy and Loganathan (2007)	0.276 Meggiolaro and de Castro (2012)	1754 Meggiolaro and de Castro (2012)
Low carbon steel (steel 20)	185000 Fatemi and Gladskyi (2013)	0.3 Fatemi and Gladskyi (2013)	365 Fatemi and Gladskyi (2013)	506 Fatemi and Gladskyi (2013)	0.159 Fatemi and Gladskyi (2013)	838 (MPa) Fatemi and Gladskyi (2013)
Titanium alloy (BT9)	118000 Fatemi et al. (2010)	0.37 Fatemi et al. (2010)	910 Fatemi et al. (2010)	1080 Fatemi et al. (2010)	Stress-strain curve Fatemi et al. (2010)	Stress-strain curve Fatemi et al. (2010)

Table 3.6: Fatigue limit of materials.

Material		Fatigue limit (MPa)	Loading conditions	Reference
EN3B	Combined tension-torsion @10^6 cycles	192.4 / 148.7 / 188.2 / 141.3	R=-1 ϕ=0 / R=0 ϕ=0 / R=-1 ϕ=90 / R=0 ϕ=90	Susmel and Taylor (2008)
C40	Combined tension-torsion @2x10^6 cycles	101 / 99.6 / 67.9 / 66.8	R=-1 ϕ-0 / R=-1 ϕ=90 / R=0 ϕ=0 / R=0 ϕ-90	Atzori et al. (2006)
SS304	@10^6-10^7 cycles	240	Reverse bending	B.S.S.A. ((Undated))
Low carbon steel (Steel 20)	Smooth specimen @10^6 cycles	200	Fully reversed	Fatemi and Gladskyi (2013)
	Notched specimen @10^6 cycles	90	Fully reversed	
Titanium alloy BT9	@10^7 cycles	654		AZoM.com (2013)

R= minimum stress / maximum stress, ϕ = phase angle

3.12   FINITE ELEMENT ANALYSIS MODELLING

To get the stress distribution response time history for the applied loadings on the test specimens considered in this study, structural analysis using FEA was conducted. Details of the simulation models and meshes developed for the said purpose are given in the following.

3.12.1 EN3B Specimen

A solid bar with a notch is used for testing, with the geometry shown in Figure 3.17 (Susmel and Taylor, 2008). The FEA model with applied load as moment (N.mm) and normal force (N) along axis and fixed support ($Ux = Uy = Uz = URx = URy = URz = 0$) and mesh with 10 node tetrahedrons are shown in Figure 3.18. Stresses are monitored at the notch root as this is a stress concentration zone and a critical location for fatigue life estimation.
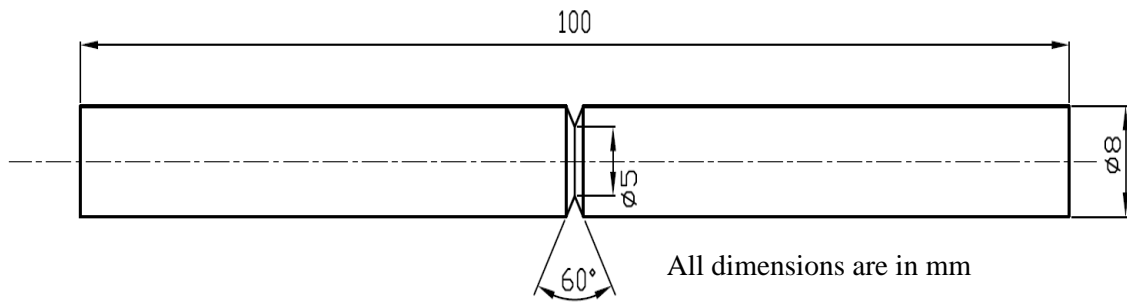
Figure 3.17: Geometry detail of EN3B specimen with notch radius 1.25 mm.

(a) Loading and constraints   (b) Finite element model

(c) Fine mesh around notch
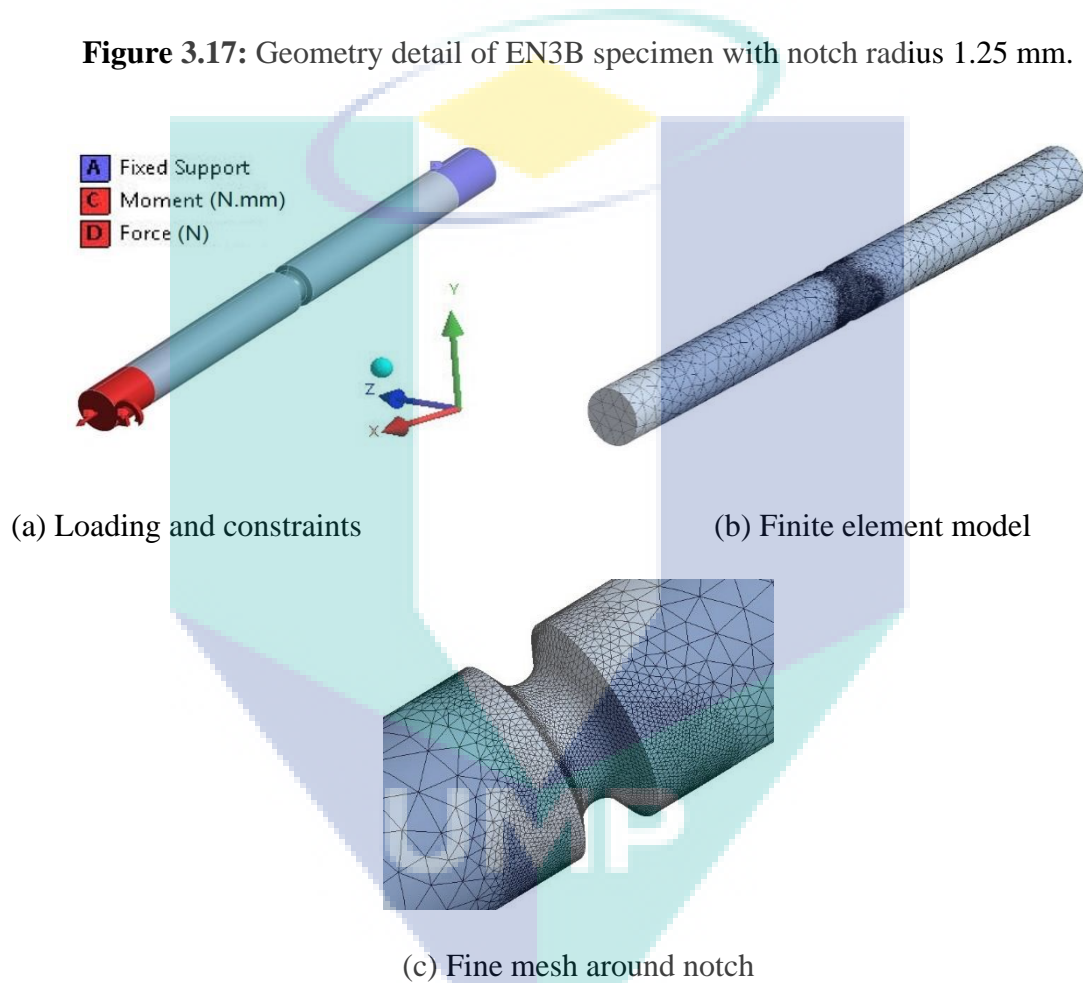
Figure 3.18: Structural and finite element model for EN3B specimens with loading and boundary conditions.

3.12.2 C40 Specimen

A notched solid bar is used with geometry details shown in Figure 3.19 (Atzori et al., 2006). The FEA model with applied load as moment (N.mm) and normal force (N) along axis and fixed support and mesh with 10 node tetrahedrons are shown in

Figure 3.20. Stresses are monitored at the notch root as this is a stress concentration zone and a critical location for fatigue life estimation.

All dimensions are in mm

Figure 3.19: Geometry detail of C40 specimen with length 200 mm.

(a) Loading and constraints   (b) Finite element model

(c) Fine mesh around notch
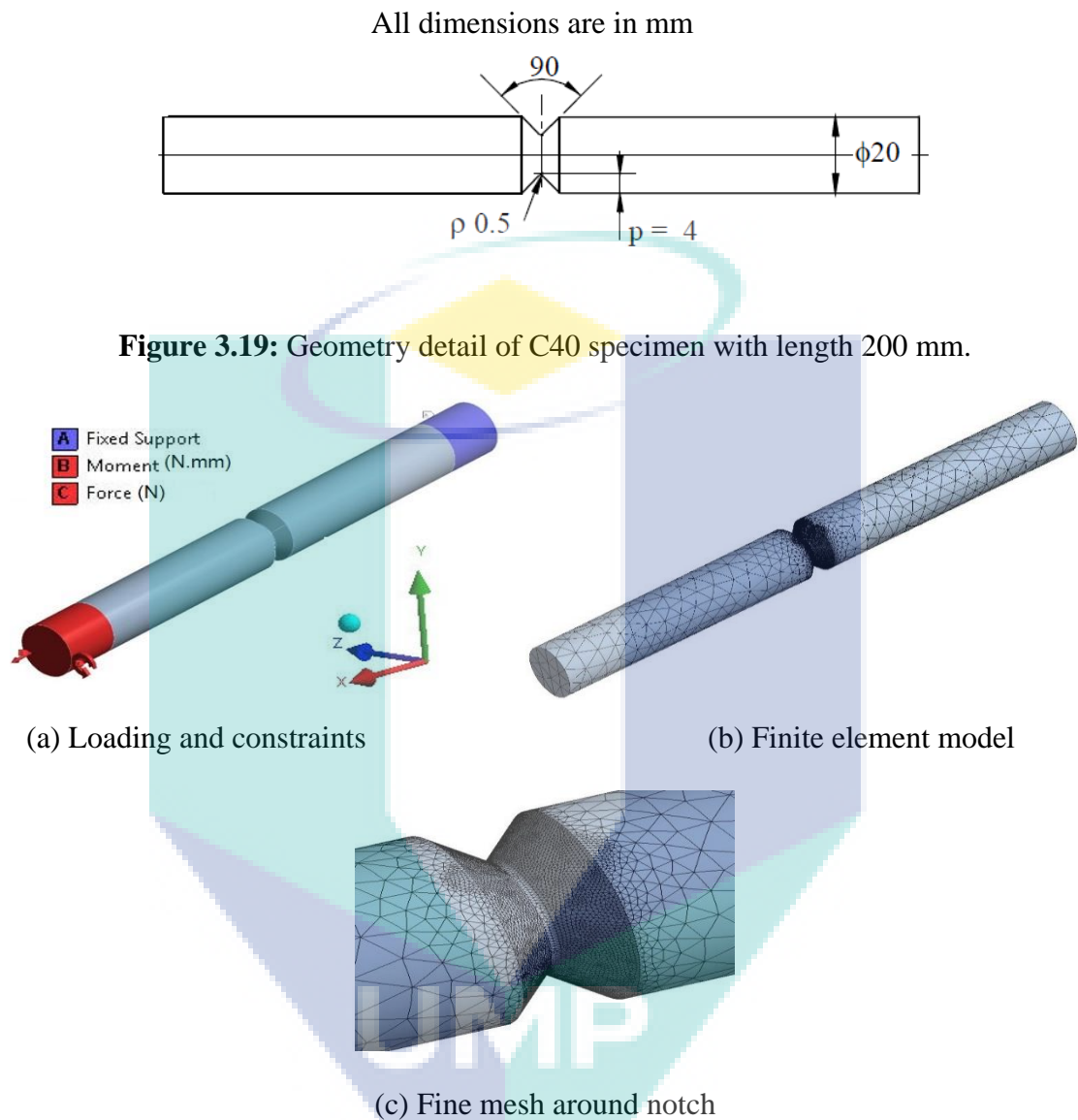
Figure 3.20: Structural and finite element model for C40 specimen with loading and boundary conditions.

3.12.3 SS304 Specimen

Hollow cylinder specimens are used with geometry details in Figure 3.21 (Itoh et al., 1995). The FEA model with applied load as torsional displacement (mm) and axial displacement (mm) along axis and fixed support and mesh with 20 node hexahedrons are shown in Figure 3.22, with flanges removed as they are only for

physical clamping. Stresses are monitored at the centre of the gauge length for fatigue life estimation.

All dimensions are in mm
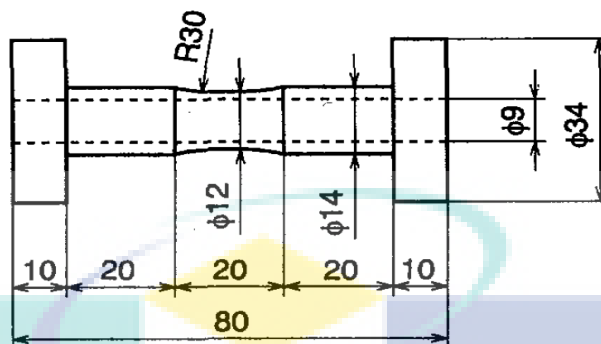
Figure 3.21: Geometry detail of SS304 specimen.

(a) Loading and constraints   (b) Finite element model

(c) Mesh around gauge length
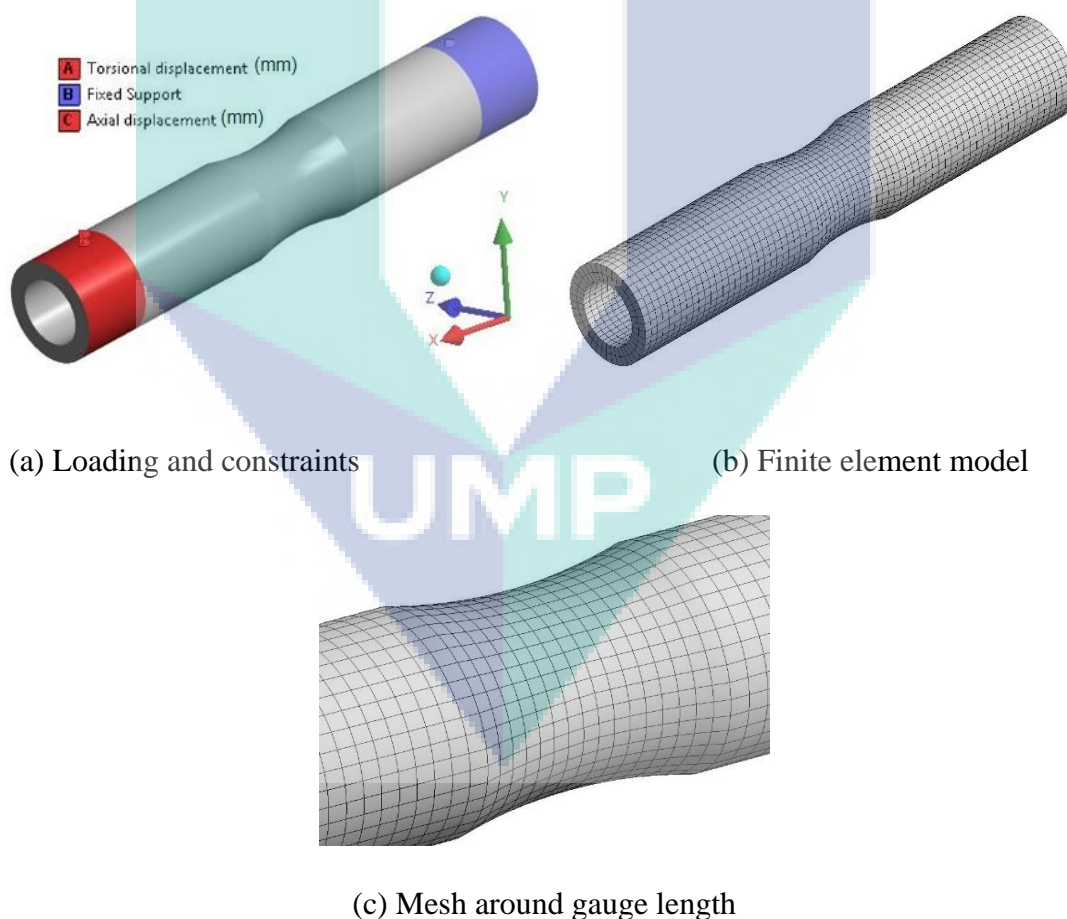
Figure 3.22: Structural and finite element model for SS304 specimen with loading and boundary conditions.

3.12.4 Low Carbon Steel (Steel 20) Specimen

A thin-walled tubular specimen is used with geometry shown in Figure 3.23. The specimen had a 3.4 mm diameter through thickness transverse hole at the middle of the gauge length (Fatemi and Gladskyi, 2013). The FEA model with applied load as moment (N.mm) and normal force (N) along axis and fixed support and mesh with 10 node tetrahedrons are shown in Figure 3.24, where stresses are monitored on the hole circumference at the locations identified by (Fatemi and Gladskyi, 2013) experimentally.

All dimensions are in mm
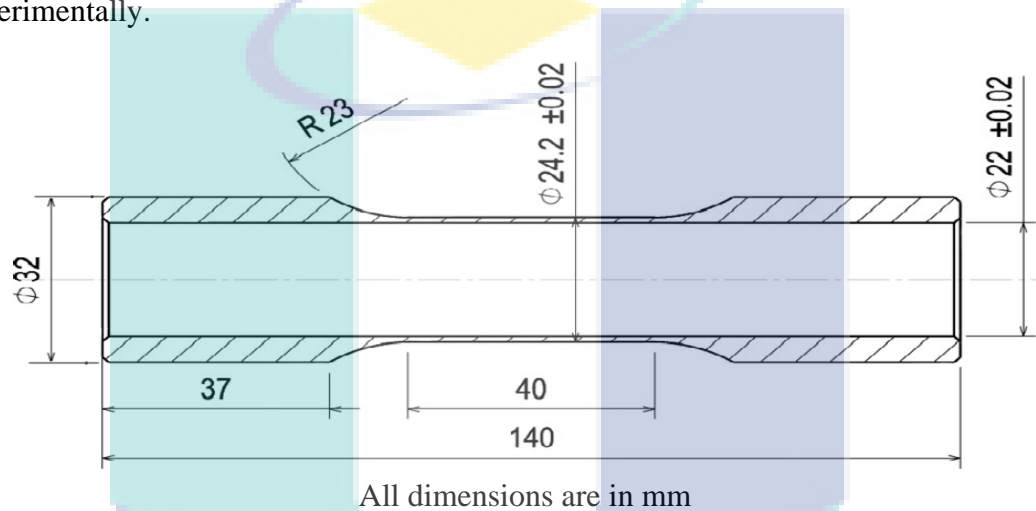
Figure 3.23: Geometry detail of low carbon steel (Steel 20) specimen.
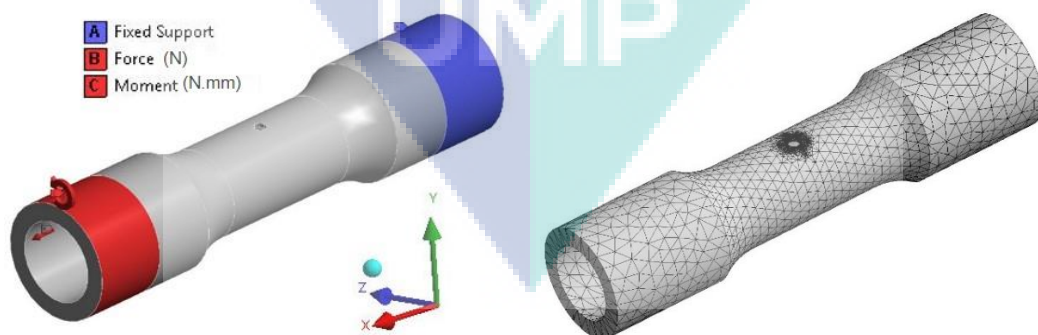
(a) Loading and constraints   (b) Finite element model

Figure 3.24: Structural and finite element model for low carbon steel (Steel 20) specimen with loading and boundary conditions.
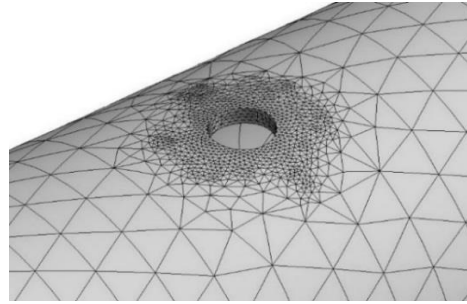
(c) Fine mesh around hole

Figure 3.24: Continued.

3.12.5 Titanium Alloy (BT9) Specimen

Tubular specimens are used for titanium alloy BT9 with geometry details shown in Figure 3.25 (Fatemi et al., 2010). The FEA model with applied load as torsional displacement (mm) and axial displacement (mm) along axis and fixed support and mesh with 20 node hexahedrons are shown in Figure 3.26, where stresses are monitored at the centre of the gauge length. The solid specimen is shown in Figure 3.27, with 4 mm diameter, gauge length of 19 mm and a sweep mesh of 20 node hexahedrons with size of 0.75 mm.
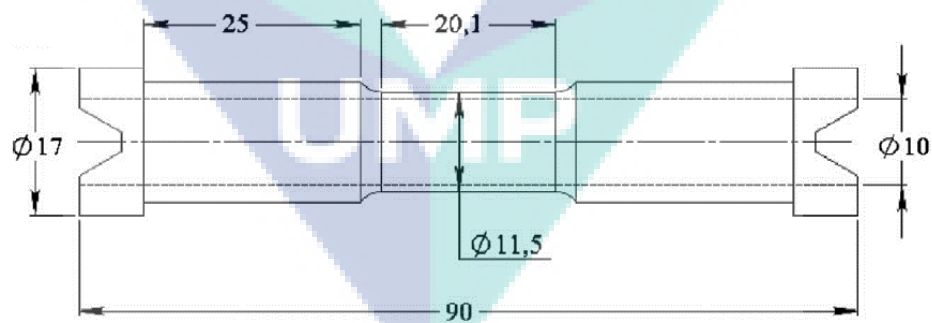
All dimensions are in mm.

Figure 3.25: Geometry detail of titanium alloy BT9 tubular specimen

(a) Loading and constraints

(b) Finite element model

(c) Mesh around gauge length
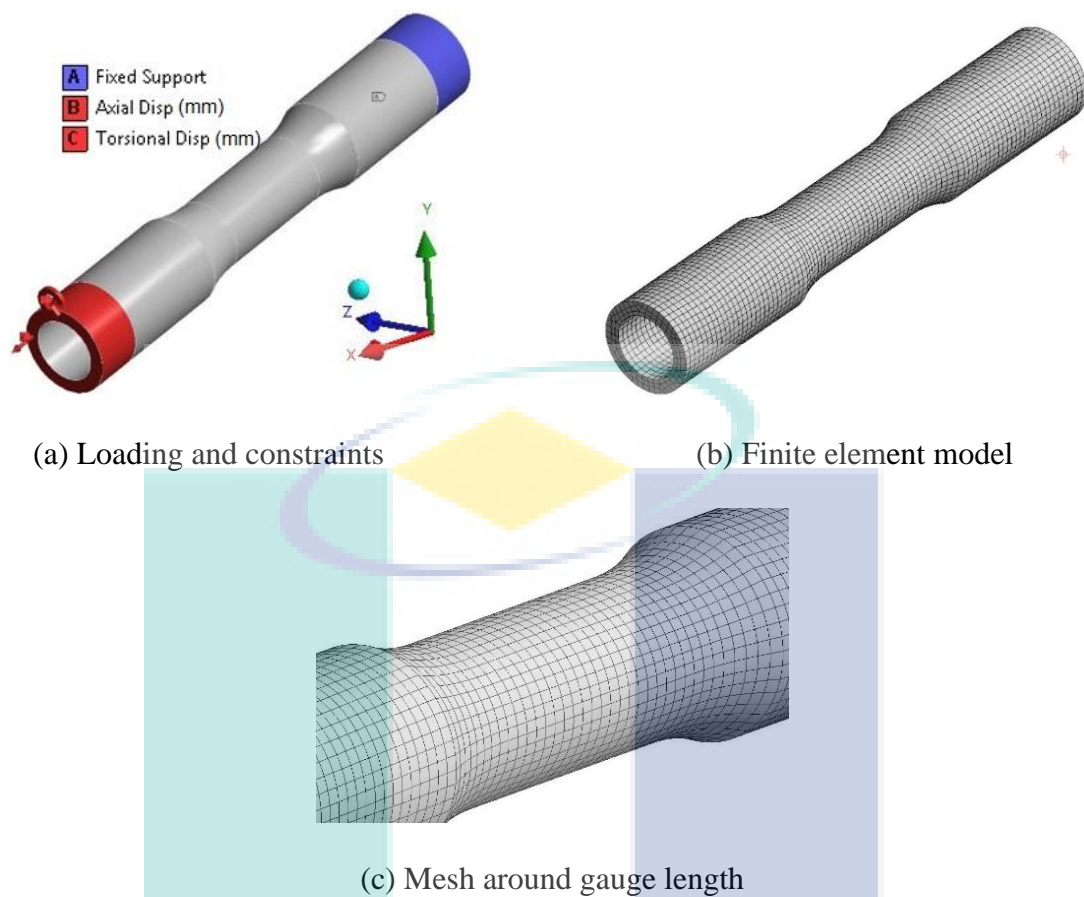
Figure 3.26: Structural and finite element model for titanium alloy BT9 tubular specimen with loading and boundary conditions.

(a) Loading and constraints

(b) Finite element model
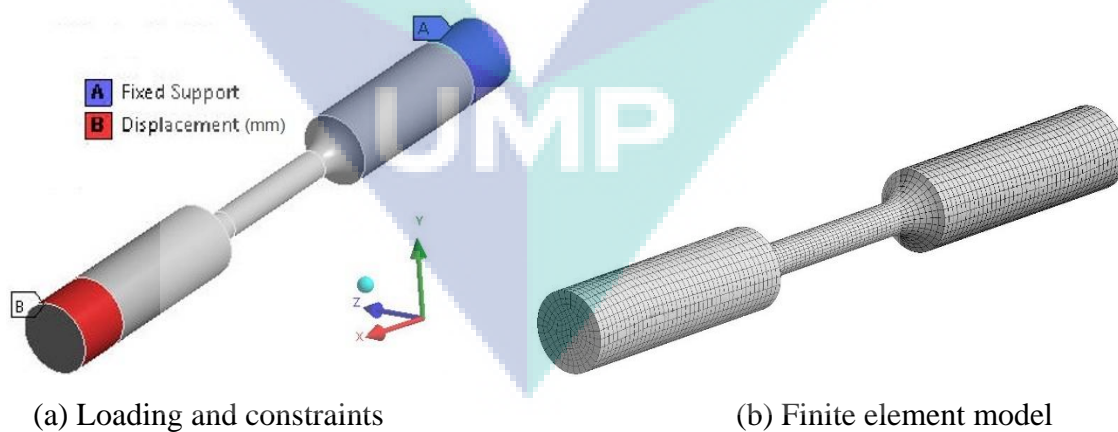
Figure 3.27: Structural and finite element model for titanium alloy BT9 solid specimen with 4 mm diameter and 19 mm gauge length with loading and boundary conditions.

3.13   MESH CONVERGENCE OF FINITE ELEMENT MODELS

Finite element models of specimens generated in Section 3.12 are verified for the mesh convergence by examining the von Mises stress, Tresca stress and maximum principal stress with respect to the mesh size. To reduce both the solution cost (CPU time) and limitation of storage space, the number of nodes and elements has to be kept to the minimum with acceptable convergence of the stress magnitude. The minimum mesh size is set for either gauge length or notch, depending on the shape of the specimens. There follow the details of the mesh type selection and convergence of mesh tests for the respective specimens with the minimum mesh size selected for each FEA model.

3.13.1   Mesh Type Selection

Selection of the right techniques for meshing is based on the geometry, model topology, analysis objectives and engineering judgement. The geometries of the specimens (Section 3.12) consist of radial notch, hollow tubular geometry and tubular with a hole. It is generally accepted that at stress concentration areas the mesh quality should be high. As quadratic hexahedral elements (20 nodes) are robust and preferred for good and accurate results (Bishop and Sherratt, 2000; Wang et al., 2004), they are the preferred choice to mesh the specimen geometries. Quadratic tetrahedral (10-node) are also good and can be used in any condition (Wang et al., 2004), but usually result in a larger number of elements compared to hex mesh, although tetrahedral elements can capture the typical geometry features easily. In this study hexahedral elements are only used where the geometry allows the sweep meshing scheme to generate hex mesh. The sweep meshing scheme is the easiest method to create structured hexahedral mesh along a body having a topologically uniform cross-section. In this scheme where the geometry is characterized by source and target faces which are topologically similar, the hexahedral mesh is swept (extruded) between the source and target along a single logical axis bounding the swept hexahedra between the source and target surfaces (Scott et al., 2005). For other specimen geometries where there is a sharp change of area, as in radially notched specimens, or a non-symmetric feature like a hole in the circumference, tetrahedral (10-node) mesh is used because it is quicker to generate, as there is no need

to simplify the geometry to accommodate hexahedral mesh and provide results with good accuracy.

For this study, specimens of five different materials are considered and to mesh their FEA models the mesh type is selected as follows: the EN3B and C40 specimens, which have a radial notch, are meshed with 10-node tetrahedral elements, the steel 20 specimen, which has a notch hole in its circumference, is meshed with 10-node tetrahedral elements, the SS304 and titanium alloy BT9 specimens have uniform cross-sectional areas with respect to the area topology, and are thus meshed with 20-node hex. elements using a sweep meshing scheme.

3.13.2 Identification of Mesh Size

The convergence of the stress was considered as the main criterion to select the mesh size, with the number of nodes and elements small enough to keep the FE analysis within the limitations of computational time and storage capacity. The finite element mesh for each specimen model was generated using the hexahedral and tetrahedral elements, as mentioned in the previous section. The maximum principal stress, Tresca stress and von Mises stress are checked for convergence at the critical locations of the respective specimens. Figure 3.28 shows the variation of the stresses for the different specimens at critical locations, as well as change in the FE model size for each specimen, in terms of the number of nodes and elements, with respect to element size. For the EN3B specimen, the variation in the stresses and size of the FE model as a function of mesh size around the critical region are shown in Figures 3.28(a) and 3.28(f) respectively. The maximum percentage difference between stresses for mesh size smaller than 0.175 mm is approximately 0.24%. However, as the mesh size decreases from 0.175 mm to 0.15 mm, the FE model size increases by 1.5 times with respect to the number of nodes as well as elements. Thus the mesh size of 0.175 mm is selected for the critical region and 2 mm global mesh size for FE analysis of the EN3B specimen in order to keep the FE model efficient in stress estimation as well as computational time and storage capacity. Similarly, for the C40 specimen, variation of the stress and size of the FE model as a function of mesh size is shown in Figures 3.28(b) and 3.28(g) respectively. After the mesh size of 0.3 mm, the stress corresponding to the lower mesh

size of 0.25 mm has a difference of 0.24% with the stress obtained for 0.3 mm, and the FE model size increases by approximately 1.4 times in the number of nodes and elements. Thus the mesh size of 0.3 mm is selected for the critical region and 4 mm global mesh size to keep the FE model smaller in size for stress approximation as well as to lessen the computational time and storage capacity. For the SS304 specimen, the stress variation and the size of FE model with respect to mesh size are shown in Figures 3.28(c) and 3.28(h) respectively. For mesh sizes smaller than 1.0 mm, the maximum difference between stress values is approximately 0.2%. However, the FE model size for the mesh size of 0.5 mm increases by 5 times in node numbers and 6 times in element numbers, so the 1.0 mm mesh size is the most appropriate size for the gauge length and 1.5 mm for the global mesh size to keep the CPU time and storage capacity requirement at the minimum.

For the steel 20 specimen, variation of the stress and size of FE model with respect to mesh size is shown in Figures 3.28(d) and 3.28(i) respectively. For stresses at mesh sizes less than 0.25 mm, the maximum difference between stress values is approximately 0.24%. The FE model size increases by a factor of 2.0 for the number of nodes and elements when the mesh size is reduced from 0.25 mm to 0.15 mm. Hence, the mesh size of 0.25 mm is selected for the critical region of the notch hole and 3 mm for the global mesh size, so that the converged stresses are obtained with reduced CPU load and storage requirement.

For the titanium alloy BT9 specimen, the stress and FE mode size variation with respect to mesh size are shown in Figures 3.28(e) and 3.28(j). The stress variation chart shows no variation of stress values with change in mesh size. This is due to the low elastic modulus of the material which makes the material hard enough to show only very small deflections against applied loads, leading to very small distortions in the geometry. Thus with the combination of the applied load and mesh size, the model is already in the converged stress region (NAFEMS, (Undated)). Hence, to keep the CPU time and storage requirement low with mesh not to be distorted around the gauge length, the mesh size of 1.0 mm is selected, because, compared with the size of FE model for 0.75 mm mesh size, the number of nodes and elements increased by a factor of approximately 2.0.
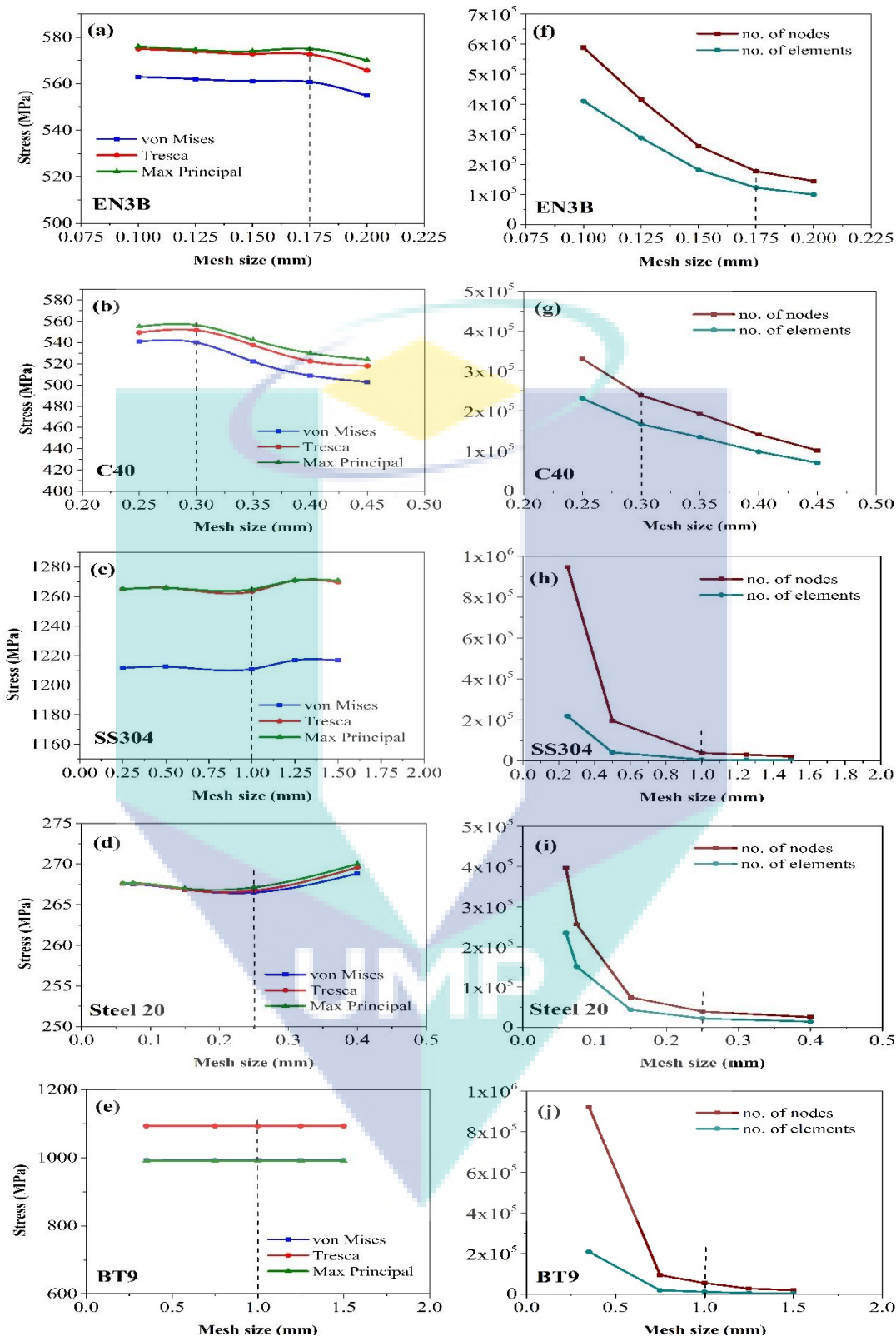
Figure 3.28: Mesh size versus calculated FEA stresses (a–e) and mesh size versus no. of nodes and elements of FEA model (f–j).

3.13.3 Verification of FEA Models

The developed FEA models are verified by comparing the calculated stress values by FEA from the applied stress, and stress reported in source data in case of applied strain. The calculated stresses are within 4% error is shown in Table 3.7.

Table 3.7: Comparison of calculated and actual stresses in considered specimens.

Material of specimen	Stress value in source data (MPa)	Calculated stress from FEA (MPa)	error (%)
EN3B	150	150.4	0.27
C40	119.3	123	3.0
SS304	732	740	1.0
Low carbon steel (Steel 20)	106	105.95	0.04
Titanium alloy BT9	735	707	3.8

3.14   SUMMARY

In this chapter, the selection of parameters for the proposed model equation has been discussed and the selected parameters are highlighted. The two proposed equations for fatigue parameters are defined on the basis of strain energy type combination and separate stress–strain terms combined in summation form. The working of the proposed model is explained in detail, and the calculation process for critical plane determination with the incremental angle method and newly proposed GA-based method is explained. The development of tools like interactive spreadsheets used in the calibration set-up with the GA is discussed. The process of calculating the calibrations from the GA is explained in detail, and the fatigue life estimation procedure is described using the proposed fatigue life estimation method. Finally, details of the experimental data from already published literature used for validation of the proposed model are given, and details of the loading cases, material used and data of the FEA models used in the validation exercise are presented with mesh convergence and validation of the FEA models. Performance analysis of the proposed fatigue life models and new critical plane estimation method against various material and loading conditions is presented in Chapter 4.

CHAPTER 4

RESULTS AND DISCUSSION

4.1   INTRODUCTION

This chapter presents the performance analysis for the proposed multiaxial fatigue life estimation model. The experimental fatigue life results from published literature are used for the purpose of validating the developed model. A comparative analysis between the two fatigue parameter models is presented. Performance is analysed by comparison with the experimental fatigue life data of various materials against different loadings, taken from the published literature. The results of the proposed model are compared with the fatigue life models available in commercial fatigue life code, including the Fatemi–Socie and endurance function models. The efficiency of the genetic algorithm-based critical plane estimation methods is analysed in comparison with the conventional incremental angle method.

4.2   COMPARATIVE ANALYSIS OF PROPOSED MULTIAXIAL FATIGUE MODELS

The proposed fatigue life prediction model is formulated with two fatigue parameter expressions based firstly on the strain–energy approach, having shear and normal strain energy terms (Model-1), and secondly on summation of the stress and strain terms (Model-2) using the discrete contribution of stress–strain terms, as described in Section 3.5. The comparative performance of the proposed fatigue life prediction models is evaluated against a set of complex profiles representing various levels of proportional, non-proportional and multiaxial loading conditions, according to the loading profiles in Table 3.4. The experimental fatigue life results of SS304 (Itoh et al., 1995) for the above-mentioned loadings are utilized for comparative analysis. Two

sets of axial and shear strain loads are applied, as given in Table 4.1 and designated as Set 1 and Set 2 (Itoh et al., 1995).

The experimental fatigue life for each axial and shear strain set and loading path (Table 3.4) is given in Table 4.2. From the profile paths (Table 3.4), Path 5 and Path 12 are selected for calibration as they characterize in-phase, i.e. fully proportional, and completely out-of-phase, i.e. non-proportional loading, Figure 4.1. (Kida et al., 1997). Set 1 and Set 2 of the axial and shear strain loads (Table 4.1) are used for the Path 5 proportional (in-phase) and Path 12 non-proportional (out-of-phase) loading conditions for calibration with the two proposed multiaxial fatigue models, Model-1 and Model-2. Hence, eight sets of calibrated coefficients are obtained in order to predict fatigue life with different combinations of load sets and profile paths, as presented in Table 4.3.

(a) Path 5   (b) Path 12
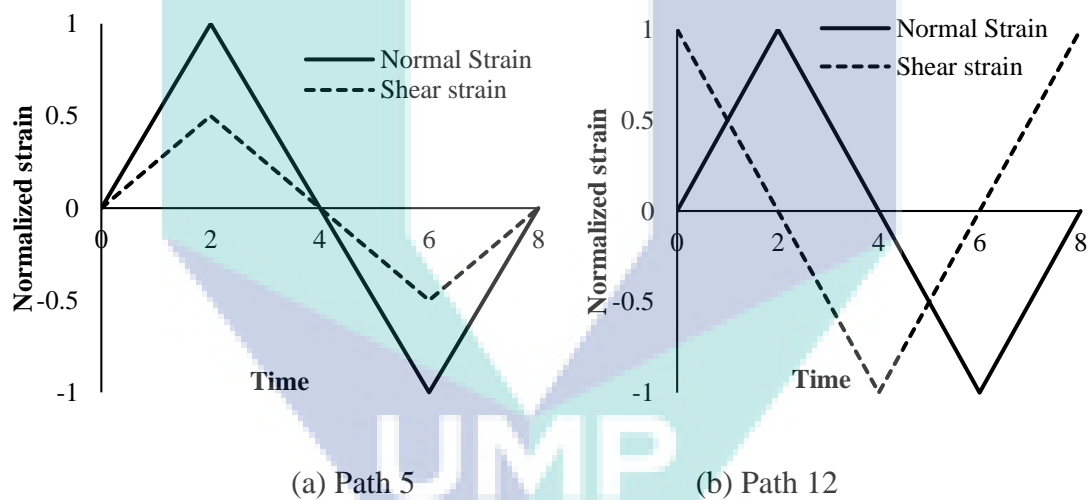
Figure 4.1: Normal and shear strain with respect to time.

Table 4.1: Applied axial and shear strain load sets for SS304 specimen.

	Set 1	Set 2
Axial strain (%)	0.5	0.8
Shear strain (%)	0.87	1.39

Table 4.2: Predicted fatigue life by Model-1 and Model-2 with respective loading for SS304 specimen.

Path no.	Load set no.	Experimental life (cycles) (Itoh et al., 1995)	Predicted fatigue life (cycles)			
			Model-1		Model-2	
			Path 5 Proportional (in-phase)	Path 12 Non-proportional (out-of-phase)	Path 5 Proportional (in-phase)	Path 12 Non-proportional (out-of-phase)
1	1	9500	88019	6162	14469	4227
	2	1400	8423	746	2623	639
2	1	20000	71932	5441	14318	4140
	2	2100	7586	659.5	2231.6	549
3	1	2400 (1200 blocks)	16920	1806	11541	3456
	2	820 (410 blocks)	2785	242	2187	514
4	1	3400 (1700 blocks)	17825	1868	12112	3742
	2	900 (450 blocks)	2751	238	2421	532
6	1	9700	18731	1911	14372	4382
	2	2600	2749	239	2435	633
7	1	18000	18582	1935	13456	3874
	2	1700	2842	246	2498	586
8	1	2050	12987	1435	14559	5025
	2	470	4551	394	6735	1177
9	1	2950	25744	2851	11363	3867
	2	660	2696	234	2442	492
10	1	2600	26073	2822	24215	8204
	2	320	4525	388	7611	1198
11	1	14400	26493	2593	13810	4256
	2	1200	3513	304	3186	592
13	1	3200 (1600 blocks)	33272	3201	10567	3096
	2	1000 (500 blocks)	4662	423	2035	435
Paths used for calibration						
5	1	17500	----	----	-----	----
	2	3200	----	----	-----	----
12	1	4750	----	-----	----	----
	2	710	----	-----	----	----

Table 4.3: Calibrated coefficients from genetic algorithm for SS304.

		Calibrated coefficients							
Model-1									
		K (×10^{-01})	R	V	a_1	a_2		m	σ_L
Set 1	**Path 5**	4.12201	1.040395	24.8	0.205004	0.267898		1	169
	Path 12	3.83043	1.022177	12.3	0.484119	0.527805		1	178
Set 2	**Path 5**	9.25598	0.35938	32.1	0.571430	0.073620		1	172
	Path 12	9.16228	0.76214	29.2	0.235450	0.335700		1	191
Model-2									
		K (×10^{-05})	R	V	a_1	a_2	a_3	a_4	m	σ_L

		K (×10^{-05})	R	V	a_1	a_2	a_3	a_4	m	σ_L
Set 1	**Path 5**	3.05670	0.099895	888	0.219796	0.369444	0.546368	0.53614	1	225
	Path 12	6.90730	0.177681	907	0.087341	0.666236	0.595491	0.65008	1	216
Set 2	**Path 5**	7.27490	0.105526	902	0.383121	0.874629	0.519770	0.59175	1	214
	Path 12	29.9000	0.226573	880	0.024449	0.420024	0.579126	0.91491	1	218

Table 4.4: No. of iterations for calibration of model using GA.

Path no.	Strain set no.	Number of iterations for calibration	
		Model-1	Model-2
5	1	6750	13500
	2	6750	13500
12	1	6750	13500
	2	6750	6750

The number of iterations required to calibrate the fatigue model coefficients for each developed multiaxial fatigue model with both of the profile paths selected for calibration and applied strain load sets are presented in Table 4.4. It is observed that the proposed fatigue life Model-1 requires fewer iterations compared to the number of iterations required for Model-2, hence leading to reduced CPU resource consumption and processing time. This is attributed to the higher number of variables (a_3 and a_4) needing to be calibrated in Model-2 in order to find the optimized values of variables when applying the genetic algorithm (GA) approach. However, for a combination of the non-proportional loading condition (Path 12) and strain Set 2, the number of iterations for Model-2 is equal to the number of iterations required by Model-1 for the calibration of the proposed fatigue model. This is due to the inherent randomness in GA, resulting in fewer iterations being needed to achieve the objective of minimum error defined for

calibration of the model coefficients by the GA. The results of fatigue life estimation using Model-1 and Model-2 are presented in Table 4.2, which gives the predicted fatigue life determined from each set of calibrated coefficients (Table 4.3) by the respective load Sets 1 and 2. The comparison between the predicted and experimental fatigue life (Itoh et al., 1995) is shown in Figure 4.2. The solid line on Figure 4.2 represents perfect correlation between the experimental and predicted fatigue life, and the dotted lines represent factor of two and five goodness bands. It is observed that the estimated fatigue life from the proposed model with Model-1 and Model-2 shows good correlation with the experimental fatigue life results (minimum difference with experimental results is 0.4% and 3.5%) when using the coefficients calibrated from profile Path 12. The improved results with minimum error are due to the fact that Path 12 is a better approximation of non-proportional and complex loading compared to the proportional loading case (Path 5).

Comparing the predicted fatigue life using the proposed fatigue model with Model-1 and Model-2, less scatter is observed in the predicted fatigue life results using Model-2 than when using Model-1. This is attributed to the discrete stress–strain terms present in Model-2, contributing individually to calibration as well as fatigue life prediction. The benefit of using discrete terms is in accommodating small variations in the loading path due to the increased number of variables included in Model-2 compared to Model-1. However, calibration of the model from a characteristic profile and the subsequent fatigue life prediction using different profiles become more difficult with the application of Model-2 due to additional coefficients. For different profiles, the individual contribution of each stress and strain parameter in Model-2 changes. Consequently, maintaining accuracy is more difficult when applying Model-2 than Model-1, where two stress–strain terms are combined together into one term, so that only a single coefficient is to be dealt with.

For profile Paths 1, 2 and 11, when the fatigue life is estimated by Model-2 with both sets of applied axial and shear strains loading given in Table 4.1, and for calibration of the fatigue model coefficients with profile Path 5, more accurate estimations result, with a minimum difference of 0.4% with respect to the experimental results. The reason is that Paths 1, 2, 5 and 11 have rotation of the principal strain

(a) Model-1 and Set 1

(b) Model-1 and Set 2

(c) Model-2 and Set 1

(d) Model-2 and Set 2
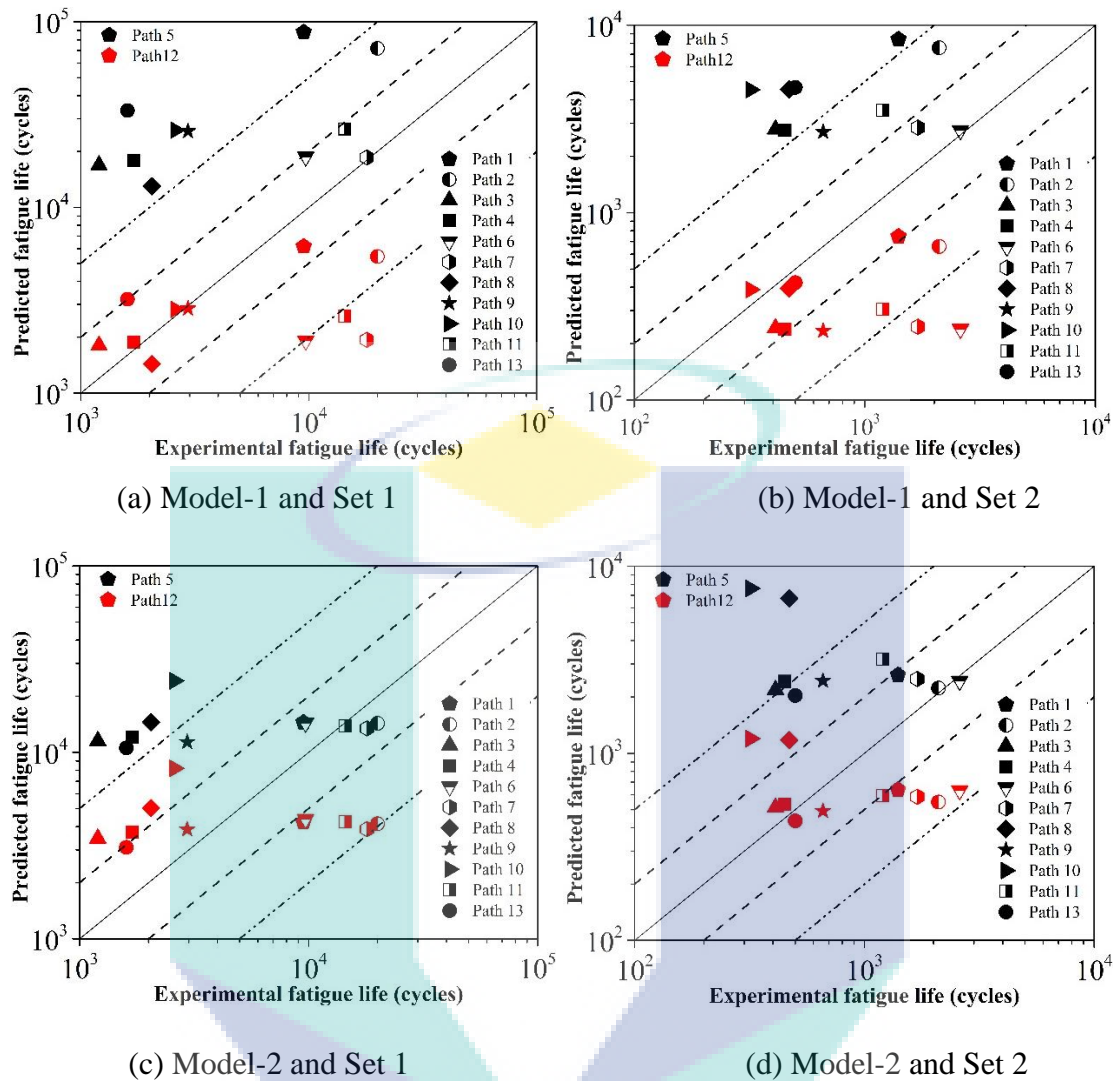
Figure 4.2: Predicted fatigue life (cycles) versus experimental fatigue life for SS304 specimen against various loading profiles and applied strain loadings.

direction as a common factor, while Paths 1, 2 and 5 also have two principal strain directions in common (Itoh et al., 1995). Hence Path 5 is a suitable candidate to be a characteristic profile for Paths 1, 2 and 11. Therefore the model coefficients determined by using Path 5 estimated the fatigue life with good accuracy. In profile Paths 1 and 2, the maximum principal strain alternates between 0° and 45°, while in profile Path 11 the planes of maximum principal strain continuously rotate (Itoh et al., 1995). Since the proposed fatigue model gives accurate results with Model-2, it can be observed that application of proposed fatigue life Model-2 efficiently handles the rotation of the principal strain directions in fully reversed loading. For profile Paths 3 and 4, when the fatigue life is predicted by Model-1 using the coefficients calibrated from strain Set 1

and profile Path 12 (Table 4.3), very good accuracy is observed with a minimum 1.0% difference.

The predicted fatigue life is compared with the number of blocks instead of the number of cycles in the experimental results, as profile Paths 3, 4 and 13 are counted as two cycles per block, because one cycle is defined as a full straining for both axial and shear cycles (Itoh et al., 1995). This shows that Model-1 can better capture the direction of strain changing at zero strain, as happens in profile Paths 3 and 4 (Itoh et al., 1995). This is due to the combined terms containing stress and strain quantities, where the direction (sign) of the stress will drive the effect of the whole combined term. Hence Model-1 can better capture the effect of changing directions of strains from compressive to tensile and vice versa.

Profile Paths 6 and 7 are nearly proportional, especially Path 6, as a large number of small loading steps results in nearly proportional loading (Itoh et al., 1995; Kida et al., 1997). For Paths 6 and 7, fatigue life prediction from the proposed fatigue life Model-1 and Model-2 shows better accuracy with model coefficients calibrated by profile Path 5 than by Path 12, with minimum differences of 0.3% and 8% respectively. Profile Paths 8, 9 and 10 have rectangular or box-strain history; Paths 8 and 9 retrace the loading path after one half cycle while Path 10 characterizes a continuous path (Itoh et al., 1995; Kida et al., 1997). The results of the estimated fatigue life from Model-1 show agreeable accuracy, with coefficients of the model calibrated with Path 12 showing a minimum of 0.4% difference from the experimental results. Profile 11 and 12 show the phase difference between normal and shear strains (Kida et al., 1997), while Path 13 has a retrace of strain-path added from Path 12. For the estimated fatigue life for Path 11, the proposed fatigue life model with Model-1 and Model-2 results in a mixed response for model coefficients calibrated with Path 5 and Path 12. The resultant mixed effect is attributed to the 45° phase difference between the axial and shear strain for Path 11, which is intermediate between Path 5 and Path 12, as Path 5 is in-phase and Path 12 is out-of-phase (Kida et al., 1997). For Path 13, the proposed fatigue model application with model coefficients calibrated with profile Path 12, for both Model-1 and Model-2, predicted the fatigue life with good accuracy, with a minimum 1% and 3% difference respectively against the experimental data.

Hence, it can be concluded that the predicted fatigue life from the proposed fatigue Model-1 and Model-2 is in good agreement with the experimental results. The number of iterations required for Model-1 is approximately 50% less than for Model-2 due to the smaller number of variables to be calibrated. Relatively scattered results are obtained with Model-1. Scattered results are also reported for the energy-based fatigue parameter (Ince and Glinka, 2014). However, the smaller number of iterations required for model coefficients calibrated with Model-1, as well as the complexity involved in dealing with various profiles using Model-2 containing separate stress-strain terms, make Model-1 a better candidate for fatigue parameter estimation. Therefore, the model with combined stress–strain terms, i.e. Model-1, will be used for fatigue life prediction as well as the proposed fatigue life model performance analysis.

4.3 PERFORMANCE OF PROPOSED MODEL WITH DIFFERENT MATERIALS AND LOADING CONDITIONS

In this section the performance of the proposed model is analysed against different materials and loading conditions. These include experimental results from already published literature for carbon steel C40 (Atzori et al., 2006), low carbon steel EN3B (Susmel and Taylor, 2008), low carbon steel (steel 20) (0.24% C, 0.25% Si, 0.45% Mn, 0.2%Cr and balance Fe) (Fatemi and Gladskyi, 2013), stainless steel SS304 (Itoh et al., 1995) and titanium alloy (BT9) (0.081% Fe, 0.06% C, 0.3% Si, 3.4% Mo, 0.018% N, 6.5% Al, 1.58% Zr, 0.006% H) (Fatemi et al., 2010). The performance is analysed against loading conditions with, in-phase and out-of-phase tension and torsion load, complex loadings with various non-proportional factors involved and block loads containing axial, torsion and out-of-phase loading segments.

4.3.1 C40 Carbon Steel with In-Phase and Out-of-Phase Loading

The experimental fatigue life results for C40 carbon steel (Atzori et al., 2006) under in-phase and out-of-phase loading with zero and positive mean is used to verify the accuracy of the proposed fatigue life model in fatigue life prediction. The specimen is a notched solid bar shown in Figure 3.19. The objective of this analysis is to evaluate the performance of the proposed model for loading with the mean stress effect as well as to validate the newly proposed method of linear interpolation of fatigue model

calibrated coefficients on the basis of applied load amplitude in order to improve the prediction accuracy of fatigue life. Table 4.5 presents the applied load with loading conditions and experimental and predicted fatigue life with respect to the number of calibration points. The predicted fatigue life is analysed against the experimental results for applied loads and the number of calibration points, where R is the ratio of σ_{min} and σ_{max}, where σ_{min} and σ_{max} are minimum and maximum stress respectively.

Table 4.5: Predicted fatigue life of C40 steel.

Normal and shear stress at net area (σ_a, τ_a) (MPa)	Experimental cycles to failure (N_f) $\times 10^6$ (Atzori et al., 2006)	Predicted cycles to failure (N_p)$\times 10^6$	
		One calibration point (CP$_1$)	Two calibration points (CP$_1$ and CP$_2$)
R= -1 and phase = 0			
101 (CP2)	2.0	2.32	1.43
129.75	0.18	0.109	0.347
159.92	0.072	0.06	0.105
179	0.21	0.041	0.054
200 (CP1)	0.027	0.0268	0.0268
221	0.012	0.02	0.0157
R=-1 and phase = 90			
99.6 (CP2)	2.0	0.06	1.182
119.5	0.94	0.032	0.24
140	0.285	0.02	0.072
160.25	0.044	0.0128	0.028
180	0.016	0.0113	0.016
199.7 (CP1)	0.011	0.009	0.0094
R=0 and phase = 0			
67.9 (CP2)	2.0	0.217	1.98
79.72	0.79	0.15	0.664
99.56	0.35	0.12	0.478
119	0.157	0.056	0.069
138.58	0.0477	0.046	0.06
158.1 (CP1)	0.026	0.0234	0.023
R=0 and phase = 90			
66.8 (CP2)	2.0	0.102	1.84
89.55	0.34	0.064	0.287
119.3	0.094	0.036	0.07
138.75	0.034	0.026	0.036
158.1 (CP1)	0.022	0.021	0.0215

In the case of loading with zero mean, $\sigma_{min} = \sigma_{max}$ with σ_{min} having a negative sign, R is -1. Similarly, in the case of loading with a positive mean, $\sigma_{min} = 0$ and $\sigma_{amplitude} = \sigma_{max}/2$, and R is 0. From each load set (with respect to R and phase), two

loads are selected for calibration, identified as CP_1 and CP_2 in Table 4.5. Fatigue life is estimated for the other load sets, initially using one calibration point CP_1. Furthermore, Table 4.6 presents the calibrated coefficients determined from the proposed GA-based calibration method for CP_1 and CP_2, where the calibrated coefficients are determined for each load by interpolation with respect to the magnitude of loading between the two limits CP_1 and CP_2.

Table 4.6: Calibrated coefficients from genetic algorithm for C40 carbon steel.

Load point (MPa)	Calibrated coefficients						
	K (×10⁻⁰¹)	R	V	a_1	a_2	m	σ_L
			$R = -1$ and phase $= 0$				
101	3.42547	0.599584	21.7	0.206696	0.324086	1	87
200	4.12513	0.493662	40.3	0.116364	0.284852	1	80
			$R = -1$ and phase $= 90$				
99.6	6.55282	0.799797	38.4	0.205202	0.525045	1	83
199.7	3.52097	0.230151	48.5	0.270758	0.232341	1	79
			$R = 0$ and phase $= 0$				
67.9	1.82930	0.68675	25.7	0.22701	0.449320	1	53
158.1	5.50956	1.031381	22.6	0.462611	0.734568	1	47
			$R = 0$ and phase $= 90$				
66.8	3.22295	0.860883	28.3	0.541942	0.175393	1	51
158.1	4.18124	0.554612	36.7	0.753561	0.251289	1	48

The results of fatigue life from the proposed fatigue life model predicted with CP_1 only, as well as with the interpolation scheme with CP_1 and CP_2, are presented in Figure 4.3, against the experimental fatigue life by Atzori et al. (2006). In the case of R = -1 in-phase load, the predicted results from the proposed model (Figure 4.3(a)) are in good agreement with the experimental results when the calibrated coefficients are determined using CP_1 only. Similarly, the results from the proposed model using calibrated coefficients obtained from the interpolation scheme between CP_1 and CP_2 are also in good correlation with the experimental results. Both calibration schemes give a minimum difference of approximately within 3% (R^2 value of 0.96) between the predicted and experimental results. Similarly, for out-of-phase load, with the CP_1 calibrated coefficients, i.e. single load point calibration, the predicted fatigue life shows significant variations compared to the experimental data (Figure 4.3(b)). The variations are more pronounced at the load points away from the calibration load point CP_1 and the predicted life is greatly underestimated with decreasing loads. This confirms the

ineffectiveness of a single load point calibration in capturing the fatigue life behaviour completely for a range of loads. The results of the two load point calibration method, i.e. interpolation of coefficients between CP1 and CP2, are in good agreement with the experimental data. The predicted fatigue life from the proposed model with the interpolation scheme shows approximately within 4% difference (R^2 value of 0.96) from the experimental fatigue life. Variations in the predicted fatigue life results for the middle range of the applied load domain are due to the observed scatter in the experimental data. Brighenti and Carpinteri (2012) reported that variations are observed in predicted fatigue life against experimental data with scatter in the endurance function model for loading conditions with zero mean.

(a) R= -1 and Phase=0°   (b) R= -1 and Phase=90°

(c) R=0 and Phase=0°   (d) R=0 and Phase=90°
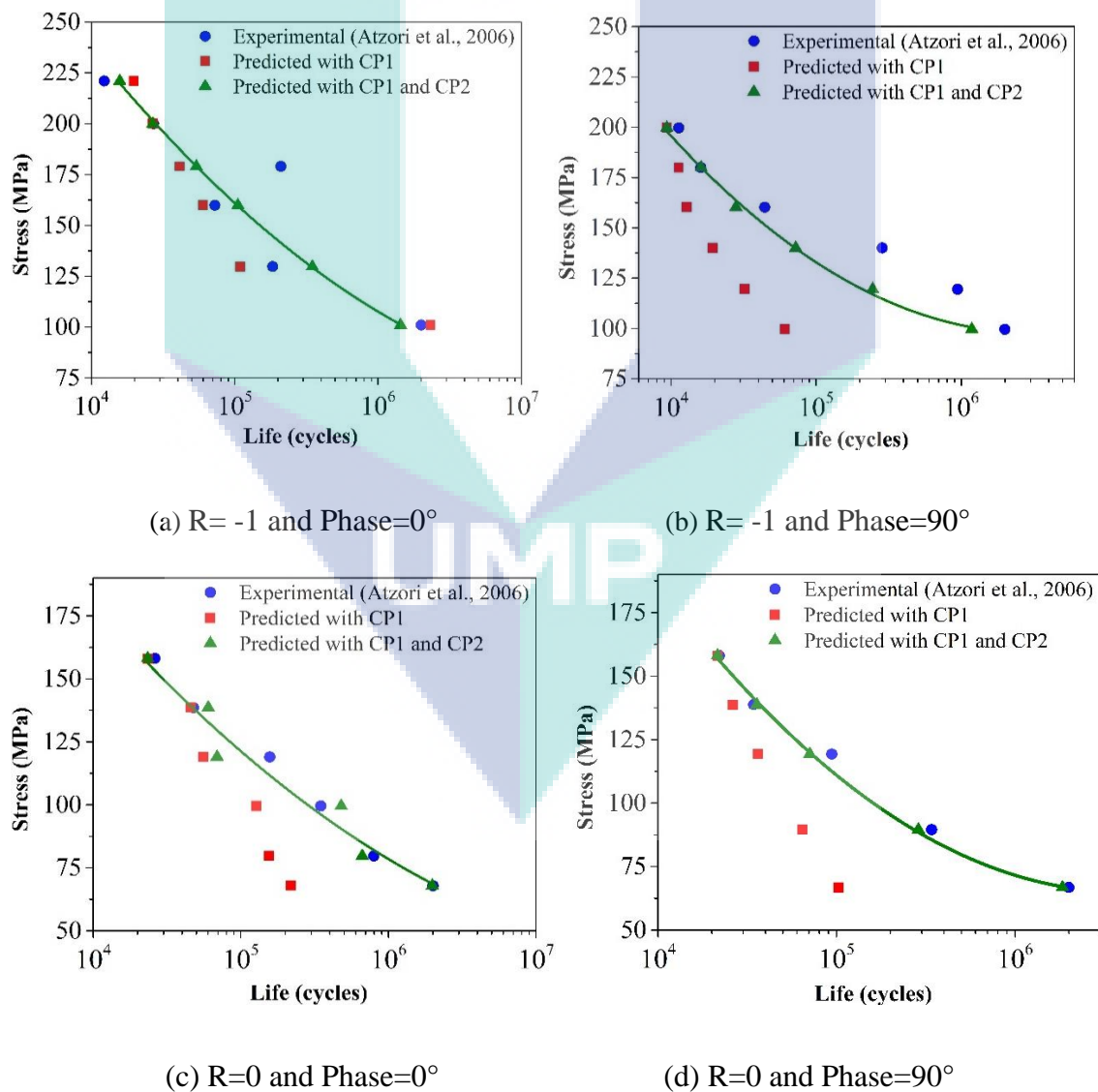
Figure 4.3: Predicted versus experimental life for C40 steel with respect to stress ratio (R) and phase difference.

For the conditions having R = 0 with in-phase and out-of-phase loading, the predicted fatigue life results from the proposed model with single point CP_1 calibration show a deviation from the experimental results. At decreased loads, i.e. away from the calibration point CP_1 load, a gradually diverging trend is observed in the predicted fatigue life. The predicted life is on the conservative side but with 15 to 20% difference (R^2 value of 0.87) from the experimental fatigue life, when shifting from the low-cycle to high-cycle region. As the selected load point CP_1 has fatigue life in the low-cycle region. This shows the inability of the single point calibration method to accurately predict fatigue life. With coefficients obtained from the interpolation scheme, i.e. interpolation between two load points (CP_1 and CP_2), the predicted fatigue shows good agreement with experimental fatigue life data, but on the slightly conservative side. The predicted fatigue follows the trend of experimental life accurately with a difference of approximately 2% (R^2 value of 0.99). The order of magnitude is similar for the proposed model and experimental data at corresponding load points.

The results obtained show the effectiveness of using more than one load point for the calibration of the proposed model coefficients. The effectiveness of the proposed model is evident for proportional as well as non-proportional loading cases. Estimation of the coefficients of the proposed model using GA (Table 4.6) is accompanied with an inherent flexibility of accommodating any kind of loading condition, as well as iterative improvement of the solution by applying the evolutionary algorithm (Brighenti and Carpinteri, 2012).

4.3.2 EN3B Steel Alloy with In-Phase and Out-of-Phase Loading

The performance of the proposed fatigue life model for EN3B steel alloy against the experimental results (Susmel and Taylor, 2008) for zero and positive mean as well as in-phase and out-of-phase tension and torsion loadings are presented. The specimen used for fatigue life prediction is a solid notched bar with a diameter of 8.0 mm, shown in Figure 3.17. The performance is analysed for loading with mean stress as well as scatter in the experimental results by Susmel and Taylor (2008). The proposed model coefficients calibrated using the proposed GA-based calibration method for two and

three load points are shown in Table 4.7. Accurate fatigue life prediction results are obtained in the case of three load points with the proposed interpolation scheme, compared to the two load point calibration of the model coefficients. The additional calibration point is selected at a load point in between the two extreme load points within the studied range for R = 0 and phase = 90 case, as shown in Table 4.8. Fatigue life is predicted for the applied normal and shear stress, where R has the same meaning as defined in the previous section. From each load set (with respect to R and phase) as in Table 4.8, two load points are selected for calibration and identified as CP_1 and CP_2. A third load point CP_3 is selected for the R= 0 and phase = 90° load set, as this set has enough load points to be used for performance analysis life after three are selected as calibration points. Fatigue life is estimated using interpolated coefficients based on the normal stress data for each load.

Table 4.7: Calibrated coefficients from genetic algorithm for EN3B steel alloy.

Load point (MPa)	$K (\times 10^{-01})$	R	V	a_1	a_2	m	σ_L
				Calibrated coefficients			
			R = -1 and phase = 0				
180	9.30498	0.724	20.8	0.480175	0.443722	1	138
275	12.0781	0.517	31.9	0.529860	0.318603	1	134
			R = -1 and phase = 90				
200	10.8000	0.811	27.3	0.42238	0.527092	1	138
285	11.3507	0.396	18.5	0.49135	0.331566	1	136
			R = 0 and phase = 0				
150	12.2399	0.952	26.8	0.273191	0.523005	1	104
190	11.7468	0.750	23.0	0.509624	0.484350	1	123
			R = 0 and phase = 90				
145	9.12036	0.843	21.3	0.21777	0.44642	1	139
170	8.81021	0.359	20.1	0.207048	0.289171	1	138
235	9.63454	0.457	31.1	0.330776	0.249027	1	137

Results of predicted fatigue life from the proposed fatigue life model using two-point and three-point interpolations of coefficients are presented in Figure 4.4 along with the experimental life by Susmel and Taylor (2008). For the case of the load set with R = -1 and phase = 0, it is observed that the fatigue life predicted by the proposed fatigue life model is on the conservative side. The predicted life for a load point of 200 MPa normal stress is higher than the experimental life. This increase in the predicted

fatigue life for the mentioned load point is due to the slight scatter in the experimental data, resulting in a deviation from the model behaviour at other load points. Results from the proposed fatigue life model are in good agreement with the experimental data, showing approximately 2% difference in estimating the fatigue life for the R = -1, phase = 0 case. For the case of the load set with R = -1 and phase = 90, the predicted fatigue life from the proposed fatigue life model is in good correlation with the published experimental results.

Table 4.8: Predicted fatigue life for EN3B steel.

Normal stress at net area (σ_a) (MPa)	Shear stress at net area (τ_a) (MPa)	Experimental fatigue life (cycles) (Susmel and Taylor, 2008)	Predicted fatigue life (cycles)	
			Two calibration points (CP_1 & CP_2)	Calibration points (CP_1 - CP_3 & CP_3-Cp_2)
R = -1 and phase = 0				
180 (CP_2)	103.9	2174897	1786431	---
190	109.7	1400006	807181	---
200	115.5	437907	445531	---
230	132.8	188480	135909	---
259.6	155.9	82952	58167	---
275 (CP_1)	158.8	46254	42878	---
R = -1 and phase = 90				
200 (CP_2)	115.5	2100000	1869827	---
230	132.8	245935	184465	---
250	144.3	79328	79388	---
260	150.1	314817	68753	---
270	155.9	59622	42365	---
285 (CP_1)	164.5	34338	28869	---
R = 0 and phase = 0				
150 (CP_2)	150	844615	759879	---
160	160	370618	169407	---
165	165	249286	119982	---
170	170	110056	86524	---
180	180	28108	51294	---
190 (CP_1)	190	34298	31123	---
R = 0 and phase = 90				
145 (CP2)	145	2581210	2303300	2303300
150	150	2500000	1317299	839787
155	155	367445	704303	363447
160	160	304439	444139	195065
170 (CP3)	170	112944	230905	81354
180	180	49200	131045	58199
190	190	52000	84352	45785
200	200	67873	48555	31242

| 235 (CP1) | 135.7 | 59243 | 53559 | 53559 |

The predicted fatigue life is lower than the experimental fatigue life, resulting in safe mechanical designs. The minimum difference between the predicted fatigue life and the experimental data is less than 1%. The difference in the predicted fatigue life and the experimental data at the load point with 260 MPa normal stress load is attributed to the scatter in the experimental results The experimental fatigue life shows a higher than expected fatigue life as compared to the behaviour of fatigue lives from other load values, as observed in Figure 4.4(b). In general, the results of predicted fatigue life from the proposed model are accurate with respect to experimental data for the load set with R = - 1 and phase = 90.

(a) R = -1 and Phase = 0°   (b) R = -1 and Phase = 90°

(c) R = 0 and Phase = 0°   (d) R = 0 and Phase = 90°
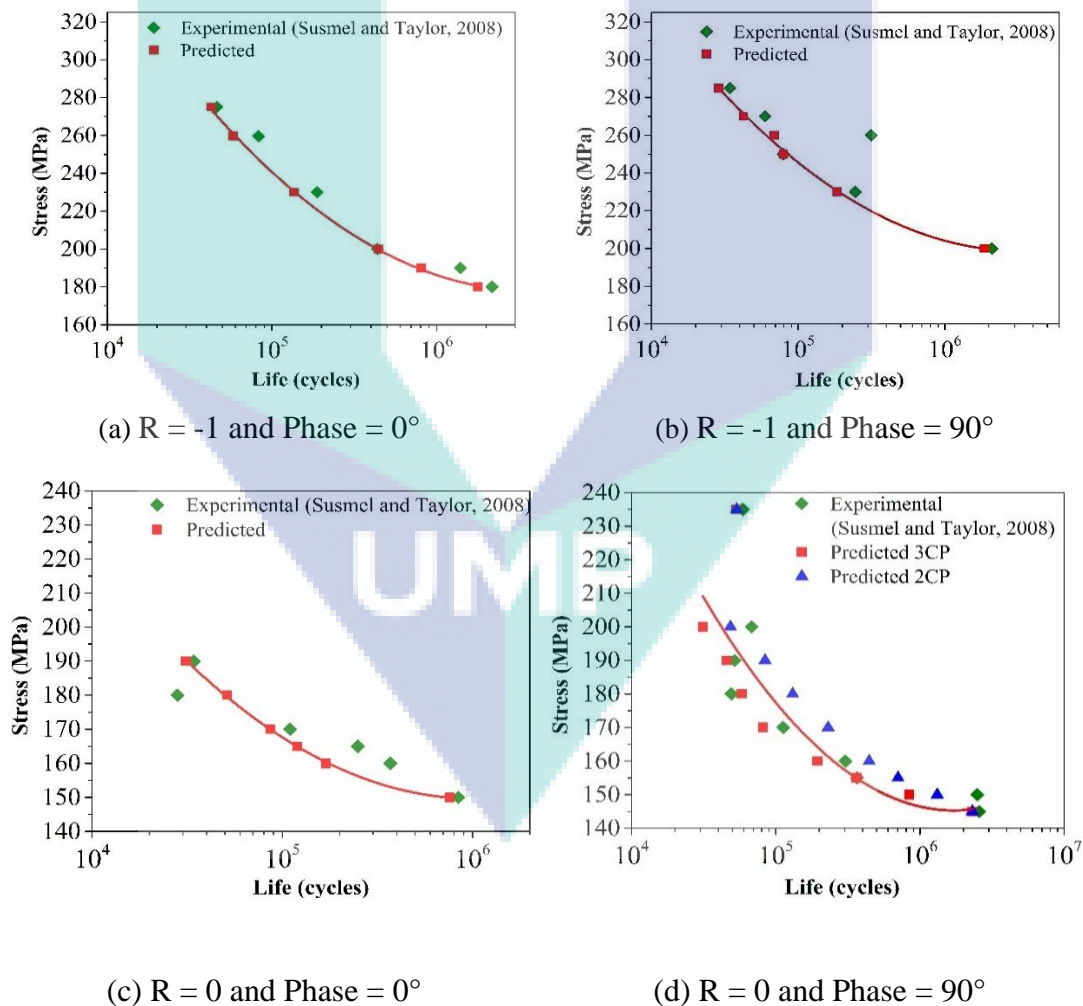
Figure 4.4: Predicted versus experimental life against applied normal stress for EN3B steel with respect to stress ratio (R) and phase difference.

For the load case of R = 0, phase = 0, the predicted fatigue life results are presented in Table 4.8. The results are on the conservative side, as the predicted fatigue life is lower than the experimental fatigue life, which is generally favourable for safe designs. However, at a normal stress load value of 180 MPa, the experimentally obtained fatigue life is lower than the predicted life. This is attributed to scatter in the experimental data, as shown in Figure 4.4(c). This is not representative of the typical behaviour of EN3B material with respect to other load points. For the remaining load values, the estimated fatigue life from the proposed model is in good agreement with the experimental data, showing a difference of approximately 2%. For the load set with R = 0 and phase = 90, the fatigue life is estimated using model coefficients determined from two and three calibration points. The results for predicted and experimental fatigue life are presented in Figure 4.4(d). The fatigue life predicted by interpolating the model coefficients between the two calibration points, CP_1 and CP_2, is generally overestimated, especially in the region away from CP_1 and CP_2, with more than 10% difference. A significant improvement in fatigue life prediction accuracy is obtained when three-point calibration is used, with an additional calibration point CP_3 at 170 MPa load in the interpolation scheme. The predicted fatigue life resulting from the three-point calibration shows good agreement with the experimental fatigue life within a minimum 1% difference. The estimated fatigue lives provide a good averaged representation of the EN3B behaviour even with the scatter in the experimental results. Hence, in summary, the use of additional calibration points improves the fatigue life prediction accuracy. Greater fatigue life prediction efficiency can be achieved with fewer calibration points for a range of load magnitudes. Hence, the number of experiments is reduced, leading to cost-effective experimental testing for generating the calibration data.

4.3.3 Low Carbon Steel (Steel 20) with Axial and Torsion Loading

The experimental fatigue life results of low carbon steel (steel 20 alloy) with a chemical composition 0.24% C, 0.25% Si, 0.45% Mn, 0.2%Cr and balance Fe (Ukranian-Standard, 1988; Fatemi and Gladskyi, 2013), under fully reversed, load-controlled fatigue tests with sinusoidal load waveforms are used for performance analysis of the proposed model. In a load-controlled fatigue test, a sequence of stress

amplitudes is obtained by applying cycles of stress amplitudes to the test specimen until failure (Gale and Totemeier, 2003). The sinusoidal load waveform is a combination of fully reversed axial and torsion cycles applied as a set of repeating blocks. In this section, the fatigue life prediction results for axial and torsion load cycles are discussed. The performance of the proposed fatigue life model for notched components in cases of axial and torsion loading is evaluated with interpolation of the calibration coefficient technique. A thin-walled tubular specimen with a circular hole as a notch in the centre of the gauge length (shown in Figure 3.23) is used for the analysis.

The critical location for fatigue failure in the specimen in the case of axial and torsion load is dependent on the stress distribution around the notch hole for both axial and torsional loading conditions, as shown in Figures 4.5(a) and 4.5(b). The critical fatigue failure location is determined by applying axial and torsion load in the FEM. The stress distribution is obtained around the periphery of the notch hole showing stress concentration regions. Angles around the circumference of the notch hole are according to Figure 4.5(c). As seen from the stress distribution patterns obtained on the notch hole circumference, the critical location for fatigue failure in tension and torsion loading is observed at different orientations around the circumference. For axial loading, the critical locations are at $0°$ and $180°$ while for torsion loading the critical locations are observed at $45°$ and $135°$ around the hole circumference. The results are in agreement with the experimentally observed crack locations for the respective loading, as shown in Figures 4.5(d) and 4.5(e) (Fatemi and Gladskyi, 2013). The magnitudes of applied normal (axial) and torsion stress used for the analysis of the experimental and predicted fatigue life with the experimental and predicted orientations of the critical plane are presented in Table 4.9. From each of the axial and torsion load set, calibration points are selected at two load values labelled as CP_1 and CP_2 in Table 4.9, assuming that the range of experimental data is completely defined by the selected load values. The calibration coefficients for low carbon steel determined from the proposed GA-based calibration method are shown in Table 4.10. From the axial load set, the stress amplitude of 106 MPa is not selected as the calibrated load. This is in order to check the possibility of extrapolation in determination of the calibration coefficient in addition to the interpolation scheme. Extrapolation with respect to CP_1 and CP_2 in the normal stress load set is used for determining the calibrated coefficients for the 106 MPa load.

(a) For axial load   (b) For torsion load

(c) Angle designation

(d)   Crack location for axial load   (e) Crack location for torsional load
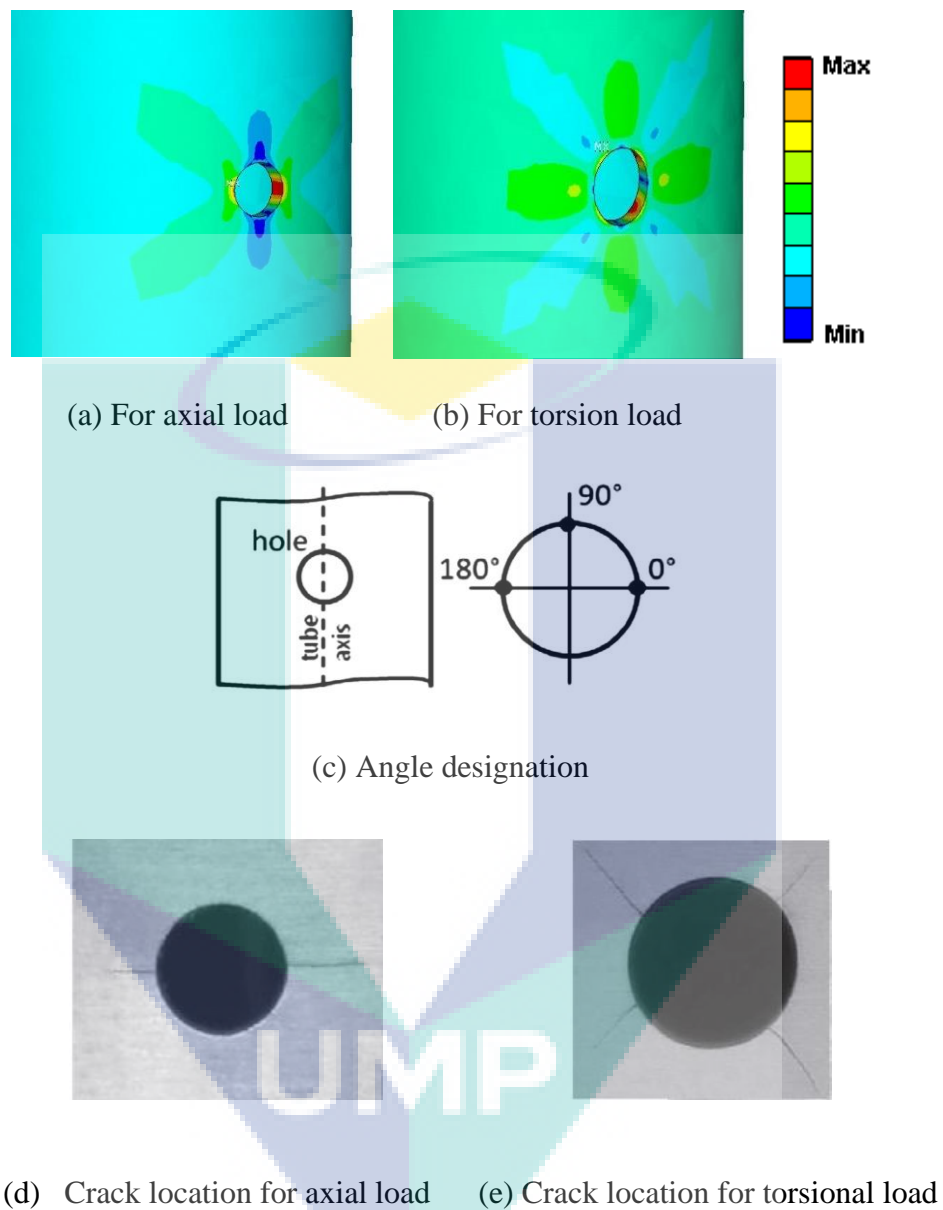
Figure 4.5: Stress distribution, angle designation and crack locations around notch hole.

The results of the predicted fatigue life for axial and torsion loading conditions using the proposed fatigue life model are given in Figure 4.6. In the case of axial loading, application of the proposed model with the interpolation technique for the model coefficients predicted fatigue life results that are in good agreement with published experimental fatigue life results (Fatemi and Gladskyi, 2013) with a difference of approximately 2%. The model coefficients are also determined using

extrapolation of the calibrated coefficients for a load of 106 MPa. However, the results obtained from the extrapolation show a smaller value of coefficient 'K' than the coefficient value determined from calibration scheme, as shown in Table 4.10. This can lead to negative value of the coefficient at lower load values. Negative coefficients are unrealistic and contrary to the definition of the model. Hence the extrapolation technique is not recommended to determine the model coefficients. In order to use two load points for the calibration of the model coefficients, the selected load points must cover the range of studied loads for interpolation, i.e., the selected loads points must be at the extremes of the studied range of loads.

Table 4.9: Predicted fatigue life for low carbon steel (steel 20).

Applied nominal stress (MPa)	Experimental life (cycles) (Fatemi and Gladskyi, 2013)	Predicted life (cycles)	Critical plane orientation (deg.)	
			Experimental (Fatemi and Gladskyi, 2013)	Predicted
Normal stress				
269 (CP1)	315	302	5	0
250	495	441	4	0
200	2115	1466	2	0
144 (CP2)	20900	19618	2	0
106	140500	135551	0	0
Shear stress				
149 (CP1)	5659	5502	45	45
121	34700	15963	45	45
87	198000	107501	45-48	45
65 (CP2)	1150000	906000	--	45

Table 4.10: Calibrated coefficients from genetic algorithm for low carbon steel (steel 20).

Load point (MPa)	Calibrated coefficients						
	K (×10^{-01})	R	V	a_1	a_2	m	σ_L
Normal stress							
269	15.23	0.075118	20.8	2.612265	1.77667	1	81
144	6.937	0.303484	21.9	2.485315	2.20052	1	84
106	9.934	0.301521	24.1	1.957164	1.730195	1	76
Shear stress							
149	9.838	0.348106	17.3	1.236188	1.154545	1	88
65	4.231	0.226825	17.7	1.038966	1.274541	1	84
Extrapolated							
106	4.415	0.372907	22.2	2.446722	2.329704	1	85

(a) Normal stress   (b) Shear stress
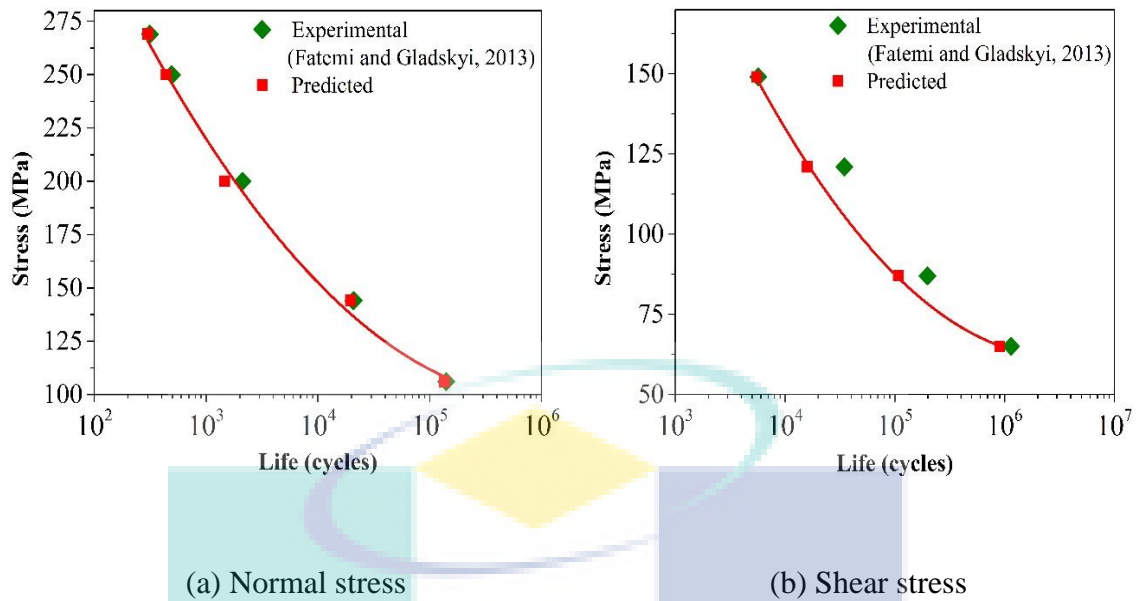
Figure 4.6: Predicted versus experimental fatigue life for low carbon steel (steel 20) with applied normal and shear stress.

The predicted fatigue life for the load of 106 MPa in Table 4.9 is determined by using model coefficients calibrated from the proposed calibration scheme (Table 4.10). Critical plane orientations estimated on critical locations identified earlier, i.e. 0° and 45°, using the proposed model are presented in Table 4.9. The results are in good correlation with experimental observations, showing a maximum 5° difference between the predicted critical angles and the experimental data for the normal load of 269 MPa. For other loading conditions, the predicted critical plane angles are similar to the experimental results.

For torsional loading the estimated fatigue lives are on the conservative side with a difference of approximately 5% from the experimental results. Scatter in the experimental results leads to underestimated fatigue life, especially at 121 MPa load. Underestimation of the predicted fatigue life may be attributed to the use of fewer cycles for the load of 65 MPa as the experimental fatigue life, i.e. 1.15×10^6 cycles. According to the results reported by Fatemi and Gladskyi (2013), the experimental fatigue life is greater than 1.15×10^6 cycles. Critical plane orientations estimated using the proposed multiaxial fatigue model are presented in Table 4.9. The results are in good agreement with experimental observations, showing a maximum 3° difference

between the predicted critical angles and the experimental data for the shear load of 87 MPa. The predicted critical plane orientation is accurate, showing only a difference of 3–5° compared with the experimentally obtained critical plane orientation results. Hence, it can be observed that the predicted orientation of critical planes has no effect on the underestimation of the predicted result. Therefore, it can be concluded that the conservative estimation of fatigue life is due to the scatter in the experimental results for the fatigue life in the torsional loading case.

4.3.4 Low Carbon Steel (Steel 20) with Blocks of Axial and Torsion Loads

Experimental fatigue life data for various combinations of axial and torsional loading cycles (Fatemi and Gladskyi, 2013) are presented in Figure 4.7. Axial cycles of 144 MPa normal stress and torsion cycles of 149 MPa shear stress are applied. Blocks of loads are identified as 'A' for axial and 'T' for torsion with the respective number of cycles in the block. The calibrated coefficients for the proposed model for the above-mentioned normal and torsion load are shown in Table 4.10. The estimated fatigue life from the proposed model using Eq. (3.26) is reported in Table 4.11. It is observed that for the loading block with 1000 axial and 100 torsion cycles (A1000-T100), the fatigue life estimated by the axial calibrated model is on the conservative side compared with the experimental data. It is observed that this load block is dominated by axial load cycles (Fatemi and Gladskyi, 2013). Hence, the number of axial cycles with respect to the number of blocks observed in Table 4.11 for A1000-T100 is very similar to the fatigue life obtained with axial loads only for the same magnitude of 144 MPa (Table 4.9). Hence, when the fatigue life is predicted by the proposed model, damage due to torsion cycles is added to the cumulative damage that occurred due to the axial cycles in the block, resulting in a smaller number of blocks to failure. In the case of fatigue life with torsion calibration, the predicted fatigue life is overestimated with relatively good accuracy. However, the resultant higher accuracy is an anomalous result in this case. This is attributed to the fact that the critical points for torsion loading, i.e. 45° and 135°, as seen in Figure 4.5(b), are different from the critical points for axial loading, i.e. 0° and 180°. The stress distribution is different at the critical point locations for axial and torsion loadings, so the calibrated coefficients determined using torsion

load are based on a different stress distribution from that actually present at the critical location for the A1000-T100 load block, i.e. 0° and 180°.
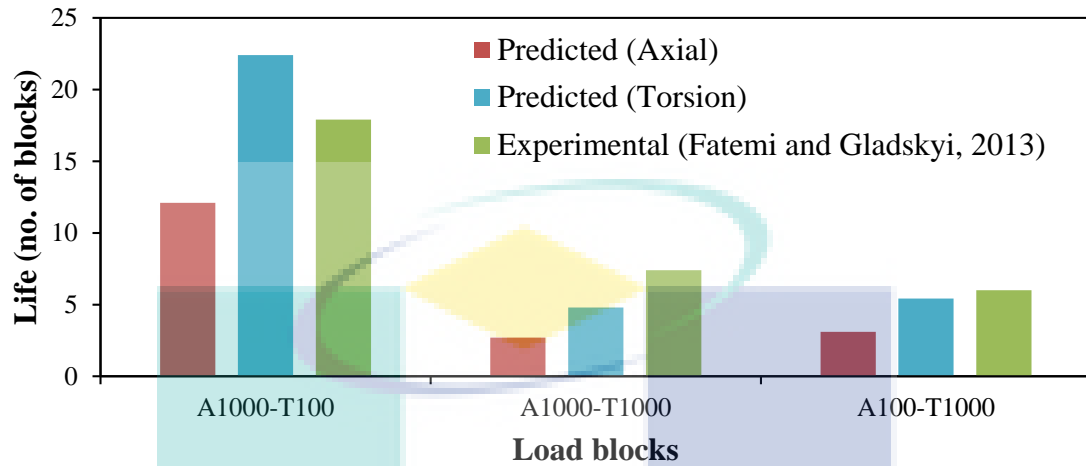
Figure 4.7: Predicted and experimental fatigue life for block loading for low carbon steel (steel 20).

Table 4.11: Fatigue life for block loads with respect to each calibration for low carbon steel (steel 20).

Loading combination	Applied nominal stress (MPa)		Fatigue Life(blocks)		
	Normal	Shear	Experimental (Fatemi and Gladskyi, 2013)	Predicted, calibrated by:	
				Axial load	Torsion load
A1000-T100			17.9	12.1	22.4
A1000-T1000	144	149	7.4	2.7	4.8
A100 / T1000			6.0	3.1	5.42

In the case of the load block with A1000-T1000, the number of cycles with respect to the number of blocks to failure (Table 4.11) shows the beneficial effects of axial loading on the torsion cycles in the experimental fatigue life. More torsion cycles are required to fail the material compared to the pure torsion case (Table 4.11) (Fatemi and Gladskyi, 2013). When fatigue life is estimated using the proposed model with axial calibration and the cumulative fatigue life calculated by Eq. (3.26), conservative results are obtained. The reason for this reduced accuracy is attributed to the observed beneficial effect of axial loading in the experimental results on the number of torsion cycles required to fail the specimen. A factor contributing to this observed phenomenon due to the T-stress from axial loading, which can extend the plastic zone size beyond

that present in pure torsion tests and another factor due to the increased friction during the compression part of the axial cycles. Therefore, both the plasticity and roughness induced closures may explain retardation effect of axial loading on torsion fatigue life (Fatemi and Gladskyi, 2013). This in turn leads to more applied load blocks being needed before failure. However, in the case of the fatigue life predicted from the proposed model, cumulative damage is determined by summing up the damage from each segment. Hence, the effects of axial loading on torsion cycles are not included in the cumulative damage obtained. An improved result is obtained from the proposed fatigue model with coefficients calibrated by pure torsion, in terms of better accuracy in predicting the required number of blocks to failure. This improvement in accuracy is due to the torsion calibrated coefficients, as the torsion cycles are more damaging then axial cycles, as observed from the number of cycles required to failure in Table 4.11.

Both axial and torsion cycles are equal in number when the interaction of the axial and torsion loadings is ignored. The torsion loading causes more damage than the axial with the same number of cycles. Hence, this load block is more similar to the pure torsion case. Therefore, the calibrated coefficients determined from pure torsion load predicted the fatigue life with better accuracy than the case for calibrated coefficients from pure axial load.

For the A100-T1000 load block, the number of loading blocks to failure predicted by the proposed model is conservative. This is because the locations of the critical points for torsion loading (45° and 135°) are different from the axial loading locations (0° and 180°), as shown in Figure 4.5(b). Hence the stress state is changed at both locations, i.e., the location of the critical point in axial and torsion load is different. As the block is dominated by the more damaging torsion loading cycles, the difference in estimated fatigue life between the axial calibrated model and the experimental fatigue life is as expected (Table 4.11). With the torsion calibrated model coefficients the predicted fatigue life has a minimum 14% difference from the experimental fatigue life. This is due to the fact that the A100-T1000 block primarily consists of torsion cycles, and experimental results have shown that there is no effect of axial cycles on torsion fatigue behaviour for this block load (Fatemi and Gladskyi, 2013). Thus, the predicted fatigue life has shown good agreement with the experimentally observed

fatigue life. Axial cycles cause less damage than torsion cycles, as well as being dominated by the torsion cycles. Hence there is no appreciable effect of axial cycles on the total cumulative damage in this case.

From the above discussion, it can be summarized that the inaccuracy in fatigue life estimation for block loadings is mainly due to the assumptions made to simplify the handling of block loads as segments. The damage caused by each segment is calculated by a linear cumulative rule. As the model is calibrated using pure torsion and pure axial profiles, the sequential effect of axial and torsion loadings is not captured. This can be seen from the fatigue life result of the A1000-T1000 block, where the effect of axial load on the torsion fatigue life is most prominent in the experimental results. Hence, to improve the fatigue life estimation by the proposed model, the selected calibration profiles should represent the characteristics of the loading profile under consideration (axial as well as torsion loading). The assumption of using the damage of one cycle to estimate the damage for the segment of block, resulting in an average prediction accuracy difference of 9%, is insufficient to capture the sequential effect of axial and torsion loadings. Hence, calibration is to be performed using a full or filtered profile so that only high damage cycles remain and the sequence effect of previous loading cycles can be captured.

4.3.5   Stainless Steel SS304 with Complex Profiles

The experimental fatigue life results of SS304 (Itoh et al., 1995) under complex loading profile paths are shown in Table 3.4 to evaluate the prediction accuracy of the proposed multiaxial fatigue life model. The specimen with a hollow-cylinder geometry was shown in Figure 3.21, and is evaluated against the set of complex loading profile paths in order to validate the application of simpler characteristic profiles for calibration of the proposed model coefficients. Simpler characteristic profiles are used to represent the complex profiles for the calibration of the proposed model from the experimental fatigue life results, thus making the experimental testing easier and more economical (Shamsaei and McKelvey, 2014). Hence, the validation results can be used to justify the application of simpler characteristic profiles, resulting in low-cost experiments for calibration of the proposed model in predicting fatigue life against in complex real-

world loading conditions. Profile Paths 5 and 12, characterizing in-phase and out-of-phase loading conditions, are considered as simpler profiles used for calibrating the model coefficients shown in Table 4.3 for Model-1. The capability of the proposed fatigue life model is evaluated for predicting fatigue life against other profile paths (Table 3.4) representing complex loadings. The results of fatigue life prediction are compared with the experimental fatigue life results. Loads with profile paths are applied with two sets of axial and shear strain ranges, Set 1 and Set 2, as presented in Table 4.1.

The application of two sets of strain magnitudes results in emphasizing the effect of the applied strain magnitude on fatigue life prediction by the proposed model. The predicted fatigue life results are presented in Table 4.12, determined with the four sets of calibrated coefficients for Model-1 (Table 4.3) with Set 1 and Set 2 of applied strain for profile paths other than Paths 5 and 12. A factor of 2–5 is generally used to describe the goodness band (Fatemi et al., 2010; Ince and Glinka, 2014). Hence the predicted fatigue life results with a superimposed goodness band are used, as presented in Figure 4.8. In order to evaluate the effect of magnitude on the prediction accuracy when the magnitude of load is different for calibration and at the time of fatigue life estimation. The fatigue life is estimated with Set 1 of applied strain when the model coefficients are calibrated using Set 2 of applied strain with Paths 5 and 12. Similarly, fatigue life is predicted with Set 2 of applied strain when the model coefficients are calibrated using Set 1 of applied strain with Paths 5 and 12. For the considered profile paths, one cycle is defined as a full straining for both axial and shear cycles. Thus the profile Paths 3, 4 and 13 represent two cycles per loading block (Itoh et al., 1995; Kida et al., 1997). For Paths 1, 2, 3 and 4, representing load paths with two principal strain directions and fully reversed loading, the fatigue life results show that the proposed model has successfully captured the multiaxiality present in the stresses. The proposed fatigue life model with coefficients calibrated using Path 12 predicted the fatigue life more accurately than the fatigue life predicted with coefficients calibrated using Path 5, with differences of 5–8% and 13–24% respectively. This is also clear from the profile path shapes, as the applied normal and shear strain are in-phase for Path 5, resulting in the minimum possible non-proportionality of stresses (Itoh et al., 1995), making this a less damaging path than Path 12. The proposed model calibrated from profile Path 5 predicts a higher number of cycles than the experimental results in the case of more

severe multiaxial profile paths. In contrast, the fatigue life prediction results from the proposed fatigue life model with model coefficients calibrated with profile Path 12 are in good agreement with the experimental results. This is due to the fact that prediction with Path 12 (i.e. with axial and shear strain 90° out-of-phase) generates a mutlitiaxial response. Hence, the proposed model is capable of predicting fatigue life more accurately for other profile paths having a multiaxial response.

Table 4.12: Fatigue life predicted for SS304.

Path no.	Experimental life (cycles) (Itoh et al., 1995)	Predicted life with calibration by			
		Set 1		Set 2	
		Path 5	Path 12	Path 5	Path 12
		Set 1 as applied load			
1	9500	88019	6162	26139	2156
2	20000	71932	5441	22710	1880
3	2400 (1200 blocks)	16920	1806	7160	617
4	3400 (1700 blocks)	17825	1868	7364	645
6	9700	18731	1911	7429	657
7	18000	18582	1935	7553	664
8	2050	12987	1435	5572	488
9	2950	25744	2851	11108	968
10	2600	26073	2822	10912	959
11	14400	26493	2593	10264	892
13	3200 (1600 blocks)	33272	3201	13048	1127
		Set 2 as applied load			
1	1400	19739	2138	8423	746
2	2100	17703	1930	7586	659.5
3	820 (410 blocks)	5855	719	2785	242
4	900 (450 blocks)	5898	712	2751	238
6	2600	6216	714	2749	239
7	1700	6320	737	2842	246
8	470	9905	1182	4551	394
9	660	5612	699	2696	234
10	320	9921	1170	4525	388
11	1200	7809	906	3513	304
13	1000 (500 blocks)	10026	1208	4662	423
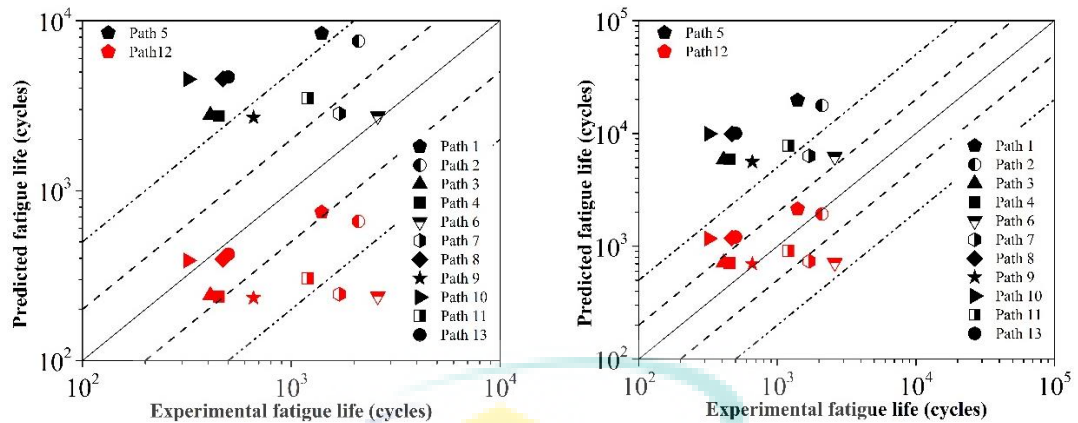
(a) 0.8 axial 1.39 shear strain (Set 2) applied load and calibration load

(b) 0.8 axial 1.39 shear strain (Set 2) applied load and 0.5 and 0.87 (Set 1)calibration load
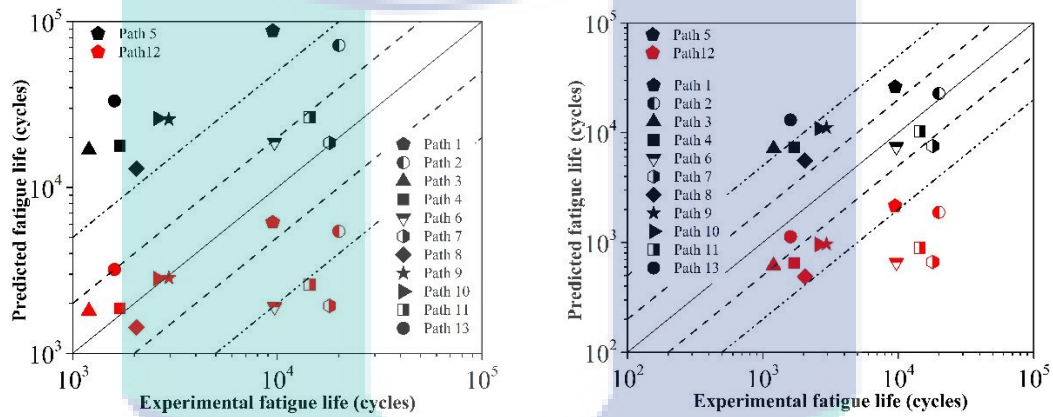
(c) 0.5 axial 0.87 shear strain (Set 1) applied load and calibration load

(d) 0.5 axial 0.87 shear strain (Set 1) applied load and 0.8 and 1.39 (Set 2) calibration load

Figure 4.8: Predicted versus experimental life for SS304 with respect to applied strain load, calibration load and load profile used for calibration.

Paths 6 and 7 are similar to Path 5 with respect to the characteristics of proportional loading. The predicted fatigue life results by the proposed fatigue life model with coefficients calibrated using Path 5 are in good agreement with the experimental fatigue life results, with a minimum difference of 1%. Similarly, profile Paths 8, 9, 10 and 13 have loading characteristics similar to Path 12. The estimated fatigue life from the proposed fatigue life model is in good accuracy, with a minimum 1–4% difference compared to the experimental results. However, the predicted fatigue life from the proposed model with Path 11 using the model coefficients calibrated with Paths 5 and 12 shows mixed results in both cases. This is due to the fact that Path 11 has a 45° phase difference between applied axial and shear strain (Kida et al., 1997), i.e. its

loading is in between Paths 5 and 12, which are fully proportional in-phase and non-proportional out-of-phase respectively. Thus Path 11 is similar to both Paths 5 and 12 with respect to the characteristics of the profile. Additionally, the fatigue life prediction accuracy of the proposed fatigue life model is evaluated for the effects of applied loads with different magnitudes used for calibration and fatigue life estimation. Hence, strain Set 1 (Table 4.1) with Paths 5 and 12 is used to calibrate the proposed model, and strain Set 2 is used to predict the fatigue life for the remaining profile paths. Similarly, strain Set 2 (Table 4.1) with Paths 5 and 12 is used to calibrate the proposed model and strain Set 1 is used to predict the fatigue life for the remaining profile paths. From the results obtained from Table 4.12, it is clear that the magnitude has a noticeable impact on the fatigue life prediction accuracy of the proposed fatigue life model. From Table 4.12, with the fatigue life predicted with Set 1, it is observed that fatigue life predicted from proposed fatigue life model with model coefficients calibrated with applied strain load Set 2 is lower than when predicted with Set 1 calibration. Calibration with the higher magnitude strain load Set 2 results in model coefficients causing more damage per applied unit load. Hence, a lower fatigue life is predicted with the smaller magnitude strain load Set 1. A combination of Path 2 and strain loading Set 2 with model coefficients calibrated using Path 5 gives more accurate predicted fatigue life than the combination of Path 2 and loading Set 1. However, the result is a mathematical coincidence without any direct technical explanation.

Fatigue life predicted by the proposed fatigue life model with strain loading Set 2 as applied load is presented in Table 4.12. The predicted life from the proposed fatigue life model with coefficients calibrated using strain loading Set 1 is higher than that predicted with model coefficients calibrated with strain loading Set 2. For Paths 2 and 9, the model coefficients are calibrated with strain loading Set 1 and Path 12. The results of the predicted fatigue life are more accurate than the results with calibration done with strain loading Set 2 and Path 12. However, this result is anomalous and purely due to the mathematics involved, lacking a direct theoretical explanation. Hence, this result cannot be used as justification of the proposed model performance. From the results obtained, it can be observed that calibration of the proposed fatigue life model is preferably performed with load magnitudes similar to the applied loads for fatigue life estimation.

From the results presented in Table 4.12, it is evident that the proposed fatigue life model is capable of handling complex multiaxial profiles. The concept of using simpler profiles representing the characteristics of the complex profiles for the calibration of the proposed model from experimental fatigue life data is verified. A fully proportional in-phase (Path 5) and non-proportional out-of-phase (Path 12) profiles are used for calibrating the proposed model coefficients and predicting the fatigue life for more complex profiles (Table 3.4). Non-proportional factors examined in the considered profiles are the two principal strain directions, fully reversed loading, rotational principal strain direction, step length and direction of loading path (Itoh et al., 1995). The proposed fatigue life model handled these factors with good accuracy (i.e. minimum 1% difference). This shows the inherent flexibility of the proposed fatigue life model with the application of the genetic algorithm. Furthermore, for application of the model, no new material constant needs to be determined, and only the FEA material model needs to be defined. A non-linear material model is essential in order to accommodate plasticity. A significant feature of the proposed fatigue life model is its simplicity in application, as only the fatigue limit is required as a material fatigue property. It is preferable that the fatigue limit used is similar to that of the loading profile used for calibration. In case of unavailability of the fatigue limit data, the model is flexible, as the fatigue limit for simple cyclic loading can be applied with a reduced fatigue limit value. This flexibility of the model is inherent due to the application of a GA capable of estimating correct behaviour with this assumption.

4.3.6 Titanium Alloy BT9 with Combination of Axial, Shear and Out-of-Phase Axial and Shear Load

The block loading used for titanium alloy BT9 (chemical composition 0.081% Fe, 0.06% C, 0.3% Si, 3.4% Mo, 0.018% N, 6.5% Al, 1.58% Zr, 0.006% H and balance Ti) consists of axial, torsion and axial–torsion out-of-phase loading segments, as shown in Figure 4.9 (Fatemi et al., 2010). The proposed model is calibrated using the axial, torsion and axial–torsion out-of-phase loadings with the experimental fatigue life presented in Table 4.13. The calibrated coefficients are presented in Table 4.14 with coefficients from the axial loads determined using a solid specimen, as the experimental fatigue life for axial load is determined using a solid specimen. Experimental fatigue life results for titanium alloy BT9 are given in Table 4.15, and were determined using the
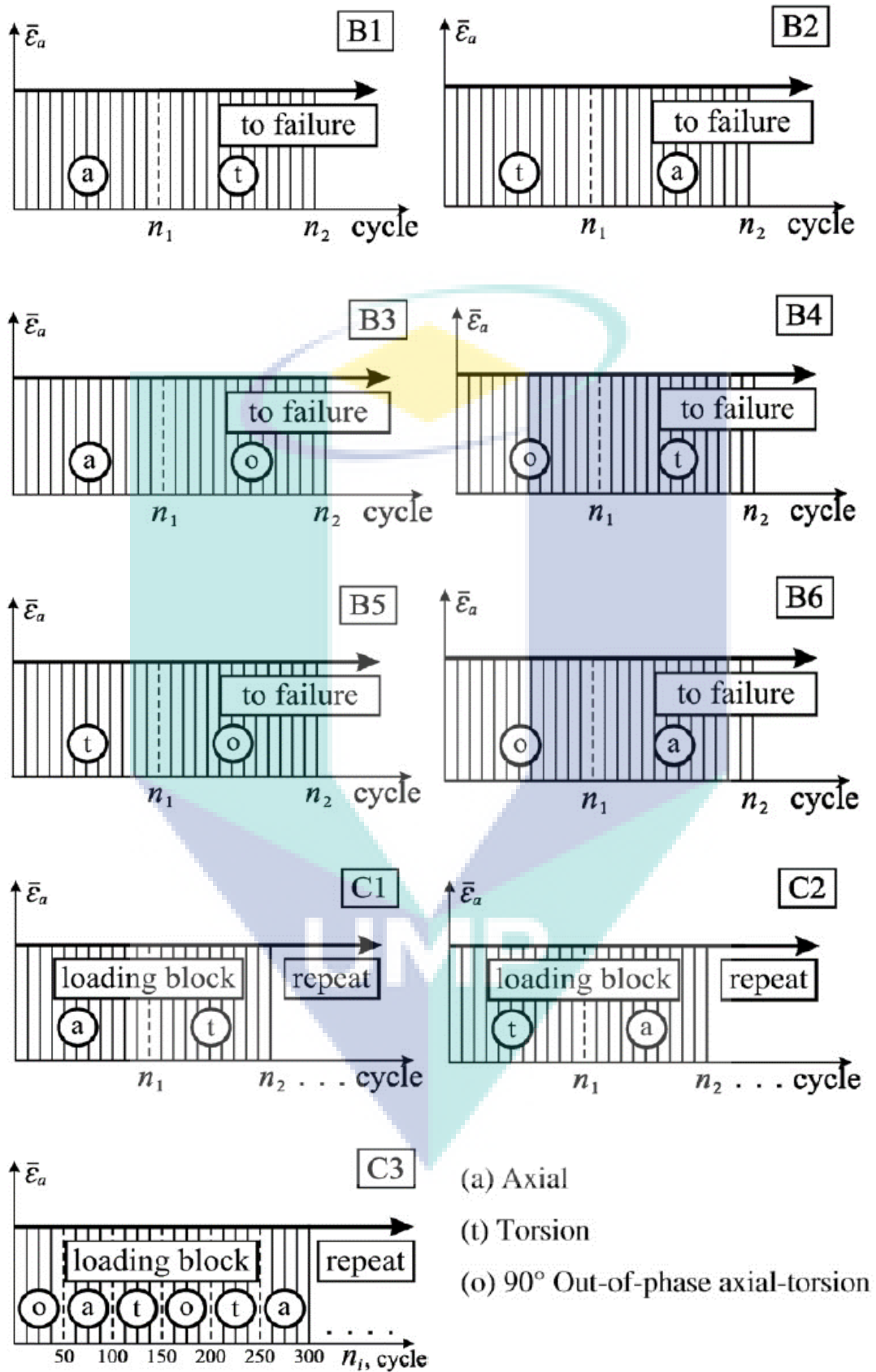
Figure 4.9: Loading blocks composed of different combinations of axial, torsion, and 90° out-of-phase axial–torsion strain paths.

tubular specimen (Fatemi et al., 2010). The mechanical properties of the alloy are listed in Table 3.5. Hollow tubular and solid bar specimens are used for the analysis and their geometry is shown in Figure 3.26 and Figure 3.27 respectively. The predicted and experimental fatigue lives for blocks of loading are presented in Table 4.15.

Table 4.13: Specimen and loads used for calibration for titanium alloy BT9.

| Specimen | Load type | Applied strain | | Cycles to failure (Fatemi et al., 2010) |
		Axial	Shear	
Solid	Axial	0.01	---	960
Tubular	Torsion	---	0.0173	498
	90° out-of-phase	0.01	0.0173	142

Table 4.14: Calibrated coefficients from genetic algorithm for titanium alloy BT9.

| | | | Calibrated coefficients | | | | |
Applied strain	$K \times (10^{-01})$	R	V	a_1	a_2	m	σ_L
Solid specimen with axial load							
0.01 axial	4.3411	0.4017	161	0.1924	1.0756	1	557
Tubular specimen with torsion							
0.0173 shear	5.0075	0.0930	130	0.1285	1.245	1	506
Tubular specimen with OOP							
0.01 axial and shear 0.0173	4.6277	0.2806	94	0.2147	2.153	1	518

Block loading is considered in the form of load segments with constant amplitude loadings with magnitudes according to Table 4.15. For each block load, the critical plane is determined by evaluating the damage by each segment of the block load and then the cumulative damage is evaluated for each plane. The plane with maximum damage is selected as the critical plane (Fatemi et al., 2010). The stress–strain response of titanium alloy BT9 is not sensitive to the loading sequence and change in strain path (Fatemi et al. (2010). Thus, the fatigue life prediction is simplified by calculating the damage for each segment of the block loads individually. Cumulative damage is then determined by summing up the individual load segments (Eq. (3.26)). Hence, the fatigue life is calculated in terms of the number of blocks required for failure.

Table 4.15: Fatigue life for block loads with respect to each calibration for titanium alloy BT9.

| Load block | Phase | Applied strain | | Cycles | No. of blocks | | | |
		Axial	Shear		Experimental (Fatemi et al., 2010)	Solid axial	Tubular torsion	Tubular OOP
B1	---	0.01	---	97	1	3.2	1.1	0.9
	---	---	0.0173	301				
B2	---	---	0.0173	398	1	2	0.7	0.57
	---	0.01	---	205				
B3	---	0.01	---	98	1	4.1	1.45	1.17
	90	0.01	0.0173	86				
B4	90	0.01	0.0173	80	1	2.1	0.66	0.55
	---	---	0.0173	384				
B5	---	---	0.0173	282	1	2.23	0.7	0.6
	90	0.01	0.0173	108				
B6	90	0.01	0.0173	61	1	5.8	2	1.65
	---	0.01	---	70				
C1(1)	---	0.01	---	40	2.5	7.5	2.6	2.11
	---	---	0.0173	130				
C1(2)	---	0.01	---	65	1.8	4.5	1.55	1.27
	---	---	0.0173	219				
C2(1)	---	---	0.0173	176	1.9	5.1	1.8	1.46
	---	0.01	---	66				
C2(2)	---	---	0.0173	209	1.4	4.6	1.6	1.3
	---	0.01	---	65				
C3	90	0.010	0.0173	50	1.6	2.54	0.9	0.72
	---	0.01	---	50				
	---	---	0.0173	50				
	90	0.01	0.0173	50				
	---	---	0.0173	50				
	---	0.01	---	50				

From Table 4.15, it can be concluded that the concept of calibration of the proposed model from characteristic profiles, which are simpler than actual loading conditions but represents their behavior, can be used in the case of fatigue life estimation of block loads. As for the block loading considered in the study, blocks consists of segments of constant amplitude axial, torsion and out-of-phase axial–torsion load (Table 4.15) are used for fatigue life prediction. The proposed model is calibrated using axial, torsion and out-of-phase axial–torsion profiles as mentioned in Table 4.13. Small error in fatigue life estimation is expected, as the profiles used for calibration have only axial, torsion or out-of-phase axial–torsion load and the block loads have a mixture of the three load types (Figure 4.9). But still the fatigue lives, i.e., the number of

blocks to failure, predicted by the proposed model are reasonably accurate with differences of 4–7%, as shown in Figure 4.10. Any improvement in the profiles used for calibration which can better represent the characteristics of the block loads will further improve the accuracy of fatigue life prediction.
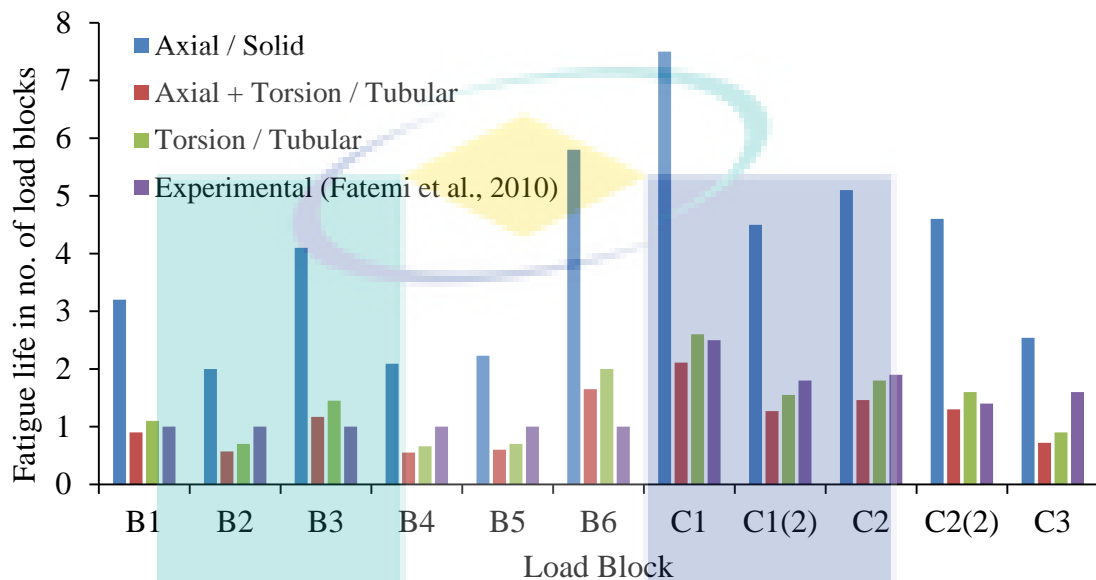
Figure 4.10: Experimental and predicted fatigue life of titanium alloy BT9 for block loads with different calibrations.

An important aspect related to selection of the specimen geometry for calibration of the proposed model is identified from the fatigue life results (Table 4.15) in the case of calibrated coefficients from the axially loaded solid specimen. The fatigue life results from this specimen show that the geometry of the specimen used for generating fatigue life data from experiments should either be similar or more precisely have a similar stress distribution to the component under study. The experimental fatigue life for the axially loaded specimen is determined by applying axial strain loads on the solid specimen shown in Figure 3.27 (Fatemi et al., 2010), and torsion as well as out-of-phase loads are applied on the tubular specimen shown in Figure 3.26. Hence, the fatigue life results from the calibration performed by the axially loaded specimen resulted in non-conservative fatigue life results for all cases.

From Table 4.15, B1 and B2, B3 and B6 and B4 and B5 are pairs of blocks that have similar segments but in the opposite order, thus the sequence effect is highlighted by examining the fatigue life results. For all cases, the predicted fatigue life is within acceptable limits, where the coefficients calibrated by the hollow specimen with torsion and out-of-phase axial–torsion load are used as shown in Figure 4.10. With reference to the experimental observation by Fatemi et al. (2010) that the material is not affected by the loading path, the damage predicted by the proposed model for each load segment is estimated separately and summed up to determine the total damage by the load block and thus the fatigue life as the number of load blocks.

For loading blocks C1 and C2, the fatigue life prediction is more accurate, which can be attributed to the number of cycles in the block segments. C series loading blocks have fewer cycles than B series loading blocks. As already mentioned in Section 3.10, the damage to the load segment is determined by multiplying the damage from one cycle by the number of cycles in that load segment. Then the damage of each load segment is summed up to determine the total damage to the loading block. This may affect the accuracy of fatigue life prediction when there are more cycles in the loading segment, because more cycles include more effects of previous loading cycles for the experimentally determined fatigue life. Hence it can be deduced that, to improve the accuracy of the proposed model and to better handle the sequence and damage accumulation effects, a full response history is required for fatigue life estimation. To reduce the size of the loading history, a filtered response history (with the most damaging cycles included) may also be an acceptable alternative to a full response history, as in general approximately 10% of filtered histories can account for 90% of the total damage (Stephens et al., 2000).

Comparison of the variation of the proposed fatigue model parameter and the Fatemi–Socie model parameter (Fatemi et al., 2010) with respect to the plane angle is shown in Figure 4.11(a) for torsion loading, and in Figure 4.11(b) for out-of-phase axial–torsion loading. The clear difference is due to the reliance of the proposed model parameter on normal and shear stress–strain to determine the parameter value, but the Fatemi–Socie model parameter follows the shear strain range to locate planes with the maximum value of strain range and then identify the critical plane among the located

planes having the maximum normal stress (Fatemi and Socie, 1988). In the case of out-of-phase axial–torsion load, the trend of the proposed model parameter has shown a clear peak to identify the critical plane, while the Fatemi–Socie model parameter has shown clear variation from the torsion case due to the applied axial load, although the identified plane is approximately the same, within ± 5°, as the proposed model parameter.
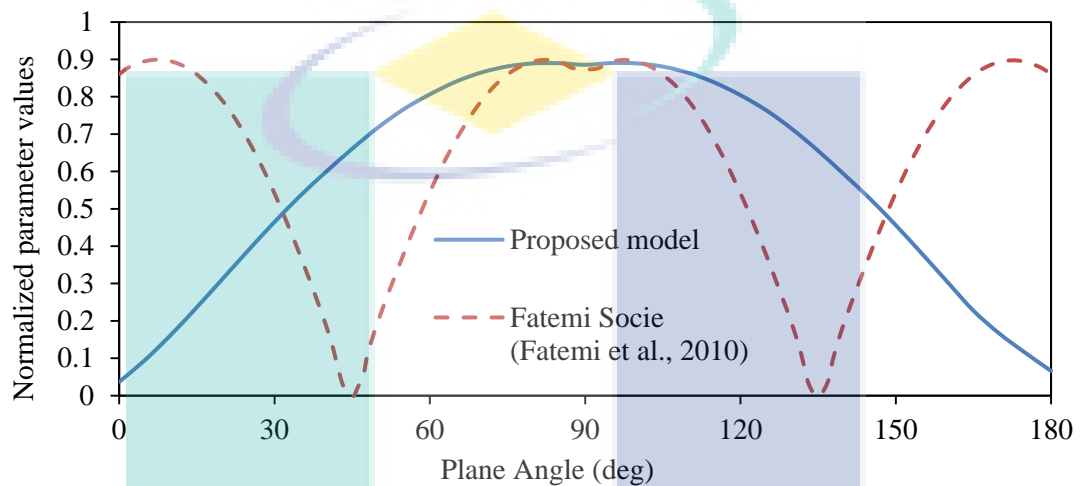
(a) Torsional loading
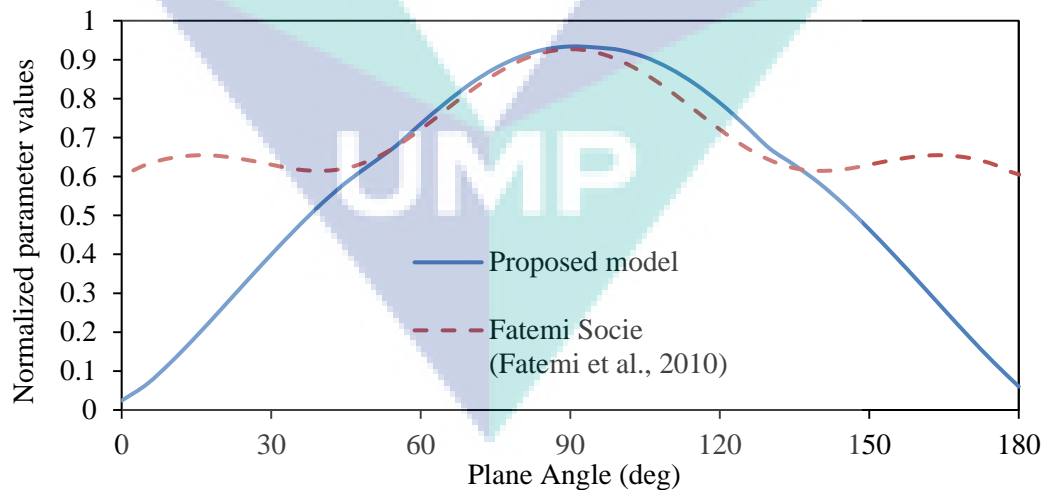
(b) Axial–torsional loading

Figure 4.11: Fatigue parameter variation for proposed and Fatemi–Socie model for titanium alloy BT9 with respect to plane angle.

The critical plane orientations predicted by the proposed model parameter, for block loads (Table 4.15), are presented in Figure 4.12, side by side with the orientations predicted by the Fatemi–Socie model parameter and observed experimentally (Fatemi et al., 2010). By comparing the orientations of the critical plane with the experimental data as shown in Figure 4.12, the proposed model predicted the critical plane orientation within approximately ±10°, which is also similar to the accuracy of predictions made by the Fatemi–Socie model. In case of B1 block, the difference between experimental and predicted values of critical plane is observed as 15°, while for blocks B2 and C2, the difference is 10°. This is due to the fact that the material Titanium alloy BT9 is a brittle material and with the application of normal, shear and out of phase normal and shear load, different mechanisms are competing with each other in causing the failure (Becker and Lampman, 2002). This results in an uncertainty in the experimentally observed critical plane orientation as it depends on the mechanism which most probably cause the actual crack to form. The fatigue parameter models are used for estimating the critical plane according to a defined criteria due to which the load block with similar load sequence resulted in similar estimation of critical plane orientation such as in case of B1 - C1 and B2 - C2. However experimentally the plane orientation is different like for B1 - C1 and for B2 - C2. This shows that the experimental critical plane results have uncertainty due to competing failure mechanisms which are resulting in deviation from the predicted results. Thus with the consideration of experimental uncertainty it can be assumed that the proposed model is able to predict the location of the critical plane and fatigue life with reasonable accuracy for block loading, even with the assumptions made to simplify the analysis, namely that the block loads consist of segments and the damage to each segment can be calculated with reference to the damage done by one cycle in that segment. The accuracy of the proposed model can be further improved by applying the block loading as a full or filtered profile so that only high damage cycles remain and the sequence effect of previous loading cycles can be captured.
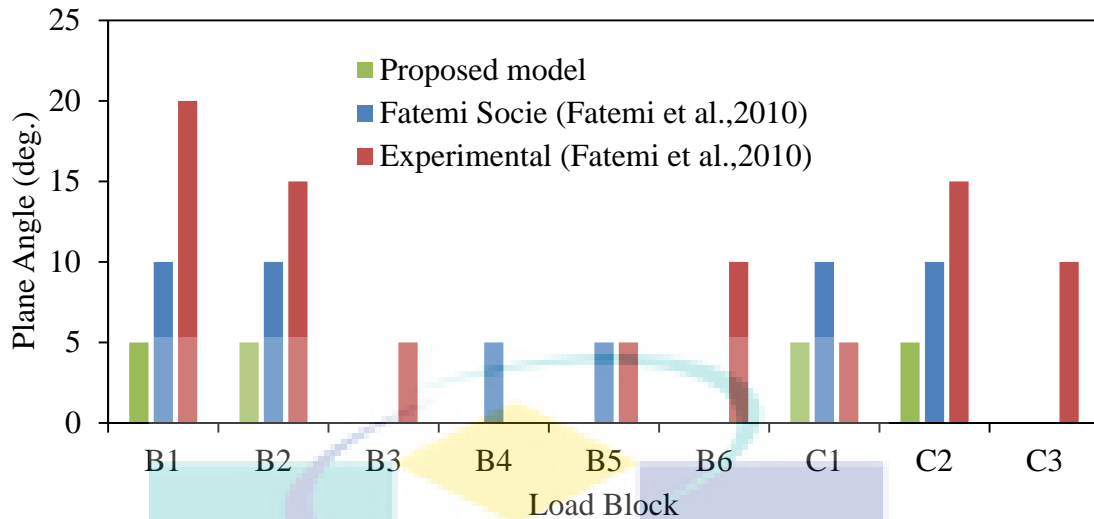
Figure 4.12: Critical plane orientation for each block loading by proposed model, Fatemi–Socie model and experimentally determined for titanium alloy BT9.

4.4 EVALUATION OF PROPOSED MODEL RESULTS WITH COMMON MULTIAXIAL FATIGUE MODELS

In this section the performance of the proposed fatigue life model is evaluated with the fatigue life models available in commercial fatigue life codes. The performance is also evaluated with the Fatemi–Socie model, which is widely accepted among researchers, and the endurance function model which uses GA for calibration. The estimated fatigue life results are compared with the experimental fatigue life for in-phase, out-of-phase and complex load paths, available from published literature.

The equivalent stress determination methods in commercial fatigue life code are absolute maximum principal, signed von Mises, signed shear, a critical plane parameter and the Wang–Brown method. In the absolute maximum principal method, the principal stress with the largest amplitude is used. For the signed von Mises method, von Mises stress with the sign of the absolute maximum principal stress is used. Maximum shear stress as per the Tresca criterion with the sign of absolute maximum principal stress is used in the signed shear method. The critical plane parameter is expressed in Eq. (4.1), while the orientation of the critical plane is defined by angle ϕ with the plane having the highest value of σ_ϕ, as shown in Figure 4.13 (HBM, 2011). The Wang–Brown method employs the parameter as defined in Eq. (2.7). The above-mentioned methods are applied with Morrow mean stress correction and Neuber elastic–plastic correction. The

Fatemi–Socie parameter as expressed in Eq. (2.9) and the endurance function model are coded for use in the study.
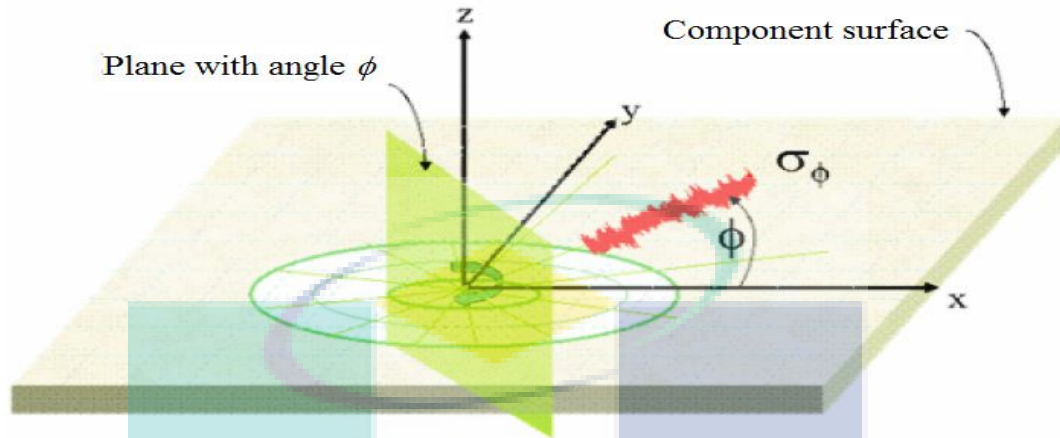
Figure 4.13: Resolution of normal stress for critical plane.

For testing with in-phase and out-of-phase loading, the experimental fatigue life results for the C40 specimen are used (Atzori et al., 2006). In the case of evaluating with complex paths, the experimental fatigue life results for SS304 are used (Itoh et al., 1995). The estimated fatigue lives from the studied models with the respective experimental life are presented in Tables 4.17 and 4.18. The experimental fatigue life results for carbon steel C40 against in-phase and out-of-phase loading with zero and positive mean, alongside the predicted fatigue life by the fatigue life estimation methods under consideration, are presented in Table 4.16. Table 4.17 presents the experimental fatigue life results for the profile paths shown in Table 3.4 and strain load Set 1 and Set 2 as presented in Table 4.1, along with the predicted fatigue life by the fatigue life estimation models under study. The critical plane locations estimated by the critical plane parameter from commercial code, the Fatemi–Socie model and the new proposed model are presented in Table 4.18. The critical plane method from commercial code does not provide variation of the fatigue parameter with plane angles data.

$$\sigma_\phi = \frac{\sigma_{XX} + \sigma_{YY}}{2} + \frac{\sigma_{XX} - \sigma_{YY}}{2} \cdot \cos 2\phi + \sigma_{XY} \sin 2\phi \qquad (4.1)$$

Table 4.16: Predicted fatigue life for C40 specimen.

Applied stress (MPa)	Fatigue life ($\times 10^4$) cycles								
	Absolute max. principal	Signed von Mises	Signed shear	Critical plane	Wang Brown[1]	Fatemi Socie[2]	Endurance function[3]	Proposed model	Experimental[4]
R = -1, phase = 0									
221	1.28	1.364	1.04	1.288	1.421	1.79	--	1.57	1.2
200	1.3	1.37	1.132	1.308	1.518	3.84	2.7	2.68	2.7
179	1.43	1.48	1.259	1.444	1.64	8.83	3.2	5.4	22
160	1.427	1.412	1.377	1.447	1.63	23	4.5	10.5	7.2
129.75	1.37	1.362	1.343	1.317	1.567	140	11	34.7	18
101	3.3	3.338	3.274	3.336	4.369	733	175	143	200
R = -1, phase = 90									
199.7	1.4	1.59	0.84	1.4	0.552	28	0.92	0.94	1.1
180	1.55	1.5	0.77	1.571	0.63	78	1.4	1.6	1.4
160.25	1.5	1.49	0.77	1.598	0.745	133	2.3	2.8	4.1
119.5	8.8	8.47	3.59	9.282	2.89	1442	14	24	94
99.6	34.45	33	11.8	36.57	7.649	7562	120	118.2	200
R = 0, phase = 0									
158	1.558	1.64	1.29	1.58	1.75	0.352	2.5	2.3	2.6
138.5	1.76	1.7	1.22	1.79	1.96	0.936	4.8	6	4.7
119	2.27	2.13	1.45	2.28	2.9	3.359	10	6.9	15
99.5	6.19	5.7	3.65	6.2	7.89	14.1	23	47.8	35
67.9	63.3	60	53.6	63.6	105	135	140	198	200
R = 0, phase = 90									
158	2.22	1.76	0.9	2.365	1.114	4.48	2	2.15	2.1
138.75	4.8	3.5	1.657	4.974	2.582	7.69	3.5	3.6	3.6
119.3	8.5	5.49	2.5	15.59	5.651	16	6.6	7	8.5
89.55	13	8.5	4.7	121.8	31.29	95.6	21	28.7	34
66.8	200	200	200	200	200	566	85	184	200

1- (Wang and Brown, 1993), 2- (Fatemi and Socie, 1988; Fatemi and Gladskyi, 2013), 3- (Brighenti and Carpinteri, 2012), 4- (Atzori et al., 2006).

The fatigue life results of the C40 specimen (Atzori et al., 2006) are shown in Figure 4.14, where it is observed that the proposed model demonstrated a steady performance in predicting the fatigue life for all four load types and magnitudes with good accuracy with differences of 1–3% against the experimental fatigue life. The fatigue life results from the models used with commercial fatigue life codes are conservative, especially at lower magnitudes. The results from the Fatemi–Socie model generally overestimated the fatigue life for both load cases, with R = -1. The fatigue life predicted by the endurance function model shows good accuracy for all load types and magnitudes. Variations in the fatigue life predicted from the above-mentioned models,

Table 4.17: Predicted fatigue life for SS304 specimen.

Path no.	Fatigue life cycles							
	Absolute max. principal	Signed von Mises	Signed shear	Critical plane	Wang Brown[1]	Fatemi Socie[2]	Proposed model	Experimental[3]
For 0.5 axial and 0.87 shear strain load (Set 1)								
1	6128	4248	2050	6128	626	158	6162	9500
2	6249	3043	1228	6464	1042	165	22710	20000
3	1061	942	756	2216	296	132	1806	1200
4	1655	1311	905	2173	454	331	1868	1700
5	2102	1783	1318	2137	2215	310	14596	17500
6	2200	1991	1157	2338	1423	188	7429	9700
7	2268	2104	1161	2391	1122	327	18582	18000
8	2429	1828	1106	2848	556	387	1435	2050
9	2545	2392	1468	4417	502	310	2851	2950
10	2622	1831	955	2894	575	405	2822	2600
11	4756	3333	1576	4897	1803	1123	10264	14400
12	6866	3599	1471	6932	1063	667	4987	4750
13	3396	2001	889	4766	305	761	1127	1600
For 0.8 axial and 1.39 shear strain load (Set 2)								
1	1399	506	233	1676	216	15	746	1400
2	1675	651	270	1712	261	16	1930	2100
3	342	264	151	718	136	31	242	410
4	499	350	189	708	176	32	238	450
5	685	518	285	699	786	33	3278	3200
6	744	567	264	768	454	29	2749	2600
7	764	535	231	780	352	17	2842	1700
8	968	749	493	1118	230	45.7	394	470
9	931	685	424	1104	149	34	699	660
10	944	533	244	1062	189	21	388	320
11	1326	870	360	1362	588	126	906	1200
12	1979	761	325	2061	382	84	689	710
13	995	396	17	1579	131	84	423	500

1- (Wang and Brown, 1993), 2- (Fatemi and Socie, 1988; Fatemi and Gladskyi, 2013),
3- (Itoh et al., 1995).

Table 4.18: Estimated locations of critical planes for SS304 specimen.

Path no.	Critical plane	Fatemi–Socie	Proposed model
Set 1 (0.5 axial and 0.87 shear strain load)			
1	90	90	90
2	90	90	90
3	60	110	110
4	60	110	110
5	60	85	100
6	60	85	80
7	70	80	80
8	60	110	120
9	120	75	110
10	110	110	100
11	70	90	80
12	80	100	80
13	90	80	80
Set 2 (0.8 axial and 1.39 shear strain load)			
1	90	90	90
2	90	90	90
3	120	105	115
4	60	75	110
5	60	95	100
6	70	90	80
7	70	90	80
8	70	80	80
9	110	75	80
10	60	110	105
11	70	90	80
12	80	95	80
13	70	95	80

except the endurance function model and the proposed model, are mainly due to the dependence on many material properties like fatigue strength exponent, fatigue strength coefficient, fatigue ductility coefficient and fatigue ductility exponent. These properties are not commonly available and in the current case are taken from more than one source, as mentioned in Table 3.5. This emphasizes the benefit of the calibration scheme introduced in the proposed model, where the model coefficients are tailored according to loading and material conditions. Thus, there is no requirement for a number of fatigue-related material properties in order to estimate the fatigue life (Shamsaei and McKelvey, 2014). In addition to this simplification, the interpolation scheme introduced for the model coefficients with the newly proposed model improved the accuracy of the

fatigue life prediction. The predicted fatigue life values from the proposed model are nearly equal to the results from the endurance function model. The similarity in results for the two models is due to the GA-based calibration scheme for the model coefficients in both cases. Fatigue life results with complex profiles for the SS304 specimen are presented in Figure 4.15. The results show that the proposed model predicted the fatigue life with good accuracy for all profile paths and magnitudes of applied loads, with differences of 1–4%.

In general, for all methods from commercial code as well as the Fatemi–Socie model, the difference in loading step size is difficult to identify, i.e., the difference in Paths 5 to 7, resulting in approximately similar predicted fatigue life for the three load paths. This simply shows that the models available in commercial fatigue life codes and already published models cannot be used universally for every type of loading condition, as identified by researchers (Mahadevan and Liu, 2005; Fatemi and Shamsaei, 2011; Macha and Niesłony, 2012; Ince and Glinka, 2014). A possible reason for the resulting inaccuracy of the Fatemi–Socie parameter is the failure of SS304 in planes experiencing maximum normal stress rather than shear in certain loading conditions (Socie and Marquis, 2000), while the Fatemi–Socie model defines the plane with the maximum shear strain range as the critical plane. The critical planes identified by the Fatemi-Socie model and the proposed model are very similar in most cases, as observed from Figure 4.16. The variation of predicted fatigue life by the Fatemi–Socie model with respect to experimental life is attributed to the definition of the parameter itself, i.e. the dependence on the maximum shear strain range only to locate the critical plane. The requirement for a number of material properties is another reason for fatigue life variation, as these material properties are defined using many variables that need to be determined from experimental data prior to fatigue life estimation. Experimental errors can be introduced when determining these variables experimentally. This highlights the drawbacks associated with different models in predicting fatigue life accurately.
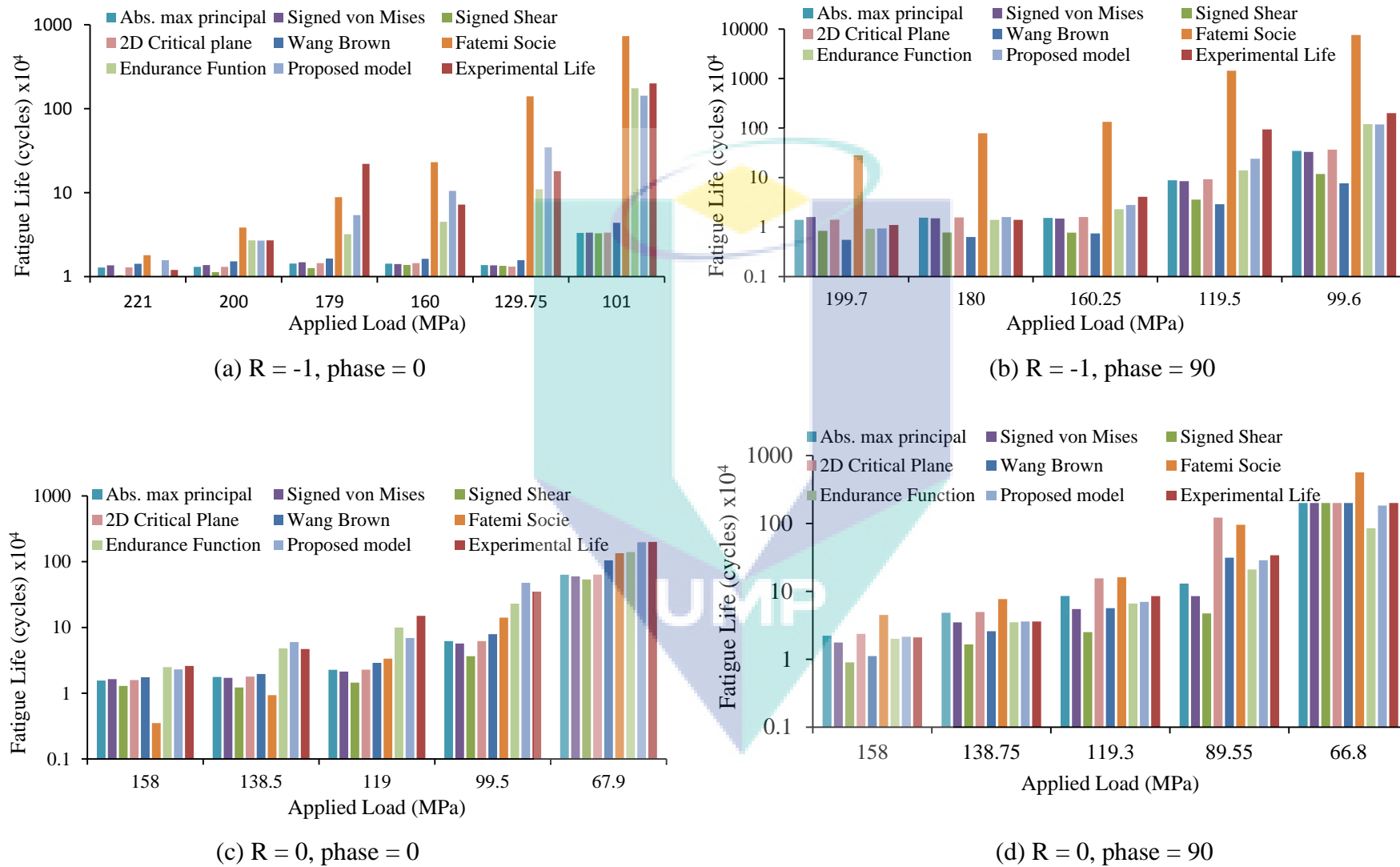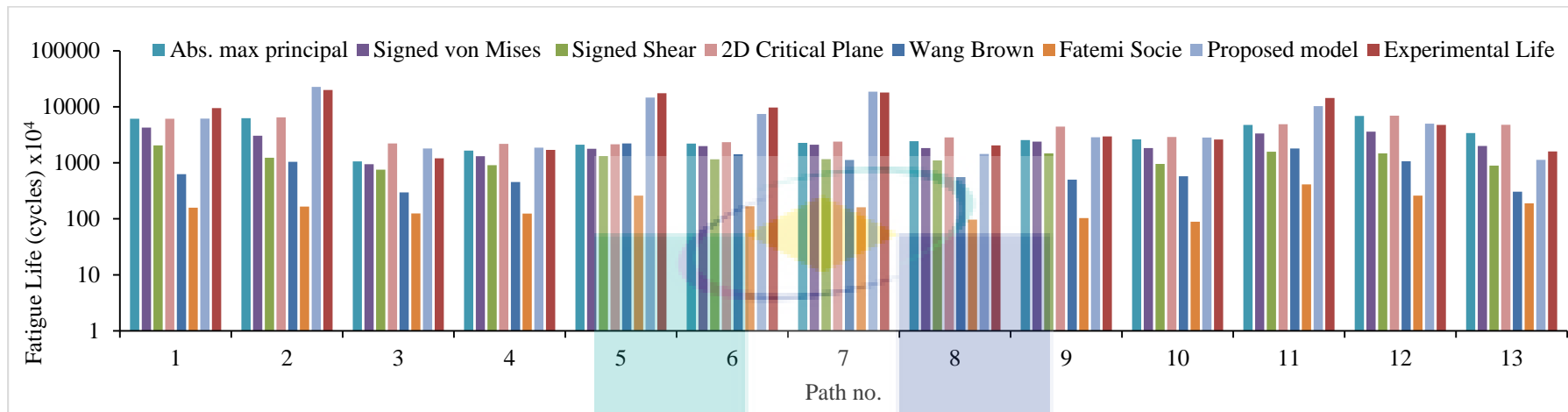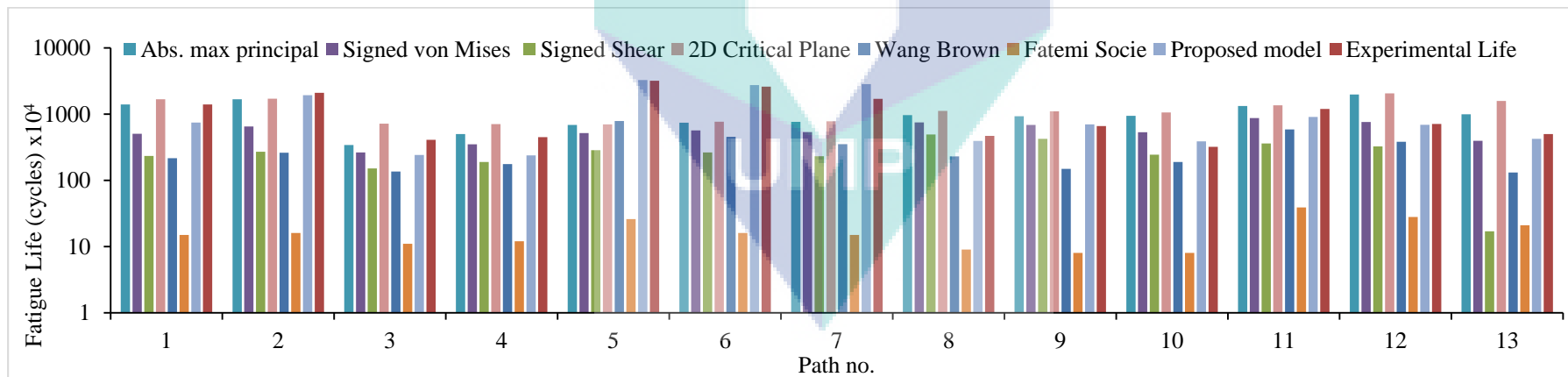
Figure 4.14: Fatigue life of C40 from various models versus experimental life.

(a) (Set 1) 0.5% axial and 0.87% shear strain.

(b) (Set 2) 0.8% axial and 1.39% shear strain

Figure 4.15: Fatigue life of SS304 from various models versus experimental life.

Critical plane estimation results are presented in Table 4.18 for the models with the critical plane location data. Figure 4.16 shows the variation of the fatigue parameter with plane angle (ϕ), as shown in Figure 3.2, which is the plane angle with the axis of the specimen. Since no variation of the parameter data is available for the critical plane model from the commercial code, the results from the critical plane model are not included in Figure 4.16. The critical plane location (Table 4.18) as well as the variation of the fatigue parameter with plane angle for the Fatemi–Socie model and the proposed model are approximately similar, except for Paths 6, 7 and 11, where Paths 6 and 7 represent the steps size in loading and Path 11 is an intermediate case between Path 5 and Path 12. For the critical plane model and Fatemi–Socie parameter, Paths 6 and 7 resulted in approximately the same location of the critical plane as Path 5. But in the case of the proposed model there is a clear shift of 20° in the critical plane location for both Set 1 and Set 2 of magnitudes of applied loading (Table 4.18). The reason for this behaviour lies in the definition of the fatigue life parameters. The critical plane model searches for the plane having the maximum resultant stress from the surface stresses along the plane normal (Figure 4.13). The Fatemi–Socie model defines the critical plane in two steps; firstly, searching for planes having the maximum shear strain range and secondly selecting from among these planes the one with the maximum normal stress as the critical plane. For Paths 5, 6 and 7, the applied strain range is the same, which results in the same critical plane location, as the initial selection of planes is made on the basis of the shear strain (Itoh et al., 1995). In the case of the proposed model, the fatigue parameter consists of strain and stress terms.

The plane with the maximum fatigue parameter is selected as the critical plane. Hence, the effect of step loading on the location of the critical plane is captured efficiently. For Path 11, the variations of the fatigue parameter with plane angle are different for the Fatemi–Socie model compared to the proposed model, as shown in Figure 4.16. The Fatemi–Socie model shows clear peaks in the fatigue parameter, while the proposed model shows a plateau behaviour for the fatigue parameter. This is attributed to the definition of the fatigue parameters. Fatemi–Socie searches for the maximum shear strain range planes and then adds the normal stress on the selected planes to determine the fatigue parameter, while the proposed model searches for planes having a combined effect of shear and normal stress and strain terms.
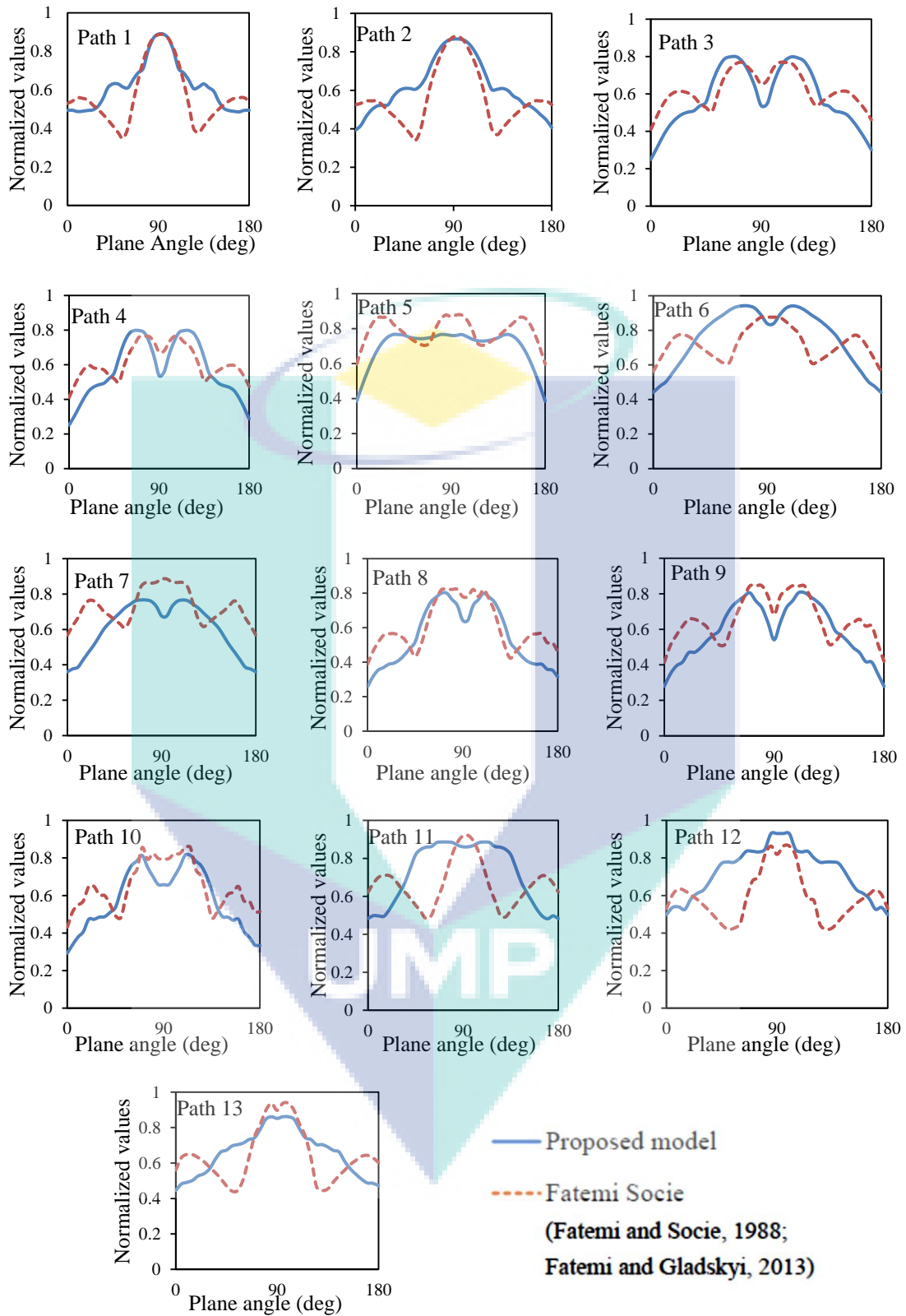
Figure 4.16: Proposed and Fatemi–Socie parameter variations with plane angle for SS304 and Set 2.

In the case of Path 11 the phase difference is 45°, which causes a mixed effect of in-phase and out of phase normal and shear stress–strain load (Kida et al., 1997). The proposed model is better able to capture that combined stress–strain effect. Hence, a wider range of planes is identified as having high fatigue parameter values compared to Fatemi–Socie, which shows a distinct peak, as seen in Figure 4.16. For Paths 1, 2, 3 and 4 the fatigue parameter variations for the proposed model and the Fatemi–Socie model are very close to each other (Figure 4.16), as are also the estimated critical plane locations as presented in Table 4.18. This shows that both models show excellent agreement in critical plane estimation for profile paths with two principal strain directions and fully reversed loading (Itoh et al., 1995). In the cases of Paths 8, 9, 10, 12 and 13, which represent load cases having a box loading path and rotation in the principal strain directions, the observed fatigue parameter variation (Figure 4.16) as well as the estimated critical plane locations (Table 4.18) are in close agreement. Hence, it can be observed that the proposed model performed in good agreement with, and in certain situations performed even better than, the fatigue life models already used in commercial codes and established in published literature.

4.5 PERFORMANCE OF DEVELOPED CRITICAL PLANE ESTIMATION TECHNIQUE

A new approach has been developed to determine the critical plane orientation using an optimization technique with a genetic algorithm. This approach is helpful in finding the critical plane according to one or more criteria simultaneously describing the critical plane properties. The performance of the proposed technique is verified by comparing the critical plane location predicted by the conventional incremental angle method with the GA-based method. The comparison is made by estimating the critical plane location for in-phase and out-of-phase loading for the C40 carbon steel specimen, given in Table 4.19, as well as for the complex loading for SS304 steel given in Table 4.20. In Table 4.19 and Table 4.20 the critical plane location predicted by the incremental method and GA-based method are presented side by side with the value of the calculated fatigue parameter. This is to show the benefit of the GA method in identifying planes with higher value fatigue parameters, which were missed by the incremental angle method.

Table 4.19: Critical planes for C40 specimen.

Loading Condition	Stress	Theta (θ) Incremental	GA	Phi (φ) Incremental	GA	Fatigue parameter Incremental	GA
R-1 Ph0	101	165	18 / 165	100	45 / 100	1.11054	1.11059 / 1.11057
	200	180	178	145	143	1.41773	1.41980
R-1 Ph90	99.6	180	180	95	93	1.07621	1.07840
	199.7	0	179	90	88	1.81711	1.82106
R0 Ph0	67.9	170	164	140	138	1.32631	1.32647
	158.1	0	179 / 0	40	141 / 39	1.52013	1.52113 / 1.52085
R0 Ph90	66.8	180	0 / 180	95	85 / 97	1.45247	1.45248 / 1.4513
	158.1	0	179 / 0	95	85 / 95	1.88255	1.88317 / 1.88262

The proposed technique based on GA optimization is applied with the objective function defined so as to maximize the fatigue parameter according to the considered fatigue life criteria. The technique coupled with GA works with a decision-based approach for the generation of critical plane orientation angles. The critical plane angles are then used to calculate the fatigue parameter for every iteration. This approach results in reduced resource consumption, avoids extra calculations on planes with smaller fatigue parameter values and decreases the effort needed to find the critical plane at the required accuracy. From the results (Tables 4.20 and 4.21), it is observed that GA-based critical plane estimation shows a least count of one degree (1°) instead of the commonly used 5° (Ince, 2012).

The technique requires only approximately 1800 iterations to locate the critical plane, i.e., the initializing set for the GA has 180 angle values with reference to the 1° least count for a range of angles from 0°–180° and the number of generations for the GA is set at 10. The total iterations that result are nearly equal in number to the iterations used for the incremental angle method with a 5° step size. However, for the incremental angle approach using the same least count, i.e. 1° step size, the number of iterations increases 18 times, to more than 32000 iterations, i.e. 181 steps for each value of θ and φ angles in order to locate the critical plane for the maximized fatigue

Table 4.20: Critical planes for SS304 specimen.

Path no.	Strain cases		Theta (θ)		Phi (φ)		Fatigue parameter	
	Axial	Shear	Incremental	GA	Incremental	GA	Incremental	GA
1	0.5	0.87	0	0	90	90	3.59584	3.59585
	0.8	1.39	0	0	90	90	4.33277	4.33277
2	0.5	0.87	0	180	90	91	3.58936	3.59028
	0.8	1.39	0	0	90	89	4.33162	4.33223
3	0.5	0.87	0	179 / 0	110	68 / 112	3.63267	3.64229 / 3.64147
	0.8	1.39	0	0	115	115	4.31325	4.31370
4	0.5	0.87	180	179	110	110	3.78136	3.78215
	0.8	1.39	180	179	110	111	4.45319	4.45605
5	0.5	0.87	175	0 / 176	35	144 / 37	2.91461	2.91645 / 2.91785
	0.8	1.39	175	174 / 0	35	37 / 144	3.45054	3.45605 / 3.45206
6	0.5	0.87	180	178	80	80	3.308001	3.30986
	0.8	1.39	180	178	80	81	3.99819	4.004143
7	0.5	0.87	180	179	80	79	3.40371	3.40552
	0.8	1.39	180	179 / 0	80	80 / 100	4.09305	4.09326 / 4.09305
8	0.5	0.87	0	179 / 0	120	62 / 116	3.54503	3.54953 / 3.53698
	0.8	1.39	180	179 / 0	80	79 / 101	4.53368	4.53555 / 4.5346
9	0.5	0.87	0	179 / 0	110	70 / 109	3.5469	3.5481 / 3.54489
	0.8	1.39	180	179 / 0	80	78 / 103	4.46761	4.47809 / 4.47752
10	0.5	0.87	180	180 / 0	100	103 / 78	3.82634	3.83397 / 3.83366
	0.8	1.39	180	179 / 0	105	104 / 76	4.55532	4.55786 / 4.55744
11	0.5	0.87	180	179	80	80	3.093013	3.093647
	0.8	1.39	180	180 / 0	80	79 / 101	3.71974	3.72325 / 3.72312
12	0.5	0.87	180	180	80	82	3.34163	3.346288
	0.8	1.39	180	180 / 0	80	80 / 100	3.943375	3.94338 / 3.94319
13	0.5	0.87	180	180	80	82	3.36139	3.366025
	0.8	1.39	180	180 / 0	80	80 / 100	3.95408	3.95423 / 3.95423

parameter. This difference in the required number of extra iterations performed in the incremental angle method is shown in Figure 4.17. Figure 4.17(a) shows the fatigue parameter results from the incremental angle set-up for C40 steel for the load set with R = -1, Phase = 90 and load point of 199.7 MPa.

The incremental angle approach results in extra calculations on points with low fatigue parameter values on the corresponding θ and φ, which are not needed for critical plane determination. The reduction in extra calculation effort when using the GA-based critical plane estimation technique is shown in Figure 4.17(b). For the same loading case, the critical plane angles θ and φ with the maximum fatigue parameter value from every generation are selected for further optimization by the GA to reach the maximum fatigue parameter value and avoid θ and φ values with small fatigue parameter values. This results in enhanced efficiency for determining the critical plane orientation in terms of the time required for long complex multiaxial and variable amplitude loading due to the smaller number of iterations required. Another advantage of using the GA-based approach is observed from the results in Tables 4.20–4.22, showing that the approach leads to the critical plane with higher fatigue parameter values than with the incremental angle method.
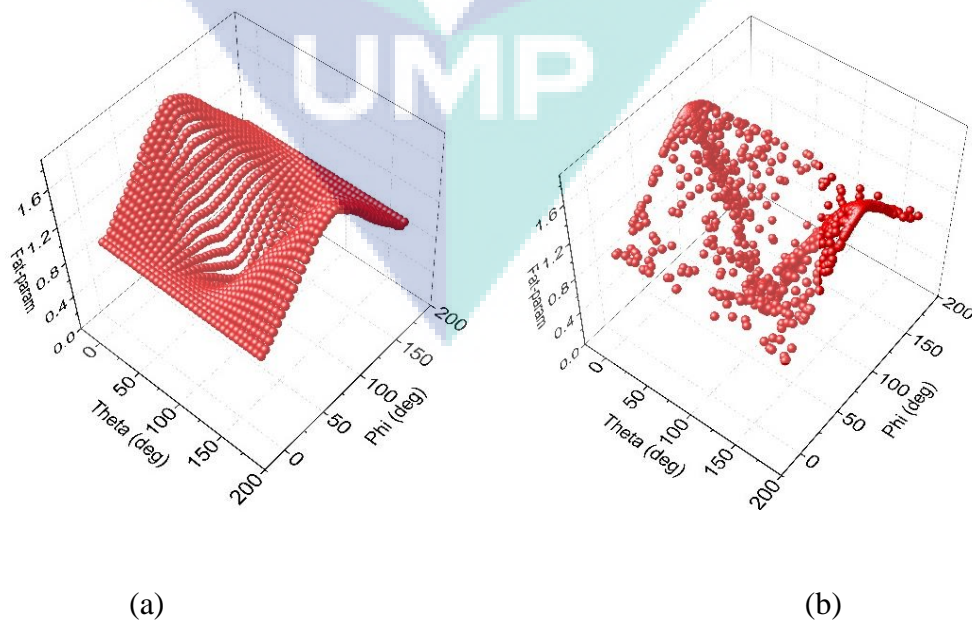

(a)   (b)

Figure 4.17: Fatigue parameter estimation for C40 steel with R-1-Ph90-199.7 MPa loading case with (a) incremental angle, (b) GA.

Due to the larger step size applied in the incremental angle method, i.e. 5°, it is possible that a plane with a higher value fatigue parameter may be missed. Where the results from the incremental angle method and GA-based method are similar, this is due to the fact that the loading profiles considered for study have small and non-random variations. Hence, few planes have maximum damage so both methods give similar results for the orientation of the critical plane.

The capability of the GA, when using the multi-objective optimization technique in order to find the critical plane with respect to more than one objective functions, is explored. The two objective functions include maximization of the proposed fatigue parameter and maximization of the variance of shear stress on the candidate plane (Susmel, 2010). The results of two-parameter critical plane estimation with the proposed parameter and maximum variance of shear using complex profiles with SS304 steel are presented in Table 4.21. Theta (θ) and phi (ϕ) are reported for the maximum proposed fatigue parameter value as well as the maximum variance of shear stress, against the respective loading profiles from Table 3.4 and loading strain Set 1 from Table 4.1. The results show the advantage of using this approach that more candidate planes are identified from the two criteria for maximum damage. For Paths 3, 4, 5, 8, 9 and 10, the critical plane locations identified by maximizing the proposed parameter and variance of shear are different, and thus additional to the planes identified by the proposed model. The benefit of the extra plane identification is also clear from the fatigue parameter values for Paths 3 and 4, where for angle values $\phi = 3°$ and 178° for the case of maximized variance of shear, the value of the proposed fatigue model parameter is noticeably lower than the maximum proposed fatigue parameter value. This shows that the critical planes identified at $\phi = 3°$ and 178° are additionally identified and would be missed by the proposed fatigue model parameter. Hence, the additional number of candidate critical planes reduces the probability of missing the plane with maximum damage (Araujo et al., 2011).

Figure 4.18 shows the comparison of variation of the proposed fatigue parameter and the variance of shear stress with respect to plane angles theta (θ) and phi (ϕ). For Paths 1 and 2 (Figures 4.18 (a) and 4.18(b)), the shear stress and normal load act alternately; hence the proposed parameter which depends on both normal and shear

stress–strain terms showed a clear peak with respect to ϕ. On the other hand, the maximum variance of shear stress showed two peaks. This is due to the dependence of the maximum variance parameter on shear stress, as shear stress has no compressive or negative value so there is a chance of more than one plane having the maximum value of stress. For Paths 3 and 4 (Figures 4.18(c) and 4.18(d)) the shear and normal load is acting simultaneously. The proposed parameter showed two peak values with respect to angle ϕ. This is due to the shear load acting in different directions when the normal load is acting as tensile. The maximum variance of shear parameter has a similar shape for Paths 1 and 2, with a shift in peak location with respect to ϕ. This may be due to the shear load acting in a similar pattern for Paths 1 to 4. For Paths 5, 6 and 7, the shear and normal load are applied in-phase in Path 5 and with different step sizes in Paths 6 and 7. The variation of the proposed fatigue parameter and variance of shear with respect to plane angles θ and ϕ are approximately the same for all three paths.

For Paths 8, 9 and 10, the difference is the compressive and tensile stress during the shear cycle and box shape continuous loading for Path 10. The proposed fatigue parameter identified more planes with high damage with Path 9 than with Path 8, while there was a definitive peak for Path 10. There is no significant difference in behaviour in variance of the shear parameter for the three paths. The proposed parameter results are logical in the sense that tensile stress causes cracks to open and helps the cracks to grow, thus causing more damage (Stephens et al., 2000). Paths 11, 12 and 13 have out-of-phase continuous loading load paths of normal and shear load. The variation of the proposed fatigue parameter for Path 11 is approximately in between the cases of Paths 5 and 12. This is due to the fact that Path 11 has a 45° phase difference, while Path 5 has 0° and Path 12 has 90°. It can be seen from Figures 4.18(e), 4.18(k) and 4.18(l) that, as the phase angle increases, the number of planes with high fatigue parameter values also increase. This is due to the rotation of the planes of maximum principal strain such that all planes are strained during some portion of the cycle (Itoh et al., 1995). Path 13 as seen from Figure 4.18(m) caused the peak with respect to phi (ϕ) to grow wider, i.e. more planes are facing damage due to the addition of retracing of the load path to Path 12.

Table 4.21: Critical plane with fatigue parameter and variance of shear stress maximized on SS 304 specimen.

Path no.	Strain cases		Theta (θ)		Phi (φ)		Value of fatigue parameter / Variance	
	Axial	Shear	Fatigue parameter maximized	Variance of shear maximized	Fatigue parameter maximized	Variance of shear maximized	Fatigue parameter maximized	Variance of shear maximized
1	0.5	0.87	180	180	90	92	3.59586 / 1916372	3.59172 / 1920103
2	0.5	0.87	0	0	89	89	3.59028 / 491969	3.59027 / 491971
3	0.5	0.87	179 / 0	0 / 0	68 / 112	94 / 3	(3.64221 / 572544) / (3.64128 / 566281)	(3.05496 / 741350) / (1.70573 / 741335)
4	0.5	0.87	0 / 180	0 / 0	69 / 111	88 / 178	(3.78169 / 573812) / (3.781601 / 571695)	(3.23537 / 755789) / (1.63726 / 755789)
5	0.5	0.87	0 / 180	0 / 0	144 / 36	167 / 77	(2.91645 / 1000228) / (2.91641 / 1016364)	(2.28644 / 2057109) / (2.29998 / 2057075)
6	0.5	0.87	178 / 0	0 / 180	80 / 100	78 / 11	(3.30974 / 1910576) / (3.30804 / 1928486)	(2.65714 / 3504013) / (2.15744 / 3502552)
7	0.5	0.87	0 / 180	180 / 0	100 / 80	100 / 80	(3.40408 / 1014914) / (3.40399 / 1024516)	(2.9106679 / 1615255) / (2.91041 / 1615246)
8	0.5	0.87	180 / 0	0 / 180	62 / 119	84 / 96	(3.54935 / 301002) / (3.54915 / 291789)	(2.71653 / 1237445) / (2.71330 / 1237415)
9	0.5	0.87	179 / 0	0 / 180	71 / 110	97 / 83	(3.54776 / 523944) / (3.54579 / 519767)	(3.29491 / 570816) / (3.30665 / 570795)
10	0.5	0.87	180 / 0	0 / 180	102 / 77	96 / 84	(3.83389 / 877440) / (3.83374 / 869146)	(3.38469 / 1196083) / (3.38125 / 1196032)
11	0.5	0.87	180 / 0	0 / 180	80 / 100	77 / 103	(3.09337 / 238782) / (3.09301 / 245077)	(2.41156 / 492025) / (2.44128 / 491816)
12	0.5	0.87	0 / 180	180 / 0	98 / 82	96 / 84	(3.34628 / 499757) / (3.34628 / 499698)	(3.07728 / 582456) / (3.07864 / 582455)
13	0.5	0.87	180 / 0	0 / 180	82 / 98	89 / 91	(3.36598 / 869464) / (3.36597 / 867814)	(3.29182 / 927009) / (3.28955 / 926999)

The variance of shear showed variations in the region with lower parameter values, which is insignificant with respect to prediction of the critical plane location. The different behaviour of the two maximized parameters with respect to the critical plane angles shows that the two objective functions result in different planes for each of the two criteria in order to estimate the maximum damage according to the respective definitions of the two parameters.

A newly proposed critical plane estimation technique using GA optimization is analysed. Direct comparisons of the incremental angle method and GA-based method have been made. The newly proposed GA-based method is found to be more efficient, reducing the required number of iterations by a ratio of 18 (approx.) and improving the accuracy from 5° to 1° for the critical location. Moreover, two fatigue parameters, the proposed parameter and variance of shear, are used simultaneously to locate the critical plane. The results show that the benefit of having more than one parameter is the identification of different critical planes from those identified when only one parameter is used. This is especially useful in the case of random and complex loadings where more than one criterion can identify candidate planes which are left out when using only one criterion.
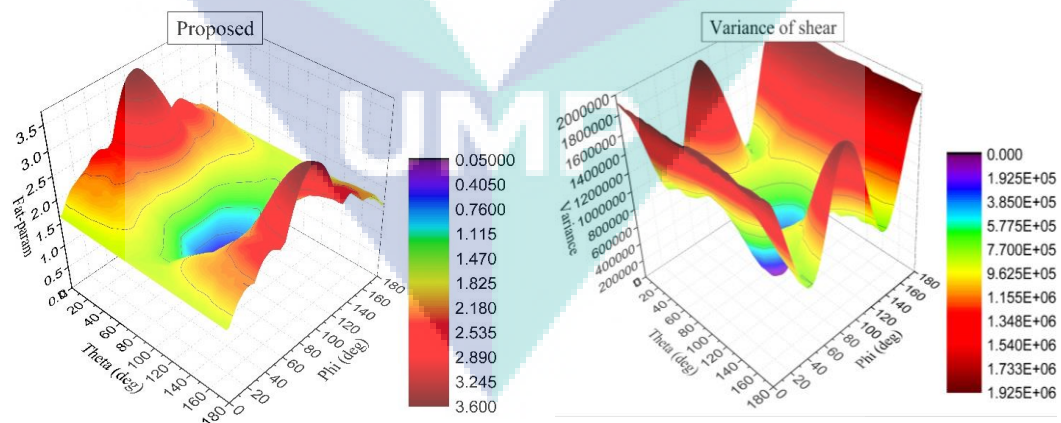
(a) Path 1

Figure 4.18: Proposed fatigue parameter and variance of shear with plane angles for SS304 specimen, Set 1 strains for profile Paths 1–13.
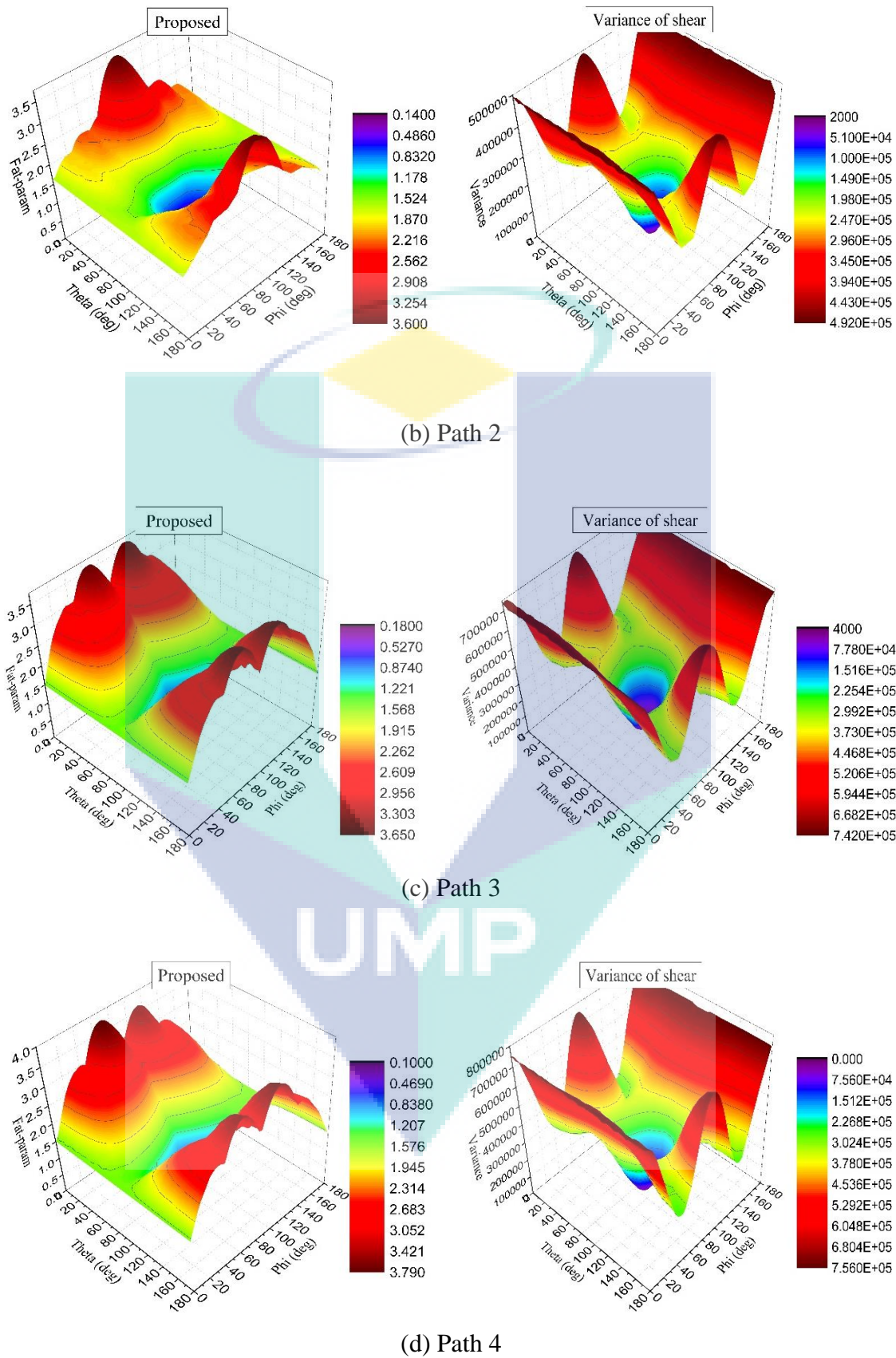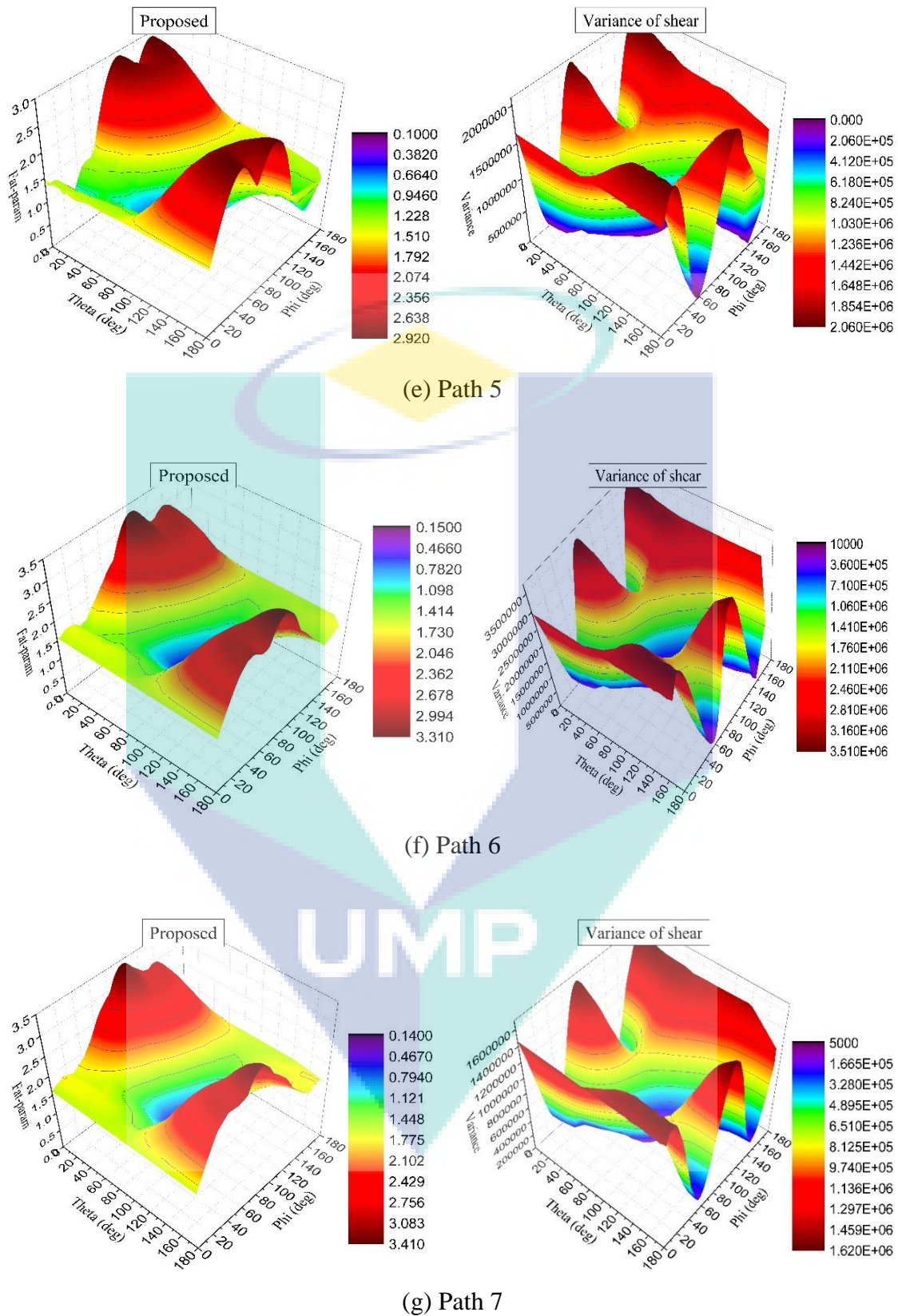
(b) Path 2

(c) Path 3

(d) Path 4

Figure 4.18: Continued.

(e) Path 5

(f) Path 6

(g) Path 7

Figure 4.18: Continued.

(h) Path 8

(i) Path 9

(j) Path 10

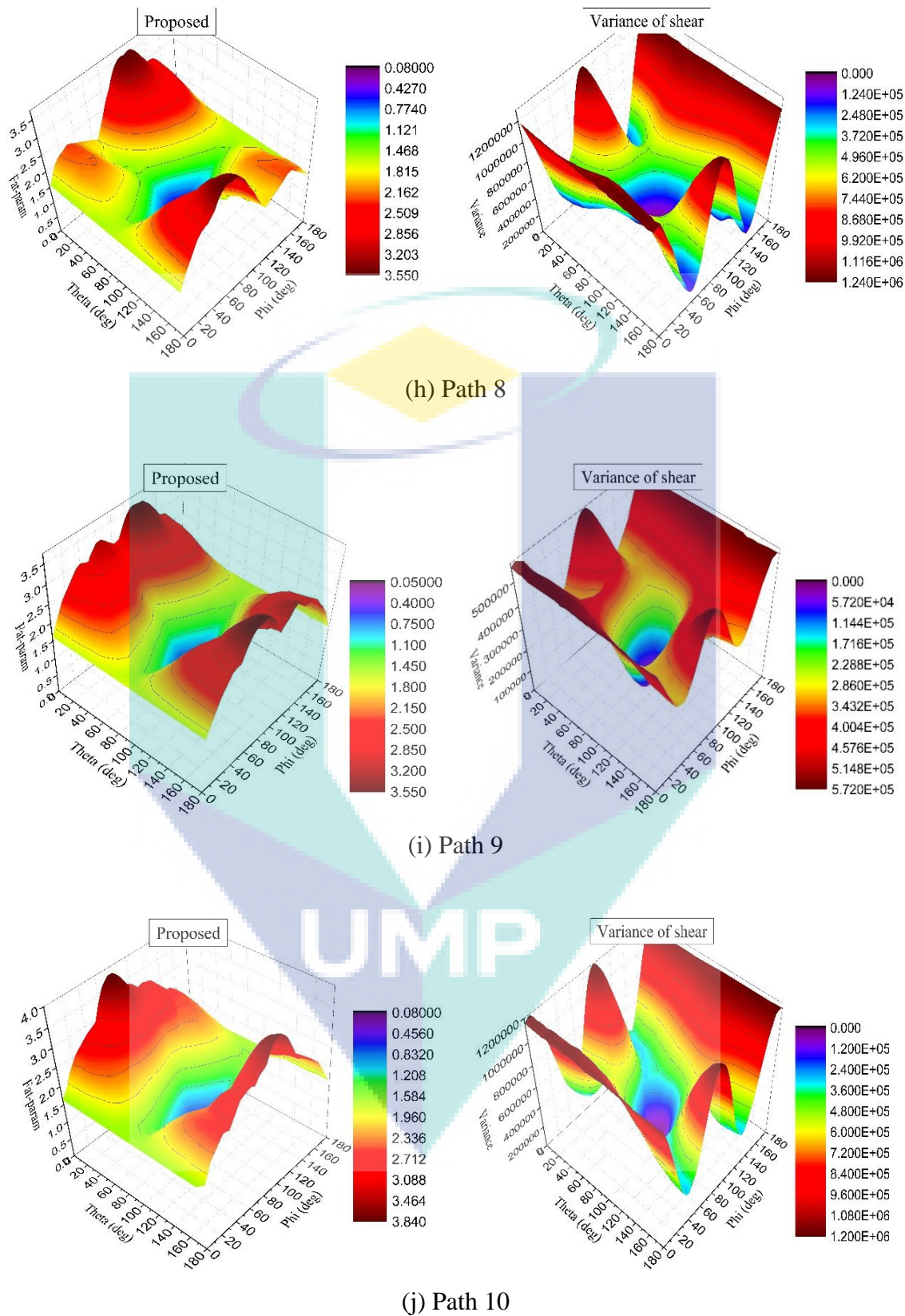**Figure 4.18:** Continued.

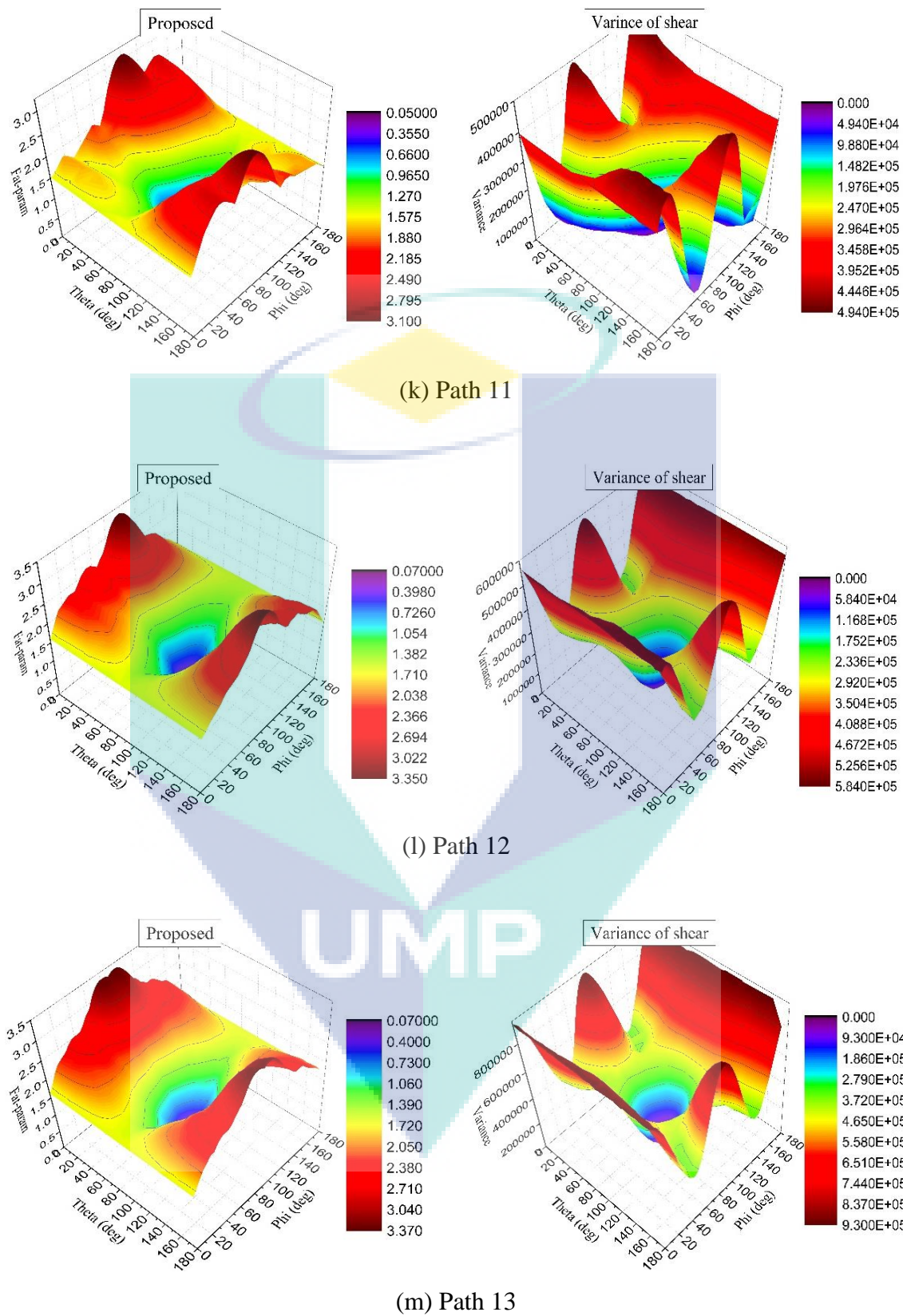(k) Path 11

(l) Path 12

(m) Path 13

Figure 4.18: Continued.

4.6   SUMMARY

The performance and accuracy of the proposed model is analysed by comparing the results with previously published experimental fatigue life results for different materials and complex loading cases. The results are found to be within reasonable accuracy. The proposed model is independent of the loading path shape in estimating the fatigue life. The damage is determined directly from the stress–strain response history, so considering different materials with the same loading is not beneficial in highlighting the features and capability of the proposed model. Hence, the experimental results for this analysis are selected in order to have various complex loading cases for different materials. The results with the proposed model are also compared with the models available in literature and commercial codes. The proposed model is found to be consistent in performance and with better accuracy in the various loading conditions. The proposed GA-based critical plane estimation method is found to more accurate than the conventional angle increment method, with the capability to use more than one critical plane criterion. A summary of these findings, contributions and recommendations for future research work will be presented in Chapter 5.
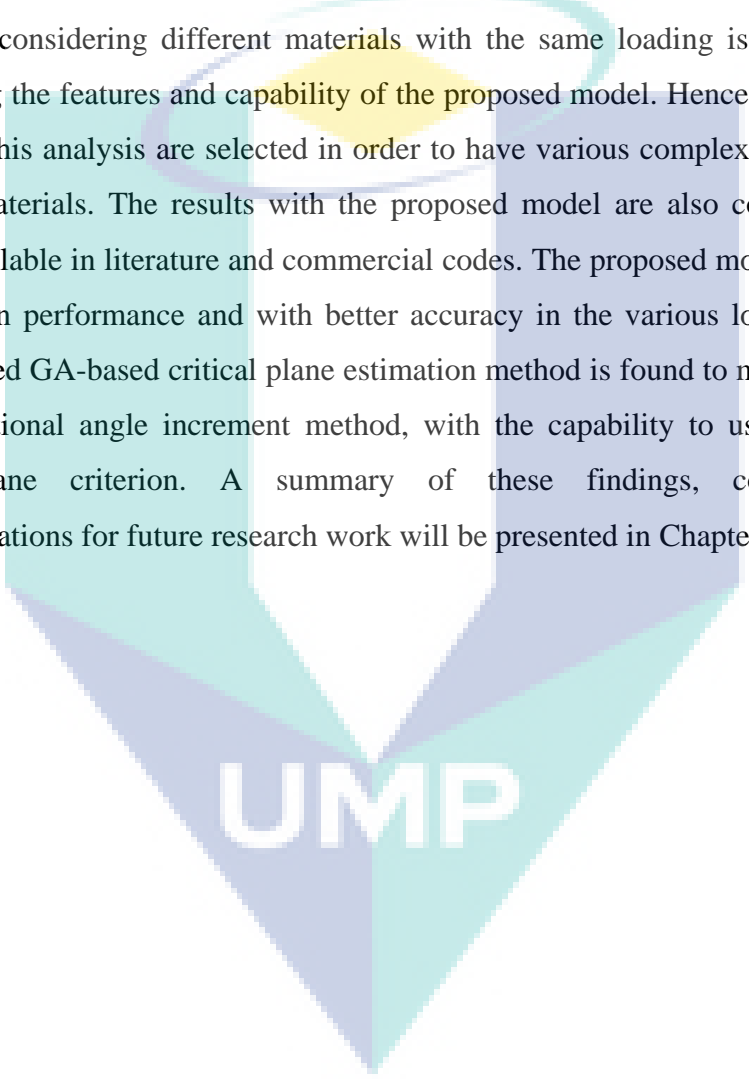
CHAPTER 5

CONCLUSIONS AND RECOMMENDATIONS

5.1   INTRODUCTION

Understanding the multiaxial fatigue problem is essential for reliability assessment and for design against multiaxial fatigue failure for mechanical components in realistic service conditions. Fatigue life evaluation of mechanical components based on experimental assessments is expensive and time-consuming. Therefore, numerical and analytical methods are essential approaches for conducting fatigue and durability analyses. The main objective of this study is to develop a multiaxial fatigue life estimation methodology which has a universal or general-purpose application for various material and loading conditions. This chapter summarizes the most important findings from the work carried out in this study. It also includes suggestions for further work.

5.2   SUMMARY OF FINDINGS

5.2.1 Modelling of Fatigue Parameter Expressions

The proposed fatigue parameter is modelled in two forms of stress–strain terms. The first form is the strain–energy type (Model-1), with the products of the strain and stress terms of normal and shear stress summed to define the fatigue parameter. The second form is the summation of normal and shear stress and strain terms (Modle-2), separately summed to define the fatigue parameter. Each term in both expressions has a coefficient associated with it that is to be calibrated using the experimental fatigue life results. This resulted in fewer coefficients needing to be calibrated for parameter

expression with Model-1. The comparative study between the two forms is performed by using the experimental fatigue life results for various complex multiaxial profiles and comparing the predicted fatigue life with the experimental results. Based on analysis of the results, both forms of parameter expression provided approximately the same level of accuracy of 1–6% for fatigue life prediction. The strain–energy form (Model-1) resulted in 50% reduction in the number of iterations required for the calibration process to determine the coefficients, compared with what is required for the summation of the stress–strain terms. Therefore, based on reduced effort and ease in calibration, the strain energy form (Model-1) is selected to be used.

5.2.2   GA-based Model Calibration

A calibration methodology is proposed to calibrate the coefficients of the proposed model based on a genetic algorithm. The major advantage of the proposed calibration method is that it only requires material data related to the stress–strain curve to generate the stress–strain response using FEM and the fatigue limit as a fatigue-related material property. The proposed methodology for calibration uses the full loading-response history in the calibration process, which means that it is independent of the loading path shapes and that the coefficients determined are the best possible representation of the fatigue behaviour. The calibration method is flexible enough to accommodate any modification in model expressions and the introduction of new coefficients without any change in the application procedure. Hence, it can be concluded that the proposed calibration method is robust to handle various loading path shape.

5.2.3   Performance Analysis

The performance of the proposed model is analysed and validated by comparative analysis with the fatigue life results for various materials and loading conditions from the published literature. The experimental fatigue life data used are based on EN3B steel alloy, carbon steel C40, SS304, titanium alloy (BT9) and low carbon steel (steel 20), with in-phase and out-of-phase loading, and applied magnitudes of loading with zero and positive means, complex loading profiles and block loads.

Including this, the proposed fatigue life model is compared with commercially available fatigue life models, i.e., absolute maximum principal, signed von Mises, signed shear, a critical plane parameter and the Wang–Brown method, including the Fatemi–Socie model and endurance function model from the published literature. Comparison with the experimental fatigue life results shows that the proposed model has predicted the fatigue life with an approximate difference of 1–5% for the loading profiles. In addition to the prediction accuracy, the benefit of the proposed interpolation scheme for calibrated coefficients is also observed where the fatigue life estimation accuracy is significantly improved, reduced from more than 10% to 1% difference. Analysis of the fatigue life prediction for the block loads showed that the proposed model, with the assumptions made to simplify the handling of block loading, predicted fatigue life with reasonable accuracy, with differences as low as 4–9%. It also highlighted the importance of characteristic profiles to correctly represent the considered loading profiles for better accuracy in fatigue life prediction with the proposed model. Comparing the fatigue life estimation of the proposed model with commercially available models including Fatemi–Socie and the endurance function model, it showed a consistent performance in the estimation of fatigue life for all cases, with differences of 1–5% for the considered loadings. Hence, it can be summarized that the proposed model has shown good consistent performance against various loading and material conditions. It can be considered as a general-purpose model for estimating the multiaxial fatigue life.

5.2.4 Critical Plane Estimation Method

The performance of the proposed approach in determining the critical plane orientation using the GA is analysed against multiaxial loading conditions. The proposed technique identified the critical plane with a better accuracy of $\pm 1°$ to $\pm 5°$ for the conventional angle increment method, with an approximate reduction of the number of iterations by a ratio of 18. In addition, the proposed approach using the multi-objective optimization also made it possible to use more than one fatigue parameter, i.e. the proposed fatigue parameter and maximum variance of shear stress, simultaneously. This resulted in additional planes being identified by the maximum variance of shear, which have low values of proposed fatigue parameter, as in the case of Paths 3 and 4 additional planes at location angles of $3°$ and $178°$ are identified. The proposed

technique can be used with more than two fatigue parameters, which may be useful in the case of random and complex loadings where more than one criterion can identify candidate planes which might be left out if using only one criterion. Thus, it can be concluded that the proposed critical plane estimation method is advantageous especially in complex random loading conditions. The application of more than one fatigue failure criteria identifies almost all of the candidate planes for fatigue failure, hence overcoming the limitation of single criterion.

The proposed multiaxial fatigue analysis methodology, including the continuum damage mechanics approach for damage estimation, critical plane-based multiaxial fatigue damage parameter and GA for calibration, is efficient, robust and reasonably accurate and suitable for use as a design tool for mechanical components in both academic and industrial applications.

5.3   CONTRIBUTIONS OF THE STUDY

The contributions of the study can be summarized as follows:

i.   A hybrid model is developed for multiaxial fatigue life analysis combining continuum damage mechanics and a critical plane-based approach. The model is independent of the applied load path shape. Hence, additional complexity and loss of the sequence of the applied load information, due to the application of cycle counting methods, is avoided.

ii.   A novel calibration scheme based on a genetic algorithm is developed for the proposed model. The scheme is capable of calibrating a number of coefficients simultaneously without requiring any new material coefficients.

iii.   A modular approach for fatigue life estimation is obtained by applying a GA-based calibration method, i.e., the model is flexible to adapt further modifications without any change in the proposed application procedure.

iv.   The proposed model is successfully applied for the estimation of fatigue life in the case of multiaxial loading conditions based on using the characteristic profiles for calibration. In addition, the interpolation scheme for coefficients calibration has remarkably improved the accuracy of fatigue life prediction.

v. A multi-parameter method is developed to locate the critical plane using the multi-objective optimization technique. More than one fatigue life criterion can be implemented simultaneously to identify additional candidate planes for fatigue failure. This technique is especially useful for complex or random loadings where the random nature of loading may result in additional planes being identified with a high level of damage.

5.4   RECOMMENDATIONS FOR FUTURE WORK

During this research, several areas of interest have been highlighted which could be of interest and worth investigating more thoroughly. These are outlined as follows:

i. Testing the proposed model against the experimental results from random profiles such as SAE-Bracket, SAE-Transmission and SAE-Suspension or CARLOS-multi profiles.

ii. Development of characteristic profiles representing the mentioned standard profiles so that the procedure of defining the characteristic profiles can be formulated and tested.

iii. A parameter to quantify the multiaxial nature of loading can be defined, such as the stress ratio or multiaxiality index, on the basis of which interpolation of calibrated coefficients can be done in the case of multiaxial loads, or where normal and shear stresses vary. Specially designed experiments can be performed with defined multiaxiality index values.

iv. Further study to incorporate the material-specific parameters for materials which fail in shear and normal stresses, e.g., weighting factors can be added in the fatigue parameter expression to speed up the procedure and to guide the GA solution towards a more accurate prediction of material behaviour.

REFERENCES

Abdullah, S., Al-Asady, N. A., Ariffin, A. K. and Rahman, M. M. 2008. A review on finite element analysis approaches in durability assessment of automotive components. *Journal of Applied Sciences.* **8**(12): 2192-2201.

Acevedoa, C. and Nussbaumer, A. 2009. Study on crack propagation in tubular joints under compressive fatigue loadings. Working paper. Fatigue Design 2009, Senlis, France: 25-26 November. pp. 1-8.

Anes, V., Reis, L., Li, B. and de Freitas, M. 2014. New cycle counting method for multiaxial fatigue. *International Journal of Fatigue.* **67**: 78-94.

Araujo, J. A., Dantas, A. P., Castro, F. C., Mamiya, E. N. and Ferreira, J. L. A. 2011. On the characterization of the critical plane with a simple and fast alternative measure of the shear stress amplitude in multiaxial fatigue. *International Journal of Fatigue.* **33**(8): 1092–1100.

Ås, S. K. 2006. *Fatigue Life Prediction of an Aluminum Alloy Automotive Component Using Finite Element Analysis of Surface Topography.* PhD. Norwegian University of Science and Technology,

Atzori, B., Berto, F., Lazzarin, P. and Quaresimin, M. 2006. Multi-axial fatigue behaviour of a severely notched carbon steel. *International Journal of Fatigue.* **28**: 485–493.

A to Z of Materials (AZoM.com). AZoM.com. 2013. Titanium Alloys - Ti5Al2Sn4Mo2Zr4Cr Properties and Applications (Online). http://www.azom.com/properties.aspx?ArticleID=2114 (19 June 2014).

British Stainless Steel Association. B.S.S.A. (Undated). Fatigue properties and endurance limits of stainless steels (Online). http://www.bssa.org.uk/topics.php?article=104 (18 June 2014).

Becker, W. T. and Lampman, S. R. (Eds.) 2002. *ASM Handbook: Volume 11. Failure Analysis and Prevention.* Mateirals Park, Ohio: ASM International.

Bishop, N. W. M. and Sherratt, F. 2000. *Finite element based fatigue calculations.* Netherlands: NAFEMS Ltd.

Bobyr, M., Altenbach, H. and Khalimon, O. 2014. On the application of the continuum damage mechanics to multi-axial low-cyclic damage. *Archive of Applied Mechanics.* p.14.

Brighenti, R. and Carpinteri, A. 2012. A notch multiaxial fatigue approach based on damage mechanics. *International Journal of Fatigue.* **39**: 122-133.

Brown, M. and Miller, K. J. 1973. Theory for fatigue under multiaxial stress–strain conditions. *Proceedings of the Institute of Mechanical Engineering,* **187**: pp. 745–756.

Brown, M. W. and Miller, K. J. 1982. Two decades of progress in the assessment of multiaxial low-cycle fatigue life. *Low-cycle fatigue and life prediction.* Amzallag, C., Leis, B. N.and Rabbe, P. (Eds.). West Conshohocken, PA: American Society for Testing and Materials, **ASTM STP 770**:482-499.

Bukkapatnam, S. and Sadananda, K. 2005. A genetic algorithm for unified approach-based predictive modeling of fatigue crack growth. *International Journal of Fatigue.* **27**(10-12): 1354-1359.

Chaboche, J. L. 1998a. Continuum Damage Mechaincs: Part II - Damage Growth, Crack Initiation and Crack Growth. *Journal of Applied Mechanics.* **55**: 65-72.

Chaboche, J. L. 1998b. Continuum Damage Mechanics: Part I - General Concepts. *Journal of Applied Mechanics.* **55**: 59-64.

Chapetti, M. D., Katsura, N., Tagawa, T. and Miyata, T. 2001. Static strengthening and fatigue blunt-notch sensitivity in lowcarbon steels. *International Journal of Fatigue.* **23**: 207-214.

Charkaluk, E., Constantinescu, A., Maïtournam, H. and Van, K. D. 2009. Revisiting the Dang Van criterion. *Procedia Engineering 1, Mesomechanics,* pp. 143-146.

Chaussumier, M., Mabru, M., Shahzad, M., Chieragatti, R. and Rezai-Aria, F. 2013. A predictive fatigue life model for anodized 7050 aluminium alloy. *International Journal of Fatigue.* **48**: 205-213.

Chu, C. C. 1995. Fatigue damage calculation using the critical plane approach. *Journal of Engineering Materials and Technology.* **117**(1): 41-49.

Crossland, B. 1956. Effect of large hydrostatic pressure on the torsional fatigue strength of an alloy steel. *Proceedings of International conference on fatigue of metals,* pp. 138–149.

Davis, L. (Ed.) 1991. *Handbook of genetic algorithms.* New York: Van Nostrand Reinhold.

Drucker, D. C. 1952. A more fundamental approach to plastic stress-strain relations. *Proceedings of the First U.S. Congress of Applied Mechanics,* pp. 487-491.

Emuakpor, O. S., George, T., Cross, C., Wertz, J. and Shen, M. H. H. 2012. A new distortion energy-based equivalent stress for multiaxial fatigue life prediction. *International Journal of Non-Linear Mechanics.* **47**: 29-37.

ESTECO. 2003. *MOGA-II - An improved Multi-Objective Genetic Algorithm*. Tec. Rep. 2003-006.

Ewing, J. A. and Humfrey, J. C. 1903. The fracture of metals under repeated alterations of stress. *Philosophical Transactions of the Royal Society.* **A200**: 241-250.

Fatemi, A. and Gladskyi, M. 2013. Notched fatigue behavior including load sequence effects under axial and torsional loadings. *International Journal of Fatigue.* **55**: 43-53.

Fatemi, A. and Shamsaei, N. 2011. Multiaxial fatigue: An overview and some approximation models for life estimation. *International Journal of Fatigue.* **33**: 948-958.

Fatemi, A., Shamsaei, N., Gladskyi, M., Panasovskyi, K. and Shukaev, S. 2010. Multiaxial fatigue of titanium including step loading and load path alteration and sequence effects. *International Journal of Fatigue.* **32**(11): 1862-1874.

Fatemi, A. and Socie, D. F. 1988. A critical plane approach to multiaxial fatigue damage including out of phase loading. *Fatgiue and Fracture of Engineering Materials and Structures.* **11**(3): 149-166.

Findley, W. N. 1959. A theory for the effect of mean stress on fatigue of metals under combined torsion and axial load or bending. *Journal of Engineering for Industry.* **Nov**: 301-306.

Fonseca, C. M. and Fleming, P. J. 1993. Genetic algorithms for multi-objective optimization: formulation, discussion and generalization. *Genetic Algorithms: Proceedings of the Fifth International Conference,* pp. 416-423.

Franulovic, M., Basan, R. and Prebil, I. 2009. Genetic algorithm in material model parameters' identification for low-cycle fatigue. *Computational Materials Science.* **45**: 505-510.

Gale, W. F. and Totemeier, T. C. 2003. *Smithells Metals Reference Book.*8th ed. Elsevier Science.

Ganjidoust, A. and M.Shariyat. 2009. A modified approach for multiaxial fatigue damage prediction. *12th International Conference on Fracture (ICF 12),* pp. 4259-4268.

Gantovnik, V. B., Anderson-Cook, C. M., Gürdal, Z. and Watson, L. T. 2003. A genetic algorithmwith memory for mixed discrete-continuous design optimization. *Computer and Structures.* **81**(20): 2003-2009.

Gao, H., Huang, H. Z., Zhu, S. P., Li, Y. F. and Yuan, R. 2014. A modified nonlinear damage accumulation model for fatigue life prediction considering load interaction effects. *The Scientific World Journal.* **2014**: 164378.

Gates, N. and Fatemi, A. 2014. Notched fatigue behavior and stress analysis under multiaxial states of stress. *International Journal of Fatigue.* **67**: 2-14.

Gates, N. R., Fatemi, A., Socie, D. F. and Phan, N. 2014. Notched fatigue behavior under multiaxial stress states. *Advanced Material Research.* **891-892**: 185-190.

Ghalami, T. Z. and Fatemi, A. 2013. Multiaxial fatigue and life prediction of elastomeric components. *International Journal of Fatigue.* **55**: 90-101.

Glinka, G., Wang, G. and Plumtree, A. 1995. Mean stress effects in multiaxial fatigue. *Fatigue and Fracture of Engineering Materials and Structures.* **18**(7/8): 755-764.

Gómez, C., Canales, M., Calvo, S., Rivera, R., Valdés, J. R. and Núñez, J. L. 2011. High and low cycle fatigue life estimation of welding steel under constant amplitude loading: Analysis of different multiaxial damage models and in-phase and out-of-phase loading effects. *International Journal of Fatigue.* **33**(4): 578-587.

Habtour, E., Connon, W., Pohland, M. F., Stanton, S. C., Paulus, M. and Dasgupta, A. 2014. Review of Response and Damage of Linear and Nonlinear Systems under Multiaxial Vibration. *Shock and Vibration.* **2014**: 1-21.

HBM. 2011. *ncode Design Life Theory Guide*.

Hofmann, F., Bertolino, G., Constantinescu, A. and Ferjani, M. 2009. Numerical exploration of the dang van high cycle fatigue criterion: application to gradient effects. *Journal of Mechanics of Materials and Structures.* **4**(2): 293-308.

Horstemeyer, M. F. and Gokhale, A. M. 1999. A void_crack nucleation model for ductile metals. *International Journal of Solids and Structures.* **36**(33): 5029-5055.

Ince, A. 2012. *Development of computational multiaxial fatigue modelling for notched components.* Ph.D. Thesis. University of Waterloo, Canada.

Ince, A. 2013. Computational multiaxial fatigue modelling for notched components. *Modeling and Numerical Simulation of Material Science.* **03**(03): 14-22.

Ince, A. and Glinka, G. 2014. A generalized fatigue damage parameter for multiaxial fatigue life prediction under proportional and non-proportional loadings. *International Journal of Fatigue.* **62**: 34-41.

Itoh, T., Ohnami, M., Sakane, M. and Socie, D. F. 1995. Nonproportional Low Cycle Fatigue Criterion for Type 304 Stainless Steel. *Journal of Engineering Materials and Technology.* **117**: 285-292.

Kandil, F. A., Brown, M. W. and Miller, K. J. 1982. Biaxial low-cycle fatigue fracture of 316 stainless steel at elevated temperatures. London: The Metals Society, **Book 280**:203-210.

Kenmeugne, B., Fotsing, B. D. S., Anago, G. F., Fogue, M., Robert, J. L. and Kenne, J. P. 2012. On the evolution and comparison of multiaxial fatigue criteria. *International Journal of Engineering and Technology.* **4**(1): 37-46.

Khandelwal, K. and El-Tawil, S. 2014. A finite strain continuum damage model for simulating ductile fracture in steels. *Engineering Fracture Mechanics.* **116**: 172-189.

Kida, S., Itoh, T., Sakane, M., Ohnami, M. and Socie, D. F. 1997. Dislocation structure and non-proportional hardening of type 304 stainless steel. *Fatigue & Fracture of Engineering Materials & Structures.* **20**(10): 1375-1386.

Klemenc, J. and Fajdiga, M. 2012. Estimating S–N curves and their scatter using a differential ant-stigmergy algorithm. *International Journal of Fatigue.* **43**: 90-97.

Klemenc, J. and Fajdiga, M. 2013. Joint estimation of E–N curves and their scatter using evolutionary algorithms. *International Journal of Fatigue.* **56**: 42-53.

Krishnapillai, K. and Jones, R. 2009. Three-dimensional structural design optimisation based on fatigue implementing a genetic algorithm and a non-similitude crack growth law. *Finite Elements in Analysis and Design.* **45**(2): 132-146.

Lampman, S. R. (Ed.) 1996. *ASM Handbook: Volume 19. Fatigue and Fracture.* Mateirals Park, Ohio: ASM International.

Lasserre, S. and Palin-Luc, T. 1998. An energy based criterion for high cycle multiaxial fatigue. *European Journal of Mechanics - A/Solids.* **17**(2): 237-251.

Lazzarin, P. and Susmel, L. 2003. A stress-based method to predict lifetime under multiaxial fatigue loadings. *Fatigue and Fracture of Engineering Materials and Structures.* **26**: 1171-1187.

Lee, Y., Pan, J., Hathaway, R. and Barkey, M. 2005. *Fatigue testing and analysis: Theory and practice.* New York: Elsevier Butterworth Heinemann.

Leila, K., Emmanuel, P. and Sylvain, L. 2010. A measure of the equivalent shear stress amplitude from a prismatic hull in the principal coordinate system. *International Journal of Fatigue.* **32**(12): 1977-1984.

Li, J., Sun, Q., Zhang, Z. P., Li, C. W. and Zhang, D. W. 2010. A New Multiaxial Fatigue Life Prediction Model Under Proportional and Nonproportional Loading. *Journal of Engineering Materials and Technology.* **132**: pp.8.

Li, J., Zhang, Z. P., Sun, Q. and Li, C. W. 2011. Multiaxial fatigue life prediction for various metallic materials based on the critical plane approach. *International Journal of Fatigue.* **33**(2): 90-101.

Liu, K. C. 1993. A method based on virtual strain energy parameters for multiaxial fatigue life prediction. *Advances in Multiaxial Fatigue.* McDowell, D. L.and Ellis, R. (Eds.). West Conshohocken, PA: American Society for Testing Materials, **ASTM STP1191**:67-84.

Liu, K. C. and Wang, J. A. 2001. An energy method for predicting fatigue life, crack orientation, and crack growth under multiaxial loading conditions. *International Journal of Fatigue.* **23**(S1): S129-S134.

Liu, Y. 2006. *Stochastic modeling of multiaxial fatigue and fracture.* Ph.D. Thesis. Vanderbilt University, USA.

Lotfi, B. and Beiss, P. 2013. Application of neural networking for fatigue limit prediction of powder metallurgy steel parts. *Materials & Design.* **50**: 440-445.

Lu, Z. and Liu, Y. 2009. Crack growth-based multiaxial fatigue life prediction. Working Paper. 12th International Conference on Fracture (ICF-12), Ottawa, Canada: 12-17 July. pp. 1-10.

Lugo, M., Jordon, J. B., Horstemeyer, M. F., Tschopp, M. A., Harris, J. and Gokhale, A. M. 2011. Quantification of damage evolution in a 7075 aluminum alloy using an acoustic emission technique. *Materials Science and Engineering: A.* **528**(22-23): 6708-6714.

Luo, C. and Chattopadhyay, A. 2011. Prediction of fatigue crack initial stage based on a multiscale damage criterion. *International Journal of Fatigue.* **33**(3): 403-413.

Macha, E. and Niesłony, A. 2012. Critical plane fatigue life models of materials and structures under multiaxial stationary random loading: The state-of-the-art in Opole Research Centre CESTI and directions of future activities. *International Journal of Fatigue.* **39**: 95-102.

Mahadevan, S. and Liu, Y. 2005. Multiaxial high-cycle fatigue criterion and life prediction for metals. *International Journal of Fatigue.* **27**(7): 790-800.

Mahadevan, S. and Liu, Y. 2007. A unified multiaxial fatigue damage model for isotropic and anisotropic materials. *International Journal of Fatigue.* **29**(2): 347-359.

Maksimovic, S. 2005. Fatigue Life Analysis of Aircraft Structural Components. *Scientific-Technical Review.* **LV**(1): 15-22.

Mamiya, E. N., Castro, F. C., Algarte, R. D. and Araújo, J. A. 2011. Multiaxial fatigue life estimation based on a piecewise ruled S–N surface. *International Journal of Fatigue.* **33**(4): 529-540.

Mamiya, E. N., Goncalves, C. A. and Araujo, J. A. 2005. Multiaxial fatigue: a stress based criterion for hard metals. *International Journal of Fatigue.* **27**(2): 177-187.

Manson, S. S. and Halford, G. R. 2006. *Fatigue and durability of structural materials.* Materials Park, Ohio: ASM International, Materials.

Marquis, G. 2010. Current trends in multiaxial fatgiue reserach and assessment. Working paper. The Ninth International Conference on Multiaxial Fatigue & Fracture (ICMFF9), University of Parma, Italy: 7-9 June. pp. 883-898.

Mayer, H. 2009. Fatigue damage of low amplitude cycles in low carbon steel. *Journal of Materials Science.* **44**(18): 4919-4929.

McDiarmid, D. L. 1991. A general criterion for high cycle multiaxial fatigue failure. *Fatigue and Fracture of Engineering Materials and Structures.* **14**(4): 429-453.

McDiarmid, D. L. 1994. A shear stress based critical-plane criterion of multiaxial fatigue failure for design and life prediction. *Fatigue and Fracture of Engineering Materials and Structures.* **7**(12): 217-226.

Meggiolaro, M. A. and de Castro, J. T. P. 2012a. An improved multiaxial rainflow algorithm for non-proportional stress or strain histories – Part I: Enclosing surface methods. *International Journal of Fatigue.* **42**: 217-226.

Meggiolaro, M. A. and de Castro, J. T. P. 2012b. An improved multiaxial rainflow algorithm for non-proportional stress or strain histories – Part II: The Modified Wang–Brown method. *International Journal of Fatigue.* **42**: 194-206.

Miao, B., Zhang, W., Zhang, J. and Jin, D. 2009. Evaluation of Railway Vehicle Car Body Fatigue Life and Durability using a Multi-disciplinary Analysis Method. *International Journal of Vehicle Structures and Systems.* **1**(4): 85-92.

Milella, P. P. 2013. *Multiaxial Fatigue.* Springer Milan.

Morrow, J. D. and Socie, D. F. 1980. Review of contemporary approaches to fatigue damage analysis. *Risk and Failure Analysis for Improved Performance and Reliability.* Burke, J. J.and Weiss, V. (Eds.). New York: Plenum Publication Corp., pp. 141-194.

NAFEMS. (Undated). The Importance of Mesh Convergence - Part 1 (Online). http://www.nafems.org/join/resources/knowledgebase/001/ (18 March 2015).

Narayanasamy, R. and Loganathan, C. 2007. The influence of friction on the prediction of wrinkling of prestrained blanks when drawing through a conical die. *Materials and Design.* **28**(3): 904-912.

Niesłony, A. and Böhm, M. 2013. Mean stress effect correction using constant stress ratio S–N curves. *International Journal of Fatigue.* **52**: 49-56.

Ninic, D. 2006. *Fatigue in Automatic Transmissions.* PhD. University of New South Wales,

Ninic, D. and Stark, H. 2007. A multiaxial fatigue damage function. *International Journal of Fatigue.* **29**(3): 533-548.

Noradila, A. L., Sajuri, Z., Syarif, J., Miyashita, Y. and Mutoh, Y. 2013. Effect of strain rates on tensile and work hardening properties for Al-Zn magnesium alloys. *IOP Conference Series: Materials Science and Engineering.* **46**: 012031.

Núñez, J. L., Calvo, S., Canales, M., Gómez, C. and Valdés, J. R. 2011. Probabilistic formulation of the multiaxial fatigue damage of Liu. *International Journal of Fatigue.* **33**(3): 460-465.

Ottosen, N. S., Stenstrom, R. and Ristinmaa, M. 2008. Continuum approach to high-cycle fatigue modeling. *International Journal of Fatigue.* **30**: 996-1006.

Palin-Luc, T., Banvillet, A. and Lasserre, S. 2003. A volumetric energy based high cycle multiaxial fatigue criterion. *International Journal of Fatigue.* **25**(8): 755-769.

Papadopoulos, I. V. 1994. A new criterion of fatigue strength for out-of phase bending and torsion of hard metals. *International Journal of Fatigue.* **16**(6): 377-384.

Papadopoulos, I. V., Davoli, P., Gorla, C., Filippini, M. and Bernasconi, A. 1997. A comparative study of multiaxial high-cycle fatigue criteria for metals. *International Journal of Fatigue.* **19**(3): 219-235.

Papuga, J. 2011. A survey on evaluating the fatigue limit under multiaxial loading. *International Journal of Fatigue.* **33**: 153-165.

Papuga, J. and Ruzicka, M. 2008. Two new multiaxial criteria for high cycle fatigue computation. *International Journal of Fatigue.* **30**(1): 58-66.

Pinto, F. 2007. *Application of evolutionary techniques to energy transfer efficiency in heat transfer problems and low consumption buildings.* PhD Thesis. University of Bolonga, Italy.

Pinto, H. n., De Jesus, A. l. M. P., Fernández-Canteli, A., Castillo, E. and Pereira, H. l. F. S. G. 2010. Analysis of Constant and Variable Amplitude Strain-Life Data Using a Novel Probabilistic Weibull Regression Model. *Journal of Pressure Vessel Technology.* **132**(6): 061401.

Rahman, M. M., Ariffin, A. K., Jamaludin, N. and Haron, C. H. 2007. Finite element based durability assessment of a free piston linear engine component. *Structural Durability and Health Monitoring.* **3**: 1-13.

Rahman, M. M., Ariffin, A. K., Rejab, M. R. M., Kadirgama, K. and Noor, M. M. 2009a. Multiaxial fatigue behaviour of cylinder head for a free piston linear engine. *Journal of Applied Sciences.* **9**(15): 2725-2734.

Rahman, M. M., Kadirgama, K., Noor, M. M., Rejab, M. R. M. and Kesulai, S. A. 2009b. Fatigue life prediction of lower suspension arm using strain-life approach. *European Journal of Scientific Research.* **30**(3): 437-450.

Reis, L., Li, B. and deFreitas, M. 2003. Multiaxial fatigue testing and analysis of metallic materials. *ANALES DE MECÁNICA DE LA FRACTURA.* **20**: 462-467.

Routara, B. C., Sahoo, A. K., Parida, K. and Padhi, P. C. 2012. Response surface methodology and genetic algorithm used to optimize the cutting condition for surface roughness parameters in CNC turning. *Procedia Engineering.* **38**: 1893-1904.

Roux, C., Lorang, X., Maitournam, H., Nguyen-Tajan, M.-L. and Quesson, B. 2013. Multi-parameter Fatigue Equivalence Loadings for Specification Applications. *Procedia Engineering.* **66**: 393-402.

Saintier, N., Palin-luc, T., Bénabes, J. and Cocheteux, F. 2013. Non-local energy based fatigue life calculation method under multiaxial variable amplitude loadings. *International Journal of Fatigue.* **54**: 68-83.

Sangid, M. D. 2013. The physics of fatigue crack initiation. *International Journal of Fatigue.* **57**: 58-72.

Schijve, J. 2003. Fatigue of structures and materials in the 20th century and the state of the art. *International Journal of Fatigue.* **25**(8): 679-702.

Schijve, J. 2009. *Fatigue of Structures and Materials.*2nd ed. Springer Science+Business Media, B.V.

Schmid, S. R., Hamrock, B. J. and Jacobson, B. O. 2013. *Fundamentals of Machine Elements.*3rd ed. CRC Press

Scott, M. A., Earp, M. N., Benzley, S. E. and Stephenson, M. B. 2005. Adaptive Sweeping Techniques. *Proceedings, 14th International Meshing Roundtable,* pp. 417-432.

Shamsaei, N. 2010. *Multiaxial fatigue and deformation including non-proportional hardening and variable amplitude loading effects.* PhD Thesis. The University of Toledo, Toledo, USA.

Shamsaei, N. and McKelvey, S. A. 2014. Multiaxial life predictions in absence of any fatigue properties. *International Journal of Fatigue.* **67**: 62-72.

Shang, D.-G., Sun, G.-Q. and Bao, M. 2010. Multiaxial fatigue damage parameter and life prediction under low cycle loading for GH4169 alloy and other structural materials. *International Journal of Fatigue.* **32**(7): 1108-1115.

Sines, G. 1955. Failure of materials under combined repeated stresses with superimposed static stress. *National Advisory Committee for Aeronautics.* **Technical Note 3495**: pp. 69.

Sines, G. 1959. Behavior of metals under complex static and alternating stresses. *Metal fatigue.* Sines, G.and Waisman, J. L. (Eds.). New York: McGraw-Hill,

Smith, K. N., Watson, P. and Topper, T. H. 1970. A Stress-Strain function for the fatigue of metals. *Journal of Materials.* **5**(4): 767-778.

Socie, D. F. and Marquis, G. B. 2000. *Multiaixal Fatigue.* Warrendale, PA, USA: SAE.

Society of Automotive Engineers. 2002. *Technical Report on Low Cycle Fatigue Properties Ferrous and Non-Ferrous Materials*. SAE J1099 (AUG2002).

Stephens, R. I., Fatemi, A., Stephens, R. R. and Fuchs, H. O. 2000. *Metal fatigue in engineering.* New York: John Wiley and Sons, Inc.

Suman, S. K. 2013. *Nonlinear Fatigue Damage Accumulation in Aircraft Engine Alloys Under Multiaixal Loading.* PhD Thesis. North Dakota State University of Agricultural and Applied Science, Fargo, North Dakota, USA.

Sun, G. Q., Wang, D. and Shang, D. G. 2013. Time-dependent multiaxial fatigue and life prediction for nickel-based GH4169 alloy. *Fatigue & Fracture of Engineering Materials & Structures.* **36**(10): 1039-1050.

Susmel, L. 2010. A simple and efficient numerical algorithm to determine the orientation of the critical plane in multiaxial fatigue problems. *International Journal of Fatigue.* **32**(11): 1875-1883.

Susmel, L. and Lazzarin, P. 2002. A bi-parametric modified Wohler curve for high cycle multiaxial fatigue assessment. *Fatigue and Fracture of Engineering Materials and Structures.* **25**: 63-78.

Susmel, L., Louks, R., Gerin, B., Draper, J. and Askes, H. 2014a. On the multiaxial fatigue assessment of complex three-dimensional stress concentrators. *International Journal of Fatigue.* **63**: 12-24.

Susmel, L. and Taylor, D. 2006. A simplified approach to apply the theory of critical distances to notched components under torsional fatigue loading. *International Journal of Fatigue.* **28**(4): 417-430.

Susmel, L. and Taylor, D. 2008. The Modified Wohler Curve Method applied along with the Theory of Critical Distances to estimate finite life of notched components subjected to complex multiaxial loading paths. *Fatigue and Fracture of Engineering Materials and Structures.* **31**: 1047-1064.

Susmel, L. and Taylor, D. 2010. An Elasto-Plastic Reformulation of the Theory of Critical Distances to Estimate Lifetime of Notched Components Failing in the Low/Medium-Cycle Fatigue Regime. *Journal of Engineering Materials and Technology.* **132**(2): 021002.

Susmel, L. and Taylor, D. 2011. The Theory of Critical Distances to estimate lifetime of notched components subjected to variable amplitude uniaxial fatigue loading. *International Journal of Fatigue.* **33**(7): 900-911.

Susmel, L. and Taylor, D. 2012. A critical distance/plane method to estimate finite life of notched components under variable amplitude uniaxial/multiaxial fatigue loading. *International Journal of Fatigue.* **38**: 7-24.

Susmel, L. and Tovo, R. 2011. Estimating fatigue damage under variable amplitude multiaxial fatigue loading. *Fatigue & Fracture of Engineering Materials & Structures.* **34**(12): 1053-1077.

Susmel, L., Tovo, R. and Socie, D. F. 2014b. Estimating the orientation of Stage I crack paths through the direction of maximum variance of the resolved shear stress. *International Journal of Fatigue.* **58**: 94-101.

Tarar, W. A. 2008. *A New Finite Element Procedure for Fatigue Life Prediction and High Strain Rate Assessment of Cold Worked Advanced High Strength Steel.* PhD. The Ohio State University,

Taylor, D. 1999. Geometrical effects in fatigue: a unifying theoretical model. *International Journal of Fatigue.* **21**(5): 413-420.

Ukranian-Standard. 1988. *Carbon structural quality steel guaged bars with special surface finish. General specifications [In Russian].* **Gost 1050-88.**

Van, K. D. 1993. Macro-micro approach in high-cycle multiaxial fatigue. *Advances in Multiaxial Fatigue.* McDowell, D. L.and Ellis, R. (Eds.). West Conshohocken, PA: American Society for Testing Materials, **ASTM STP1191**:120-130.

Varvani-Farahani, A. 2005. *Advances in Fatigue, Fracture and Damage Assessment of Materials.* WIT Press.

Vassilopoulos, A., Georgopoulos, E. and Dionysopoulos, V. 2007. Artificial neural networks in spectrum fatigue life prediction of composite materials. *International Journal of Fatigue.* **29**(1): 20-29.

Vassilopoulos, A., Georgopoulos, E. and Keller, T. 2008. Comparison of genetic programming with conventional methods for fatigue life modeling of FRP composite materials. *International Journal of Fatigue.* **30**(9): 1634-1645.

Vu, Q. H., Halm, D. and Nadot, Y. 2010. Multiaxial fatigue criterion for complex loading based on stress invariants. *International Journal of Fatigue.* **32**(7): 1004-1014.

Wang, C. H. and Brown, M. W. 1993. A Path Independent Parameter for Fatigue under Proportional and Non proportional loading. *Fatigue and Fracture of Engineering Materials and Structures.* **16**(12): 1285-1298.

Wang, E., Nelson, T. and Rauch, R. 2004. Back to Elements - Tetrahedra vs. Hexahedra. Working Paper. International ANSYS Conference, Pittsburgh, PA, United States: 24-26 May. pp. 1-16.

Zenner, H., Simburger, A. and Liu, J. 2000. On the fatigue limit of ductile metals under complex multiaxial loading. *International Journal of Fatigue.* **22**(2): 137-145.

Zhang, T., McHugh, P. E. and Leen, S. B. 2012. Finite element implementation of multiaxial continuum damage mechanics for plain and fretting fatigue. *International Journal of Fatigue.* **44**: 260-272.

Zhou, N., Zhang, J., Ju, F. and Liu, S. 2012. Genetic Algorithm Coupled with the Neural Network for Fatigue Properties of Welding Joints Predicting. *Journal of Computers.* **7**(8): 1887-1894.
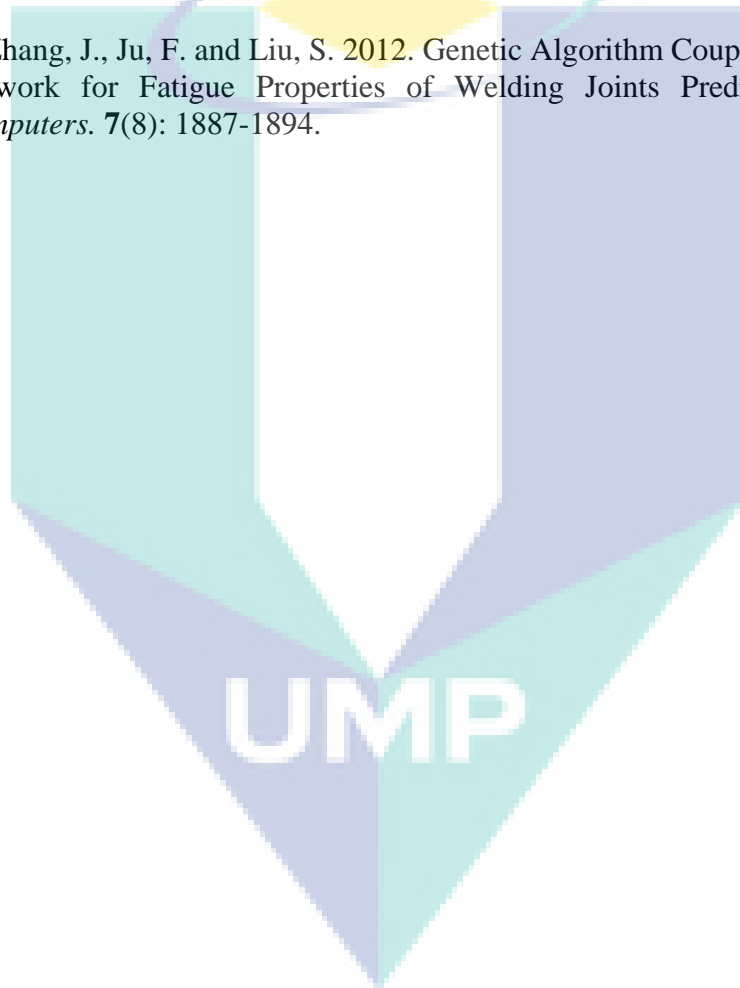
LIST OF PUBLICATIONS

1. Kamal, M. and Rahman, M.M. 2015. Continuum damage mechanics and genetic algorithm for multiaxial fatigue life modelling: a hybrid approach. *Fatigue & Fracture of Engineering Materials & Structures*. (ISI Indexed, Q1, impact factor 1.561) (Accepted)

2. Kamal, M. and Rahman, M.M. 2015. An integrated approach for fatigue life estimation based on continuum damage mechanics theory and critical plane method. *International Journal of Automotive and Mechanical Engineering*, **Volume 11:** 2756-2770. (Scopus Indexed, SNIP = 2.106)

3. Kamal, M. and Rahman, M.M. 2015. Fatigue Life Estimation Based on Continuum Mechanics Theory with Application of Genetic Algorithm. *International Journal of Automotive and Mechanical Engineering*, **Volume 11:**2686-2698.

4. Kamal, M. and Rahman, M.M. 2015. Dual-Criteria Method to Determine Critical Plane Orientation for Multiaxial Fatigue Prediction using Genetic Algorithm. *International Journal of Automotive and Mechanical Engineering*, **Volume 11:**2571-2581. (Scopus Indexed, SNIP = 2.106)

5. Kamal, M. and Rahman, M.M. 2014. Finite Element Based Fatigue Behaviour of Springs in Automobile Suspension. *International Journal of Automotive and Mechanical Engineering*, **10**:1910-1919. (Scopus Indexed, SNIP = 2.106)

6. Kamal, M., Rahman, M.M. and Rahman, A.G.A. 2014. Fatigue Life Estimation Models: a State of The Art. *International Journal of Automotive and Mechanical Engineering*, **Volume 9**: 1599-1608. (Scopus Indexed, SNIP = 2.106)

7. Kamal, M., Rahman, M.M. and Sani, M.S.M. 2013. Fatigue Life Prediction Using Simplified Endurance Function Model. *Advances in Mechanical Engineering, Issue: Advances of Artificial Intelligence in Mechanical Engineering (ADIN)*, **Volume 2013**, Article ID 581754. (ISI Indexed, Q2, impact factor 1.062)

8. Kamal, M., Rahman, M.M. and Rahman, A.G.A. 2013. Application of Multi Body Simulation for Fatigue Life Estimation. *Journal of Mechanical Engineering and Sciences*, **7**:912-923. (Scopus Indexed)

9. Kamal, M., Rahman, M.M. and Rahman, A.G.A. 2012. Fatigue Life Evaluation of Suspension Knuckle Using Multi Body Simulation Technique. *Journal of Mechanical Engineering and Sciences*, **3**:291-300. (Scopus Indexed)

10. Kamal, M. and Rahman, M.M. 2012. Study on Dynamic Behavior of Wishbone Suspension System. IOP Conference Series: *Materials Science and Engineering*, **36**(1), Article # 012019 (Scopus Indexed)

Under review and Submission

11.   Kamal, M. and Rahman, M.M. A multiaxial fatigue model based on continuum mechanics theory under complex loading conditions. (communication)

12.   Kamal, M. and Rahman, M.M. Performance study of fatigue parameter expressions for newly developed fatigue estimation model. (communication)

13.   Kamal, M. and Rahman, M.M. Fatigue life prediction of Titanium alloy for block loading using the hybrid approach of critical plane and continuum damage mechanics. (communication)
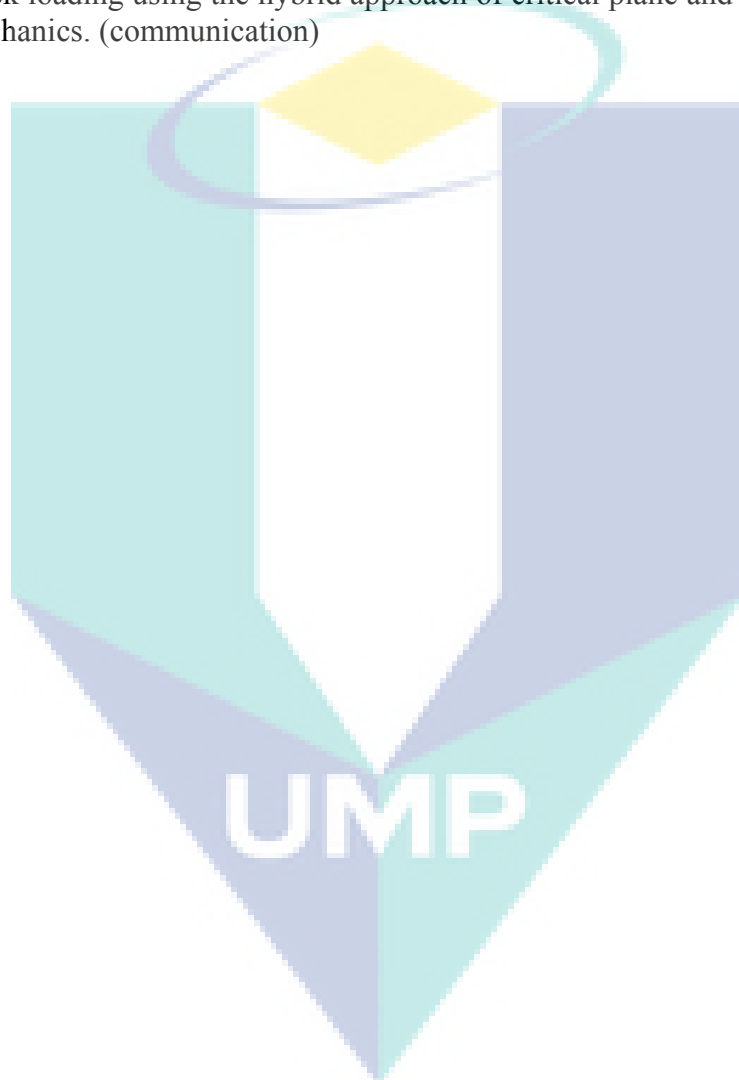
APPENDIX A1

INCREMENTAL ANGLE METHOD FOR CRITICAL PLANE

! NUMBER OF NODE AT CRITICAL LOCATION IN VARIABLE "nodenumber"

```
*dim,nloc,array,3,1
*GET,NLOC(1,1),NODE,nodenumber,loc,x
*GET,NLOC(2,1),NODE,nodenumber,loc,y
*GET,NLOC(3,1),NODE,nodenumber,loc,z

LOCAL,12,0,nloc(1,1),nloc(2,1),nloc(3,1)

wpcsys,-1

*get,N,active,,set,nset        !NUMBER OF RESULT SETS

!********************************************************

/post1
*dim,crtpstrain,array,1,4
*dim,criticalplanefinder,array,n,1371,8
*afun,deg     !change angle from radian to deg for angle functions

stopcheck=0

csys,12

*abset,Finding the critical plane,both

*do,a,1,n,1

*ABCHECK,nint(a/n*100),load step %a%

 *if,_return,gt,0,then
     stopcheck=1
 *endif

 *if,stopcheck,gt,0,exit

    set,,,,,,,a   !RESULT AT LOAD STEP READ
    i=1

  *do,theta,0,180,5
    *do,phy,0,180,5
      wpcsys,-1
      wprota,theta,,-(90-phy)
```

```
      rsys,4

      *get,CRTPSTRAIN(1,1),node,nodenumber,epto,xy
      *get,CRTPSTRAIN(1,2),node,nodenumber,epto,xz
      *get,criticalplanefinder(a,i,7),node,nodenumber,epto,x
      *get,CRTPSTRAIN(1,3),node,nodenumber,s,xy
      *get,CRTPSTRAIN(1,4),node,nodenumber,s,xz
      *get,criticalplanefinder(a,i,8),node,nodenumber,s,x


resultantshearstrain=((CRTPSTRAIN(1,1))**2+(CRTPSTRAIN(1,2))**2)**(1/2)

resultantshearstress=((CRTPSTRAIN(1,3))**2+(CRTPSTRAIN(1,4))**2)**(1/2)

      criticalplanefinder(a,i,1)=theta
      criticalplanefinder(a,i,2)=phy
      criticalplanefinder(a,i,3)=CRTPSTRAIN(1,1)
      criticalplanefinder(a,i,4)=CRTPSTRAIN(1,2)
      criticalplanefinder(a,i,5)=resultantshearstrain
      criticalplanefinder(a,i,6)=resultantshearstress

     i=i+1

    *enddo
   *enddo
*enddo
*ABFINI

!***********************************

*dim,forsorting,,n,4
*dim,strainrange,,1369,6

*do,b,1,1369,1

     *do,c,1,n

          forsorting(c,1)=criticalplanefinder(c,b,7)  !store normal strain
          forsorting(c,2)=criticalplanefinder(c,b,8)  !store normal stress
          forsorting(c,3)=criticalplanefinder(c,b,5)  !store resultant strain
          forsorting(c,4)=criticalplanefinder(c,b,6)  !store resultant shear stress


     *enddo

!******************************************************

    !normal strain range
```

```
*dim,orderforsortingmatrix,,n

*moper,orderforsortingmatrix(1),forsorting(1,1),sort,forsorting(1,1)  !SORTING
OPERATION

maxstrainnormal=forsorting(n,1)
minstrainnormal=forsorting(1,1)

*moper,orderforsortingmatrix(1),forsorting(1,1),sort,orderforsortingmatrix(1,1)
!restore matrix to original order

*del,orderforsortingmatrix,,nopr   !delete and redefined just to make sure that no
value of that matrix used by mistake

!********************************************************

!normal stress range

*dim,orderforsortingmatrix,,n

*moper,orderforsortingmatrix(1),forsorting(1,2),sort,forsorting(1,2)  !SORTING
OPERATION

maxstressnormal=forsorting(n,2)

*moper,orderforsortingmatrix(1),forsorting(1,2),sort,orderforsortingmatrix(1,1)
!restore matrix to original order

*del,orderforsortingmatrix,,nopr

!********************************************************

!Resultant shear strain !!

*dim,orderforsortingmatrix,,n

*moper,orderforsortingmatrix(1),forsorting(1,3),sort,forsorting(1,3)  !SORTING
OPERATION

maxstrainresultant=forsorting(n,3)
minstrainresultant=forsorting(1,3)

*moper,orderforsortingmatrix(1),forsorting(1,3),sort,orderforsortingmatrix(1,1)
!restore matrix to original order

*del,orderforsortingmatrix,,nopr

!********************************************************
```

```
!shear stress

*dim,orderforsortingmatrix,,n

*moper,orderforsortingmatrix(1),forsorting(1,4),sort,forsorting(1,4)  !SORTING
OPERATION

maxshearstresssultant=forsorting(n,4)

*moper,orderforsortingmatrix(1),forsorting(1,4),sort,orderforsortingmatrix(1,1)
!restore matrix to original order

*del,orderforsortingmatrix,,nopr

!**********************************************************

strainrange(b,1)=criticalplanefinder(1,b,1)

strainrange(b,2)=criticalplanefinder(1,b,2)

strainrange(b,3)=maxstrainnormal-minstrainnormal  !NORMAL STRAIN RANGE

strainrange(b,4)=maxstrainresultant-minstrainresultant  !SHEAR STRAIN RANGE

strainrange(b,5)=strainrange(b,4)*maxshearstresssultant

strainrange(b,6)=strainrange(b,5)+(strainrange(b,3)*maxstressnormal)  !paramater
combo of strain range and max shear stress on plane

*enddo        !COUNTER FOR b

!Critical plane location

*dim,orderofstrainrangematrix,,1369

*moper,orderofstrainrangematrix(1),strainrange(1,6),sort,strainrange(1,6)

rowindexformaxPARM=orderofstrainrangematrix(1369,1)

*moper,orderofstrainrangematrix(1),strainrange(1,6),sort,orderofstrainrangematrix(1,1)

*del,orderofstrainrangematrix,,nopr

theta_maxPARAM=strainrange(rowindexformaxPARM,1)
phy_maxPARAM=strainrange(rowindexformaxPARM,2)
maxPARAMETER=strainrange(rowindexformaxPARM,6)
!***********************************
```

APPENDIX A2

SINGLE PARAMETER GA BASED CRITICAL PLANE METHOD

```
Sub fatpara()

yieldstress = Sheet1.Cells(5, 2)
n = Sheet1.Cells(6, 2)

'convert degress into radians

theta = (Sheet1.Cells(7, 2)) * (3.14159 / 180)
phy = (Sheet1.Cells(8, 2)) * (3.14159 / 180)

Sheet1.Cells(7, 3) = theta
Sheet1.Cells(8, 3) = phy

Dim sortrange As Range


'a 3D array with load numbers and critical plane angles and xy and xz and resultant
shear strains "theta,phy,XY shear strain, XZ shear strain, resultant shear strain"


    'Direction cosines w.r.t. theta and phy
    a11 = Cos(theta) * Sin(phy)
    a12 = Sin(theta) * Sin(phy)
    a13 = Cos(phy)
    a21 = -Sin(theta)
    a22 = Cos(theta)
    a23 = 0
    a31 = -Cos(theta) * Cos(phy)
    a32 = -Sin(theta) * Cos(phy)
    a33 = Sin(phy)


For a = 1 To n

    'For Strains


        CRTPSTRAIN_GLC_x = Sheet1.Cells(5 + a, 7)
        CRTPSTRAIN_GLC_y = Sheet1.Cells(5 + a, 8)
        CRTPSTRAIN_GLC_z = Sheet1.Cells(5 + a, 9)
        CRTPSTRAIN_GLC_xy = Sheet1.Cells(5 + a, 10)
        CRTPSTRAIN_GLC_xz = Sheet1.Cells(5 + a, 11)
        CRTPSTRAIN_GLC_yz = Sheet1.Cells(5 + a, 12)
```

'shear strain components

CRTPSTRAIN11 = 2 * ((CRTPSTRAIN_GLC_x * a11 * a21) +
(CRTPSTRAIN_GLC_y * a12 * a22) +
(CRTPSTRAIN_GLC_z * a13 * a23) +
((CRTPSTRAIN_GLC_xy * (a11 * a22 + a12 * a21)) / 2) +
((CRTPSTRAIN_GLC_yz * (a12 * a23 + a13 * a22)) / 2) +
((CRTPSTRAIN_GLC_xz * (a13 * a21 + a11 * a23)) / 2))

CRTPSTRAIN12 = 2 * ((CRTPSTRAIN_GLC_x * a11 * a31) +
(CRTPSTRAIN_GLC_y * a12 * a32) +
(CRTPSTRAIN_GLC_z * a13 * a33) +
((CRTPSTRAIN_GLC_xy * (a11 * a32 + a12 * a31)) / 2) +
((CRTPSTRAIN_GLC_yz * (a12 * a33 + a13 * a32)) / 2) +
((CRTPSTRAIN_GLC_xz * (a13 * a31 + a11 * a33)) / 2))

'normal strain component

CRTPSTRAIN15 = (CRTPSTRAIN_GLC_x * (a11 ^ 2)) +
(CRTPSTRAIN_GLC_y * (a12 ^ 2)) +
(CRTPSTRAIN_GLC_z * (a13 ^ 2)) +
(CRTPSTRAIN_GLC_xy * (a11 * a12)) +
(CRTPSTRAIN_GLC_xz * (a11 * a13)) +
(CRTPSTRAIN_GLC_yz * (a13 * a12))

resultantshearstrain = ((CRTPSTRAIN11) ^ 2 + (CRTPSTRAIN12) ^ 2) ^ (1 / 2)

'storing calculated normal and shear stains in excel sheet for sorting maximum and minimum values

Sheet3.Cells(1 + a, 3) = CRTPSTRAIN15
Sheet3.Cells(1 + a, 4) = resultantshearstrain

'For Stresses

CRTPSTRESS_GLC_x = Sheet1.Cells(5 + a, 14)
CRTPSTRESS_GLC_y = Sheet1.Cells(5 + a, 15)
CRTPSTRESS_GLC_z = Sheet1.Cells(5 + a, 16)
CRTPSTRESS_GLC_xy = Sheet1.Cells(5 + a, 17)
CRTPSTRESS_GLC_xz = Sheet1.Cells(5 + a, 18)
CRTPSTRESS_GLC_yz = Sheet1.Cells(5 + a, 19)

'shear stress components

```
CRTPSTRAIN13    =    (CRTPSTRESS_GLC_x    *    a11    *    a21)    +
                (CRTPSTRESS_GLC_y    *    a12    *    a22)    +
                (CRTPSTRESS_GLC_z    *    a13    *    a23)    +
                (CRTPSTRESS_GLC_xy * (a11 * a22 + a12 * a21)) +
                (CRTPSTRESS_GLC_yz * (a12 * a23 + a13 * a22)) +
                (CRTPSTRESS_GLC_xz * (a13 * a21 + a11 * a23))

CRTPSTRAIN14    =    (CRTPSTRESS_GLC_x    *    a11    *    a31)    +
                (CRTPSTRESS_GLC_y    *    a12    *    a32)    +
                (CRTPSTRESS_GLC_z    *    a13    *    a33)    +
                (CRTPSTRESS_GLC_xy * (a11 * a32 + a12 * a31)) +
                (CRTPSTRESS_GLC_yz * (a12 * a33 + a13 * a32)) +
                (CRTPSTRESS_GLC_xz * (a13 * a31 + a11 * a33))


'normal stress component

CRTPSTRAIN16    =    (CRTPSTRESS_GLC_x    *    (a11    ^    2))    +
                (CRTPSTRESS_GLC_y    *    (a12    ^    2))    +
                (CRTPSTRESS_GLC_z    *    (a13    ^    2))    +    2    *
                ((CRTPSTRESS_GLC_xy    *    (a11    *    a12))    +
                (CRTPSTRESS_GLC_xz    *    (a11    *    a13))    +
                (CRTPSTRESS_GLC_yz * (a13 * a12)))

resultantshearstress = ((CRTPSTRAIN13) ^ 2 + (CRTPSTRAIN14) ^ 2) ^ (1 / 2)

'storing calculated normal and shear stress in excel sheet for sorting maximum
and minimum values

Sheet3.Cells(1 + a, 5) = CRTPSTRAIN16
Sheet3.Cells(1 + a, 6) = resultantshearstress


Next a

'maximum and minimum normal strain

Worksheets("data processing sheet").Activate

Set sortrange = Worksheets("data processing sheet").Range(Cells(2, 3), Cells(n + 1, 3))


maxstrainnormal = Application.WorksheetFunction.Max(sortrange)
minstrainnormal = Application.WorksheetFunction.Min(sortrange)


'maximum and minimum shear strains
```

```
Set sortrange = Worksheets("data processing sheet").Range(Cells(2, 4), Cells(n + 1, 4))

maxstrainresultant = Application.WorksheetFunction.Max(sortrange)
minstrainresultant = Application.WorksheetFunction.Min(sortrange)


'maximum normal stress

Set sortrange = Worksheets("data processing sheet").Range(Cells(2, 5), Cells(n + 1, 5))

maxstressnormal = Application.WorksheetFunction.Max(sortrange)


'maximum shear stress

Set sortrange = Worksheets("data processing sheet").Range(Cells(2, 6), Cells(n + 1, 6))

maxshearstresssultant = Application.WorksheetFunction.Max(sortrange)


Worksheets("sheet1").Activate

fatparam = (maxstrainresultant - minstrainresultant) * (maxshearstresssultant) +
            (maxstrainnormal - minstrainnormal) * (maxstressnormal)

Sheet1.Cells(12, 2) = fatparam


End Sub
```
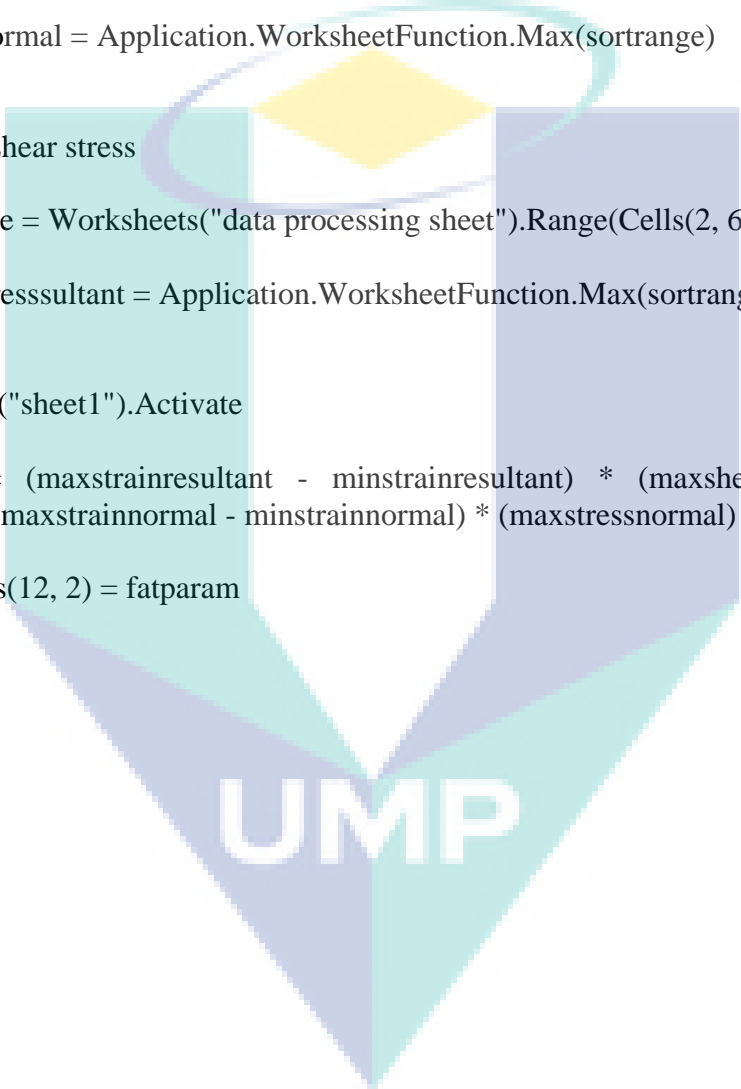
APPENDIX A3

IMPLEMENTATION OF MAXIMUM VARIANCE OF SHEAR

'Coding for maximum variance method below

theta = Sheet1.Cells(8, 2)
phy = Sheet1.Cells(7, 2)

Dim meanstress() As Double

ReDim meanstress(1, 1 To 6) As Double

increament = Sheet1.Cells(15, 2)

recsize = ((180 / increament) + 1) ^ 2
'size of matrix to store results depend on the size increment size

meanstress(1, 1) = 0 'mean of x
meanstress(1, 2) = 0 'mean of y
meanstress(1, 3) = 0 'mean of z
meanstress(1, 4) = 0 'mean of xy
meanstress(1, 5) = 0 'mean of xz
meanstress(1, 6) = 0 'mean of yz

For c = 1 To n

meanstress(1, 1) = meanstress(1, 1) + Sheet1.Cells(5 + c, 14)
meanstress(1, 2) = meanstress(1, 2) + Sheet1.Cells(5 + c, 15)
meanstress(1, 3) = meanstress(1, 3) + Sheet1.Cells(5 + c, 16)
meanstress(1, 4) = meanstress(1, 4) + Sheet1.Cells(5 + c, 17)
meanstress(1, 5) = meanstress(1, 5) + Sheet1.Cells(5 + c, 18)
meanstress(1, 6) = meanstress(1, 6) + Sheet1.Cells(5 + c, 19)

Next c

For d = 1 To 6

   meanstress(1, d) = meanstress(1, d) / n   '1-6 is X,Y,Z,XY,XZ,YZ

Next d

'Following loop make variance array filled with zeros before starting i.e. initialize with zeros

```
For r = 1 To 6
  For cl = 1 To 6

      Sheet4.Cells(1 + r, 7 + cl) = 0

   Next cl
Next r
```

'The loop to fill variance array

```
For r = 1 To 6
  For cl = 1 To 6
    For c = 1 To n

      Sheet4.Cells(1 + r, 7 + cl) = Sheet4.Cells(1 + r, 7 + cl) + ((Sheet1.Cells(5 + c, 13
                        + r) - meanstress(1, r)) * (Sheet1.Cells(5 + c, 13 + cl)
                        - meanstress(1, cl)))

    Next c

   Sheet4.Cells(1 + r, 7 + cl) = Sheet4.Cells(1 + r, 7 + cl) / n
   'divide the var terms with N (no of data points)

   Next cl
Next r
```

'at this point we will have the variance matrix C

'**
****

'NOW MODULE 1 OF THE ALGORITHM WILL BE CODED ..

```
Dim dc() As Variant
ReDim dc(6, 1) As Variant 'matrix name here is changed to "dc" as "d" exists in loop
variables

Dim m() As Variant
ReDim m(6, 1) As Variant  'm matrix in paper

Dim dct() As Variant
ReDim dct(1, 6) As Variant 'new matrix defined to sotre transpose of dc matrix

Dim vshearq() As Variant
```

ReDim vshearq(1) As Variant 'variance shear q (V(Tq) -- defined as matrix so result of matrix multiplication can be stored)

Dim record() As Double
ReDim record(1, 4)

'i = 1   'counter index intilization for record array

'here theta, phy and alpha has same meaning as in paper

'this loop will calculate variance and store them in record array with respective angles of critical planes...

'15 deg incriment is the value suggested in paper to give good results in most situations (this can be changed! With appropirate size change in record array))

vmax = 0

        theta = theta * (3.141592 / 180) 'in sin cos needs radians
        phy = phy * (3.141592 / 180)

'For Theta = 0 To 180 Step 15
   'For phy = 0 To 180 Step 15

     'For i = 1 To recsize
      For alpha = 0 To (180 * 3.141592 / 180) Step (increament * 3.141592 / 180)

      'alpha = alpha * (3.141592 / 180) 'in sin cos needs radians

      Sheet4.Cells(11, 8) = ((1 / 2) * (Sin(theta) * Sin(2 * phy) * Cos(alpha) +
                         Sin(alpha) * Sin(2 * theta) * (Cos(phy)) ^ 2))

      Sheet4.Cells(12, 8) = ((1 / 2) * (-Sin(theta) * Sin(2 * phy) * Cos(alpha) +
                         Sin(alpha) * Sin(2 * theta) * (Sin(phy)) ^ 2))

      Sheet4.Cells(13, 8) = (-(1 / 2) * Sin(alpha) * Sin(2 * theta))

      Sheet4.Cells(14, 8) = ((1 / 2) * (Sin(alpha) * Sin(2 * phy) * Sin(2 * theta)) -
                         (Cos(alpha) * Cos(2 * phy) * Sin(theta)))

      Sheet4.Cells(15, 8) = ((Sin(alpha) * Cos(phy) * Cos(2 * theta)) + (Cos(alpha) *
                         Sin(phy) * Cos(theta)))

      Sheet4.Cells(16, 8) = ((Sin(alpha) * Sin(phy) * Cos(2 * theta)) - (Cos(alpha) *
                         Cos(phy) * Cos(theta)))
      Dim var_range As Range

```
        Dim dc_range As Range          'for matrix multiplication mmult function require
cells addresses

        Worksheets("data processing").Activate

        Set var_range = Worksheets("data processing").Range(Cells(2, 8), Cells(7, 13))

        Set dc_range = Worksheets("data processing").Range(Cells(11, 8), Cells(16, 8))

        m = Application.WorksheetFunction.MMult(var_range, dc_range)
        '*moper,m,var,multi,dc    !matrix multiplication

        dct = Application.WorksheetFunction.Transpose(dc_range)  '*mfun,dcT,tran,dc
!transpose of direction cosine matrix

        For x = 1 To 6

        Sheet4.Cells(10 + x, 10) = m(x, 1)
        Sheet4.Cells(20, 7 + x) = dct(x)     'dct work with only one index not (1,x)

        Next x

        Set dct_range = Worksheets("data processing").Range(Cells(20, 8), Cells(20, 13))

        Set m_range = Worksheets("data processing").Range(Cells(11, 10), Cells(16, 10))

        vshearq = Application.WorksheetFunction.MMult(dct_range, m_range)
'*moper,vshearq,dcT,multi,m    !var(Tq)=d(transposed)*m (eq. A.5)

        If vshearq(1) > vmax Then

            vmax = vshearq(1)
            rectheta = theta
            recphy = phy
            recalpha = alpha

        End If

    Next alpha

    record(1, 1) = rectheta * (180 / 3.141592)   ' converted back to degree
    record(1, 2) = recphy * (180 / 3.141592)
    record(1, 3) = recalpha * (180 / 3.141592)
    record(1, 4) = vmax
    'i = i + 1
    'vmax = 0
  'Next i

  'Next phy
```

```vba
 'Next Theta

'MODULE 1 ENDS, WE HAVE RECORD MATRIX WITH INITIAL VALUES OF
CRITCAL PLANE ANGLES FOR MODULE 2 TO FINE TUNE

Worksheets("sheet1").Activate

Sheet1.Cells(22, 2) = record(1, 1)   'theta
Sheet1.Cells(23, 2) = record(1, 2)   'phy
Sheet1.Cells(24, 2) = record(1, 3)   'alpha
Sheet1.Cells(25, 2) = record(1, 4)   'variance

'Next j


'tempvari = 0
'max_var_row_indx = 0

'For j = 1 To recsize

  'If Sheet2.Cells(1 + j, 4) > tempvari Then
    'tempvari = Sheet2.Cells(1 + j, 4)
    'max_var_row_indx = 1 + j
  'End If

'Next j

'Sheet1.Cells(9, 2) = Sheet2.Cells(max_var_row_indx, 1)  'Theta
'S 'heet1.Cells(10, 2) = Sheet2.Cells(max_var_row_indx, 2) 'pHy
'Sheet1.Cells(11, 2) = Sheet2.Cells(max_var_row_indx, 3) ' alpha
'Sheet1.Cells(12, 2) = Sheet2.Cells(max_var_row_indx, 4) 'variance


'Worksheets("data processing").Activate

'Set sortrange = Worksheets("data processing").Range(Cells(2, 4), Cells(recsize + 1, 4))

End Sub
```

APPENDIX A4

EXTRACTION OF STRESS-STRAIN QUANTITIES ON CRITICAL PLANE

```
!To get stress-strain quantities on critical plane

/post1

wpcsys,-1

wprota,theta_maxPARAM,,-(90-phy_maxPARAM)

*dim,normalstress,,n,1
*dim,normalstrain,,n,1
*dim,shearstress,,n,3
*dim,shearstrain,,n,3

rsys,4      !note: workplane rotated in the critical plane angles

*do,a,1,n,1

   set,,,,,,,a

   *get,normalstress(a,1),node,nodenumber,s,x
   *get,normalstrain(a,1),node,nodenumber,epto,x
   *get,shearstress(a,1),node,nodenumber,s,xy
   *get,shearstress(a,2),node,nodenumber,s,xz
   *get,shearstrain(a,1),node,nodenumber,epto,xy
   *get,shearstrain(a,2),node,nodenumber,epto,xz

   shearstress(a,3)=((shearstress(a,1))**2+(shearstress(a,2))**2)**(1/2)
   shearstrain(a,3)=((shearstrain(a,1))**2+(shearstrain(a,2))**2)**(1/2)

 *enddo

! Max normal stress
!****************

*dim,orderofnormalstress,,n,1

*moper,orderofnormalstress(1),normalstress(1,1),sort,normalstress(1,1)

rowformaxnormalstress=orderofnormalstress(n,1)

*moper,orderofnormalstress(1),normalstress(1,1),sort,orderofnormalstress(1,1)

*del,orderofnormalstress,,nopr
```

```
maxnormalstress=normalstress(rowformaxnormalstress,1)
! Max normal strain range
!*********************

*dim,orderofnormalstrain,,n,1

*moper,orderofnormalstrain(1),normalstrain(1,1),sort,normalstrain(1,1)

rowformaxnormalstrain=orderofnormalstrain(n,1)
rowforminnormalstrain=orderofnormalstrain(1,1)

*moper,orderofnormalstrain(1),normalstrain(1,1),sort,orderofnormalstrain(1,1)

*del,orderofnormalstrain,,nopr

normalstrainrange = normalstrain(rowformaxnormalstrain,1)-
                    normalstrain(rowforminnormalstrain,1)

! Max shear stress
!**************

*dim,orderofshearstress,,n,1

*moper,orderofshearstress(1),shearstress(1,3),sort,shearstress(1,3)

rowmaxshrstrs_resul=orderofshearstress(n,1)

*moper,orderofshearstress(1),shearstress(1,3),sort,orderofshearstress(1,1)

*del,orderofshearstress,,nopr

maxshearstress_resul=shearstress(rowmaxshrstrs_resul,3)

! Shear strain range
!****************

*dim,orderofnormalstrain,,n,1

*moper,orderofnormalstrain(1),shearstrain(1,3),sort,shearstrain(1,3)

rowformaxshearstrain=orderofnormalstrain(n,1)
rowforminshearstrain=orderofnormalstrain(1,1)

*moper,orderofnormalstrain(1),shearstrain(1,3),sort,orderofnormalstrain(1,1)

*del,orderofnormalstrain,,nopr
```

```
shearstrainrange = shearstrain(rowformaxshearstrain,3)-
                    shearstrain(rowforminshearstrain,3)
!Mean shear and normal stress
!***********************

meannormalstress=0

meanshearstress=0

*do,a,1,n,1

    meannormalstress=normalstress(a,1)+meannormalstress
    meanshearstress=shearstress(a,3)+meanshearstress

*enddo

meannormalstress=meannormalstress/n
meanshearstress=meanshearstress/n
```
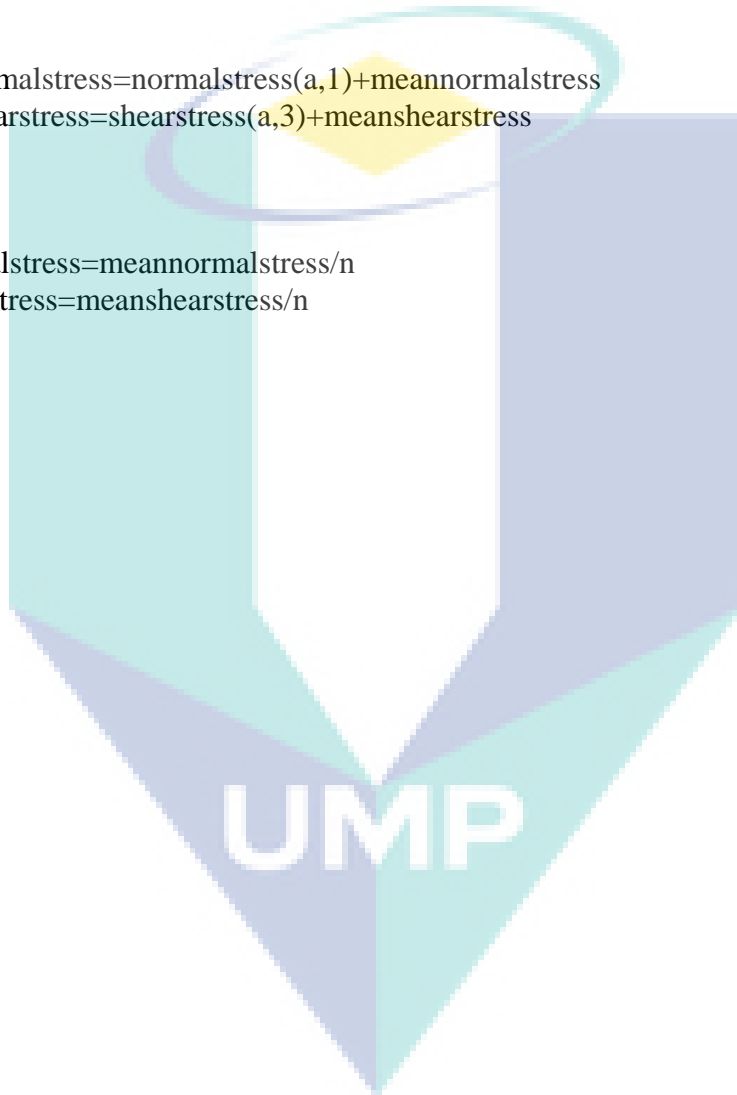
APPENDIX A5

CODING FOR DAMAGE ESTIMATION

```
Sub damage_function()

n = Sheet1.Cells(20, 3)

Dim P() As Double
Dim dP() As Double
Dim Dn() As Double

ReDim P(1 To n, 1) As Double
ReDim dP(1 To n, 1) As Double
ReDim Dn(1 To n, 1) As Double

a1      = Sheet1.Cells(7, 3)
a2      = Sheet1.Cells(8, 3)
a3      = Sheet1.Cells(9, 3)
a4      = Sheet1.Cells(10, 3)
sigma   = Sheet1.Cells(13, 3)
K       = Sheet1.Cells(5, 3)
R       = Sheet1.Cells(6, 3)
V       = Sheet1.Cells(11, 3)
m       = Sheet1.Cells(12, 3)
shearstrainrange        = Sheet1.Cells(18, 3)
normalstrainrange       = Sheet1.Cells(19, 3)
meannormalstress        = Sheet1.Cells(21, 3)
meanshearstress         = Sheet1.Cells(22, 3)
elmod                   = Sheet1.Cells(26, 3)
yieldstress             = Sheet1.Cells(27, 3)

tempP  = 0
evolve = 0
ev     = 0
a      = 1

For a = 1 To n

shearstress = Sheet1.Cells(a + 4, 6)
normalstress = Sheet1.Cells(a + 4, 7)
```

For Model-1

```
P(a, 1) = (a1 * (shearstrainrange * shearstress) + a2 * (normalstrainrange *
        normalstress))/yieldstress -  (sigma) / elmod - ev
```

For Model-2

P(a, 1) = a1 * (shearstrainrange) + a2 * (shearstress / yieldstress) + a3 *
        (normalstrainrange) + a4 * (normalstress / yieldstress) - (sigma / elmod) - ev

If P(a, 1) <= 0 Then

tempP = 0

Else

  dP(a, 1) = P(a, 1) - tempP
  tempP = P(a, 1)

   If dP(a, 1) > 0 Then

    Dn(a, 1) = K * (tempP ^ R) * dP(a, 1)
    evolve = (V * (dP(a, 1) ^ h) * (normalstress - meannormalstress) * (shearstress -
        meanshearstress)) / (elmod ^ 2)

     If evolve < 0 Then

      evolve = 0

     Else

      ev = evolve + ev

     End If
   End If
End If

Next a

'next loop

tempD = 0
totD = 0

For a = 1 To n Step 1

totD = Dn(a, 1) + tempD
tempD = totD

Next a

Sheet1.Cells(13, 11) = totD

End Sub

APPENDIX A6

CODING FOR FATIGUE LIFE ESTIMATION

```
*dim,P,,n,1
*dim,dP,,n,1
*dim,Dn,,n,1


a1=
a2=
a3=
a4=
sigma= <values of calibrated coefficients>
K=
R=
V=
m=

elmod=<elastic modulus>
yieldstress=<yield stress>

tempP = 0
evolve = 0
ev = 0



*do,a,1,n,1

!*********************************
```

For Model-1

```
P(a,1) =
        (a1*(shearstrainrange*shearstress(a,3))+a2*(normalstrainrange*normalstress(a,
        1)))/yieldstress-(sigma/Elmod)-ev
```

For Model-2

```
P(a,1) = a1*(shearstrainrange) + a2*(shearstress(a,3)/yieldstress) +
        a3*(normalstrainrange) + a4*(normalstress(a,1)/yieldstress) - (sigma/Elmod) –
        ev

!*********************************
```

```
   *if,P(a,1),LE,0,then

      tempP = 0

      *cycle

   *else

      dP(a,1) = P(a,1)-tempP
      tempP = P(a,1)

   *endif


   *if,dP(a,1),LE,0,then

      *cycle

   *else

      Dn(a,1) = K*(tempP**R)*dP(a,1)
      evolve = (V*(dP(a,1)**m)*(normalstress(a,1)-
               meannormalstress)*(shearstress(a,3)-meanshearstress)/Elmod**2)

      *if,evolve,LT,0,then

         evolve = 0

      *else

         ev = evolve+ev

      *endif

   *endif

*enddo

tempD=0
totD=0

*do,a,1,n,1

   totD=Dn(a,1)+tempD
   tempD=totd

*enddo

FatgiueLife=(1/totD)
```